Doctoral Thesis

Study on New Thermal Response Test Analysis with Partial Groundwater Flow and its Application for Ground Source Heat Pump System Design

Presented by: Hobyung Chae

Supervisor: Prof. Katsunori Nagano

北海道大学
HOKKAIDO UNIVERSITY

2021

Division of Human Environmental System

Graduate School of Engineering

Hokkaido University

CONTENTS OF THE THESIS

Nomenclature ····· VI

List of figures ····· VIII

List of tables ····· XIV

1. Introduction

1.1 Energy consumption and environmental issues 3

1.2 Ground source heat pump system 6

1.2.1 Geothermal energy utilization and resource temperature 6

1.2.2 Ground source heat pump system and its classification 7

1.2.3 Research trend and developments of GSHP system 11

1.3 Objectives and scope of the thesis 13

1.4 Outline of the thesis 13

1.5 Reference 16

2. Previous study orientation of this study

2.1 Introduction..... 23

2.2 Mathematical analysis of ground heat exchangers 25

2.2.1 Infinite Line source model..... 25

2.2.2 Infinite cylindrical source model..... 26

2.2.3 Finite line source model 27

2.2.4 Moving Line source model..... 29

2.2.5 Superposition principle for temperature response 32

2.3 Borehole thermal resistance 34

2.3.1 Fluid to pipe wall resistance 34

2.3.2 Grout resistance 36

2.4 Thermal response test.....40

2.4.1 Guideline for the TRT and the test setup 40

2.4.2 Parameter identification methods 41

2.4.3 Historical review of thermal response test 42

2.5 Orientation of this thesis 45

2.6 Reference 46

3. Estimation of fast groundwater flow: Simultaneous estimation of effective thermal conductivity and groundwater velocity in single-layer

3.1 Energy consumption and environmental issues 53
3.2 Field experiment 56
3.2.1 Site descriptions..... 56
3.2.2 Application of thermal response test 58
3.3 Analysis methodology.....61
3.3.1 Description of moving line source model..... 61
3.3.2 Borehole thermal resistance with groundwater flow 62
3.3.3 Equivalent single pipe 64
3.4 Results of thermal response test analysis 66
3.4.1 Conventional TRT analysis method..... 66
3.4.2 Borehole thermal resistance under the permeable borehole condition 67
3.4.3 Equivalent radius of the imaginary single pipe 69
3.4.4 Simultaneous estimation of the effective thermal conductivity and the groundwater velocity in single layer 70
3.5 Discussion on limitation of MLS model 72
3.6 Summary 72
3.7 Reference 73

4. Analysis of relaxation time of temperature for thermal response test: Estimation of effective thermal conductivity and groundwater velocity in multi-layer

4.1 Introduction.....79
4.2 Field experiments.....82
4.3 Methodologies.....84
4.3.1 Calculation of circulating fluid temperature..... 84
4.3.2 Multi-layer thermal response test analysis 85
4.4 Parameter estimation of multi-layer from TRT result.....88

4.4.1 Standard TRT results 88
4.4.2 Determination of the depths of the zone 89
4.4.3 Estimation of the groundwater velocity in the zones 92
4.5 Validation of the methodology 94
4.5.1 Comparison with calculated results and TRT data 94
4.5.2 Analysis results of the thermal parameters according to the end time of the TRT 95
4.6 Comparison between single and multi-layer parameters for the design of the GSHP 97
4.6.1 Comparison between the proposed method and the conventional TRT analysis method 98
4.6.2 Comparison between multi-layer and single layer for design parameters 99
4.6.3 Comprehensive review of each method 100
4.7 Summary 101
4.8 Reference 102

5. Validation of proposed TRT analysis and determination of borehole size: Life cycle cost analysis and cost reduction

5.1 Introduction 107
5.2 Heating and cooling load for target building 110
5.3 Numerical model 112
5.3.1 Governing equation 112
5.3.2 Discretized domain 112
5.3.3 Boundary conditions 115
5.4 Life cycle cost analysis of GSHP system based on multi-layer TRT analysis 118
5.4.1 Design parameters in multi-layer 118
5.4.2 Determination of the depths of the zone 118
5.4.3 Estimation of the groundwater velocity in the zones 121
5.4.4 Life cycle cost analysis 125
5.5 Determination of appropriate borehole length 129
5.5.1 Actively Thermal response test 129
5.5.2 Estimation of groundwater velocity 129

5.5.3 Appropriate borehole sizing and LCC analysis 132
5.6 Summary 139
5.7 Reference 140

6. Application of ground source heat pump system for nearly-zero energy building

6.1 Introduction 143
6.1.1 Concept of zero energy building 144
6.1.2 Investigation instance of facility technology in ZEB 146
6.2 Building characteristics 157
6.2.1 Building information 157
6.2.2 Building equipment system for HVAC 159
6.3 Features of ZEB simulation tool 162
6.3.1 Calculation of building loads based on heat balance 162
6.3.2 Floor heating and cooling system 165
6.3.3 Ground source heat pump system 169
6.4 Results of the simulation tool for ZEB 171
6.4.1 Building load 171
6.4.2 Supply water temperature for floor heating and cooling system 173
6.4.3 Prediction of the performance on the GSHP system 174
6.4.4 Long-term simulation for GSHP system according to groundwater velocity and borehole number 175
6.5 Summary 179
6.6 Reference 180

7. General conclusion and development toward zero carbon society

7.1 General conclusion of the thesis 185
7.2 Development toward zero carbon society 189
7.2.1 Plan to activate distribution of the GSHP system 189
7.2.2 Sate-of-the-art facility element technology for zero carbon society 190
7.3 Reference 194

Acknowledgements..... 195

Nomenclature

Abbreviations

ATES	aquifer thermal energy storage
ASHP	air source heat pump
BTES	borehole thermal energy storage
CTES	cavern thermal energy storage
DTES	duct thermal energy storage
FEM	finite element method
GHG	greenhouse gas
GSHP	ground source heat pump
GTES	ground thermal energy system
MLS	moving line source
PVT	photovoltaic thermal
SCW	standing column well
TRT	thermal response test
UTES	underground thermal energy system
ZEB	zero energy building

Symbols

c_{p}	specific heat capacity [J/(kg K)]
d	diameter [m]
F_o	Fourier constant [$\frac{\alpha t}{r^2}$)]
h	convective heat transfer coefficient (W/(m2 k))
k	temperature gradient with a log time scale [K/ln (t)]
L	borehole length [m]
m	flow rate [L/min]
n	data number
q	heat injection rate [W/m]
Q	heat injection [kW]
t	time (s)
T	temperature (°C)
$\bar{T}$	mean temperature (°C)
r	radius (m)

R	ratio between the distance from the borehole depth and the borehole radius ($\frac{r}{L_{bh}}$).
R_{b}	thermal resistance ((m k)/W)
R_{b}^{*}	revised borehole thermal resistance ((m k)/W)
v	Darcy velocity (m/s)
x	shank spacing between pipes
z	depth [m]

Greek letters

α	thermal diffusivity (m^2/s)
β	integration parameter
ρ	density (kg/m3)
ε	porosity
τ	elapsed time
λ	thermal conductivity (W/(m K))
φ	polar angle (°)
γ	Euler's constant, ($\gamma \doteq 0.5772$)

Subscripts

0	initial value
a	apparent
f	fluid
g	grout
bh	borehole
eff	effective
eq	equivalent
in	inside
out	outside
p	pipe
s	soil
w	water

List of figures

Chapter 1

Fig. 1. 1 Percentage of sectorial CO2 emissions in the world [2] 3

Fig. 1. 2 Projections of global net electricity generation and use in each sector [3] 4

Fig. 1. 3 Percentage of energy consumption in the building sector in the world [2] 5

Fig. 1. 4 Utilization of geothermal energy based on resource temperature 6

Fig. 1. 5 Comparison of COP and total work of GSHP and ASHP cycles based on various refrigerants [10] 7

Fig. 1. 6 Main elements of the GSHP system; (a) Ground loop, (b) Heat pump unit, and (c) Distribution system 8

Fig. 1. 7 Classification of GSHP system and type of ground heat exchanger 9

Fig. 1. 8 Schematic diagram of the open-loop system 10

Fig. 1. 9 Overall flow chart of this thesis 15

Chapter 2

Fig. 2. 1 Cost breakdown of GSHP system (Department of Energy and Climate Change, 2016) 23

Fig. 2. 2 Cost rate in each sector of GSHP system 24

Fig. 2. 3 Virtual mirror image of the finite line source 28

Fig. 2. 4 Temperature response according to borehole depth 28

Fig. 2. 5 Temperature response according to the groundwater velocity 31

Fig. 2. 6 Temperature response on the borehole wall surface according to the polar angle of groundwater flow direction 32

Fig. 2. 7 Temperature response according to the superimposed step load 33

Fig. 2. 8 Conceptual diagram of thermal resistance in a borehole 35

Fig. 2. 9 Equivalent radius methods for calculation of the grout resistance 37

Fig. 2. 10 Resistance network for a single U-tube 39

Chapter 3

Fig. 3. 1 Location of the test site: (a) the regional and local maps in East Japan, ... 56

Fig. 3. 2 Geological section and ground plan of the test site: (a) geological section at a test site, (b) vertical ground temperature profile, and (c) ground plan of a test site..... 57

Fig. 3. 3 Observation data of the water table depth, the precipitation, and groundwater and air temperatures 58

Fig. 3. 4 Schematic of the TRT machine units and the BHE 59

Fig. 3. 5 Figure of the TRT machine units and the BHE..... 59

Fig. 3. 6 Usage breakdown of mixed and pure backfill materials in GHSs from 2010 to 2018 [26] 62

Fig. 3. 7 Discretized model domain 64

Fig. 3. 8 Measurement data from the TRT: (a) temperature variation of the inlet and outlet pipes, (b) the heat injection and flow rate..... 66

Fig. 3. 9 Conventional TRT analysis using the temperature slope over logarithmic time 67

Fig. 3. 10 Streamline plots of the groundwater velocity; (A) permeable backfilled, (B) impermeable backfilled..... 68

Fig. 3. 11 Borehole thermal resistance according to the groundwater velocity; (A) permeable backfilled, (B) impermeable backfilled..... 68

Fig. 3. 12 Relationship of borehole thermal resistance between groundwater velocity and thermal conductivity of backfill material 69

Fig. 3. 13 Equivalent Radius of imaginary single pipe..... 70

Fig. 3. 14 Relationship between groundwater velocity and effective thermal conductivity of the soil..... 71

Fig. 3. 15 Curve fitting of temperature in each case 71

Chapter 4

Fig. 4. 1 Site description; (a) ground plan of the test site, (b) geological column section..... 78

Fig. 4. 2 Schematic diagram of the TRT machine units and the BHE 79

Fig. 4. 3 Relationship between dimensional temperature and the dimensional RTT..... 82

Fig. 4. 4 Flow chart of calculation 83

Fig. 4. 5 Measurement data of the TRT; (a) temperature data of inlet, outlet and average of Pt-100 sensors, (b) heat injection and flow rate 84

Fig. 4. 6 Dimensional temperature variation and RTT of the measurement data and calculated results 85

Fig. 4. 7 RTT according to the groundwater velocity 86

Fig. 4. 8 Vertical distribution of the RTT 87

Fig. 4. 9 Vertical temperature distribution during the heat injection period (a) and the heat transfer rate of each zone (b) 88

Fig. 4. 10 Temperature increment according to the heat exchanger rate and the groundwater velocity at the end of the TRT 89

Fig. 4. 11 Comparison between the calculated results and the TRT data 90

Fig. 4. 12 Temperature variation according to the end time of the TRT 91

Fig. 4. 13 Average temperature variation of the circulating fluid; Comparison between the proposed method and the conventional TRT analysis method 99

Fig. 4. 14 Average temperature variation of the circulating fluid; Comparison between multi-layer and single layer for design parameters 99

Fig. 4. 15 Average temperature variation of the circulating fluid; Comparison between multi-layer and single layer for design parameters when depth of the borehole was 40 m 100

Fig. 4. 16 Average temperature of the circulating fluid during the heating and cooling season 100

Chapter 5

Fig. 5. 1 Target building 110

Fig. 5. 2 Discretized numerical model 115

Fig. 5. 3 Comparison of temperature variation between TRT data and CFD results at inlet and outlet pipes 119

Fig. 5. 4 Temperature change of circulating fluid in each layer 120

Fig. 5. 5 Temperature distribution over depth; (a) temperature comparison between the CFD results and the DTS data over depth, (b) temperature distribution in the borehole at 60 h after heat injection 120

Fig. 5. 6 Heating and cooling loads of building 122

Fig. 5. 7 Required borehole numbers based on COP of the 30th year 124

Fig. 5. 8 Temperature change of the ground for 30 years 124

Fig. 5. 9 Cost rate of each section of the GSHP system in the previous studies [31,39,40] 126

Fig. 5. 10 Life cycle cost according to the government subsidy 127

Fig. 5. 11 Return of investment period according to the government subsidy 128

Fig. 5. 12 Geological conditions and groundwater velocity in Area 1 (Canada) [44] 130

Fig. 5. 13 Geological conditions and groundwater velocity in Area 2 (China) [43] 131

Fig. 5. 14 Relationship among the λ_a, λ_{eff} and v 131

Fig. 5. 15 Heating and cooling loads of the buildings; (a) Area 1 (Guelph, Canada), (b) Area 2 (Changzhou, China) and (c) monthly amount of heating and cooling loads 133

Fig. 5. 16 Required borehole numbers and the temperature change of the ground over time (Area 1 [Guelph, Canada]) 135

Fig. 5. 17 Required borehole numbers and the temperature change of the ground over time (Area 2 [Changzhou, China]) 136

Fig. 5. 18 Total borehole length in each case 136

Fig. 5. 19 Life cycle cost according to the government subsidy (Area 1 [Guelph, Canada]) ... 138

Fig. 5. 20 Life cycle cost according to the government subsidy (Area 2 [Changzhou, China]) 138

Chapter 6

Fig. 6. 1 World energy consumption by energy source (1990-2040, source: International Energy Outlook 2020) 143

Fig. 6. 2 Sustainable Development goals (source: United Nations) 144

Fig. 6. 3 Image of ZEB definition 145

Fig. 6. 4 Installed number of the GSHP systems in Japan 146

Fig. 6. 5 Figure of Kitakyushu Dormitory 147

Fig. 6. 6 Schematic diagram of the system Kitakyushu Dormitory 147

Fig. 6. 7 Figure of Forrester Hirosaki Park 148

Fig. 6. 8 figures of the snow melting system in Forrester Hirosaki Park 148

Fig. 6. 9 shows buildings targeting ZEB in various regions in Japan 149

Fig. 6. 10 Figure of Green Tomorrow 150

Fig. 6. 11 Concept of applied system in Green Tomorrow and figures 150

Fig. 6. 12 Figure of Eco-3L house 151

Fig. 6. 13 Schematic diagram of the applied system in the Eco-3L house..... 152

Fig. 6. 14 Figure of ZEB (Case 1)..... 153

Fig. 6. 15 Installed system in the building in Case 1 154

Fig. 6. 16 Figure of ZEB (Case 2)..... 155

Fig. 6. 17 Installed system in the building of Case 2. 155

Fig. 6. 18 Building floor plan and figures of each area..... 157

Fig. 6. 19 Conceptual diagram of equipment system..... 159

Fig. 6. 20 Figure of the ground source heat pump 160

Fig. 6. 21 Figures of earth tube system on construction site..... 161

Fig. 6. 22 Schematic diagram of the systems..... 161

Fig. 6. 23 Conceptual diagram of the heat balance 164

Fig. 6. 24 Conceptual diagram of the floor heating system 166

Fig. 6. 25 Net thermal resistance between adjacent meshes 166

Fig. 6. 26 Conceptual diagram of the supply water pipe 168

Fig. 6. 27 Weather data; (a) outdoor temperature and (b) global radiation 171

Fig. 6. 28 Heating and cooling loads of building..... 172

Fig. 6. 29 Monthly amount of heating and cooling loads 172

Fig. 6. 30 Floor surface temperature over time. 173

Fig. 6. 31 Supplied water temperature for heating and cooling 173

Fig. 6. 32 Variation of the EWT (T1,in)..... 174

Fig. 6. 33 Variation of SCOP over time 175

Fig. 6. 34 Calculated results for 30 years according to borehole number: (a) annual mean ground temperature, (b) SCOP for heating and (c) annual electric consumption..... 176

Fig. 6. 35 Calculated results (Case 1) for 30 years according to groundwater velocity [Layer 1: 20 m ($\lambda_{\mathrm{eff}} + v$), Layer 2: 65 m ($\lambda_{\mathrm{eff}}$)]: (a) annual mean ground temperature, (b) SCOP for heating and (c) annual electric consumption..... 177

Fig. 6. 36 Calculated results (Case 2) for 30 years according to groundwater velocity [Layer 1: 40 m ($\lambda_{\mathrm{eff}} + v$) Layer 2: 45 m ($\lambda_{\mathrm{eff}}$)]: (a) annual mean ground temperature, (b) SCOP for heating and (c) annual electric consumption..... 178

Chapter 7

Fig. 7. 1 Conceptual image of vacuum insulation panel 147

Fig. 7. 2 Conceptual image of energy-storage system 147

Fig. 7. 3 Conceptual image of Building Energy Management System 149

List of tables

Chapter 2

Table 2. 1 Empirical coefficient for a shape factor of the borehole 38

Table 2. 2 Research of the TRT analysis methods..... 44

Chapter 3

Table 3. 1 Filed measurement methods for estimation of groundwater velocity..... 54

Table 3. 2 Specification of TRT machine units..... 60

Table 3. 3 RMSE of cases..... 70

Chapter 4

Table 4. 1 Conditions of Zones 86

Table 4. 2 Results of the thermal parameter according to the end time 92

Chapter 5

Table 5. 1 Building information and parameters.....111

Table 5. 2 Conditions of the thermal response test.....116

Table 5. 3 Boundary conditions applied in CFD model.....117

Table 5. 4 Conditions of parameters in each layer 118

Table 5. 5 RMSE and temperature error in each layer 121

Table 5. 6 Monthly heating and cooling loads 122

Table 5. 7 Calculation conditions and total length of BHEs 124

Table 5. 8 Initial cost in each case..... 128

Table 5. 9 Thermal properties of each layer in Area 1 132

Table 5. 10 Thermal properties of each layer in Area 2 132

Table 5. 11 Conditions of each case in Area 1 and Area 2 134

Chapter 6

Table 6. 1 Classification of zero energy building 145
Table 6. 2 Thermal conductivity and thickness on the wall 158
Table 6. 3 Thermal conductivity and thickness on the ceiling 158
Table 6. 4 Thermal conductivity and thickness on the floor 158
Table 6. 5 Q value for each region [5] 162
Table 6. 6 Monthly amount of heating and cooling loads 172

Chapter 1.

Introduction

1.1.Energy consumption and environmental issues

Global climate change increasingly has a negative influence not only on ecosystems but also on human health and the economy. According to EEA (European Environment Agency) report [1], the regions in Europe are already facing adverse impacts of a changing climate such as rising sea levels, flooding and droughts. The large amounts of greenhouse gases (GHG) by human activities are released into the atmosphere, resulting in changing the global climate. Two-thirds of the GHG emissions are related to energy use for heating, electricity generation and transport. In Europe, burning fossil fuels are the largest emitter of the GHG, responsible for 78 % of total E.U. emissions in 2015 [1,2].

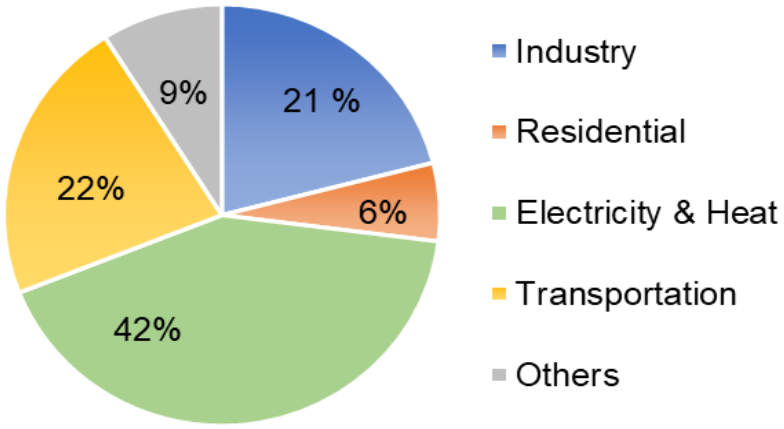

Fig. 1. 1 Percentage of sectorial CO2 emissions in the world [2]

The U.S. Energy Information Administration (EIA) predicted that world energy consumption would grow by nearly 50% between 2018 and 2050 [3]. Increasing the energy demand results from rising income, urbanization. It is a major cause of environmental pollution and significantly impacts global warming. Most of this growth comes from developing countries. Moreover, this growth focused on regions where strong economic growth is driving demand, particularly in Asia. A stable energy supply is essential to ensure economic growth since the energy demand trend has been increased. Therefore, it is necessary to present some of the significant solutions on climate change and the energy demand in the world for the next generation.

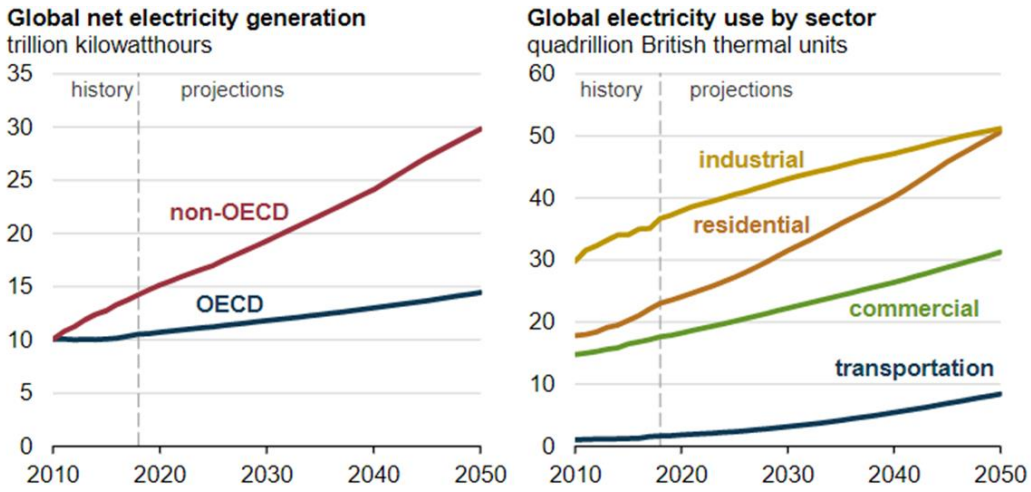

Fig. 1. 2 Projections of global net electricity generation and use in each sector [3]

Many countries and European commitments make an effort to mitigate climate change and organized the Paris Climate Agreement in 2015. In the agreement, 195 countries adopted the universal and legally global climate deal. Through the global climate agenda of the Paris Climate Agreement, E.U. has enforced to limit climate rise and energy use by 2020. The first targets for climate and energy until 2020 were to cut 20 % of the GHG emissions and energy consumption compared to 1990 levels and improve 20 % of energy efficiency. Their final goal is to mitigate GHG emissions by 80-95 % by 2050.

The building sector accounts for a third of the energy use and the GHG emissions in the world for air conditioning [2,4,5]. It needs to suggest the countermeasure to provide a sustainable and safe energy supply and mitigate the environmental problem. The GHG emissions related to energy use can be cut in two ways; changing fossil fuels to clean energy sources with non-combustibility and reducing overall energy consumption by improving the system performance and building insulation in the building sector.

Sustainable energy supply systems using renewable energy sources such as solar power, wind power and ocean energy [6–9] have been researched to good progress during the past century. However, the systems have limitations on external influences such as weather and local characteristics. On the contrary, geothermal energy can be used anywhere, regardless of the external influence. The ground source heat pump (GSHP) system utilizing geothermal energy has been regarded as a highly efficient and environmental-friendly system. The GSHP system can reduce GHG emissions compared with conventional heating, ventilation, and air conditioning

(HVAC) systems. It alleviates the heat island effect in major cities by ejecting the heat to the ground effectively. It is also possible to reduce GHG emissions and energy consumptions by using the GSHP system. This chapter explains the individual components of the GSHP system. Also, the research trend and future studies of the GSHP system are described.

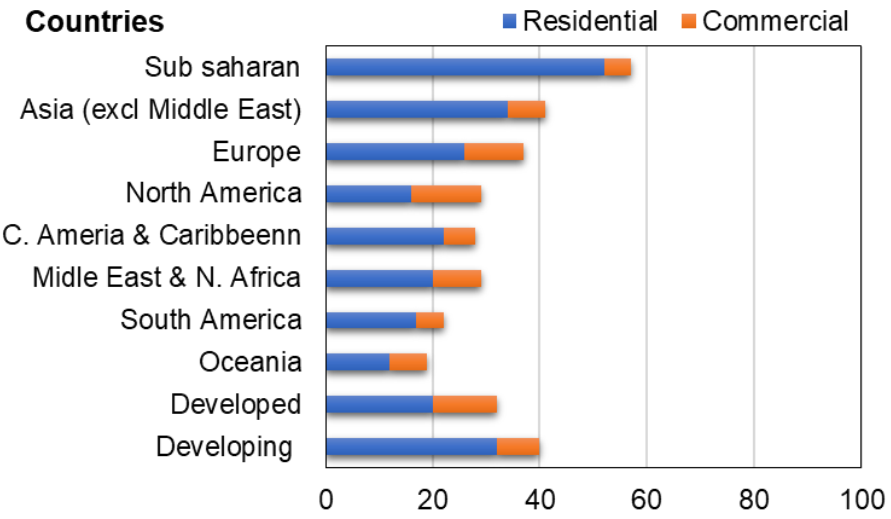

Fig. 1. 3 Percentage of energy consumption in the building sector in the world [2]

1.2. Ground source heat pump system

1.2.1. Geothermal energy utilization and resource temperature

The main factors that determine the use of geothermal resources depend on the resource temperature. Fig. 1.4 shows the utilization of global geothermal energy by temperature category. In general, there is no clear distinction between categories, but the geothermal power industry has used the top three temperature categories (a, b and c) based on economic power generation. Rankine cycle power plants have proven that they can economically produce electricity above 90 °C. These systems are called 'direct use' because there is no energy conversion process for electricity generation. However, most regions have soil temperatures between 10 and 20°C. The condition includes in the fourth category (d), which can utilize the GSHP systems.

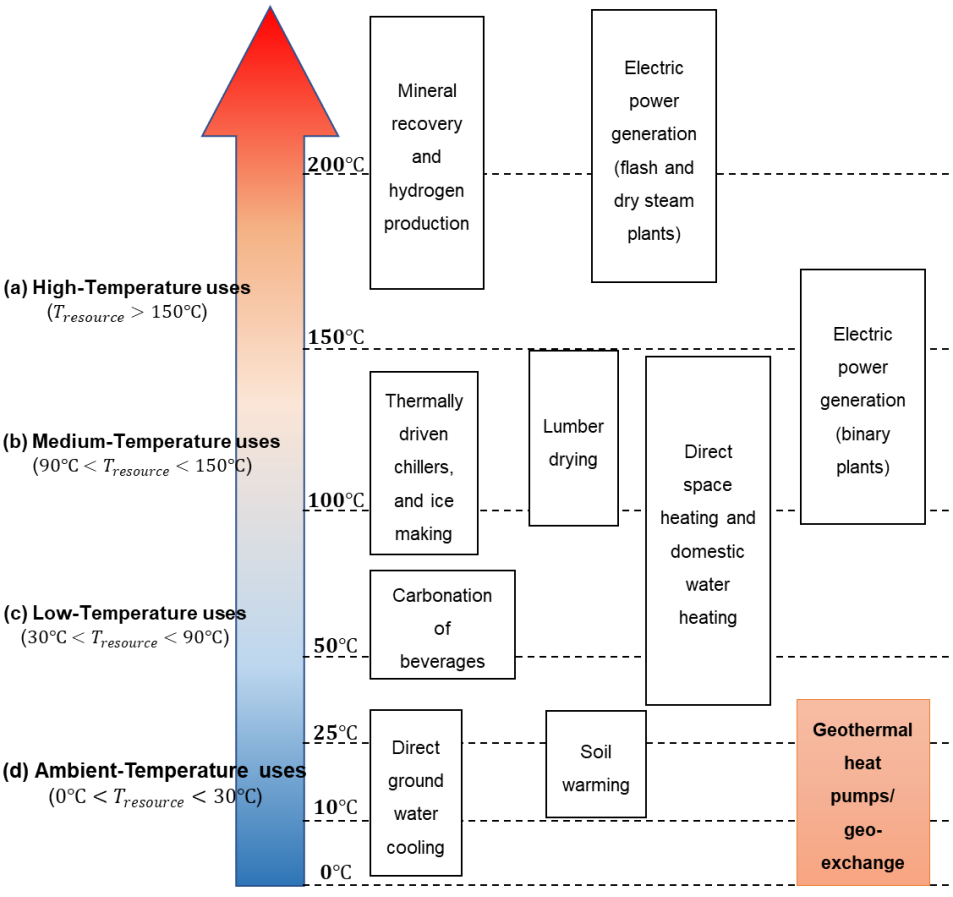

Fig. 1. 4 Utilization of geothermal energy based on resource temperature

1.2.2. Ground source heat pump system and its classification

The ground thermal energy system (GTES) is classified into the following three types. The first is the underground thermal energy system (UTES), which stores unused heat sources into the ground as a heat storage body. There are four types of UTES: aquifer thermal energy storage (ATES), borehole thermal energy storage (BTES), cavern thermal energy storage (CTES) and duct thermal energy storage (DTES). The second is the one that directly uses the heat of the ground without using a heat pump. It melts snow by circulating the heat medium (antifreeze) such as earth tube. The third is the ground source heat pump (GSHP) system, which uses a heat pump to use the retained enthalpy of the ground and groundwater as a heat source. Here, this chapter will explain the GSHP system, which is the most mainstream.

The GSHP systems utilizing the ground as a heat source or heat sink have been widely recognized as a high-performance and environmental-friendly system for heating, cooling and supplying hot water in houses and buildings. The systems can offer more high performance than an air source heat pump (ASHP) system because it uses a tremendous heat capacity and a stable temperature range of 10-20℃ of the ground. Fig. 1.5 shows the performance comparison between the GSHP system and the ASHP system according to various refrigerants [10]. In general, the heat pump (water cooled chiller) using the ground source also has higher efficiency than the heat pump (air cooled chiller) unit using air source even when the heat source temperature is the same. In addition, the GSHP systems do not need a defroster.

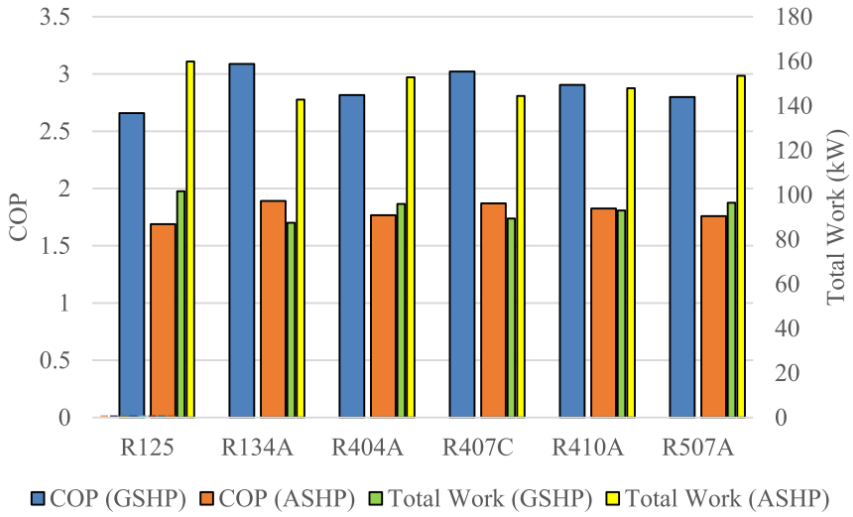

Fig. 1. 5 Comparison of COP and total work of GSHP and ASHP cycles based on various refrigerants [10]

The GSHP system generally consists of three main components: heat pump units, distribution systems and borehole heat exchangers (BHE). Fig. 1.6 indicates the ground loop, heat pump unit, and distribution system. The heat pump is a device that transfers thermal energy using the refrigeration cycles for heating and cooling of the buildings. The distribution system is a device that supplies the heat from the heat pump to the building inside through the air ducts and water pipes. The BHEs reject/absorb heat to/from the surrounding ground. In particular, the BHEs represent the main component of the GSHP system, and a proper design of the BHE leads to better thermal performance. The GSHP systems are classified by the type of ground loop.

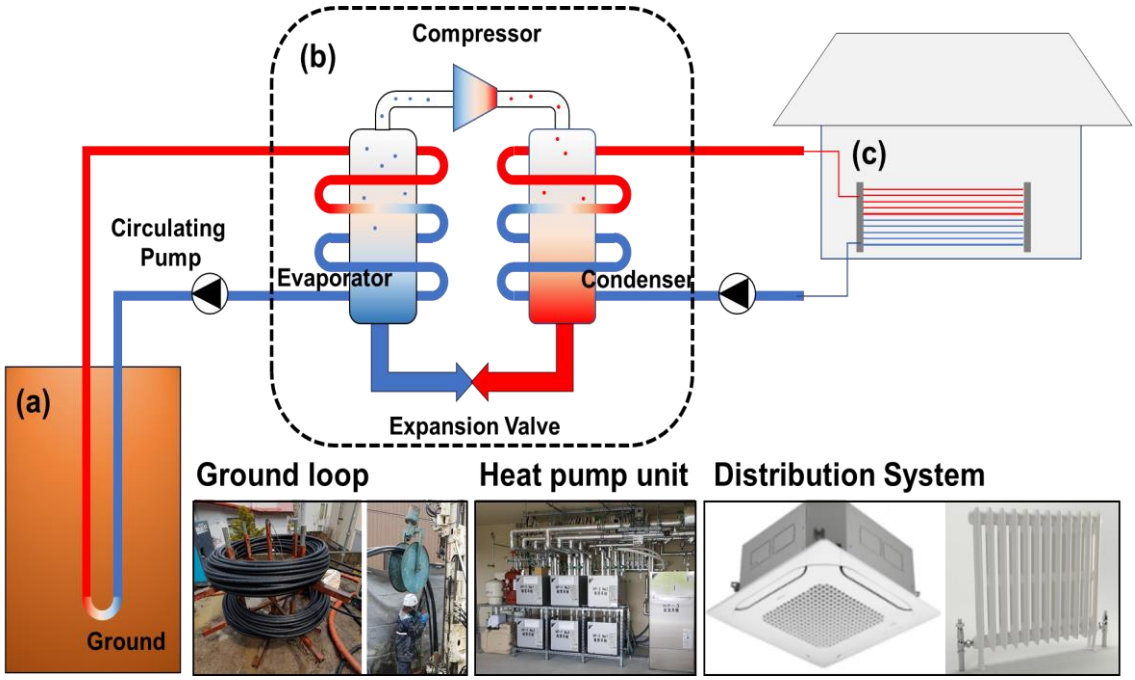

Fig. 1. 6 Main elements of the GSHP system; (a) Ground loop, (b) Heat pump unit, and (c) Distribution system

The GSHP systems can be classified into two main categories; the open-loop system and the closed-loop system. Fig. 1.7 shows the classification of the GSHP according to the type of ground heat exchanger. Since the open type uses groundwater [11–13] and lake water [14,15] directly as a heat source, its efficiency is higher than the closed type. The open-loop type using standing column well (SCW) is one of the representative systems shown in Fig. 1.8. The BHEs of the open-loop type draw the groundwater from wells in a semi-open loop arrangement. The type of system is typically used in specific geology where water is found in the rock fractures. The ground heat exchanger in such systems composed the vertical borehole filled with groundwater up to the water

table level. An open-well system has the advantages of low cost and high efficiency, but a large water yield from a surface or groundwater well is often not possible. Even if possible, there may not be a reasonable way to get the groundwater back into the environment. As installations become more extensive, the use of an open-well system may become less feasible because hundreds of gallons of the yield and/or reinjection would be required. Although the open-loop system has a high performance, it has regional restrictions: it cannot apply to areas where the lake is not in the vicinity, or the groundwater is not pumped. Also, it is a possibility for the ground environment to contaminate because of the direct use of groundwater.

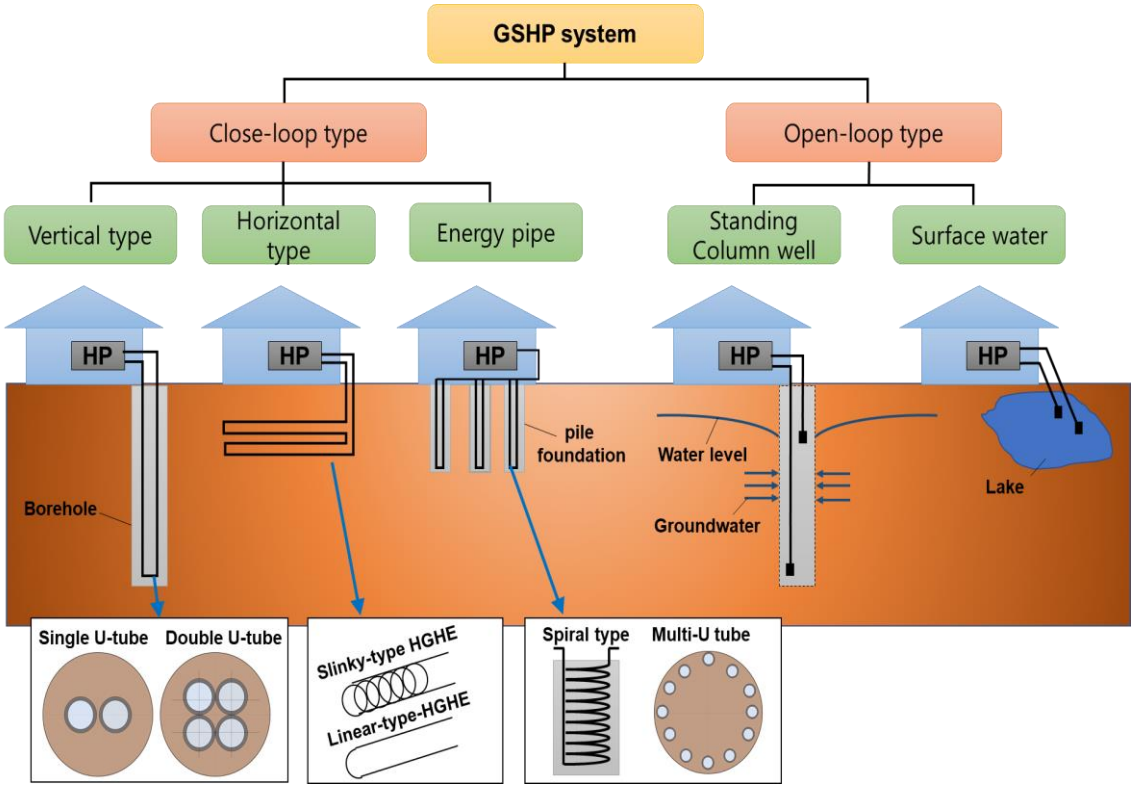

Fig. 1. 7 Classification of GSHP system and type of ground heat exchanger

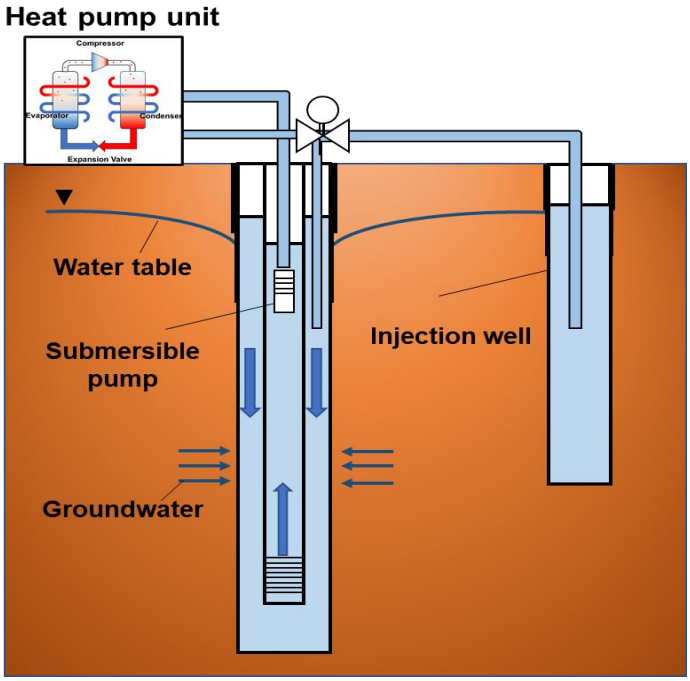

Fig. 1. 8 Schematic diagram of the open-loop system

The closed-loop type system circulates an antifreeze solution or water through a closed-loop buried in the borehole. The heat exchanger transfers the heat flux between the ground and the antifreeze solution in the closed-loop. The closed-type has an extensive range of applications when the underground is used as a heat source. In Europe and the United States, the GSHP system is widely used, and there are many examples of closed-type installation [16–18].

The closed-type system is generally classified into three types; vertical loop type, horizontal loop type and energy pile system. The horizontal type [19–22] and energy pile system [23,24] have been studied to reduce the expensive drilling cost for the borehole instead of the vertical loop type. In particular, the energy pile needs no additional cost for the borehole because the heat exchanger is installed in the steel file used as the foundation of the building. However, the horizontal type cannot supply a stable heat source because it is greatly affected by external disturbances. It also requires plenty of space for the installation of the heat exchanger. Since all building does not need the foundation, there are restrictions on installing the energy pile system. In addition, these systems have lower system performance than the vertical type.

The vertical type is the most used type of the GSHP system, and it has high-efficiency performance without space restrictions compared to other types. More generally, the advantages of the GSHP system with the vertical type are listed below.

- Energy-saving, carbon dioxide emission reduction effect.
- High efficiency of the heat pump by reducing the temperature difference on the secondary side as a heat source.
- Alleviation of the heat island phenomenon in the downtown during the cooling period.
- Performance improvement effect as defrost is unnecessary when using in cold climates.
- It is possible to supply heating, cooling and hot water supply.

On the other hand, the disadvantage of the system is the expensive installation cost. Construction of the GSHP system with the vertical closed-loop requires boreholes of 80-150 m. The installation cost of the BHEs, including the drilling, accounts for 50 % of the total cost of the GSHP system. Since the GSHP system is relatively expensive compared to other heat sources such as the ASHP system, introducing the GSHP system for heating and cooling is not more widely distributed and used. Therefore, a method to reduce the initial installation cost of the GSHP system is essential for the future task for the widespread use of the system.

1.2.3. Research trend and developments of GSHP system

The concept of a heat pump was proposed by Thomson [25] to heating and cooling buildings, and the heat pump using the ground source was first patented by Zoelly [26] in the 1910s. The first reports of groundwater heat pumps were published in the 1930s [27]. For the next ninety years, each component of the GSHP system has been developed to improve performance. This chapter describes the research status of the GSHP system, and the development and future possibilities of the system are discussed.

The new BHEs type has been continuously reported to reduce the initial installation cost of the BHE, accounting for a high portion of the overall system cost. According to cost data for approximately 140 residential and commercial facilities in the United States, the cost of a ground heat exchanger occupies between 20 and 60 % of the total system cost. The recognition that ground heat exchangers are the dominant cost factor of the GSHP systems has been driving better borehole heat exchangers. Numerous attempts have been made to develop improved borehole heat exchanger configurations, including double U-tubes [28,29], triple U-tubes [30], a spiral tube [31–33] and coaxial heat exchangers [34–36]. In recent years, an "oval" design of the U-tube has been studied to reduce borehole thermal resistance [37,38]. However, the installation time and the cost could be higher than a single U-tube.

The new development trend is related to near-zero energy buildings (NZEB) [39,40] and energy flexible buildings [41–43]. The NZEBs are defined as a building with very high energy performance. The low amount of energy required in these buildings is covered to a very significant extent by energy from renewable sources produced on-site or nearby. The energy flexibility of a building is the ability to manage its energy demand and generation according to local climate conditions. The building can also support the electricity system based on the requirements of the surrounding grids. The GSHP systems are highly desirable for the NZEBs and energy flexible buildings. The generated electricity from photovoltaic panels can readily be consumed with the GSHP system for a very high-efficiency heating/cooling on-site. With the development of the GSHP system and photovoltaic thermal (PVT) system, the GSHP combining PVT (GSHP-PVT) systems have proposed to solve features of thermal imbalance for geothermal energy and intermittency for photovoltaic system in the building energy field. There is a lot of research focused on the design and optimization of GSHP-PVT systems in recent years. Abu-Rumman et al. [44] mentioned that the GSHP-PVT hybrid system can improve 9.5 % of the electricity production efficiency and 30% of the average coefficient of performance (COP) of the heat pump. Sakellariou et al. [45] carried out the numerical simulation to clarify the energy performance of GSHP-PVT. The optimal operation strategies are also proposed under different operation modes for the GSHP-PVT system [46–48].

While a lot of research on the GSHP system has been in progress, the essential research of the system is to evaluate the system performance and design the BHEs, based on the heat exchange rate between the heat exchanger and the soil. The heat exchange rate depends on the thermal property of the soils. In the 1980s, when research on the GSHP system was actively proceeding, the researchers recognized that understanding the thermal properties of soils is significant to design the system. Mogensen proposed the thermal response test (TRT) to determine the thermal property of the soils. After that time, many researchers proposed the TRT analysis method. The research on the estimation of the groundwater flow has been started in recent years. Many studies have reported on the advection effect and the performance of the GSHP systems [49–53]. Although the effect of groundwater flow on the performance of the GSHP system has been reported, there are few studies estimating the intensity of the groundwater flow in the field. To design a more accurate GSHP system, it is necessary to estimate the groundwater velocity.

1.3. Objectives and scope of the thesis

The design tool reflecting the groundwater flow is needed to predict the performance of the GSHP system and make an accurate introduction design. In particular, many areas in Japan have rapid groundwater flows due to their geographical characteristics. However, most of the GSHP system is not designed by reflecting the effect of the groundwater flow, and the BHEs are installed by estimating the heat exchange heat of 5-7 kW for the borehole depth of 80-100 m.

The main objective of this research is to propose a new thermal response test analysis estimating partial groundwater flow and to develop its application for ground source heat pump system design. The proposed approaches enable more accurate performance predictions of the GSHP systems during a long-term operating system. The initial installation cost of the GSHP system can also reduce by suggesting appropriate borehole sizing based on the thermal properties in multi-layer of the ground. The application tool is developed to predict the energy consumption of the building, based on the GSHP system being able to calculate multi-borehole configuration under the conditions with the multi-layer with groundwater flows. The tool can combine with other components to evaluate zero energy building.

1.4. Outline of the thesis

This thesis consists of seven chapters, and followings are brief description on each chapter. Fig 1.9 describes the overall flow chart of this thesis.

Chapter 1 describes the causes of the environmental problems, and their response on which many countries make an effort to solve. In terms of these global issues, the contribution of the GSHP system is reported to reduce GHG emissions and energy consumptions. In addition, the general background concerning the GSHP system following contents are introduced: kinds of type, advantages and disadvantages, Research trend and developments.

Chapter 2 provides theories regarding analysis methodology to predict the ground temperature and the circulating water temperature to the heat flux. Also, the historical review of thermal response test is reported.

Chapter 3 suggests a practical TRT method to determine the groundwater velocity and the

effective thermal conductivity simultaneously. The approximate formula of an equivalent single pipe is proposed to calculate the temperature change of the circulating fluid under the borehole backfilled into the permeable material. The radius of the equivalent single pipe is determined by the groundwater velocity, based on the numerical approach results. The approach is useful to estimate the design parameter in on-site TRT. The groundwater velocity and the effective thermal conductivity are determined by the iteration parameter estimation method. The method provides the best-fit parameters through the minimum root mean square error (RMSE) between the TRT data and calculated results.

Chapter 4 proposes a novel TRT analytical method to estimate the groundwater velocity and the effective thermal conductivity in a multi-layer. The new idea called 'relaxation time of temperature (RTT)' is introduced; the moment when the temperature in the borehole recovers a certain level compared to that at stopping the heating. The RTT has grouped the ground into vertical zones with similar thermal properties. Finally, the temperature increments of the circulating fluid based on the determined zones and the heat exchange rates are calculated according to the groundwater velocities, using the MLS theory. These results are compared with the measured temperature data from each zone, and its best-fitting value yields the groundwater velocities.

Chapter 5 verifies the effectiveness of the multi-layer TRT analysis method and proposes the method to reduce the initial cost of the GSHP system by determining the appropriate borehole size. The required borehole number is determined by the system performance in the 30th year after operating the GSHP system, based on the parameters estimated by the TRT analysis methods. The initial and operating costs are calculated to analyze the life cycle cost (LCC) of the GSHP system. The return of investment (ROI) period is analyzed by comparing it with an air source heat pump system.

Chapter 6 introduces the application of ground source heat pump system for nearly-zero energy building. The application tool is developed to predict the energy consumption of the building, based on the GSHP system being able to calculate multi-borehole configuration under the conditions with the multi-layer with groundwater flows.

Chapter 7 summarizes general conclusions of this thesis and development toward zero carbon society.

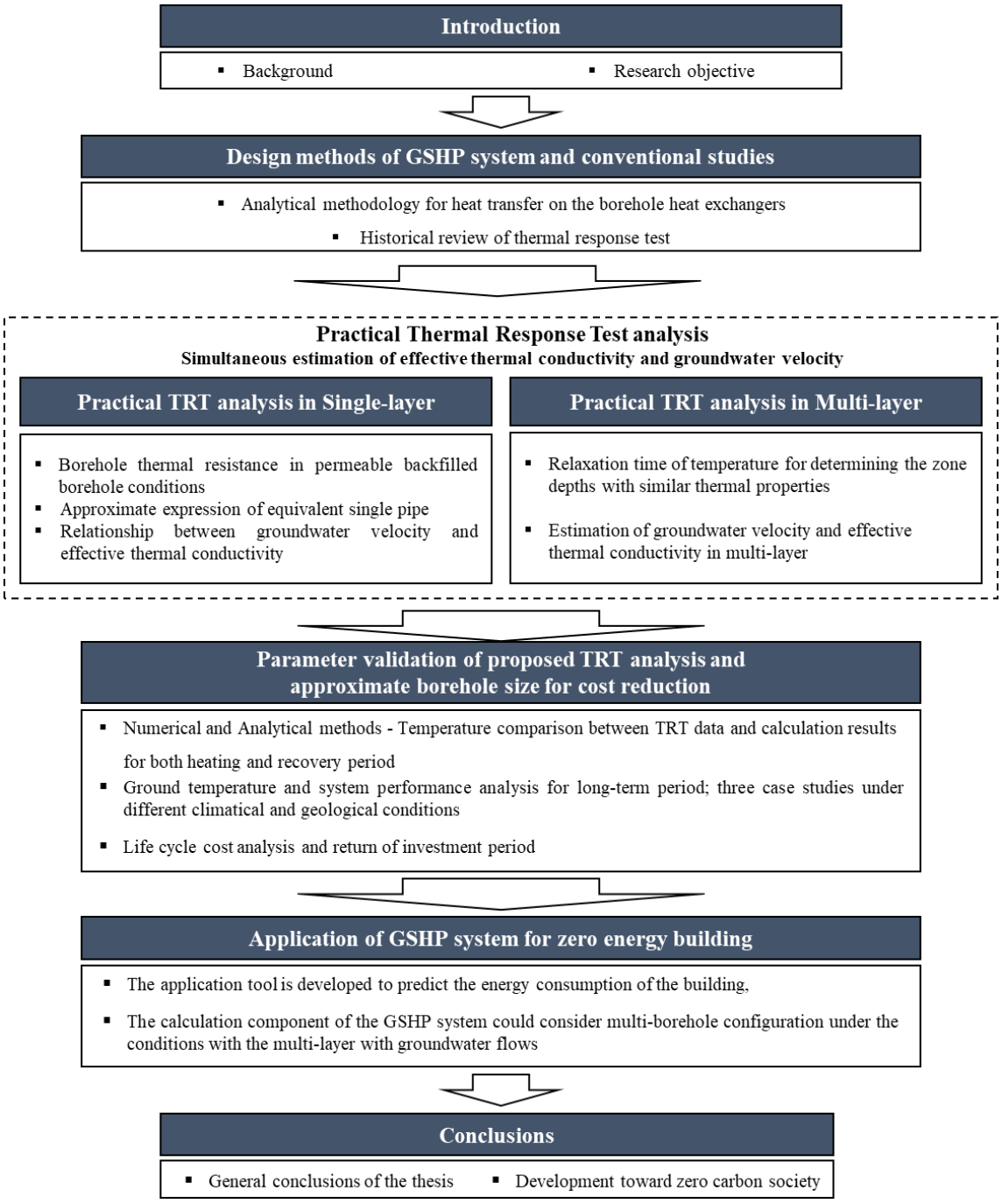

Fig. 1. 9 Overall flow chart of this thesis

1.5. Reference

[1] EEA, Climate change, impacts and vulnerability in Europe 2016, 2017. https://www.eea.europa.eu/publications/climate-change-adaptation-and-disaster.

[2] P. Nejat, F. Jomehzadeh, M.M. Taheri, M. Gohari, M.Z. Muhd, A global review of energy consumption, CO2 emissions and policy in the residential sector (with an overview of the top ten CO2 emitting countries), Renew. Sustain. Energy Rev. 43 (2015) 843–862. doi:10.1016/j.rser.2014.11.066.

[3] US Energy Information Administration, Int. Energy Outlook 2019. (n.d.).

[4] Z. Liu, W. Xu, C. Qian, X. Chen, G. Jin, Investigation on the feasibility and performance of ground source heat pump (GSHP) in three cities in cold climate zone, China, Renew. Energy. 84 (2015) 89–96. doi:10.1016/j.renene.2015.06.019.

[5] B. Rosselló-Batle, A. Moià, A. Cladera, V. Martínez, Energy use, CO2 emissions and waste throughout the life cycle of a sample of hotels in the Balearic Islands, Energy Build. 42 (2010) 547–558. doi:10.1016/j.enbuild.2009.10.024.

[6] M. Melikoglu, Current status and future of ocean energy sources: A global review, Ocean Eng. 148 (2018) 563–573. doi:10.1016/j.oceaneng.2017.11.045.

[7] F. Díaz-González, A. Sumper, O. Gomis-Bellmunt, R. Villafáfila-Robles, A review of energy storage technologies for wind power applications, Renew. Sustain. Energy Rev. 16 (2012) 2154–2171. doi:10.1016/j.rser.2012.01.029.

[8] M.S. Buker, S.B. Riffat, Building integrated solar thermal collectors - A review, Renew. Sustain. Energy Rev. 51 (2015) 327–346. doi:10.1016/j.rser.2015.06.009.

[9] A.K. Shukla, K. Sudhakar, P. Baredar, A comprehensive review on design of building integrated photovoltaic system, Energy Build. 128 (2016) 99–110. doi:10.1016/j.enbuild.2016.06.077.

[10] S. Maddah, M. Goodarzi, M.R. Safaei, Comparative study of the performance of air and geothermal sources of heat pumps cycle operating with various refrigerants and vapor injection, Alexandria Eng. J. (2020). doi:10.1016/j.aej.2020.07.009.

[11] A.P. Athresh, A. Al-Habaibeh, K. Parker, Innovative Approach for Heating of Buildings Using Water from a Flooded Coal Mine Through an Open Loop Based Single Shaft GSHP System, Energy Procedia. 75 (2015) 1221–1228. doi:10.1016/j.egypro.2015.07.162.

[12] A. Nguyen, P. Pasquier, D. Marcotte, Influence of groundwater flow in fractured aquifers on standing column wells performance, Geothermics. 58 (2015) 39–48.

doi:10.1016/j.geothermics.2015.08.005.

[13] J.H. Cho, Y. Nam, H.C. Kim, Performance and feasibility study of a Standing Column Well (SCW) system using a deep geothermalwell, Energies. 9 (2016) 1–13. doi:10.3390/en9020108.

[14] X. Chen, G. Zhang, J. Peng, X. Lin, T. Liu, The performance of an open-loop lake water heat pump system in south China, Appl. Therm. Eng. 26 (2006) 2255–2261. doi:10.1016/j.applthermaleng.2006.03.009.

[15] Y. Wang, K.K.L. Wong, Q.H. Liu, Y.T. Jin, J. Tu, Improvement of energy efficiency for an open-loop surface water source heat pump system via optimal design of water-intake, Energy Build. 51 (2012) 93–100. doi:10.1016/j.enbuild.2012.04.013.

[16] B. Sanner, Current status of ground source heat pumps in Europe, Proc. 9th Int. Conf. Therm. Energy Storage Futur. (2003) 695–703. http://buildingphysics.com/Futurestock 1.pdf.

[17] L. Rybach, B. Sanner, Geothermal Heat Pump Development: Trends and Achievements in Europe, 2017. doi:10.1142/9781786342324_0008.

[18] L. Rybach, B. Sanner, Ground-source heat pump systems - the European Experience, GHC Bull. (2000) 16–26. http://www.sanner-geo.de/media/art4.pdf.

[19] H. Esen, M. Inalli, M. Esen, K. Pihtili, Energy and exergy analysis of a ground-coupled heat pump system with two horizontal ground heat exchangers, Build. Environ. 42 (2007) 3606–3615. doi:10.1016/j.buildenv.2006.10.014.

[20] P.M. Congedo, G. Colangelo, G. Starace, CFD simulations of horizontal ground heat exchangers: A comparison among different configurations, Appl. Therm. Eng. 33–34 (2012) 24–32. doi:10.1016/j.applthermaleng.2011.09.005.

[21] M.J. Kim, S.R. Lee, S. Yoon, G.H. Go, Thermal performance evaluation and parametric study of a horizontal ground heat exchanger, Geothermics. 60 (2016) 134–143. doi:10.1016/j.geothermics.2015.12.009.

[22] K. Kupiec, B. Larwa, M. Gwadera, Heat transfer in horizontal ground heat exchangers, Appl. Therm. Eng. 75 (2015) 270–276. doi:10.1016/j.applthermaleng.2014.10.003.

[23] Y. Nam, H.B. Chae, Numerical simulation for the optimum design of ground source heat pump system using building foundation as horizontal heat exchanger, Energy. 73 (2014) 933–942. doi:10.1016/j.energy.2014.06.108.

[24] C.P. Jacovides, G. Mihalakakou, An underground pipe system as an energy source for cooling/heating purposes, Renew. Energy. 6 (1995) 893–900. doi:10.1016/0960-1481(95)00101-7.

[25] W. Thomson, On the Economy of the Heating or Cooling of Buildings by means of Currents of Air, Proc. Philos. Soc. Glas. III. (1853) 269–272.

[26] H. Zoelly, Ground Source Heat Pump in Swiss Patent, 59350, 1912.

[27] T.G.N. Haldane, The heat pump - an economical method of producing low-grade heat from electricity, J. Inst. Electr. Eng. 68 (1930) 666–703.

[28] S. Kumar, K. Murugesan, Optimization of geothermal interaction of a double U-tube borehole heat exchanger for space heating and cooling applications using Taguchi method and utility concept, Geothermics. 83 (2020) 101723. doi:10.1016/j.geothermics.2019.101723.

[29] G.A. Florides, P. Christodoulides, P. Pouloupatis, Single and double U-tube ground heat exchangers in multiple-layer substrates, Appl. Energy. 102 (2013) 364–373. doi:10.1016/j.apenergy.2012.07.035.

[30] A. Zarrella, M. De Carli, A. Galgaro, Thermal performance of two types of energy foundation pile: Helical pipe and triple U-tube, Appl. Therm. Eng. 61 (2013) 301–310. doi:10.1016/j.applthermaleng.2013.08.011.

[31] H. Li, K. Nagano, Y. Lai, A new model and solutions for a spiral heat exchanger and its experimental validation, Int. J. Heat Mass Transf. 55 (2012) 4404–4414. doi:10.1016/j.ijheatmasstransfer.2012.03.084.

[32] Jalaluddin, A. Miyara, Thermal performance and pressure drop of spiral-tube ground heat exchangers for ground-source heat pump, Appl. Therm. Eng. 90 (2015) 630–637. doi:10.1016/j.applthermaleng.2015.07.035.

[33] B. Dehghan B., Experimental and computational investigation of the spiral ground heat exchangers for ground source heat pump applications, Appl. Therm. Eng. 121 (2017) 908–921. doi:10.1016/j.applthermaleng.2017.05.002.

[34] M.S. Saadi, R. Gomri, Investigation of dynamic heat transfer process through coaxial heat exchangers in the ground, Int. J. Hydrogen Energy. 42 (2017) 18014–18027. doi:10.1016/j.ijhydene.2017.03.106.

[35] R.A. Beier, J. Acuña, P. Mogensen, B. Palm, Borehole resistance and vertical temperature profiles in coaxial borehole heat exchangers, Appl. Energy. 102 (2013) 665–675. doi:10.1016/j.apenergy.2012.08.007.

[36] S. Morchio, M. Fossa, On the ground thermal conductivity estimation with coaxial borehole heat exchangers according to different undisturbed ground temperature profiles, Appl. Therm. Eng. 173 (2020) 115198. doi:10.1016/j.applthermaleng.2020.115198.

[37] A.A. Serageldin, Y. Sakata, T. Katsura, K. Nagano, Performance enhancement of

borehole ground source heat pump using single U-tube heat exchanger with a novel oval cross-section (SUO) and a novel spacer, Sustain. Energy Technol. Assessments. 42 (2020) 100805. doi:10.1016/j.seta.2020.100805.

[38] A.A. Serageldin, Y. Sakata, T. Katsura, K. Nagano, Thermo-hydraulic performance of the U-tube borehole heat exchanger with a novel oval cross-section: Numerical approach, Energy Convers. Manag. 177 (2018) 406–415. doi:10.1016/j.enconman.2018.09.081.

[39] R. Dufo-López, J.L. Bernal-Agustín, New methodology for the generation of hourly wind speed data applied to the optimization of stand-alone systems, Energy Procedia. 14 (2012) 1973–1978. doi:10.1016/j.egypro.2011.12.1097.

[40] L. Danza, L. Belussi, G. Guazzi, I. Meroni, F. Salamone, Durability of technologies in the keeping of ZEB's performances, Energy Procedia. 148 (2018) 138–145. doi:10.1016/j.egypro.2018.08.041.

[41] S.Ø. Jensen, A. Marszal-Pomianowska, R. Lollini, W. Pasut, A. Knotzer, P. Engelmann, A. Stafford, G. Reynders, IEA EBC Annex 67 Energy Flexible Buildings, Energy Build. 155 (2017) 25–34. doi:10.1016/j.enbuild.2017.08.044.

[42] R. Li, G. Dane, C. Finck, W. Zeiler, Are building users prepared for energy flexible buildings?—A large-scale survey in the Netherlands, Appl. Energy. 203 (2017) 623–634. doi:10.1016/j.apenergy.2017.06.067.

[43] G. Reynders, R. Amaral Lopes, A. Marszal-Pomianowska, D. Aelenei, J. Martins, D. Saelens, Energy flexible buildings: An evaluation of definitions and quantification methodologies applied to thermal storage, Energy Build. 166 (2018) 372–390. doi:10.1016/j.enbuild.2018.02.040.

[44] M. Abu-Rumman, M. Hamdan, O. Ayadi, Performance enhancement of a photovoltaic thermal (PVT) and ground-source heat pump system, Geothermics. 85 (2020) 101809. doi:10.1016/j.geothermics.2020.101809.

[45] E.I. Sakellariou, A.J. Wright, P. Axaopoulos, M.A. Oyinlola, PVT based solar assisted ground source heat pump system: Modelling approach and sensitivity analyses, Sol. Energy. 193 (2019) 37–50. doi:10.1016/j.solener.2019.09.044.

[46] L. Xia, Z. Ma, G. Kokogiannakis, S. Wang, X. Gong, A model-based optimal control strategy for ground source heat pump systems with integrated solar photovoltaic thermal collectors, Appl. Energy. 228 (2018) 1399–1412. doi:10.1016/j.apenergy.2018.07.026.

[47] L. Xia, Z. Ma, G. Kokogiannakis, Z. Wang, S. Wang, A model-based design optimization strategy for ground source heat pump systems with integrated photovoltaic

thermal collectors, Appl. Energy. 214 (2018) 178–190. doi:10.1016/j.apenergy.2018.01.067.

[48] S. Andrew Putrayudha, E.C. Kang, E. Evgueniy, Y. Libing, E.J. Lee, A study of photovoltaic/thermal (PVT)-ground source heat pump hybrid system by using fuzzy logic control, Appl. Therm. Eng. 89 (2015) 578–586. doi:10.1016/j.applthermaleng.2015.06.019.

[49] A. Angelotti, L. Alberti, I. La Licata, M. Antelmi, Energy performance and thermal impact of a Borehole Heat Exchanger in a sandy aquifer: Influence of the groundwater velocity, Energy Convers. Manag. 77 (2014) 700–708. doi:10.1016/j.enconman.2013.10.018.

[50] J.C. Choi, J. Park, S.R. Lee, Numerical evaluation of the effects of groundwater flow on borehole heat exchanger arrays, Renew. Energy. 52 (2013) 230–240. doi:10.1016/j.renene.2012.10.028.

[51] C.K. Lee, H.N. Lam, A modified multi-ground-layer model for borehole ground heat exchangers with an inhomogeneous groundwater flow, Energy. 47 (2012) 378–387. doi:10.1016/j.energy.2012.09.056.

[52] J. Hecht-Méndez, M. De Paly, M. Beck, P. Bayer, Optimization of energy extraction for vertical closed-loop geothermal systems considering groundwater flow, Energy Convers. Manag. 66 (2013) 1–10. doi:10.1016/j.enconman.2012.09.019.

[53] H. Wang, C. Qi, H. Du, J. Gu, Thermal performance of borehole heat exchanger under groundwater flow: A case study from Baoding, Energy Build. 41 (2009) 1368–1373. doi:10.1016/j.enbuild.2009.08.001.

Chapter 2.

Previous study and orientation of this study

2.1. Introduction

Ground source heat pumps connect with the borehole heat exchangers (BHE) and the distribution system. The type of the BHEs is determined by its form and use, as mentioned in Chapter 1. Among them, the GSHP system with the vertical closed-loop has been mainly used in many commercial and residential buildings owing to high efficiency and small spaces for the installation. However, the system has a high initial cost because of the cost of drilling and borehole backfilling. According to Department of Energy and Climate Change report [1], the initial cost of the BHEs of the vertical loop type accounts for 50% in the GSHP system, and the drilling cost is around 60% on the part of the BHEs shown in Fig. 2. 1. Fig 2.2 also shows the cost rate in each section of the GSHP system in countries [2–4]. Therefore, it is necessary for a solution on the proper sizing and numbers of the BHEs, based on understanding the geological thermal properties. The design of the BHEs without pre-investigation of geological thermal properties made the system increase the initial installation cost; in case of the small capacity of the BHEs needs the additional heat source system, or in case of the large capacity of the BHEs causes unnecessarily expensive.

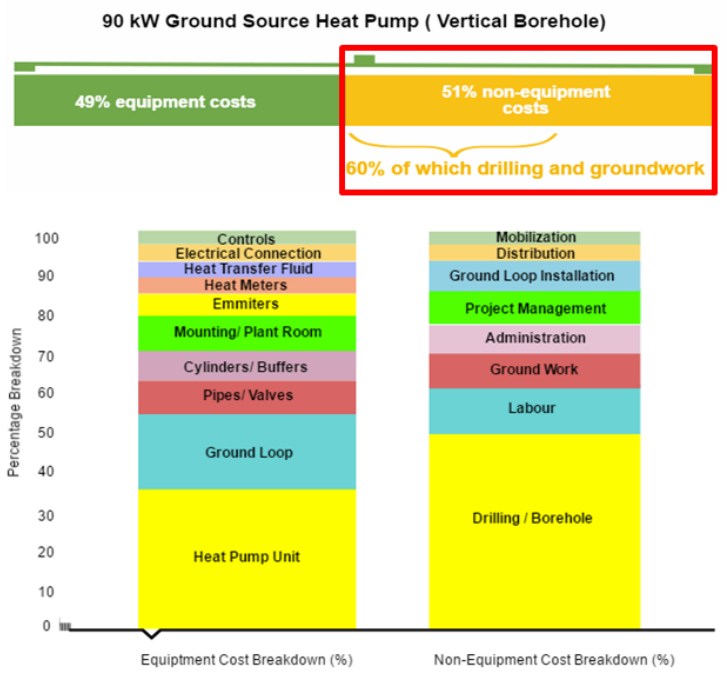

Fig. 2. 1 Cost breakdown of GSHP system (Department of Energy and Climate Change, 2016)

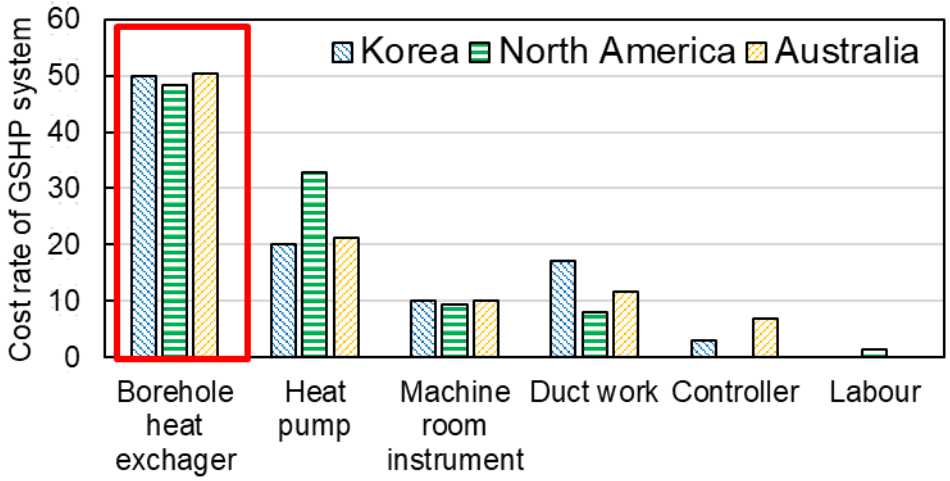

Fig. 2. 2 Cost rate in each sector of GSHP system

The essential process for the design of the BHEs is to predict the circulating fluid temperature entering to the heat pump response to the building loads. The other prediction is to calculate the accurate heat exchange rate between the BHEs and the surrounding soil, based on the thermal properties of the soil. In this process, the borehole thermal resistance should be considered with the borehole and pipe size, shank spacing between pipes and the backfill materials. This Chapter will explain the heat transfer process between the circulating fluid and the ground. The estimation methods for the design parameter are also described through in situ thermal response test (TRT). In Chapter 2.2, the analysis methodology for the heat transfer process is accounted for the heat transfer between the BHE and surrounding soil. The detailed procedures and the comparison of each model will be explained. Chapter 2.3 deals with the borehole thermal resistance between the fluid in the U-tube and the borehole wall. Finally, the historical review of the TRT is presented in Chapter 2.4.

2.2. Mathematical analysis of ground heat exchangers

2.2.1. Infinite Line source model

Infinite line source (ILS) approach is the pure conduction heat transfer process with an infinite line source continuously generating constant heat flux. Ingersoll et al. [5] modified Kelvin's line source theory to solve the heat transfer solution between the GHE and the surrounding soil.

$$T(r,t) - T_0 = \frac{q}{4\pi\lambda}\int_x^\infty \frac{1}{u} e^{-u}\, du = \frac{q}{4\pi\lambda} \cdot E_1(x), \quad \text{here } x = \frac{r^2}{4\alpha t} \tag{2-1}$$

Gautschi and Cahill [6] gave a series expansion of the exponential integral, using a Maclaurin series and Euler constant. Eq. 2-2 indicates a Maclaurin series for e^n.

$$e^n = \sum_{n=0}^{\infty} \frac{x^n}{n!} = 1 + x + \frac{x^2}{2!} + \frac{x^3}{3!} + \cdots \tag{2-2}$$

Substituting $-u$ for n in Eq. 2-2 can be expressed.

$$e^{-u} = 1 - u + \frac{u^2}{2!} - \frac{u^3}{3!} + \cdots \tag{2-3}$$

e^{-u} is applied to well function $W(u)$ in Eq. 2-4

$$\begin{aligned} W(u) &= \int_u^\infty \frac{1}{u} e^{-u}\, du = \int_u^\infty \left(1 - u + \frac{u^2}{2!} - \frac{u^3}{3!} + \cdots\right) du \\ &= \left[\ln u - u + \frac{u^2}{2 \cdot 2!} - \frac{u^3}{3 \cdot 3!} + \cdots\right]_u^\infty \\ &= \lim_{u\to\infty}\left(\ln u - e^{-u}\left(1 + \frac{1}{2} + \frac{1}{3} + \cdots\right)\right) - \left(\ln u - u + \frac{u^2}{2 \cdot 2!} - \frac{u^3}{3 \cdot 3!} + \cdots\right) \end{aligned} \tag{2-4}$$

$$\gamma = \lim_{u\to\infty}\left(1 + \frac{1}{2} + \frac{1}{3} + \cdots \frac{1}{n} - \ln u\right) = 0.5772 \tag{2-5}$$

Here, γ is Euler constant, and the exponential integral function, $W(u)$, substitutes simplified $E_1(x)$.

$$E_1(x) = -\gamma - \ln x - \sum_{n=0}^{\infty} \frac{(-1)^n x^n}{n \cdot n!} \tag{2-6}$$

Carslaw and Jaeger [6] also give a simplified form for large values of t with a maximum error in the temperature rise of 2% when $t > \frac{5r^2}{\alpha}$ [7]. Eq. 2-7 indicates the simplified ILS model from Eq. 2-1.

$$T(r,t) = \frac{q}{4\pi\lambda}\left(\ln\left(\frac{4\alpha t}{r^2}\right) - \gamma\right) + T_0 \tag{2-7}$$

The ILS model can calculate the temperature response of the imaginary borehole wall with constant heat flux based on the following assumptions.

- The ground is regarded as a homogeneous and semi-infinite medium, and its physical properties do not change.
- The effects of the ground surface are neglected.
- The initial temperature of the media is uniform.
- The heat source is an infinite line source with constant heat flux.
- The heat diffuses only in the horizontal direction, neglecting the direction of the borehole axis.

2.2.2. Infinite cylindrical source model

Infinite cylinder source approach is the pure conduction heat transfer process with an infinite cylinder source (ICS) generating heat continuously from time zero. The ICS model can be better reproduced in the borehole geometry when the thermal properties of the borehole backfill material and the soil are different [8]. The following equation describes the ICS model.

$$T(r,t) - T_0 = \frac{q}{\lambda_{\text{eff}}} \cdot G(F_o, R) \tag{2-8}$$

Here, $G(F_o, R)$ is the cylindrical source function as described by Ingersoll [5], F_o is Fourier constant ($\frac{\alpha t}{r^2}$), R is the ratio between the distance from the borehole depth and the borehole radius ($\frac{r}{L_{bh}}$).

$$G(F_o, R) = \frac{1}{\pi^2}\int_0^{\infty} f(\beta)d\beta \tag{2-9}$$

$$f(\beta) = \left(e^{-\beta^2 F_o} - 1\right)\cdot\frac{J_0(\beta)Y_1(\beta) - Y_0(\beta)J_1(\beta)}{\beta^2\left(J_1^2(\beta) + Y_1^2(\beta)\right)}d\beta \tag{2-10}$$

Eq (2-10) are Bessel functions of the first and second kinds.

2.2.3. Finite line source model

The ILS and ICS models can provide the temperature responses, and their methods are relatively simple. However, they do not consider the axial temperature gradients and the end effect at the borehole bottom side. It makes the error when the temperature response is calculated over a year. Therefore, the two-dimensional nature of ground heat transfer should be used when a more accurate prediction of the temperature response is required for a long-term period.

Eskilson [9] published the two-dimensional approach in which a finite line source (FLS) model. The FLS model considers the temperature response at a point (r, z) resulting from a constant heat flux per unit length in the finite borehole length. Fig. 2.3 shows a virtual mirror image of the finite line source, and Fig. 2.4 indicates the temperature response according to borehole depth. The analytical solution has been derived for a constant surface temperature equal to the undisturbed ground temperature.

$$T(r,z,t) = \frac{q}{4\pi\lambda_{\text{eff}}}\int_0^H \left\{\frac{\text{erfc}\left(\frac{\sqrt{r^2+(z-h)^2}}{2\sqrt{\alpha t}}\right)}{\sqrt{r^2+(z-h)^2}} - \frac{\text{erfc}\left(\frac{\sqrt{r^2+(z+h)^2}}{2\sqrt{\alpha t}}\right)}{\sqrt{r^2+(z+h)^2}}\right\}dh \tag{2-11}$$

Here,

$$\text{erfc}(x) = \frac{2}{\pi}\int_x^{\infty}\exp(-\beta^2)\,d\beta \tag{2-12}$$

Eq (2-11) can be rewritten in a dimensionless form as;

$$\Theta(R,Z,F_o) = \int_0^1 \left\{\frac{\text{erfc}\left(\frac{\sqrt{R^2+\left(Z-H'\right)^2}}{2\sqrt{F_o}}\right)}{\sqrt{R^2+\left(Z-H'\right)^2}} - \frac{\text{erfc}\left(\frac{\sqrt{R^2+\left(Z+H'\right)^2}}{2\sqrt{F_o}}\right)}{\sqrt{R^2+\left(Z+H'\right)^2}}\right\}dH' \tag{2-13}$$

Here, dimensionless variables are introduced as; $Z = z/H$, $R = r/H$, $Fo = \alpha t\ /H^2$, and $\Theta = 4\pi\lambda_{\text{eff}} t\ /q$.

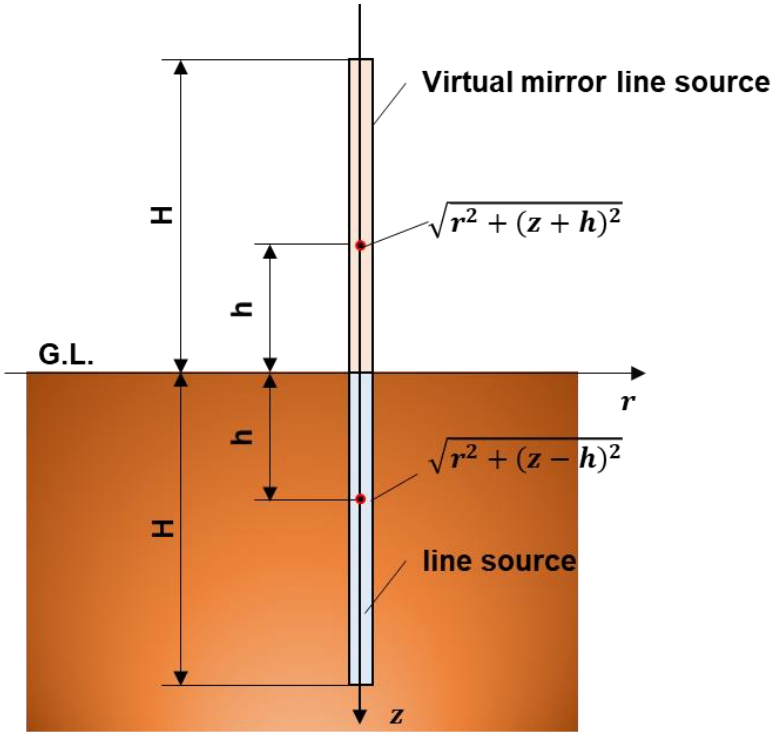

Fig. 2. 3 Virtual mirror image of the finite line source

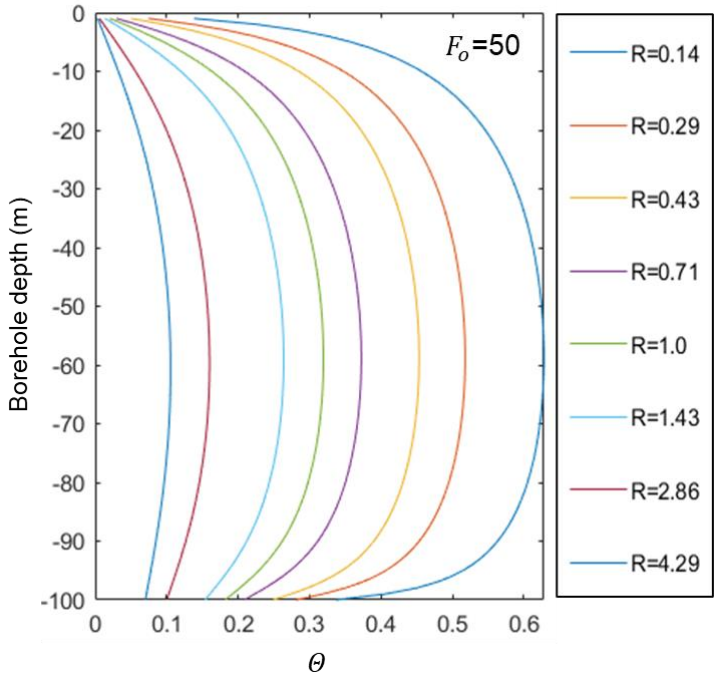

Fig. 2. 4 Temperature response according to borehole depth

2.2.4. Moving Line source model

The moving line source approach is an analytical solution of the heat transfer in the infinite porous media, considering both conductions in the fluid and solid phase and the advection by the groundwater flow. The analytical solution was introduced by Carslaw and Jaeger [8], and Diao et al. [10] modified it to apply to the subsurface environment. The heat transfer equation in the porous material is combined from the energy equation both in fluid and in solid.

- Energy equation in fluid:

$$(\rho c)_{\mathrm{w}} \frac{\partial T}{\partial t} + (\rho c)_{\mathrm{w}} \nabla \cdot (uT) = \lambda_{\mathrm{w}} \nabla^2 T \tag{2-14}$$

- Energy equation in solid:

$$(\rho c)_{\mathrm{s}} \frac{\partial T}{\partial t} = \lambda_{\mathrm{s}} \nabla^2 T \tag{2-15}$$

The effective thermal conductivity and the volumetric specific heat are weighted by the porosity of the water-saturated soil.

$$\lambda_{\mathrm{eff}} = \varepsilon \lambda_{\mathrm{w}} + (1 - \varepsilon) \lambda_{\mathrm{s}} \tag{2-16}$$

$$(\rho c)_{\mathrm{eff}} = \varepsilon (\rho c)_{w} + (1 - \varepsilon)(\rho c)_{s} \tag{2-17}$$

Eq. 2-14 and Eq. 2-15 are combined to Eq. 2-18.

$$(\rho c)_{\mathrm{eff}} \frac{\partial T}{\partial t} + (\rho c)_{\mathrm{w}} \nabla \cdot (uT) = \lambda_{\mathrm{eff}} \cdot \nabla^2 T \tag{2-18}$$

$$(\rho c)_{\mathrm{eff}} \frac{\partial T}{\partial t} + (\rho c)_{\mathrm{w}} \nabla \cdot \left(u_x \frac{\partial T}{\partial x} + u_y \frac{\partial T}{\partial x} \right) = \lambda_{\mathrm{eff}} \left(\frac{\partial^2 T}{\partial x^2} + \frac{\partial^2 T}{\partial y^2} \right) \tag{2-19}$$

Here,

$$\frac{\lambda_{\mathrm{eff}}}{\rho_{\mathrm{eff}} C_{\mathrm{p,eff}}} = \alpha \tag{2-20}$$

$$\frac{(\rho c)_{\mathrm{w}}}{(\rho c)_{\mathrm{eff}}} \cdot u = U \tag{2-22}$$

Eq. 2-19 is simplified as;

$$\frac{\partial T}{\partial t} = \alpha\left(\frac{\partial^2 T}{\partial x^2} + \frac{\partial^2 T}{\partial y^2}\right) - \left(U_x \frac{\partial T}{\partial x} + U_y \frac{\partial T}{\partial x}\right) \tag{2-23}$$

Carslaw and Jaeger [8] give the following integral formulation as a solution to Eq. 2-24.

$$\theta(x, y, \tau) = \frac{q}{4\pi\lambda_{\text{eff}}} \int_0^{\tau} \frac{1}{(\tau - \tau')} \times \exp\left[-\frac{[x - U(\tau - \tau')]^2 + y^2}{4\alpha(\tau - \tau')}\right] d\tau' \tag{2-24}$$

Here, a new parameter, η is used

$$\eta = 4\alpha(\tau - \tau')/r^2 \tag{2-25}$$

$$(\tau - \tau') = \eta r^2/4\alpha \tag{2-26}$$

Eq. 2-27 is obtained by the integration by substitution from Eq. 2-26.

$$\frac{d\eta}{d\tau'} = -4\alpha/r^2 \tag{2-27}$$

$$d\tau' = -\frac{d\eta}{4\alpha/r^2} \tag{2-28}$$

Eq. 2-29 is described by substituting Eqs. 2-25 - 2-28 to Eq. 2-24.

$$(x, y, \tau) = \frac{q}{4\pi\lambda_{\text{eff}}} \int_0^{\tau} \frac{4\alpha}{\eta r^2} \times \exp\left[-\frac{r^2 - 2xU(\tau - \tau') + U^2(\tau - \tau')^2}{4\alpha(\tau - \tau')}\right] \times -\frac{d\eta}{4\alpha/r^2} \tag{2-29}$$

$$\theta(x, y, \tau) = \frac{q}{4\pi\lambda_{\text{eff}}} \exp\left(\frac{Ux}{2\alpha}\right) \int_0^{\tau} -\frac{1}{\eta} \times \exp\left[-\frac{1}{\eta} - \frac{U^2 r^2 \eta}{16\alpha^2}\right] d\eta \tag{2-30}$$

Here, $r = \sqrt{x^2 + y^2}$

The integral boundaries are changed by the new parameter, η

$$\begin{Bmatrix} \tau \to 0 \\ 0 \to 4\alpha\tau/r^2 \end{Bmatrix} \tag{2-31}$$

The changed integral boundaries are substituted to Eq. 2-32.

$$\theta(x,y,\tau)=\frac{q}{4\pi\lambda_{\text{eff}}}\exp\left(\frac{Ux}{2\alpha}\right)\int_0^{\frac{4\alpha\tau}{r^2}}\frac{1}{\eta}\times\exp\left[-\frac{1}{\eta}-\frac{U^2r^2\eta}{16\alpha^2}\right]d\eta \quad (2\text{-}32)$$

The coordinated polar form is expressed as follows;

$$\theta(r,\varphi,\tau)=\frac{q}{4\pi\lambda_{\text{eff}}}\exp\left(\frac{Ur}{2\alpha}cos\varphi\right)\int_0^{\frac{4\alpha\tau}{r^2}}\frac{1}{\eta}\times\exp\left[-\frac{1}{\eta}-\frac{U^2r^2\eta}{16\alpha^2}\right]d\eta \quad (2\text{-}33)$$

Eq. 2-30 can be rewritten in a dimensionless form as

$$\Theta(R,\varphi,F_o)=\exp\left(\frac{R}{2}cos\varphi\right)\int_0^{\frac{4F_o}{R^2}}\frac{1}{2\eta}\times\exp\left[-\frac{1}{\eta}-\frac{R^2\eta}{16}\right]d\eta \quad (2\text{-}30)$$

Here, Θ is the non-dimensional temperature response ($=\frac{2\pi\lambda_{\text{eff}}\theta}{q}$), R is the non-dimensional radial coordinate ($=\frac{r}{L}=\frac{Ur}{\alpha}$), L is a characteristic length ($=\frac{\alpha}{U}$), F_o is the non-dimensional time ($=\frac{U^2\tau}{\alpha}$).

Fig. 2.5 shows the temperature response according to the groundwater velocity. Fig 2.6 illustrates the temperature response on the borehole wall surface according to the polar angle (φ) of groundwater flow direction. The faster groundwater velocity led to the rapid temperature converges. It was also confirmed that the temperature response differed different depending on the polar angle of groundwater flow direction.

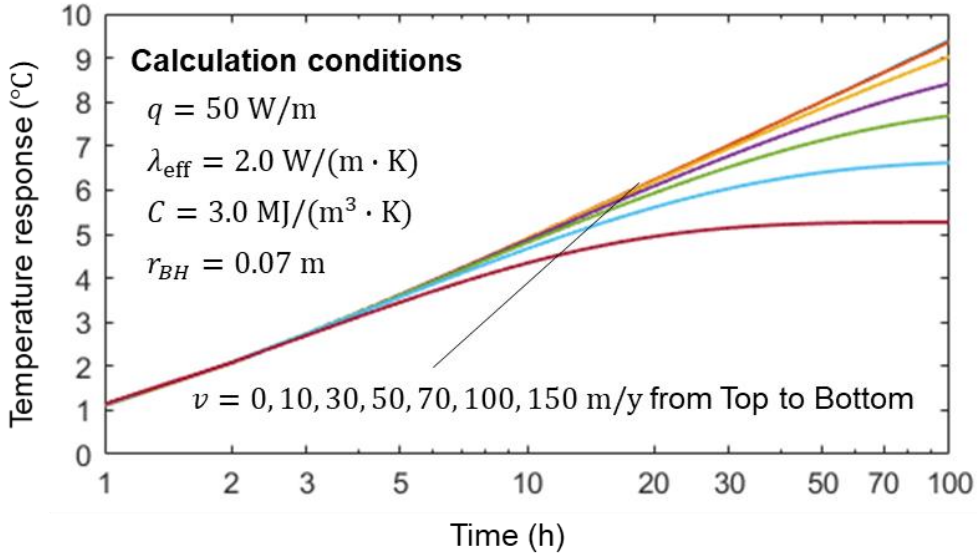

Fig. 2. 5 Temperature response according to the groundwater velocity

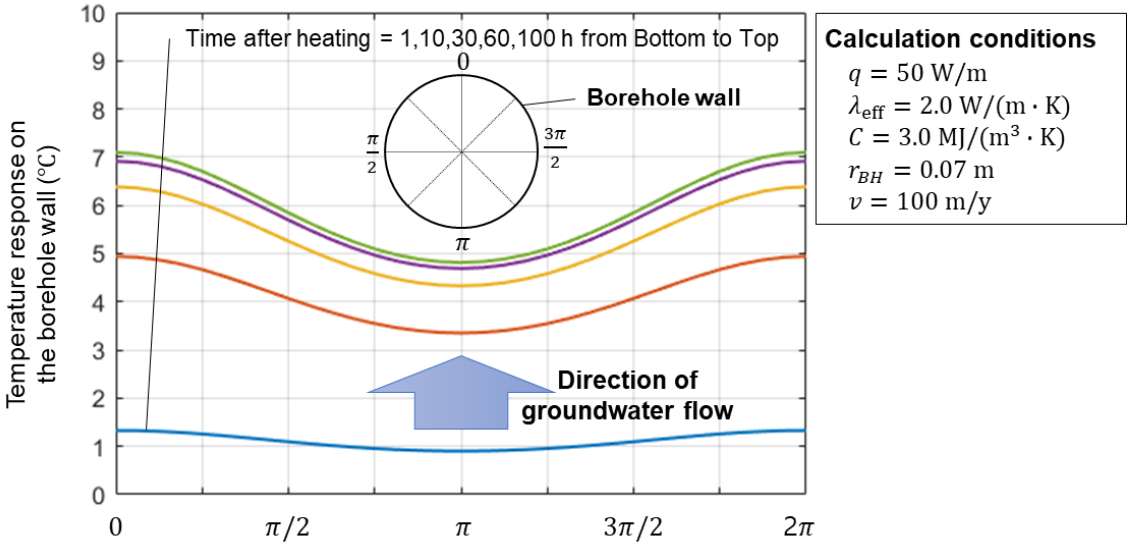

Fig. 2. 6 Temperature response on the borehole wall surface according to the polar angle of groundwater flow direction

2.2.5. Superposition principle for temperature response

In the actual operation of the GSHP system, the heat injection or ejection by the GHE varies according to the building loads. Therefore, it needs analytical approaches that can calculate the temperature response corresponding to the varying loads. The principle of the temporal superposition can provide the temperature response of the assumed borehole wall by considering the time-dependent heat flux [11–14]. The temporal responses are determined by the individual step function according to the time-variable flux. The temperature response applied to the temporal superposition of the ILS model can be expressed in Eq. 2-31. Fig. 2.7 shows the temperature response in the borehole wall according to time-dependent heat flux.

$$T_{\text{bh}}(t) - T_0 = \sum_{i=1}^{N} \frac{q_i - q_{i-1}}{4\pi\lambda_{\text{eff}}} E_1\left(\frac{r^2}{4\alpha(t_N - t_{n-1})}\right) \tag{2-31}$$

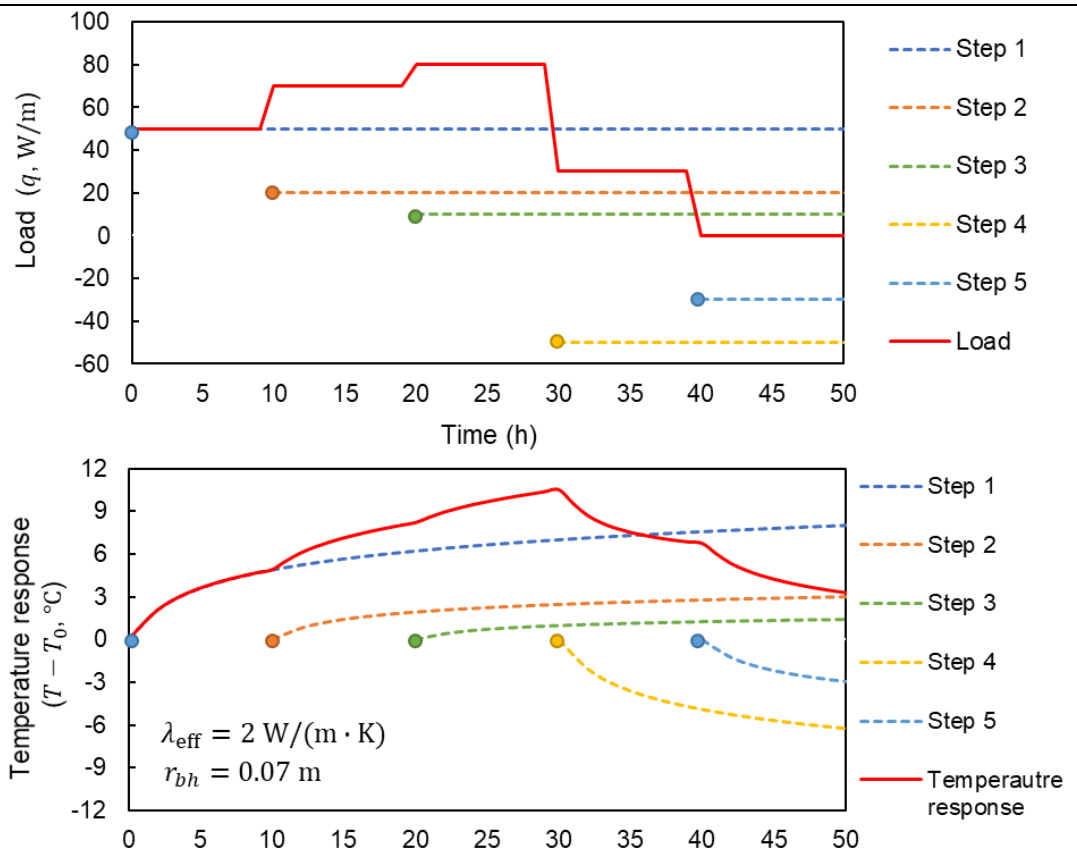

Fig. 2. 7 Temperature response according to the superimposed step load

2.3. Borehole Thermal resistance

The BHEs reject/extract heat to/from the ground. The heat transfer process is transient considering long time-scale and large-distance because the ground is regarded as an infinite medium with infinite thermal capacity. These processes were dealt with in Chapter 2.2. On the other hand, the heat transfer process in the borehole is considered short length and time scale, using thermal resistances. The heat transfer between the heat carrier fluid in the pipes of the U-tube and the borehole wall is treated in a quasi-steady condition. The borehole thermal resistance can be defined;

$$R_{\mathrm{b}} = \frac{T_{\mathrm{f}} - T_{\mathrm{b}}}{q_{\mathrm{b}}} \tag{2-32}$$

$$T_{\mathrm{f}} = \frac{T_{\mathrm{f},1} - T_{\mathrm{f},2}}{2} \tag{2-33}$$

Here, T_{b} is the mean borehole surface temperature, and q_{b} denotes the heat transfer rate per unit length of the borehole in the ground. $T_{\mathrm{f},1}$ and $T_{\mathrm{f},2}$ are the fluid temperatures in each leg of the tube.

The borehole thermal resistance is the critical performance characteristic of the GHE. The lower the thermal resistance leads to the better the performance. This Chapter deals with methods for calculating the borehole thermal resistance, which accounts for short-circuiting between the upward- and downward- flowing legs of the GHE. Also, it describes the differences between their methods.

2.3.1. Fluid to pipe wall resistance

The concept of borehole thermal resistance can be indicated as a series sum of the resistances. The total borehole resistance is calculated by the sum of the pipe resistance and grout resistance. Fig. 2.8 shows a conceptual diagram of thermal resistance in a borehole. The pipe resistance includes the convective resistance of the fluid in the pipe and the conductive resistance of the pipe. The pipe resistance is typically calculated for a single pipe and then divided by the total number of pipes:

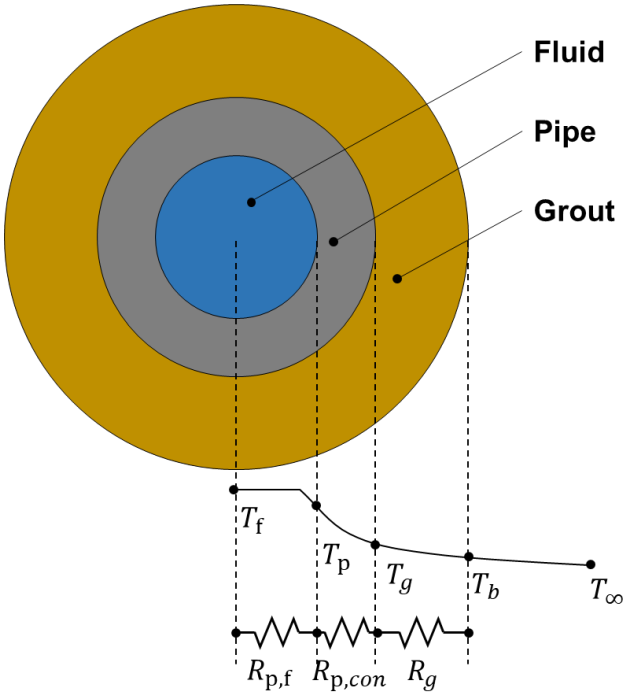

Fig. 2. 8 Conceptual diagram of thermal resistance in a borehole

$$R_b = R_g + \frac{R_p}{N} = R_g + \frac{R_{p,con} + R_{p,f}}{N} \tag{2-34}$$

Here, where N is a single (2) or a double (4) U-tube, respectively. The variable N accounts for the fact that pipe resistances are in parallel.

The conductive resistance of the pipe is derived from the steady-state heat conduction for the radial system. The heat convection of the fluid in the pipe is calculated by considering the flow rate and viscosity of the fluid, diameter and shapes of the pipe, etc.

$$R_{p,con} = \frac{1}{2\pi\lambda_p} \ln\left(\frac{r_{p,o}}{r_{p,i}}\right) \tag{2-35}$$

$$R_{p,f} = \frac{1}{2\pi r_{p,in} h_f} \tag{2-36}$$

Convective heat transfer efficiency at the inner surface of the pipe, h_f, is calculated by the Nusselt number (Nu). Nu is a function of the roughness of the surface and the flow velocity.

$$h_{\mathrm{f}} = \frac{Nu\lambda_{\mathrm{f}}}{2r_{\mathrm{p,in}}} \tag{2-37}$$

$$Nu = \frac{(F/8)(\mathrm{Re} - 1000)Pr}{1 + 12.7(F/8)^{1/2}(Pr^{2/3} - 1)} \tag{2-38}$$

The Nusselt number is valid under the conditions of the Reynolds number ($3 \times 10^3 \leq Re \leq 5 \times 10^6$) and the Prandtl number ($0.5 \leq Pr \leq 2000$).

$$Re = \frac{\rho_{\mathrm{f}} v_{\mathrm{f}} d_{\mathrm{p,in}}}{\mu_{\mathrm{f}}} = v_{\mathrm{f}} d_{\mathrm{p,in}} / \upsilon_{\mathrm{f}} \tag{2-39}$$

$$Pr = \mu_{\mathrm{f}} c_{\mathrm{f}} / \lambda_{\mathrm{f}} \tag{2-40}$$

The friction factor, F, can be obtained from Eq. 2-41

$$F = (0.79\ln(Re) - 1.64)^{-2} \tag{2-41}$$

2.3.2. Grout resistance

Many methods and approaches have been proposed for calculating grout resistance between pipes and borehole wall. These are mainly classified into three categories; equivalent radius methods, empirical formulas, and multipole method.

The equivalent radius methods are to assume two or more pipes as an equivalent pipe. The grout resistance is then calculated by considering one-dimensional radial heat conduction between the outer wall of an equivalent pipe and the borehole wall, as shown in Fig. 2.9 indicates the equivalent radius methods for calculating the grout resistance. The following Eq. 2-42 is the formula to calculate the grout resistance. The alternate equivalent radius expressions indicate in Eq. 2-43 – 45, which accounts for the effects of shank spacing [15–17].

$$R_{\mathrm{g}} = \frac{1}{2\pi\lambda_{\mathrm{g}}} \cdot \ln\left(\frac{r_{\mathrm{bh}}}{r_{\mathrm{eq}}}\right) \tag{2-42}$$

$$r_{\mathrm{eq}} = \sqrt{2} \cdot r_{\mathrm{p,out}} \tag{2-43}$$

$$r_{eq} = \sqrt{r_{p,out} \cdot s} \tag{2-44}$$

$$r_{eq} = 0.414 \cdot r_{p,out} + 0.5 \cdot x \tag{2-45}$$

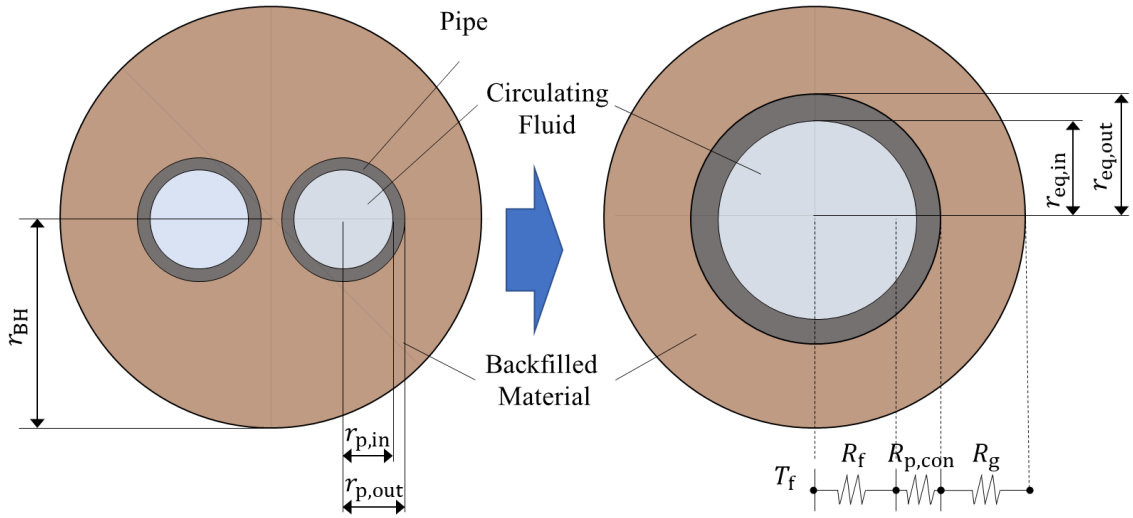

Fig. 2. 9 Equivalent radius methods for calculation of the grout resistance

The empirical formulas to calculate the borehole thermal resistance is by using empirical relationships derived from curve fitting of experimental and/or numerical data. Numerical data is derived from simulations of steady-state two-dimensional heat conduction in boreholes. One of the most popular empirical methods by Paul [18] was developed to calculate the grout thermal resistance using the well-established concept of two-dimensional conduction shape factor. The Eq. 2-44 and 2-45 indicate the form of the empirical method. Empirical coefficients (B_0 and B_1) for a shape factor of the borehole (S_b) indicate in Table 2.1.

$$R_g = \frac{1}{S_b \lambda_g} \tag{2-44}$$

$$S_b = B_0 \left(\frac{r_b}{r_{p,out}} \right)^{B_1} \tag{2-45}$$

Table 2. 1 Empirical coefficients for a shape factor of the borehole

Configuration	B_0	B_1
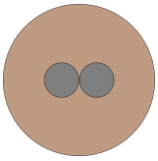	20.10	-0.9447
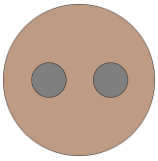	17.44	-0.6052
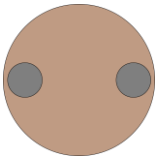	21.91	-0.3796

The counter-flow heat exchange between the pipes is important for the axial temperature variation. The temperature fields in the borehole could be represented by the thermal network, using the multipole method [19–21]. Fig. 2.10 shows the resistance network for a single U-tube. The resistance network is based on the relations between heat flows.

$$q_1 = \frac{T_{\mathrm{f1}} - T_{\mathrm{bh}}}{R_{1\mathrm{b}}} + \frac{T_{\mathrm{f1}} - T_{\mathrm{f2}}}{R_{12}} \tag{2-46}$$

$$q_2 = \frac{T_{\mathrm{f2}} - T_{\mathrm{bh}}}{R_{2\mathrm{b}}} + \frac{T_{\mathrm{f1}} - T_{\mathrm{f2}}}{R_{12}} \tag{2-47}$$

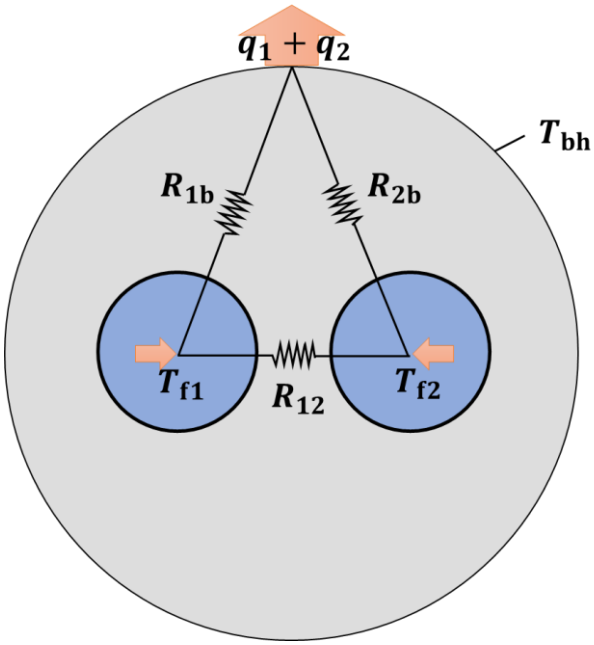

Fig. 2. 10 Resistance network for a single U-tube

Here, q_1 and q_2 are heat flux, R_{1b} and R_{2b} are thermal resistances between pipes and the borehole wall, and R_{12} is the fluid-to-fluid thermal resistance between pipes. The network determines is the total internal resistance (R_a) between the upward and downward flowing legs of the U-tube by setting the heat flows. The concept of total internal resistance is important to understand the effective borehole thermal resistance, which is the thermal resistance between the circulating fluid of the supply and return side and the average borehole wall temperature.

$$R_a = \frac{R_{12}(R_{1b} + R_{2b})}{R_{1b} + R_{2b}} \tag{2-48}$$

2.4. Thermal response test

2.4.1. Guideline for the TRT and the test setup

The design of the BHEs is significant to achieve optimum operating efficiency and the minimum design cost of the GSHP system. It depends on the accurate estimation of the thermal properties of soils and the borehole thermal resistance, which are the main key factors for the design of the BHEs. In particular, the effective thermal conductivity of soils decides the heat exchange rate between the BHEs and the ground. The higher effective thermal conductivity of the soil leads to a large amount of heat exchange and the better performance of the GSHP system. Kavanaugh [22] mentioned that the 10% error of the soil thermal conductivity of the soil causes the 5% design error in the BHE and 1 % capacity error of the heat pump. Therefore, it is necessary to accurately determine the effective thermal conductivity of the soil to design the GSHP system.

Several methods have been introduced to estimate geothermal properties; soil and rock identification [23], experimental testing of drill cutting [24] and in-field probes [25]. The most common and well-used method is thermal response test (TRT) presented by Mogensen in 1983 [26]. The first mobile test equipment for TRT has also developed at Luleå Technical University in Sweden [27] and Oklahoma State University in the United States [28]. With the development of the TRT technology, the TRT has popularized figuring out the thermal properties of the soil more easily.

The regulation standardization for The TRT is necessary to guarantee the design quality of the GSHP system. The proposal for guidance on the TRT was developed by the International Energy Agency (IEA) in Annex 13 "Wells and Boreholes" and ASHRAE handbook in “Geothermal energy”. The guideline for the TRT and the test setup is as follows;

- The TRT should be carried out for 36 to 48 h at least.
- The heat injection is considered in the range of 50 to 80 W per meter. The values are the expected peak loads on the U-tubes for an actual heat pump system.
- The accuracy of temperature measured by devices is less than ±0.3 K.
- Flow rates supply to maintain a temperature difference of 3.7 to 7.0 K between the inlet and outlet pipes.
- Data should be record at interval of 10 min at least.
- All pipes located above ground are insulated to prevent an effect of disturbance.

2.4.2. Parameter identification methods

The TRT is an onsite test to continuously inject the heat to circulating fluid in U-tubes and measure their temperature changes at an inlet and outlet of the U-tube. The direct method is analyzed the average temperature measured in inlet and outlet pipes by using an infinite line source model with least-squares approximation [29]. In this method, the heat transfer in the direction of the borehole axis is neglected, including the heat flux across the surface and down the borehole floor. The process of heat conduction in the ground is simplified one-dimensionally. The average temperature of the circulating fluid in the ground loop as a function of time with a constant heat injection is calculated by Eq. 2-7 and Eq. 2-34. The temperature slope over logarithmic time results in the effective thermal conductivity of the soil (Eq 2-50). The borehole thermal resistance is also calculated in Eq 2-51.

$$T_{\mathrm{f}}(t) = \frac{q}{4\pi\lambda}\ln(t) + \frac{q}{4\pi\lambda}\left\{\ln\left(\frac{4\alpha}{r_b^2}\right) - \gamma\right\} + R_{\mathrm{b}} \cdot q + T_0 \tag{2-49}$$

$$\lambda_{\mathrm{s}} = \frac{q}{4\pi k} \tag{2-50}$$

$$R_{\mathrm{bh}} = \frac{T_{\mathrm{f}}(t) - T_0}{q} - \frac{1}{4\pi\lambda}\left\{\ln\left(\frac{4\alpha}{r_b^2}\right) - \gamma\right\} \tag{2-51}$$

The direct method has several important limitations to apply the field test. First, a linear trend is not always obvious for all temperature curves. Second, the effect of variable heat injection is ignored. It causes power outages, electrical thermal failures or other unexpected events.

The iterative algorithm parameter estimation method is widely used to identify unknown thermal properties using TRT data. Estimation procedures are usually iterative with the goal of enforcing agreement between the mathematical model and the TRT data. The parameter estimation covers some basic problems. The first problem is choosing the objective function to minimize. The second is how to minimize the objective function. A determination of the function to minimize is used by the root mean squared error (RMSE). This method can estimate the groundwater velocity and effective thermal conductivity at the same time. The amount of information under the parameter estimation procedure decides the quality and quantity of the TRT data and the mathematical model. Some studies have been used to the iterative algorithm parameter estimation method to determine the groundwater velocity and effective thermal conductivity [30–33]. They determined the design parameters from the conditions of the

minimum RMSE. The parameters are decided under 0.1 K of the RMSE between the calculated results and TRT data.

2.4.3. Historical review of thermal response test

Mogensen [26] first proposed an experimental method to determine the thermal resistance between a thermal fluid and a borehole wall in a vertical loop. A water cooler to supply constant cooling was used with a circulation pump and a thermometer. This test equals a principle of the transient needle probe used to measure the thermal conductivity of solids. The transient needle probes typically contain electrical heating and a temperature sensor inside a metal sheath of 5 to 6 mm in diameter and 100 to 500 mm in length. Mogensen expanded this method to the entire borehole as a probe and a U-tube as a "line source". Although his purpose is to determine borehole thermal resistance, Mogensen mentioned that ground thermal conductivity could be estimated. The method has been called thermal response test (TRT) and has been widely used to estimate the effective thermal conductivity and borehole thermal resistance after the development of the mobile test equipment [27, 28].

The analysis methodologies of the TRT have been validated over the past several decades [34–36]. The first practical applications were started in the 1980s and early 1990s [26]. Afterward, the possibility of utilizing the TRT as part of a field survey began to materialize in the design of the GSHP system. In 1995, portable TRT equipment was developed by Luleå Technical University, and Oklahoma State University with a private company based in Oklahoma developed the portable TRT equipment, independently [27, 28]. Both test rigs used an electric resistance heater to apply step heat pulses to the ground and estimated the ground thermal properties of the BHE at depths of 10 to 100 m, approximately. Other test equipment was also developed in the Netherlands. This equipment used a heat pump instead of an electric resistance heater to make the lower temperature inside the BHE.

The first comparison of the TRT analysis results was carried out at areas in Belgium, it showed the reproducibility of the TRT results [37]. Austin [38] validated the TRT results and analytical procedures for core-type boreholes in laboratory experiments based on the thermal conductivity of individual core samples.

Even today, the most popular TRT evaluation method is the infinite linear heat source based on heat transfer theory. In the 1950s in the United States, this calculation method was propagated for ground loop design [29]. For the first mobile tests, the thermal conductivity was determined

and then used an approximation (Eq. 2-50 and Eq. 2-51). Based on this formula, the evaluation of the TRT has been performed up to date. The line-source approach is a relatively simple evaluation method, and there is a suitable method for validating results through sequential evaluation called “stepwise evaluation”. However, the validity of the TRT results obtained with this evaluation method is highly dependent on stable test conditions and sufficient accuracy of the sensor.

Since the first proposal for the TRT analysis, many researchers have focused on the more accurate methods for estimating the thermal properties of the ground. Table 2.1 shows the research on the TRT analysis methods. The research was carried out to estimate the design parameters based on TRT results and verified their values.

Some researchers have been proposed to determine the thermal properties in the multi-layer, by using the optical fiber distributed temperature sensing (DTS) technique [39–44]. Fujii et al. [42] utilized the optical fiber DTS to measure the temperature-time profile of the circulating fluid of each layer in the U-tubes. The measured profiles were history-matched with the cylindrical source function [29]. Sakata et al. [39] also proposed the multilayer-concept TRT by using the optical fiber DTS and determined the stepwise ground thermal conductivity with the depth of each sub-layer. Their approach methods were an uncomplicated and practical use for the TRT analysis to estimate thermal properties in multi-layer. The some researches [45–50] also suggested the TRT operating time to be the minimum time that is enough to estimate the thermal properties.

Wagner et al. [51] conducted both a tank experiment and a field experiment of the TRT to determine the hydraulic conductivity in an aquifer. They set ranges of hydraulic conductivity according to the properties of the soil, such as grain size, thermal conductivity, porosity, etc. Each value of those properties was utilized to calculate the temperature of the circulating fluid based on the moving line source (MLS) model. The calculated temperature results were then compared with the TRT data. The optimal fitting result yielded the hydraulic conductivity of the soil. Verdoya et al. [33] carried out the field TRT during both periods; the heating period and after stopping the heating injection. They estimated the groundwater velocity and effective thermal conductivity by using minimum RMSE (root mean square error) between the calculated results from the MLS model and TRT data.

Signorelli et al. [49] made the three-dimensional TRT model and examined the temperature on the borehole wall affected by the groundwater flow. As a result, the effective thermal conductivity was increased over the groundwater velocities were higher than 0.1 m/day. Gehlin et al. [52] evaluated the effective thermal conductivities at fracture zones with the groundwater

flow, using the two-dimensional finite element method. Katsura et al. [53] also developed a simulation model in the multi-layer to investigate the relation between the temperature response on the borehole wall and the groundwater velocity.

Most studies determine the weight-average values of the parameters for the installed borehole length. Although the methods for estimating parameters are useful in predicting the performance of the GSHP system, they could not suggest an appropriate borehole length to reduce the initial cost of the BHEs. Although the methods have been proposed to determine the design parameters in multi-layer by using the optical distributed temperature sensor recently, there is no method to suggest the estimation method which estimates groundwater velocity and the effective thermal conductivity of the soil in multi-layer. Therefore, it is necessary for the TRT analysis method to determine the groundwater velocity and the effective thermal conductivity of the soils to reduce the initial cost and the performance prediction of the GSHP system.

Table 2. 2 Research of the TRT analysis methods

	Only conduction			Conduction and advection		Unknown parameter				
	ILS model		ICS model	MLS model						
	Single-layer	Multi-layer	Single-layer	Single-layer	Multi-layer	λ_{eff}	R_{bh}	C	λ_g	v
Reference	[54,55]					O	O			
	[56]					O				
	[57]		[57]			O	O	O		
			[58,59]			O	O		O	
		[39–42,60]				O	O			
				[32,61,62]		O	O			O
Application	Simple process	Proper design of borehole size	Consideration of the borehole thermal resistance	Consideration of both conduction and advection						

2.5. Orientation of this thesis

The many areas in Japan have many mountains mainly composed of 1000-m-class resulted from Quaternary volcanic events. The ground basements have formed soft rocks and various coarse deposits. The ground slope is also high because the distance between the interior and the sea is short, compared to other countries. These geological conditions bring about rapid groundwater flow. These conditions could be expected to improve the performance of the system and reduce the initial cost of the GSHP system. However, since methods for estimating groundwater velocity on-site are not formalized, the many cases for the design of the GSHP system have not applied to reflect the groundwater velocity as the design parameter. It causes an increase in the installation cost of the GSHP system due to overdesign and is a hindrance to the extensive diffusion of the system.

The orientation of this thesis is to propose a new thermal response test analysis estimating partial groundwater flow and to develop its application for ground source heat pump system design. In particular, this thesis proposes quantitative partial groundwater in the multi-layer and appropriate borehole size. Compared to conventional evaluations in the fixed borehole depth, the proposed method could suggest performance change according to the depth of the borehole and an appropriate borehole depth. It is able to reduce the initial installation cost of the GSHP system by providing the proper borehole depth. In addition, the application tool is developed to predict the energy consumption of the building, based on the GSHP system being able to calculate multi-borehole configuration under the conditions with the multi-layer with groundwater flows. it could be coupled with the other components, which are renewable systems.

2.6. Reference

[1] Department of Energy and Climate, Potential Cost Reductions for Ground Source Heat Pumps, 2016.

[2] D. Tanguay, Fundamental Economic Analysis of Ground Source Heat Pump Markets in North America, 12th IEA Heat Pump Conf. (2017) 1–11.

[3] K.C. Lee, J.H. Hong, H.J. Kong, A Study of Comparative Economic Evaluation for the System of Ground Source Heat Pump and District Heating and Cooling:Focusing on the Analysis of Operation Case, Korean J. Air-Conditioning Refrig. Eng. 28 (2016) 103–109. doi:10.6110/kjacr.2016.28.3.103.

[4] Q. Lu, G.A. Narsilio, G.R. Aditya, I.W. Johnston, Economic analysis of vertical ground source heat pump systems in Melbourne, Energy. 125 (2017) 107–117. doi:10.1016/j.energy.2017.02.082.

[5] L.R. Ingersoll, O.J. Zobel, A.C. Ingersoll, Heat Conduction With Engineering, Geological, and Other Applications, 1954.

[6] W. Gautschi, W. Cahill, Exponential integral and related functions. In: Abramowitz M,Stegun I, Handbook of Mathematical Functions with Formulas, Graphs, and Mathematical Tables. National Bureau of Standards, Washington, D.C., 1964.

[7] G. Hellström, Ground heat storage: Thermal analyses of duct storage systems, University of Lund, Sweden., 1991. http://search.proquest.com/docview/303983441?accountid=14357.

[8] H.S. Carslaw, J.C. Jaeger, Conduction of Heat in Solids, Phys. Today. 15 (1962) 74–76. doi:10.1063/1.3057871.

[9] P. Eskilson, Thermal Analysis of Heat Extraction Boreholes, Univ. Lund. (1987) 222.

[10] N. Diao, Q. Li, Z. Fang, Heat transfer in ground heat exchangers with groundwater advection, Int. J. Therm. Sci. 43 (2004) 1203–1211. doi:10.1016/j.ijthermalsci.2004.04.009.

[11] C. Eklöf, S. Gehlin, A Mobile Equipment for Thermal Response Test, (Master's Thesis). Lulea Univ. Technol. Sweden. (1996). https://pure.ltu.se.

[12] J. Raymond, R. Therrien, L. Gosselin, R. Lefebvre, A Review of Thermal Response Test Analysis Using Pumping Test Concepts, Ground Water. 49 (2011) 932–945. doi:10.1111/j.1745-6584.2010.00791.x.

[13] C. Yavuzturk, J.D. Spitler, Short time step response factor model for vertical ground loop heat exchangers, ASHRAE Trans. 105 (1999) 475–485.

[14] W. Choi, R. Ooka, Interpretation of disturbed data in thermal response tests using the infinite line source model and numerical parameter estimation method, Appl. Energy. 148 (2015) 476–488. doi:10.1016/j.apenergy.2015.03.097.

[15] J. Claesson, A. Dunand, Heat Extraction From the Ground By Horizontal Pipes. a Mathematical Analysis., 1983.

[16] Y. Gu, D.L. O'Neal, Development of an equivalent diameter expression for vertical U-tubes used in ground-coupled heat pumps, ASHRAE Trans. 104 (1998) 347–355.

[17] J.E. Bose, J.D. Parker, F.C. McQuiston, Design/data Manual for Closed-loop Groundcoupled Heat Pump Systems, Am. Soc. Heating, Refrig. Air-Conditioning Eng. (1985) 1985.

[18] N.D. Paul, The Effect of Grout Thermal Conductivity on Vertical Geothermal Heat Exchanger Design and Performance, 1996.

[19] A. Minaei, M. Maerefat, A new analytical model for short-term borehole heat exchanger based on thermal resistance capacity model, Energy Build. 146 (2017) 233–242. doi:10.1016/j.enbuild.2017.04.064.

[20] S. Javed, J. Spitler, Accuracy of borehole thermal resistance calculation methods for grouted single U-tube ground heat exchangers, Appl. Energy. 187 (2017) 790–806. doi:10.1016/j.apenergy.2016.11.079.

[21] R.A. Beier, M.S. Mitchell, J.D. Spitler, S. Javed, Validation of borehole heat exchanger models against multi-flow rate thermal response tests, Geothermics. 71 (2018) 55–68. doi:10.1016/j.geothermics.2017.08.006.

[22] S.P. Kavanaugh, Rafferty K., Ground Source Heat Pumps — Design of Geothermal Systems for Commercial and Institutional Building, Am. Soc. Heating, Refrig. Air-Cond. Eng. Atlanta,. (1997) 1997.

[23] J.E. Bose, Soil and rock classification for design of ground-coupled heat pump systems - field manual., Electr. Power Res. Inst. (1989) 1989.

[24] J.H. Sass., A.H. Lachenbruch, R.J. Munroe, Thermal Conductivity of Rock from Measurement on Fragments and its Application to Heat-Flow Determinations, J. Geophys. Res. 76 (1971) 3391–3401.

[25] C. A, An Approach To Determine the Thermal Conductivity And Diffusivity, Oklahoma State Univ. (1976).

[26] P. Mogensen, Fluid to Duct Wall Heat Transfer in Duct System Heat Storage. : Proceedings of the International Conference on Subsurface Heat Storage in Theory and Practice, Stock. Sweden. (1983) 652–657.

[27] C. Eklöf, S. Gehlin, TED – a mobile equipment for thermal response test, Luleå Tech. Univ. (1996).

[28] W. Austin, C. Yavuzturk, Development of an in-situ system and analysis procedure for measuring ground thermal properties, ..ASHRAE Trans. 106 (2000) 365–79.

[29] H.S. Carslaw, J.C. Jeager, Conduction of Heat in solids, Oxford University Press, Oxford, 1959.

[30] V. Wagner, P. Bayer, G. Bisch, M. Kübert, P. Blum, Hydraulic characterization of aquifers by thermal response testing: Validation by large-scale tank and field experiments, Water Resour. Res. 50 (2014) 71–85. doi:10.1002/2013wr013939.

[31] V. Wagner, P. Blum, M. Kübert, P. Bayer, Analytical approach to groundwater-influenced thermal response tests of grouted borehole heat exchangers, Geothermics. 46 (2013) 22–31. doi:10.1016/j.geothermics.2012.10.005.

[32] H. Chae, K. Nagano, Y. Sakata, T. Katsura, T. Kondo, Estimation of fast groundwater flow velocity from thermal response test results, Energy Build. 206 (2020) 109571. doi:10.1016/j.enbuild.2019.109571.

[33] M. Verdoya, G. Imitazione, P. Chiozzi, M. Orsi, E. Armadillo, C. Pasqua, Interpretation of Thermal Response Tests in Borehole Heat Exchangers Affected by Advection, World Geotherm. Congr. 2015. (2015) 19–25.

[34] A.-R. Choudhary, An approach to determine the thermal conductivity and diffusivity of a rock in situ, Oklahoma State University, 1976. http://scholar.google.com/scholar?hl=en&btnG=Search&q=intitle:An+approach+to+determine+the+thermal+conductivity+and+diffusivity+of+a+rock+in+situ#0.

[35] J. Claesson, P. Eskilson, Conductive Heat Extraction to a deep Borehole: Thermal Analysis and Dimensioning Rules, Energy. 13 (1988) 509–527.

[36] G. Hellström, Ground Heat Storage, Thermal Analy sis of Duct Storage Systems Theory, Doctoral Thesis, LTH, Lund (1991), 1-262, Lund University, 1991.

[37] B. Sanner, G. Hellström, J. Spitler, S. Gehlin, Thermal Response Test – Current Status and World-Wide Application, Proc. World Geotherm. Congr. (2005) 24–29.

[38] W.A. AUSTIN, Development of an in Situ System for Measuring Ground Thermal Properties, 1995.

[39] Y. Sakata, T. Katsura, K. Nagano, Multilayer-concept thermal response test: Measurement and analysis methodologies with a case study, Geothermics. 71 (2018) 178–186. doi:10.1016/j.geothermics.2017.09.004.

[40] Y. Sakata, T. Katsura, K. Nagano, M. Ishizuka, Field analysis of stepwise effective thermal conductivity along a borehole heat exchanger under artificial conditions of groundwater flow, Hydrology. 4 (2017) 1–12. doi:10.3390/hydrology4020021.

[41] J. Kallio, N. Leppäharju, I. Martinkauppi, M. Nousiainen, Geoenergy research and its utilization in Finland, Spec. Pap. Geol. Surv. Finl. 2011 (2011) 179–185.

[42] H. Fujii, H. Okubo, K. Nishi, R. Itoi, K. Ohyama, K. Shibata, An improved thermal response test for U-tube ground heat exchanger based on optical fiber thermometers, Geothermics. 38 (2009) 399–406. doi:10.1016/j.geothermics.2009.06.002.

[43] U. Günzel, H. Wilhelm, Estimation of the in-situ thermal resistance of a borehole using the Distributed Temperature Sensing (DTS) technique and the Temperature Recovery Method (TRM), Geothermics. 29 (2000) 689–700. doi:10.1016/S0375-6505(00)00028-6.

[44] B.M. Freifeld, S. Finsterle, T.C. Onstott, P. Toole, L.M. Pratt, Ground surface temperature reconstructions: Using in situ estimates for thermal conductivity acquired with a fiber-optic distributed thermal perturbation sensor, Geophys. Res. Lett. 35 (2008) 3–7. doi:10.1029/2008GL034762.

[45] S.J. Austin WAI, Yavuzturk C, Development of an insitu system and analysis procedure for measuring ground thermal properties, ASHRAE Trans. (2000) 1–19.

[46] P.R. Smith MD, In situ testing and thermal conductivity testing, Proc. Geoexchange Tech. Conf. Expo. Stillwater, Oklahoma State Univ. (1999).

[47] S.P. Kavanaugh, L. Xie, C. Martin, Investigation of Methods for Determining Soil and Rock Formation Thermal Properties From Short-Term Field Tests, Atlanta. (2000).

[48] S.E.A. Gehlin, G. Hellström, Comparison of four models for thermal response test evaluation, ASHRAE Trans. 109 (2003) 131–142.

[49] S. Signorelli, S. Bassetti, D. Pahud, Thomas Kohl, Numerical evaluation of thermal response tests, Geothermics. 36 (2007) 141–166.

[50] ASHRAE, ASHRAE handbook - HVAC applications, chapter 34 Geothermal energy, 2011.

[51] V. Wagner, P. Bayer, G. Bisch, M. Kubert, P. Blum, M. Kübert, P. Bayer, Hydraulic characterization of aquifers by thermal response testing: Validation by large-scale tank and field experiments, WATER Resour. Res. 46 (2014) 71–85. doi:10.1016/j.geothermics.2012.10.005.

[52] S.E.A. Gehlin, G. Hellström, 12. Influence on thermal response test by groundwater flow in vertical fractures in hard rock, Renew. Energy. 28 (2003) 2221–2238. doi:10.1016/S0960-1481(03)00128-9.

[53] T. Katsura, K. Nagano, S. Takeda, Y. Nakamura, 13. An investigation on relation beween groundwater advection and thermal response by the thermal prove method, Soc. Heating, Air-Conditioning Sanit. Eng. Japan. 112 (2006) 51–59.

[54] V. Wagner, P. Bayer, M. Kübert, P. Blum, Numerical sensitivity study of thermal response tests, Renew. Energy. 41 (2012) 245–253. doi:10.1016/j.renene.2011.11.001.

[55] M.H. Sharqawy, S.A. Said, E.M. Mokheimer, M.A. Habib, H.M. Badr, N.A. Al-Shayea, First in situ determination of the ground thermal conductivity for boreholeheat exchanger applications in Saudi Arabia, Renew. Energy. 34 (2009) 2218–2223. doi:10.1016/j.renene.2009.03.003.

[56] X. Zheng, L. Zhang, Q. Ren, H. Qian, A thermal response method of calculating a soil's thermal properties when backfill material information is unavailable, Energy Build. 56 (2013) 146–149. doi:10.1016/j.enbuild.2012.09.020.

[57] X. Yu, Y. Zhang, N. Deng, J. Wang, D. Zhang, J. Wang, Thermal response test and numerical analysis based on two models for ground-source heat pump system, Energy Build. 66 (2013) 657–666. doi:10.1016/j.enbuild.2013.07.074.

[58] S.P. Kavanaugh, Simulation and experimental verification of vertical ground-coupled heat pump systems, Oklahoma State Univ. Stillwater, USA, PhD Thesis. (1985) 194.

[59] M. Li, A.C.K. Lai, Parameter estimation of in-situ thermal response tests for borehole ground heat exchangers, Int. J. Heat Mass Transf. 55 (2012) 2615–2624. doi:10.1016/j.ijheatmasstransfer.2011.12.033.

[60] A. Mcdaniel, J. Tinjum, D.J. Hart, Y. Lin, A. Stumpf, L. Thomas, Geothermics Distributed thermal response test to analyze thermal properties in heterogeneous lithology, Geothermics. 76 (2018) 116–124. doi:10.1016/j.geothermics.2018.07.003.

[61] V. Wagner, P. Bayer, G. Bisch, M. K€ubert, P. Blum, Hydraulic characterization of aquifers by thermal response testing: Validation by large-scale tank and field experiments, WATER Resour. Res. 50 (2014) 71–85.

[62] A. Angelotti, F. Ly, A. Zille, On the applicability of the moving line source theory to thermal response test under groundwater flow : considerations from real case studies, Geotherm. Energy. (2018). doi:10.1186/s40517-018-0098-z.

Chapter 3.

Estimation of fast groundwater flow:

Simultaneous estimation of effective thermal conductivity and groundwater velocity in single-layer

3.1. Energy consumption and environmental issues

Ground source heat pump (GSHP) system has been widely used as a high-performance system for heating, cooling and supplying hot water in houses and buildings [1,2]. However, an inaccurate design of the borehole heat exchangers (BHE), one of the main elements of the GSHP system, makes the GSHP system be over/under-designed, and it results in a high initial cost of the system [3,4]. It is necessary to design the proper length and numbers of the BHE and predict the heat extraction/injection from/to the ground, based on the properties of soil.

Mogensen [5] proposed a thermal response test (TRT) to examine the thermal properties of soil; mainly an effective thermal conductivity of the soil and a borehole thermal resistance. The TRT is conducted by continuously heating a circulating fluid in the U-tube and measuring the temperature variation at an inlet and an outlet of U-tubes over time. These temperature data are usually analyzed by the infinite line source (ILS) model with the least-square method [6]. The method is useful in urbanized cities or flat plains where the ground mainly consists of consolidated rocks with relatively low permeability and slow groundwater flow [7]. However, the analysis approach is not valid in some specific areas with steep ground slopes and high permeable aquifers, such as valleys, hills and alluvial fans. The reason is that the ILS model considers only conduction heat transfer. In these areas, the TRT analysis results analyzed by the conventional method results in high effective thermal conductivity [8–11]. Chiasson et al. [8] mentioned that the high values cause the BHEs to be over/under-designed. Therefore, the BHEs should be designed by considering the groundwater velocity as well as the effective thermal conductivity. Also, it is needed for the analysis method to simultaneously determine the groundwater velocity and the effective thermal conductivity from the TRT data.

Table 1 describes the three field measurement methods that are mainly used to estimate groundwater velocity. One of the methods is an observation-well method in which the groundwater velocity is estimated as a product of hydraulic conductivity and hydraulic gradient observed from three wells. Although this method has been frequently used in practice, the hydraulic conductivity is sensitively variable in several orders of magnitude according to porosity at each depth in any location. In other ways, the groundwater tracer method is utilized to measures the groundwater velocity using the groundwater tracer, which is an ionized substance, water temperature and solid particles. However, those direct measurement methods in the borehole do not necessarily agree with the actual velocities around the borehole due to casing and mud cake

effects and are relatively expensive to use. The field measurement methods also have a high measurement range of the groundwater velocity.

Table 3. 1 Filed measurement methods for estimation of groundwater velocity

Classification	Methods (Instrument)	Measurement range
Observation-well method	hydraulic conductivity and hydraulic gradient (Darcy's law)	3.2×10^{-6} to 5.2×10^{-5} m/s, (10 to 1640 m/y)
Groundwater tracer	To trace the electrical conductivity of the water containing the tracer (Ionized substances, water temperature, solid particles)	4.6×10^{-6} to 1.0×10^{-5} m/s, (150 to 1000 m/y)
Flowmeter	Colloidal Borescope (Laser Beam and Camera sensors)	$v \geq 1.2 \times 10^{-2}$m/s, ($v \geq$ 378,400 m/y)
	Horizontal heat pulse flowmeter (Heater and thermistors)	7.5×10^{-4} to 6.6×10^{-2} m/s, (23,600 to 2,082,400 m/y)
	Groundwater acoustic doppler velocimeter (Ultrasonic indicator)	1×10^{-4} to 2.4 m/s, (3150 to 75,686,400 m/y)

The numerical simulation approaches have been used to mimic the TRT and calculate the temperature change of circulating fluid under the ground conditions with advection effect. Signorelli et al. [7] made the three-dimensional TRT model and examined the temperature on the borehole wall affected by the groundwater flow. As a result, the effective thermal conductivity was increased over the groundwater velocities were higher than 0.1 m/day. Gehlin et al. [12] evaluated the effective thermal conductivities at fracture zones with the groundwater flow, using the two-dimensional finite element method. Katsura et al. [13] also developed a simulation model in the multi-layer to investigate the relation between the temperature response on the borehole wall and the groundwater velocity. However, these numerical approaches required a high cost, technique, time and effort. Furthermore, it is difficult to estimate the thermal properties of the ground, by utilizing the measured data from the TRT in the test site.

As an alternative to the numerical methods, moving line source (MLS) theory was introduced by Carslaw and Jaeger [6], and Diao et al. [14] modified the theory to apply to the subsurface environment. Wagner et al. [15,16] conducted both the field TRT and a laboratory experiment, and the MLS model was applied to estimate thermal properties of the ground. They utilized the hydrogeological characterization of the penetrated subsurface and presented the relationship between the effective thermal conductivity and the groundwater velocity. Verdoya et al. [17] carried out the field TRT during both periods; the heating period and after stopping the heating injection. They estimated the groundwater velocity and effective thermal conductivity by using minimum RMSE (root mean square error) between the calculated results from the MLS model and TRT data. Although they provided the TRT analysis method to be able to estimate the groundwater velocity and the effective thermal conductivity by using the MLS model, the condition of the ground velocity was less than 100 m/y. Above all things, there is no report which is the TRT results analyzing the rapid groundwater flow over 100 m/y. It is unclear that the MLS model is useful to estimate the effective thermal conductivity and the groundwater velocity in the condition with the rapid groundwater flow. It is necessary for a positivistic case study to carry out the TRT analysis utilizing the MLS model for simultaneous estimation of the groundwater velocity and effective thermal conductivity in conditions over 100 m/y of the groundwater velocity.

This study suggests a practical TRT method to determine the groundwater velocity and the effective thermal conductivity simultaneously. The MLS model is verified for application of the TRT analysis under conditions over 100 m/y of groundwater velocity. The TRT is carried out in Kazuno City, Japan, which is an alluvial gravel deposit. The geological conditions in the test site mainly consist of sandy gravel, which is a porous material with high permeability. This study proposed the approximate formula of an equivalent single pipe to calculate the temperature change of the circulating fluid under the borehole backfilled into the permeable material. The radius of the equivalent single pipe is determined by the groundwater velocity, based on the numerical approach results. The temperature change of the circulating fluid is calculated by the MLS model with the equivalent single pipe. The groundwater velocity and the effective thermal conductivity are determined by the iteration parameter estimation method. The method provides the best-fit parameters through the minimum root mean square error (RMSE) between the TRT data and calculated results.

3.2. Field experiment

3.2.1. Site descriptions

The test site was in Kazuno City (40°19'N and 140°78'E), Akita Prefecture, Japan, shown in Fig 3.1. Akita Prefecture is located in East Japan of Honshu Island, which is the main island in Japan. The region has many mountains mainly composed of 1000-m-class resulted from Quaternary volcanic events. The primary basement consisted of soft rocks and various coarse deposits, and total precipitation is about 1700 mm/y. These conditions made the region high slopes and fast-flowing rivers along the valleys. Fig 3.1 (c) illustrates the geological cross-section in Kazuno City [18]. Kazuno City has formed to be alluvial gravel deposits over 100 m surround with the steep-slope valleys and the Yoneshiro river. These geological and topographical conditions provide reasonable assumptions in which the groundwater flows rapidly in the test site.

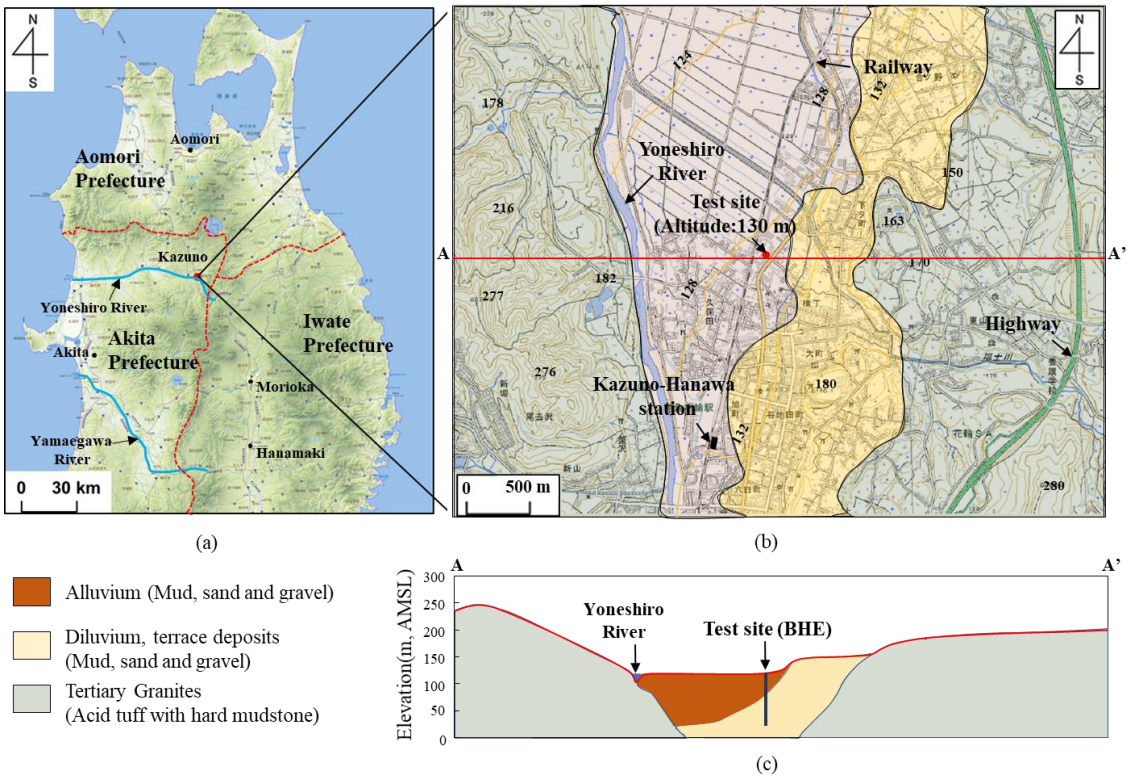

Fig. 3. 1 Location of the test site: (a) the regional and local maps in East Japan, (b) the test site in Kazuno City, and (c) geological cross-section

Fig 3.2 (a) describes a geological section of the test site. The ground of test site mainly composed of gravel, gravelly sand and sandy gravel. The thickness-weighted averages of the thermal conductivity, volumetric heat capacity for the saturated soils were estimated to be $2.4\ \mathrm{W/(m \cdot K)}$ and $3.0 \times 10^6\ \mathrm{J/(m^3 \cdot K)}$, respectively [19,20]. Fig 3.2 (b) indicates the vertical temperature distribution before the TRT is carried out. The undisturbed ground temperature was constant to be 12.3 below 10 m of G.L. Fig. 3.2 (c) shows a ground plan of the test site. Four BHEs were connected to the GSHP system to cooling and heating for the three-floor building and were installed at intervals of 4 m. The TRT was conducted marked No. 3.

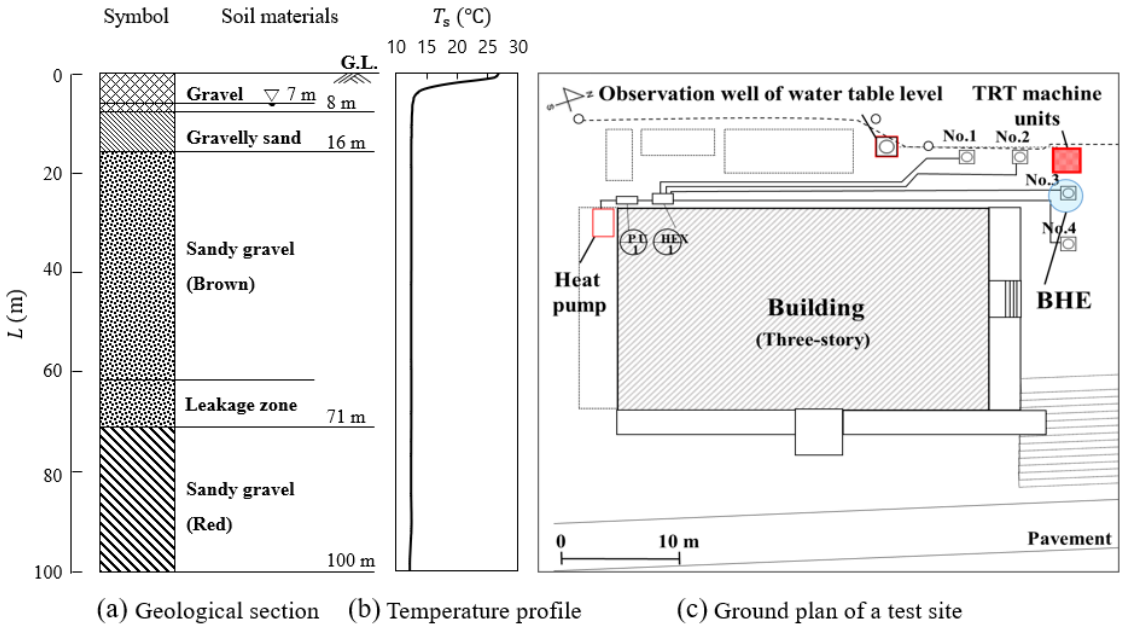

Fig. 3. 2 Geological section and ground plan of the test site: (a) geological section at a test site, (b) vertical ground temperature profile, and (c) ground plan of a test site

Fig 3.3 indicates the meteorologic observation data such as the water table level, the groundwater temperature, the precipitation, and the outdoor temperature. The observation data were measured at 10-minute intervals for three months. During the measuring period, the average, maximum and minimum temperatures of the outdoor temperature were 20.4 ℃, 28.1 ℃and 14.2 ℃, respectively. The water table level was in a range of 7.7 to 6.5 m of G.L., and it was affected by precipitation. The groundwater temperature was about 12.3°C, and it is the same value as the undistributed ground temperature.

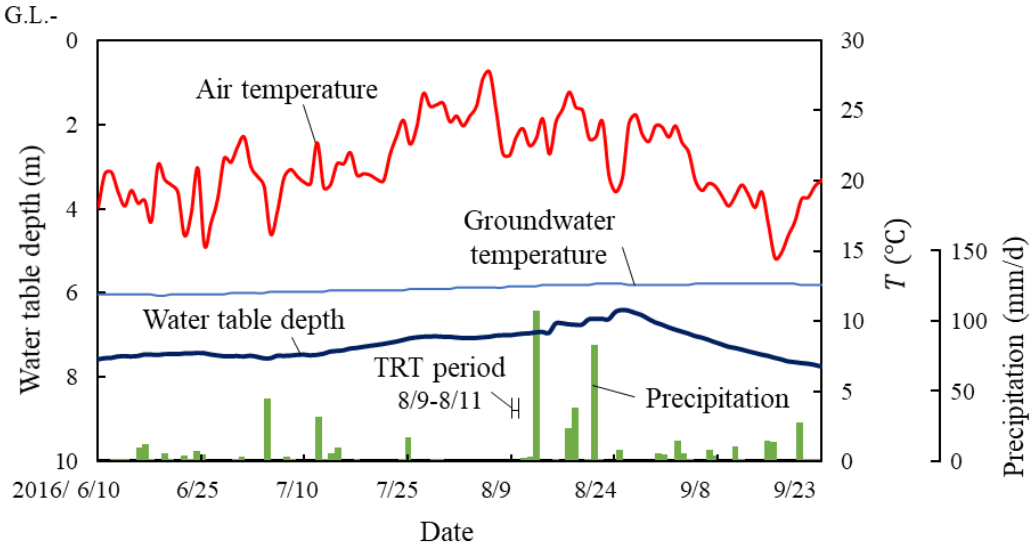

Fig. 3. 3 Observation data of the water table depth, the precipitation, and groundwater and air temperatures

3.2.2. Application of thermal response test

Fig 3.4 describes the schematic of the TRT machine units and the BHE, and Fig 3.5 indicates a figure of the in-situ TRT. The TRT equipment consisted of an electric heater, a circulating pump, a flow meter, a data logger and temperature sensors. Each equipment monitored the data at an interval of one minute, and its specifications are shown in Table 3.2. The depth and diameter of the BHE were 100 m and 146 mm, respectively. The double U-tube made of high-density polyethylene was inserted into the borehole without spacers. The inner and outer diameters of the U-tube were 25 and 32 mm, respectively. The borehole backfill material was silica sand, and it was filled in the borehole from the ground surface [21–23]. The external pipes on the ground surface were covered with the thermal-insulated material to minimize heat loss.

The TRT was carried out from the 9th to the 11th of August, 2016. During the test period, the maximum and minimum outdoor temperatures were 26.4°C and 17.7°C, respectively. The TRT machine supplied the constant heat injection of 6 kW and maintained the water flow rate of 20 L/m. TRT was performed for 60 hours while measuring the inlet and outlet temperature of the U-Tubet.

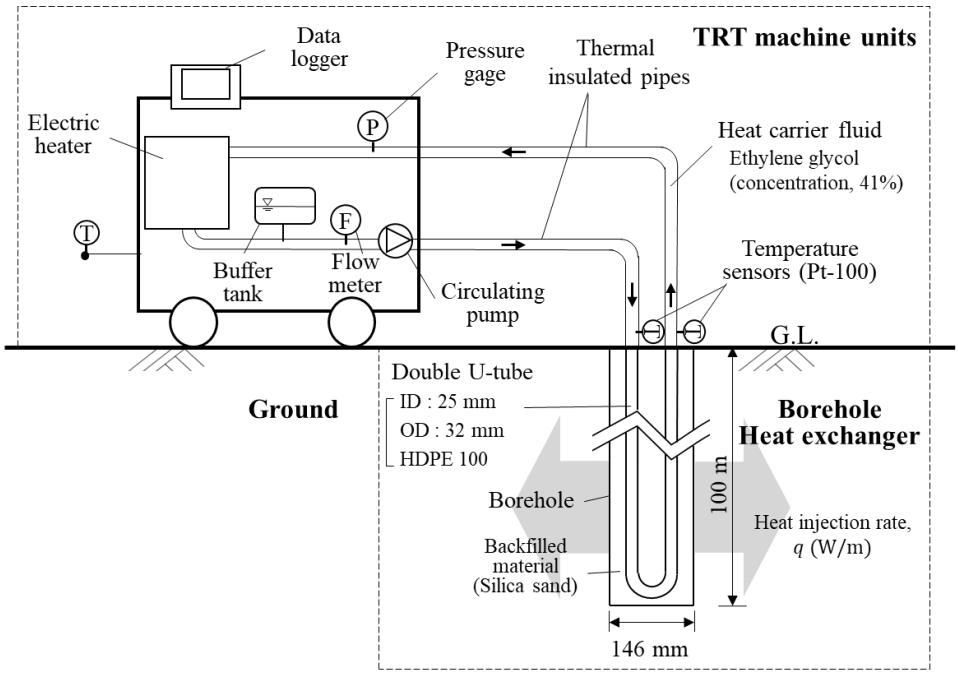

Fig. 3. 4 Schematic of the TRT machine units and the BHE

Fig. 3. 5 Figure of the TRT machine units and the BHE

Table 3. 2 Specification of TRT machine units

Unit	Specification
Electric heater	Single phase AC 200 V Maximum output power: 6 kW
Circulating pump	Single phase AC 200 V Electric power consumption: 260 W
Flow meter	Range of the flow velocity: 0.1 to 10 m/s Fluid temperature: -10 to 130 °C Electric power consumption: 12 W
Pt-100 sensor	Measured range: -30 to 200 °C Error range: $\pm 0.15+0.002 \cdot T$

3.3. Analysis methodology

3.3.1. Description of moving line source model

The moving line source model is an analytical solution of the heat transfer in the infinite porous media, considering the conduction in the fluid and solid phase and the advection by the groundwater flow. The analytical solution is driven under the following assumptions: 1) The ground is regarded as a homogeneous and semi-infinite medium, and its physical properties do not change with temperature. 2) The effects of the ground surface are neglected. 3) The initial temperature, T_0, of the media is uniform. 4) The heat source is an infinite line source with constant heat flux. Under the conditions, the time-dependent temperature responses are calculated in the coordinate system (r, φ), and the temperature response in the medium, $\theta = T - T_0$, can be obtained by means of the Green's function method in Eq (3).

$$\theta(r,\varphi,t) = \frac{q}{4\pi\lambda_{\text{eff}}} \exp\left(\frac{vr}{4\alpha_{\text{eff}}} cos\varphi\right) \int_0^{\frac{r^2}{4\alpha_S t}} \frac{1}{\beta} \exp\left(-\frac{1}{\beta} - \frac{v^2 r^2 \beta}{16\alpha_{\text{eff}}^2}\right) d\beta \tag{3-1}$$

The mean circulating fluid temperature is obtained by the borehole thermal resistance and the temperature response when the r is assigned to be the borehole radius, r_b.

$$T_{\text{f}}(t) = \frac{1}{2\pi} \int_0^{2\pi} \theta(r_{\text{b}}, \varphi, t) d\varphi + R_{\text{b}} q + T_0 \tag{3-2}$$

On the other hand, when the Darcy velocity, v, is zero, Eq. 3-2 is simplified to be Eq. 3-3, which is the ILS model. The apparent effective thermal conductivity is calculated with the temperature gradient, k, as a result of a linear equation with the logarithm of time. The apparent effective thermal conductivity is calculated in Eq. 3-4 [6].

$$T_{\text{f}}(t) = \frac{q}{4\pi\lambda_{\text{eff}}} \ln(t) + \frac{q}{4\pi\lambda_{\text{eff}}} \left\{ \ln\left(\frac{4\alpha_{eff}}{r_b^2}\right) - \gamma \right\} + R_{\text{b}} \cdot q + T_0 \tag{3-3}$$

$$\lambda_{\text{eff}} = \frac{q}{4\pi k} \tag{3-4}$$

3.3.2. Borehole thermal resistance with groundwater flow

A borehole backfill material is generally classified into three types; non-permeable, very low permeable, permeable material. There are guidelines for backfilling the borehole in European countries (Germany, Switzerland, Austria) and South Korea [24] after inserting the U-tubes. They used the non-permeable or the very low permeable material to prevent groundwater contamination. However, some countries such as Japan [25] and China have no restrictions on the guideline of the backfill material. Javadi et al. [26] investigated statistical data on which the backfill materials were used in the world, and they have summarized the results in Fig 3.6 and Table 3.2. In Japan, the BHEs usually consisted of the single/double U-tubes without spacers and the permeability materials such as silica sand for grouting [21–23,26]. The silica sand was inserted into the borehole from a ground surface up toward the bottom side of the borehole. Approximately, the material is filled in the upper side of the borehole until 3-5 m of GL. The surrounding soil then refills the borehole by soil pressure, and the pipes without spacers are closed to the borehole center. This series of procedures result in the different borehole thermal resistance between conditions of the permeable material and nonpermeable material. The previous studies [26–28] have suggested the borehole thermal resistance considering only conduction heat transfer regardless of the intensity of groundwater flow. Whereas, the borehole thermal resistance in the borehole condition backfilled with permeable material depends on both the thermal conductivity and the groundwater velocity. therefore, it is necessary to present the borehole thermal resistance considering both the thermal conductivity of the backfill material and groundwater velocity.

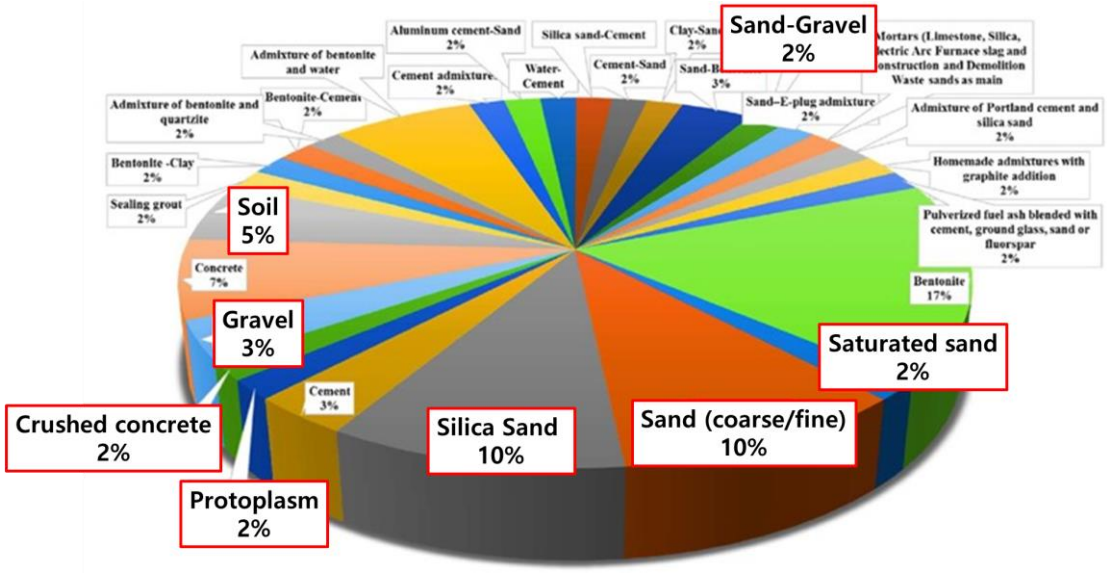

Fig. 3. 6 Usage breakdown of mixed and pure backfill materials in GHSs from 2010 to 2018 [26]

Table 3.2. Proportion of backfill materials

Type	Material (%)	Proportion (%)
Non permeable material	Bentonite(17), Concrete(7), Cement(3), Mortars(2), Sealing grout(2)	31
Very low permeable material	Admixture of bentonite and water(6), Homemade admixtures with graphite addition(2), Pulverized fuel ash(2), Bentonite-Clay(2), Admixture of bentonite and quartzite(2), Admixture of Portland cement and silica sand(2), Cement admixture(2), Aluminum cement-sand(2), Water-Cement(2), Silica sand-Cement(2), Cement-Sand(2), Clay-Sand(2), Sand Bentonite(2), Sand-E-plug admixture(2)	33
Permeable material	Silica Sand(10), Sand(10), Soil(5), Gravel(3), Sand-gravel(2), Saturated Sand(2), Protoplasm(2), Crushed Concrete(2)	36

The numerical simulation was performed to calculate the borehole thermal resistance under conditions, in which the groundwater passes through the inside borehole. A two-dimensional finite volume model (FVM) using the commercial software, ANSYS FLUENT was applied. Fig. 3.7 illustrates the discretized model. The soil domain was extended for 1 m in +X and − X directions, and 1 m in +Y and − Y direction. The geometry was divided into subdomains to optimize mesh element numbers and decrease computation time. The subdomains were the geometry of the pipes, the borehole, and the soil and its mesh element sizes were 1, 8, and 50 mm with a tetrahedral mesh, respectively. The boundary wall of the soil domain and the inner pipe is applied for Dirichlet boundary condition to evaluate the borehole thermal resistances quantitatively. The wall temperature of the soil and the inner pipe domain was assigned to be 0 and 1 °C, respectively. The groundwater flows with the constant velocity from the right side wall of the soil domain to +X direction.

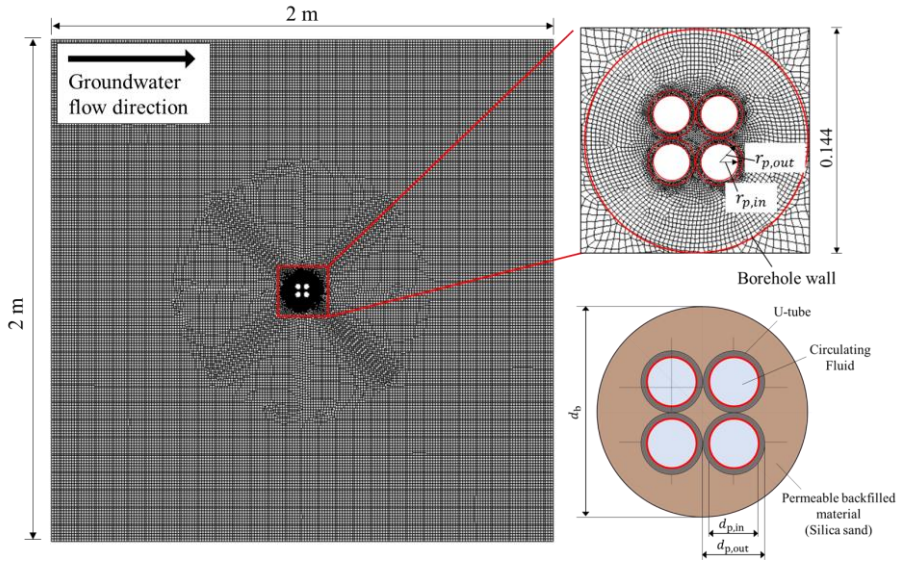

Fig. 3. 7 Discretized model domain

The borehole thermal resistance was calculated proportionally to the temperature difference between the borehole and the pipe wall divided by the heat flux in Eq. 3-5. These values were calculated from numerical simulation results according to variable conditions. The effective thermal conductivity of the soil and borehole domain was applied from 1 to 3 $\mathrm{W/(m\,K)}$ at intervals of 0.1 $\mathrm{W/(m\,K)}$ and the groundwater velocity was applied from 0 to 2000 m/y at intervals of 10 $\mathrm{m/y}$

$$R_{\mathrm{bh}} = \frac{\overline{T_{\mathrm{bh}}} - \overline{T_{\mathrm{p,in}}}}{q} \tag{3-5}$$

3.3.3. Equivalent single pipe for borehole thermal resistance in permeable backfilled borehole condition

In this study, the borehole was filled into the silica sand from the ground surface. It is expected for the backfill material to be filled in 3-5 m of the upside borehole part approximately. Another part of the borehole was refilled with the surrounding soil by the soil pressure. In this case, the boundary between the borehole wall and the ground becomes unclear and the pipes are buried by the surrounding soil. The groundwater can pass through the inside borehole. The conventional calculation methods of the borehole thermal resistance only considering the conduction heat transfer is unsuitable to calculate the circulating temperature under these

conditions.

This study proposes the approximate formula of the equivalent single pipe to calculate the circulating fluid temperature. The equivalent single pipe takes accounts of the temperature increase due to the borehole thermal resistance in the permeable backfilled borehole conditions. The radius of the equivalent singe pipe was determined by the minimum value between the average inside temperature of the U-tubes in the numerical approch and the average temperature calculated by the MLS model on the arbitrary radius. The equivalent pipe radius can be usefully used to determine the groundwater velocity and the effective thermal conductivity without considering the temperature rise due to the borehole thermal resistance in the permeable backfilled borehole conditions.

$$r_{\mathrm{eq}}(\lambda_{\mathrm{eff}}, v) = \min f = \left(\overline{T_{\mathrm{FEM,p,in}}(\lambda_{\mathrm{eff}}, v)} - \overline{T_{\mathrm{MLS}}\left(r_{\mathrm{eq}}, \lambda_{\mathrm{eff}}, v\right)} \right) \tag{3-6}$$

$$\overline{T_{\mathrm{MLS}}\left(r_{\mathrm{eq}}, \lambda_{\mathrm{eff}}, v\right)} = \frac{1}{2\pi} \int_0^{2\pi} \theta\left(r_{\mathrm{eq}}, \varphi, \lambda_{\mathrm{eff}}, v, t\right) d\varphi + T_0 \tag{3-7}$$

3.4. Results of thermal response test analysis

3.4.1. Conventional TRT analysis method

Fig. 3.8 shows the measured data for TRT: Fig. 3.8 (a) shows the temperature data of the inlet and outlet at the pipes, and Fig. 3.8 (b) indicates the flow rate and heat injection during the TRT period. Each data was measured at an interval of one minute. The temperature of the inlet and outlet increased maintaining 4.6℃ of the temperature difference. The flow rate and the heat injection were 20 L/min and 5.88 kW, respectively.

Fig. 3.9 indicates the conventional TRT analysis using the temperature slope over logarithmic time. This method uses the ILS model of Eqs. 3-3 and 3-4, utilizing the temperature data of the TRT for 12-60 h [30,31]. As a result, the temperature slope was 0.51 ℃/ln(t), and apparent effective thermal conductivity was estimated to be 9.14 W/(m·K). The reason for the high value is due to the high thermal dispersion by the effect of advection.

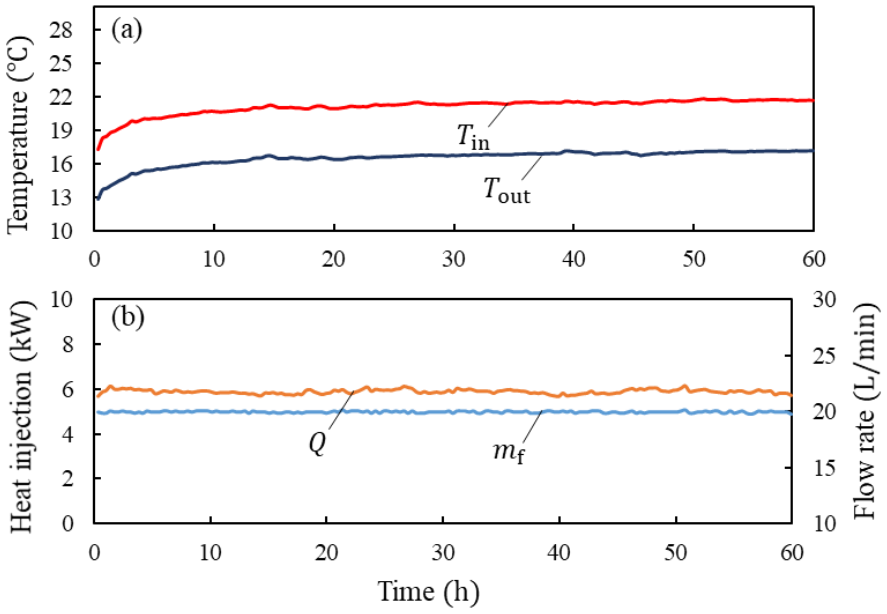

Fig. 3. 8 Measurement data from the TRT: (a) temperature variation of the inlet and outlet pipes, (b) the heat injection and flow rate

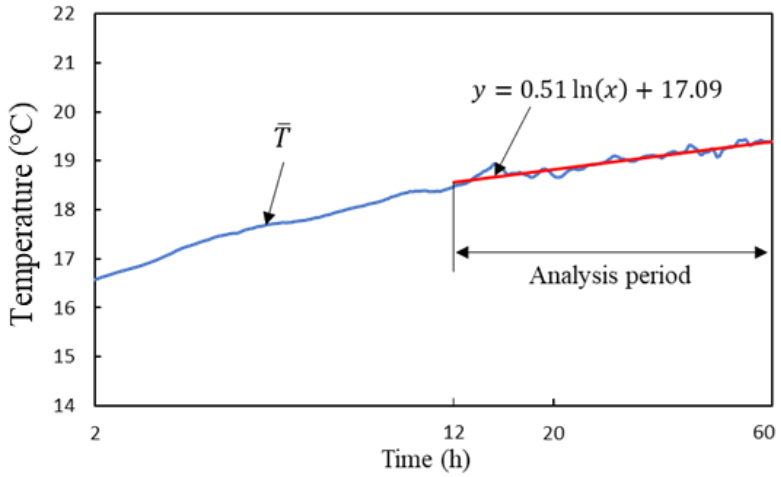

Fig. 3. 9 Conventional TRT analysis using the temperature slope over logarithmic time

3.4.2. Borehole thermal resistance in the borehole backfilled with the permeable material

Fig. 3.10 indicates the streamline plots of the groundwater velocity around the borehole. Fig. 3.11 demonstrates the results of the borehole thermal resistance according to the groundwater velocity between conditions on which the borehole is backfilled with the permeable or impermeable. The borehole thermal resistance was 0.092 (m·K)/W until the groundwater velocity is 70 m/y in both cases. On the other hand, the borehole thermal resistance in the permeable borehole backfilled condition was decreased by the advection effect. Therefore, it is necessary to propose the calculation method of the borehole thermal response in regard to the groundwater velocity, because the conventional methods considering only conduction heat transfer cause the high borehole thermal resistance in the permeable borehole backfilled conditions with the rapid groundwater flow.

Fig. 3.12 shows the relationship of borehole thermal resistance between groundwater velocity and thermal conductivity of backfill material. The borehole thermal resistance was calculated based on Eq. 3-5. As a result, the borehole thermal resistance decreased as the groundwater flow increased. On the other hand, the reduction ratio in the borehole resistance was more influenced in the condition of low thermal conductivity of the backfilled material.

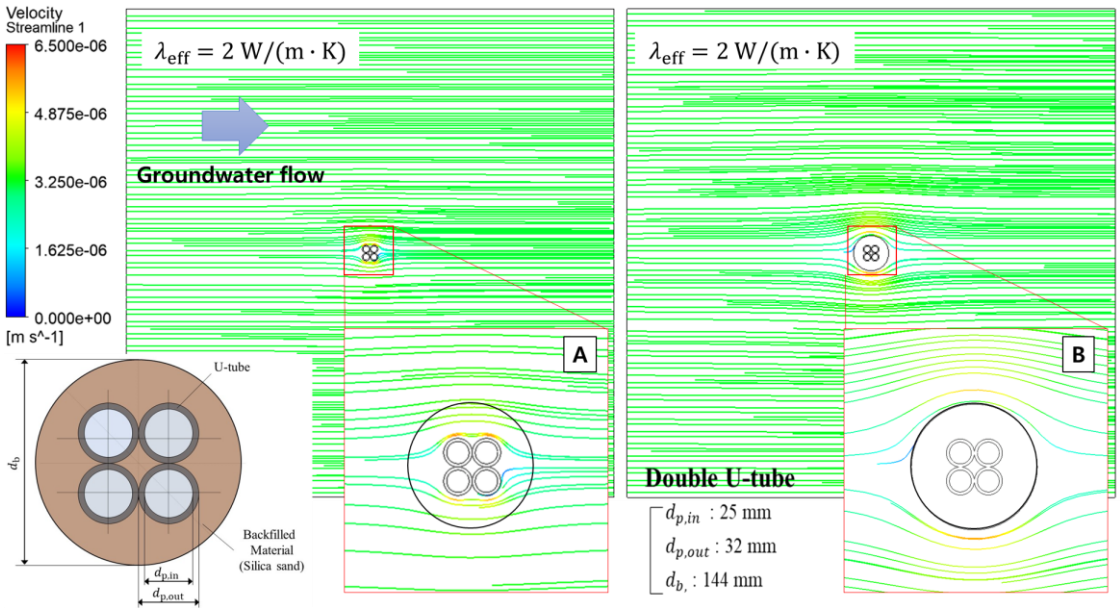

Fig. 3. 10 Streamline plots of the groundwater velocity; (A) permeable backfilled, (B) impermeable backfilled

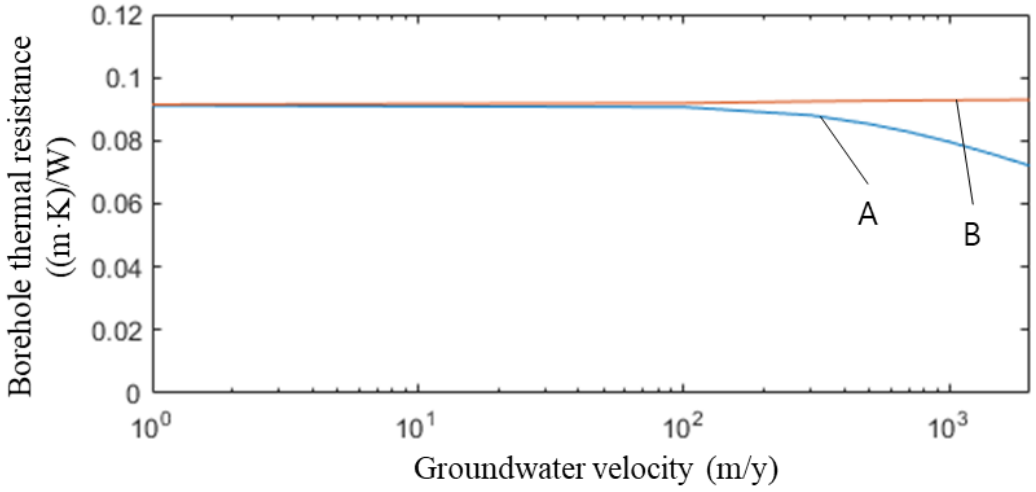

Fig. 3. 11 Borehole thermal resistance according to the groundwater velocity; (A) permeable backfilled, (B) impermeable backfilled

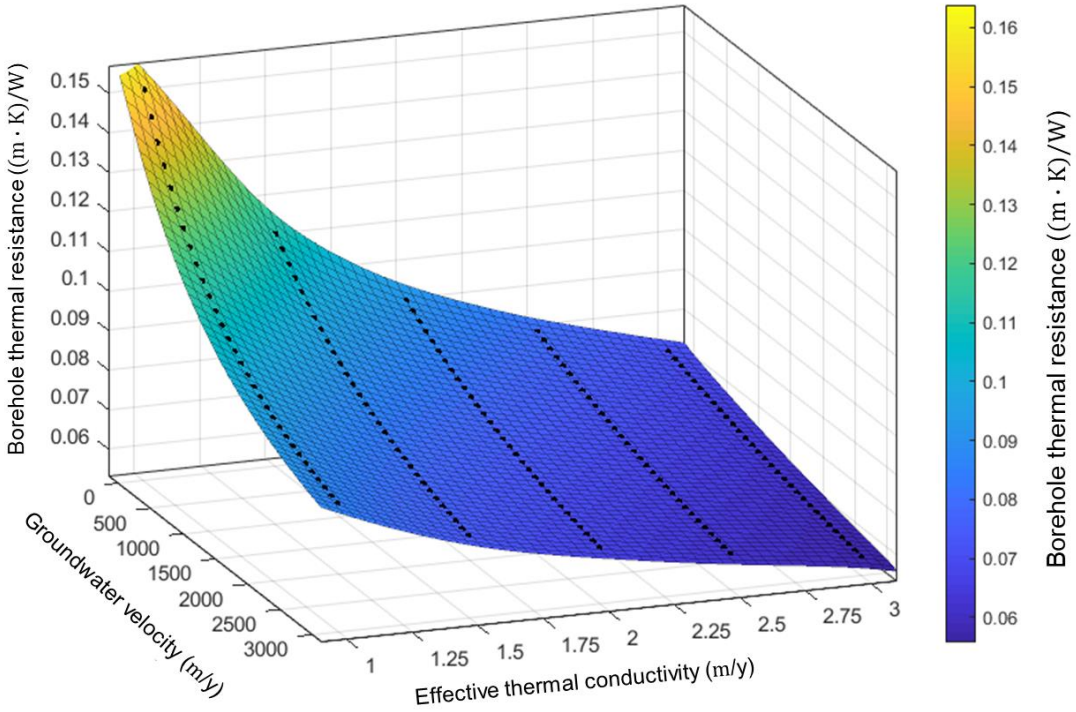

Fig. 3. 12 Relationship of borehole thermal resistance between groundwater velocity and thermal conductivity of backfill material

3.4.3. Equivalent radius of the imaginary single pipe

Fig. 3.13 indicates the equivalent radius of imaginary single pipe. The equivalent radius was determined by the minimum temperature difference based on Eq 3-6. The approximate formula for the equivalent radius was derived to be Eq. 3-8. The equivalent radius is less than 8% of temperature error between the numerical results and the calculated results of the MLS model. The temperature errors are acceptable to analyze the TRT results to estimate the effective thermal conductivity and the groundwater velocity.

$$r_{\mathrm{eq}}(v) = 19.39/(820.4 + v) \tag{3-8}$$

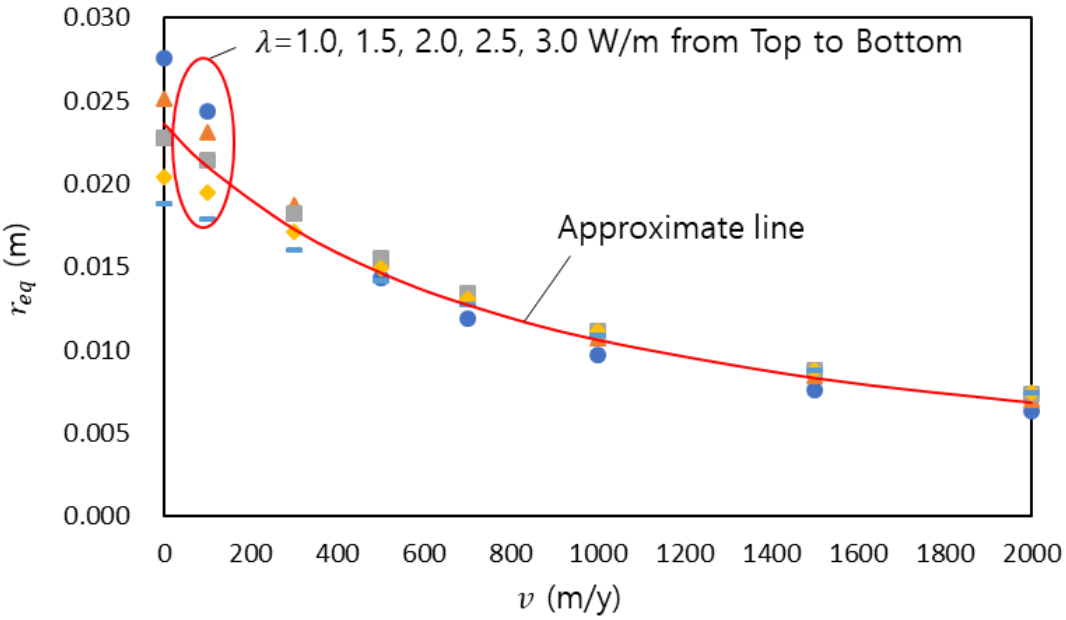

Fig. 3. 13 Equivalent Radius of imaginary single pipe

3.4.4. Simultaneous estimation of the effective thermal conductivity and the groundwater velocity from the TRT result

Fig. 13 illustrates the relationship between the groundwater velocity and the effective thermal conductivity of the soil in the test site. The relationship is derived by the iterative parameter estimation method between the TRT data and calculated results of MLS model applied the equivalent radius. The best fitting as the minimum RMSE is calculated when the groundwater velocity and the effective thermal conductivity were 120 m/y and 4.7 $\mathrm{W/(m\,K)}$, respectively. On the other hand, the RMSE in the case of 2.4 $\mathrm{W/(m\,K)}$ of the effective thermal conductivity estimated from the geological column section of the test site was relatively high value. Fig. 3. 15 shows the Curve fitting of temperature in each case, and Table 3.3 indicates the RMSE result of cases.

Table 3. 3 RMSE of cases

Case	λ_s (W/(m K))	v (m/y)	*RMSE*
Case 1	2.4	700	0.67
Case 2	4.7	120	0.10

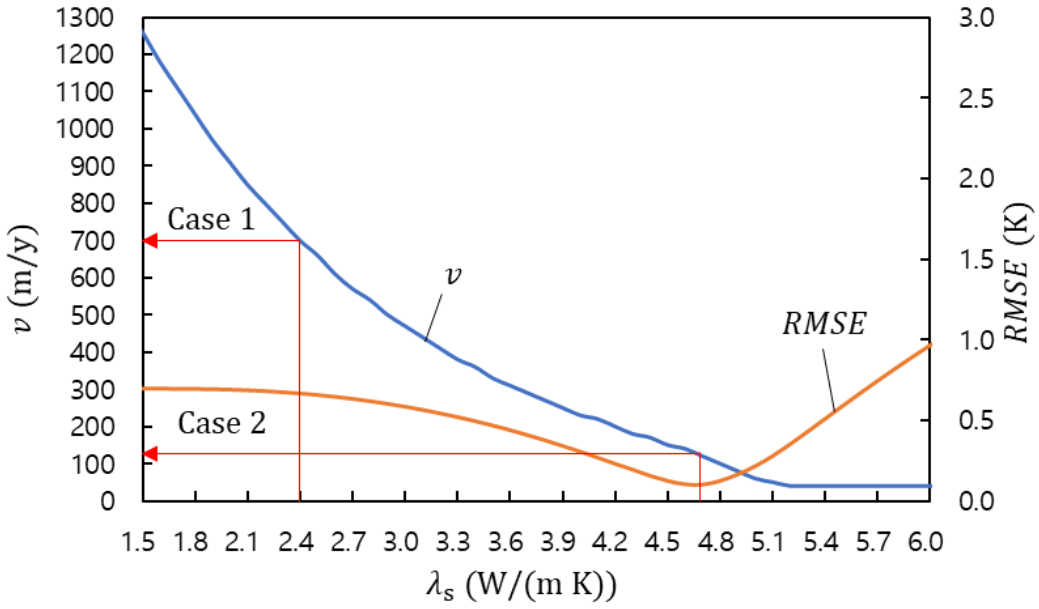

Fig. 3. 14 Relationship between groundwater velocity and effective thermal conductivity of the soil

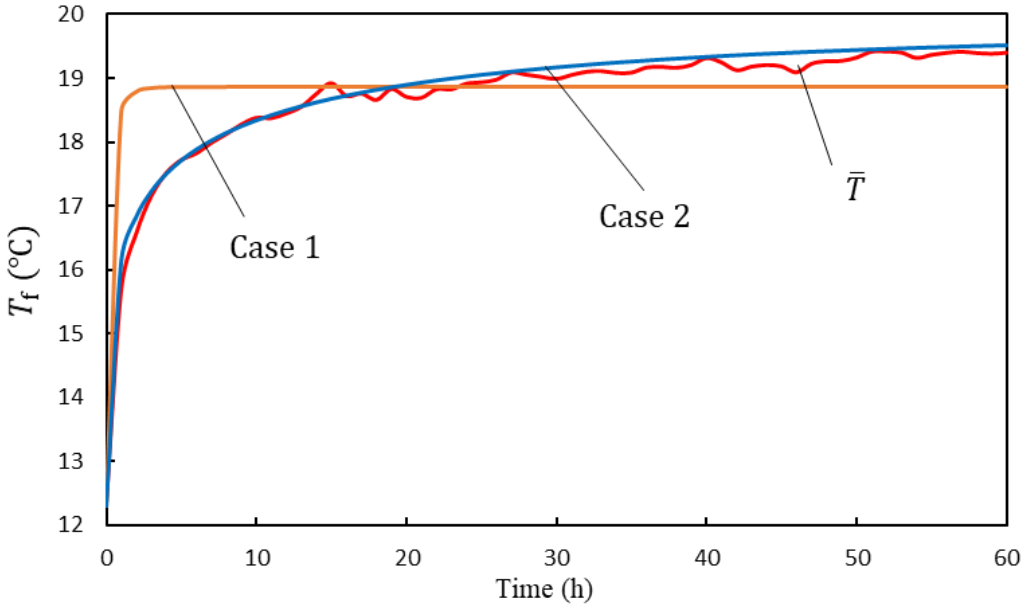

Fig. 3. 15 Curve fitting of temperature in each case

3.5. Discussion on limitation of MLS model

This study suggested a practical TRT method to determine the groundwater velocity and the effective thermal conductivity, using the MLS model. Also, MLS were verified for application of the TRT analysis under conditions over 100 m/y of groundwater velocity. As a result, the estimated effective thermal conductivity is much higher than that of the geological column section. The assumptions of the MLS model resulted in higher effective thermal conductivity; The ground is the homogeneous and semi-infinite porous medium, and the groundwater flows with the constant velocity in whole depth. On the other hand, the ground in practice was composed of heterogeneous porous media, and the groundwater flows with different velocities in each layer. In the test site where the TRT was carried out, there is a high probability that the rapid groundwater flows in the specific layers. This condition caused high effective thermal conductivity to represent weight-average values by the MLS model. Notwithstanding, the presented approach can contribute to the design of the BHE in response to the annual building heat loads under the porous backfill borehole, reflecting the weight-average thermal conductivity of soil and the groundwater velocity.

3.6. Summary

This chapter proposed a practical approach for the determination of the groundwater flow velocity and the effective thermal conductivity of soil using the MLS theory, simultaneously. The TRT was carried out in Kazuno City, Japan, and the conventional TRT analysis results presented that apparent effective thermal conductivity was 9.14 W/(m K). The borehole thermal resistance was calculated by numerical simulation, considering the groundwater velocity under the conditions that inside borehole was filled by the porous material having a high permeability. The radius of an equivalent single pipe instead of the borehole radius was applied to the MLS model to calculate the circulating fluid temperature, including the temperature increase by the grout thermal resistance. The approximate expression of the equivalent radius calculated by linear regression analysis was suggested. The groundwater velocity and the effective thermal conductivity of the soil are determined by using root mean square error between the calculated results and the TRT data. As a result, the groundwater velocity based on the effective thermal conductivity of the ground column section was calculated in 120 m/y and 4.7 W/(m K). The practical approach method could use standard TRT data for analysis without additional auxiliary equipment and complex simulation algorithms, designing the BHE in response to the annual building heat loads.

3.7. Reference

[1] A. Mustafa Omer, 01. Ground-source heat pumps systems and applications, Renew. Sustain. Energy Rev. 12 (2008) 344–371. doi:10.1016/j.rser.2006.10.003.

[2] M. Ozturk, 02. Energy and exergy analysis of a combined ground source heat pump system, Appl. Therm. Eng. 73 (2014) 360–368. doi:10.1016/j.applthermaleng.2014.08.016.

[3] S.K. Kim, G.O. Bae, K.K. Lee, Y. Song, 03. Field-scale evaluation of the design of borehole heat exchangers for the use of shallow geothermal energy, Energy. 35 (2010) 491–500. doi:10.1016/j.energy.2009.10.003.

[4] L. Valizade, 04. Ground Source Heat Pumps, J. Clean Energy Technol. 1 (2013) 216–219. doi:10.7763/JOCET.2013.V1.49.

[5] P. Mogensen, Fluid to duct wall heat transfer in duct system heat storages.pdf, (1983) 652–657.

[6] H.S. Carslaw, J.C. Jeager, Conduction of Heat in solids, Oxford University Press, Oxford, 1959.

[7] S. Signorelli, S. Bassetti, D. Pahud, Thomas Kohl, Numerical evaluation of thermal response tests, Geothermics. 36 (2007) 141–166.

[8] A.D. Chiasson, S.J. Rees, J.D. Spitler, Preliminary assessment of the effects of groundwater flow on closed-loop ground-source heat pump systems, ASHRAE Trans. 106 (2000).

[9] A. Angelotti, L. Alberti, I. La Licata, M. Antelmi, 08. Energy performance and thermal impact of a Borehole Heat Exchanger in a sandy aquifer: Influence of the groundwater velocity, Energy Convers. Manag. 77 (2014) 700–708. doi:10.1016/j.enconman.2013.10.018.

[10] D. Banks, J. Withers, R. Freeborn, 09. An overview of the results of In-situ Thermal Response Testing in the UK, Proc. Effstock Conf. Stock. Sweden. (2009).

[11] H. Fujii, 10. Practice and interpretation of thermal response tests, Geotherm. Res. Soc. Japan. 28 (2006) 245–257.

[12] S.E.A. Gehlin, G. Hellström, 12. Influence on thermal response test by groundwater flow in vertical fractures in hard rock, Renew. Energy. 28 (2003) 2221–2238. doi:10.1016/S0960-1481(03)00128-9.

[13] T. Katsura, K. Nagano, S. Takeda, Y. Nakamura, 13. An investigation on relation beween groundwater advection and thermal response by the thermal prove method, Soc.

Heating, Air-Conditioning Sanit. Eng. Japan. 112 (2006) 51–59.

[14] N. Diao, Q. Li, Z. Fang, Heat transfer in ground heat exchangers with groundwater advection, Int. J. Therm. Sci. 43 (2004) 1203–1211. doi:10.1016/j.ijthermalsci.2004.04.009.

[15] V. Wagner, P. Blum, M. Kübert, P. Bayer, Analytical approach to groundwater-influenced thermal response tests of grouted borehole heat exchangers, Geothermics. 46 (2013) 22–31. doi:10.1016/j.geothermics.2012.10.005.

[16] V. Wagner, P. Bayer, G. Bisch, M. Kübert, P. Blum, Hydraulic characterization of aquifers by thermal response testing: Validation by large-scale tank and field experiments, Water Resour. Res. 50 (2014) 71–85. doi:10.1002/2013wr013939.

[17] M. Verdoya, G. Imitazione, P. Chiozzi, M. Orsi, E. Armadillo, C. Pasqua, Interpretation of Thermal Response Tests in Borehole Heat Exchangers Affected by Advection, World Geotherm. Congr. 2015. (2015) 19–25.

[18] 18. Geological survey of Japan, (n.d.). https://www.gsj.jp/HomePageJP.html.

[19] G. Dalla Santa, F. Peron, A. Galgaro, M. Cultrera, D. Bertermann, J. Mueller, A. Bernardi, 19. Laboratory Measurements of Gravel Thermal Conductivity: An Update Methodological Approach, Energy Procedia. 125 (2017) 671–677. doi:10.1016/j.egypro.2017.08.287.

[20] I.N. Hamdhan, B.G. Clarke, 20. Determination of Thermal Conductivity of Coarse and Fine Sand Soils, Proc. World Geotherm. Congr. 2010. (2010) 1–7. doi:10.1137/120866701.

[21] G Shrestha G, Y. Uchida, S. Kuronuma, S. Yamaya, M. Katsuragi, S. Kaneko, N. Shibasaki, M. Yoshioka, 23. Performance evaluation of a ground-source heat pump system utilizing a flowing well and estimation of suitable areas for its installation in Aizu Basin, Japan, Hydrogeology. 25 (2017) 1437–1450.

[22] T. Saito, S. Hamamoto, E.E. Mon, T. Takemura, H. Saito, T. Komatsu, P. Moldrup, 24. Thermal properties of boring core samples from the Kanto area, Japan: Development of predictive models for thermal conductivity and diffusivity, Soils Found. 54 (2014) 116–125. doi:10.1016/j.sandf.2014.02.004.

[23] H. Fujii, 25. Interpretation of thermal response test in ungrouted U-tube ground heat exchangers, Geotherm. Res. Soc. Japan. 32 (2010) 31–40.

[24] Ministry of Trade, Industry and Energy of South Korea, (n.d.).

[25] Ministry of the environment of Japan, (n.d.). https://www.env.go.jp/en.

[26] H. Javadi, S.S.M. Ajarostaghi, M.A. Rosen, M. Pourfallah, A comprehensive review of

backfill materials and their effects on ground heat exchanger performance, Sustain. 10 (2018). doi:10.3390/su10124486.

[27] M.H. Sharqawy, E.M. Mokheimer, H.M. Badr, Effective pipe-to-borehole thermal resistance for vertical ground heat exchangers, Geothermics. 38 (2009) 271–277. doi:10.1016/j.geothermics.2009.02.001.

[28] D. Marcotte, P. Pasquier, On the estimation of thermal resistance in borehole thermal conductivity test, Renew. Energy. 33 (2008) 2407–2415. doi:10.1016/j.renene.2008.01.021.

[29] Inc. ANSYS, ANSYS FLUENT Theory Guide, 2013. doi:10.1016/0140-3664(87)90311-2.

[30] S. Gehlin, 27. Thermal Response Test - Method, Development and Evaluation, 2002.

[31] International Energy Agency (IEA), 28. IEA ECES ANNEX 21:Thermal Response Test(TRT)-Final report, (2013).

Chapter 4.

Analysis of relaxation time of temperature for thermal response test:

Estimation of effective thermal conductivity and groundwater velocity in multi-layer

4.1. Introduction

Ground source heat pump (GSHP) system has been recognized as a high-performance and environmental-friendly system [1–3]. The system produces higher performance than the air source heat pump (ASHP) system because it utilizes the ground as a stable heat source. The vertical closed-loop system, one of the GSHP systems, has been preferred because of its high efficiency as well as minimized installation space requirements in expensive neighborhoods [4]. The successful use and installation of the system rely on the design of the borehole heat exchangers (BHE). The design of the BHEs depends on the estimation of the effective thermal conductivity of the soil and borehole thermal resistance as the design parameters.

Thermal response test (TRT) proposed by Mogensen [5] is in-situ test to determine the thermal properties of the ground. The TRT continuously injects the heat flux and measures the circulating fluid. The measured temperature data is analyzed by an infinite line source (ILS) model with a least-squares approximation [6]. Its simple process led to frequent use in the practice. Although this method considers only the conduction heat transfer, it brings about no significant problems when the groundwater is less than 0.1 m/day [7]. However, the rapid groundwater flow results in high effective thermal conductivity. The high value causes the BHEs to be over/under-designed. Considering only heat conduction transfer makes the ground temperature increase or decrease more than the ground is in practice during the long-term system operating. Accordingly, it is necessary to reflect not only the thermal properties of the soil but also the groundwater velocities when the BHEs are designed in the areas having rapid groundwater flow.

The groundwater flow can improve the heat transfer efficiency of the ground and lead to better performance of the GSHP system. Many researchers have studied the effect of groundwater on the performance of the GSHP system [8–12]. In practice, however, the BHE has not been designed by reflecting the groundwater velocity in the site. It is a difficult task to determine the groundwater velocity from the TRT analysis. Wanger et al. [13] mentioned that the analytical approach in the advection-influenced conditions could be considered when the Darcy velocity exceeds 0.1 m/day. Another reason is the TRT operating time. The TRT tends to be operated within a limited time due to the required construction time and cost in practice. The previous research [7,14–18] suggested the TRT operating time to be the minimum time that is enough to estimate the thermal properties. Whereas the operating time of the TRT needs to be long enough to notice the effect of the groundwater flow. This evidence can be clearly seen in the temperature change according to the Darcy velocity [19]. The suggested TRT operating time is too short to determine

the groundwater velocity from the TRT data.

Wagner et al. [19] conducted both a tank experiment and a field experiment of the TRT to determine the hydraulic conductivity in an aquifer. They set ranges of hydraulic conductivity according to the properties of the soil, such as grain size, thermal conductivity, porosity, etc. Each value of those properties was utilized to calculate the temperature of the circulating fluid based on the moving line source (MLS) model. The calculated temperature results were then compared with the TRT data. The optimal fitting result yielded the hydraulic conductivity of the soil. Although demonstrating appropriate results, their approach required not only sufficient preliminary investigation for the thermal parameters of the soils but also the iteration calculation of 10,000 times. In a previous work of our research team [20], the practical approach was proposed for the simultaneous determination of the groundwater velocity and the effective thermal conductivity of the soil. The method also produced the relationship between the groundwater velocity and the effective thermal conductivity. As a result, the effective thermal conductivity and the groundwater velocity were estimated at 4.7 $W/(m \cdot k)$ and 120 m/y, respectively. Although the result was well-matched with a comparison between the TRT data and calculated temperature results, the apparent effective thermal conductivity was much higher than that of the sandy gravel, which is main the soil in the test site. The reason for the high value is that the ground was considered as a homogeneous medium based on the estimation methodology of the MLS model. Therefore, the TRT data should be analyzed by considering the ground as a heterogeneous medium. It is needed to divide the ground into layers having different thermal properties when the TRT data is analyzed.

Some researchers have been proposed to determine the thermal properties in the multi-layer, by using the optical fiber distributed temperature sensing (DTS) technique [21–26]. Fujii et al. [24] utilized the optical fiber DTS to measure the temperature-time profile of the circulating fluid of each layer in the U-tubes. The measured profiles were history-matched with the cylindrical source function [6]. Sakata et al. [21] also proposed the multilayer-concept TRT by using the optical fiber DTS and determined the stepwise ground thermal conductivity with the depth of each sub-layer. Their approach methods were an uncomplicated and practical use for the TRT analysis to estimate thermal properties in multi-layer. However, their methods could not estimate the groundwater velocity It is important to understand the effective thermal conductivity and the groundwater velocity of each layer, which is used as the design parameters of the GSHP system.

Therefore, this study proposes a novel TRT analytical method to estimate the groundwater velocity and the effective thermal conductivity of each geological layer. For simplicity, the layers

are grouped into vertical zones within the depth of the borehole. The theoretical methodologies and the experimental measurements are needed to estimate the groundwater flow velocity and the effective thermal conductivity. First, the temperatures in the U-tube are measured according to the depth at an interval of 0.5 m from the optical fiber DTS. The temperature is also monitored both during the heat injection and stopping the heat supply. Second, the new idea called 'relaxation time of temperature (RTT)' is introduced; the moment when the temperature in the borehole recovers a certain level compared to that at stopping the heating. The vertical distribution of the RTT that is calculated from the recovery temperature of each depth determines the depth of the zone, which is a vertical segment of the borehole. Third, the heat exchange rate of the zones is needed. It can be calculated from the vertical temperature profile of the circulating fluid during the heat supply. Finally, the temperature increments of the circulating fluid based on the determined zones and the heat exchange rates are calculated according to the groundwater velocities, using the MLS theory. These results are compared with the measured temperature data from each zone, and its best-fitting value yields the groundwater velocities. The proposed methodology is evaluated by comparing to the realistic operation data of the GSHP system for a long-term period in Kauno City, Japan.

4.2. Field experiments

Fig. 4.1 describes a ground plan and a geological column section of the test site. The test site located in Kazuno City (40°19'N and 140°78'E), Japan. The ground mainly composed of gravel, gravelly sand and sandy gravel. The effective thermal conductivity of the soils was expected in the range of 1-3 $W/(m \cdot k)$ on considerations based on the geometric column section [27–29]. The thickness-weighted average value of the effective thermal conductivity was approximately estimated to be 2.4 $W/(m \cdot k)$ when the soils were saturated in the water. The air-conditioned space was 143 m^2 in the three-floor building. The GSHP system operates to heating and cooling to the building. The system was composed of an inverter-driven heat pump unit, and its capacities for heating and cooling were 31.5/7.4 and 28.0/7.0 kW, respectively. Four BHEs were connected to the heat pump unit. The depth of the boreholes was 100 m, and the borehole diameter was 144 mm. The double U-tube without spacers was installed in the boreholes. The inside and outside diameter of the pipe were 32 and 25 mm, respectively. The borehole backfill material was dry silica sand, and it was inserted in the borehole from the ground surface.

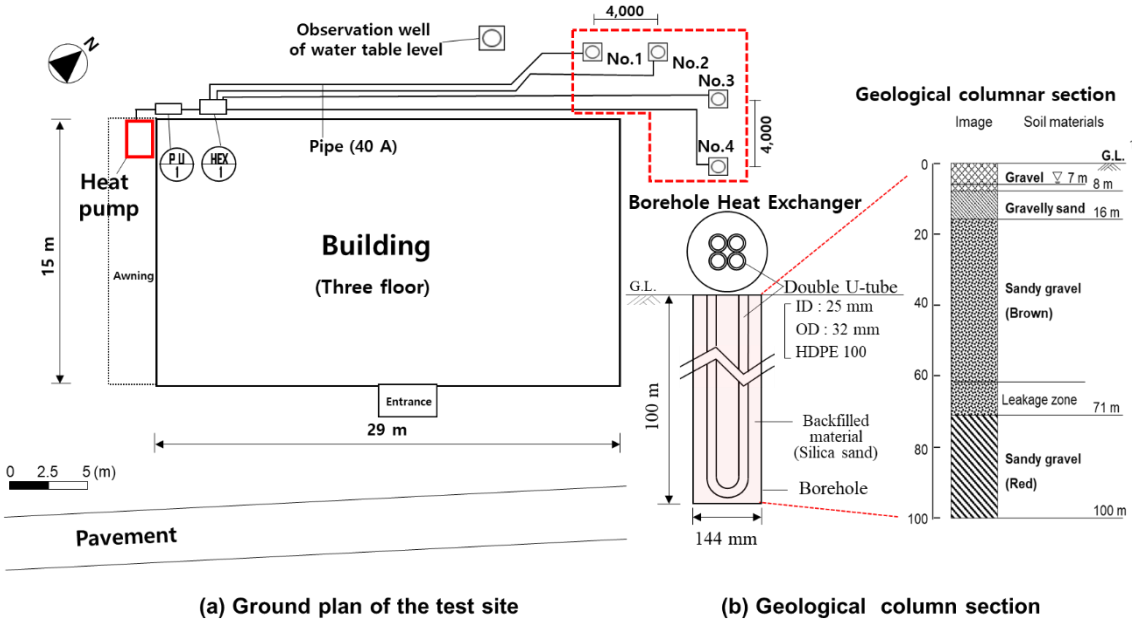

(a) Ground plan of the test site (b) Geological column section

Fig. 4. 1 Site description; (a) ground plan of the test site, (b) geological column section

Fig. 4.2 shows the schematic diagram of the TRT. The TRT was carried out during the long-term period to figure out the effect of the groundwater flow. The TRT operating time was 198 h after heat injection. The two optical fiber DTSs were inserted in the supply and return side of the U-tube. These DTSs measured the vertical profile of the temperature of the circulating fluid from the inlet/outlet side of the pipes to the bottom side of the U-tube at intervals of 0.5 m. The vertical profile is measured during the heat injection period and is continually monitored after finishing the heat injection for 198 h. The undistributed temperature was 12.0 °C before the TRT. The TRT was carried out in No.3 BHE, showing in Fig. 4.1.

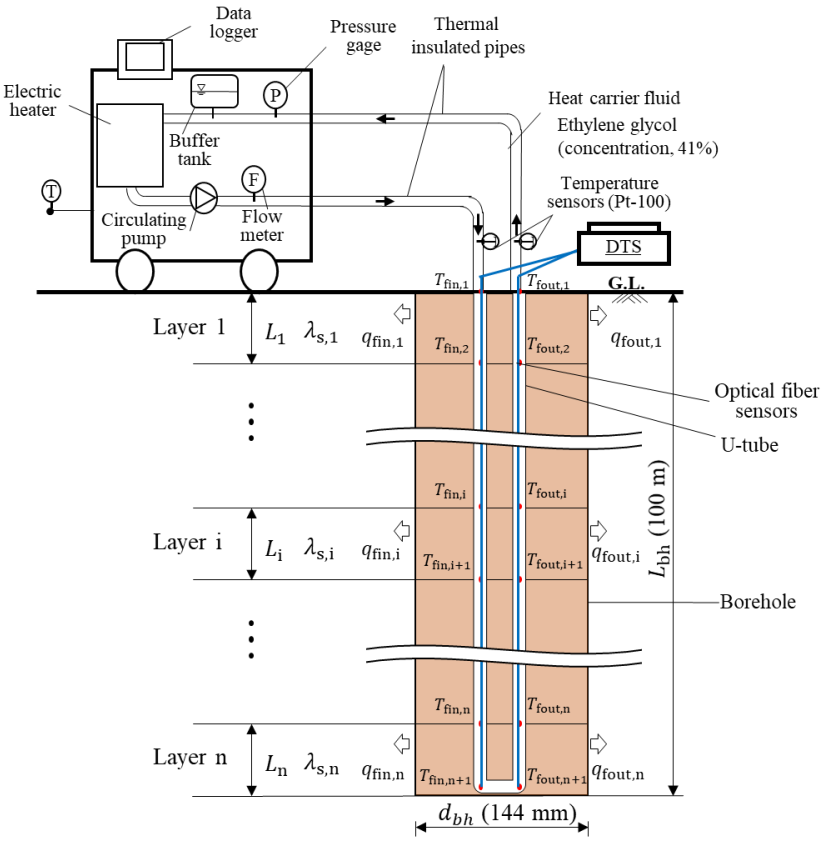

Fig. 4. 2 Schematic diagram of the TRT machine units and the BHE

4.3. Methodologies

4.3.1. Calculation of circulating fluid temperature

The moving line source (MLS) model [6] is used to analyze the TRT data for the estimation of the groundwater velocity and the effective thermal conductivity of the soil. The alternative flow speed, U, was introduced from the relationship between the Darcy velocity, v, and the moving medium of the line source theory [30] in Eq. 4-1. The time-dependent temperature increase can be obtained depending on the polar coordinate (r, φ) with the heat flux and the alternative flow speed in Eq. 4-2.

$$U = vc_{\mathrm{w}}\rho_{\mathrm{w}}/c_{\mathrm{eff}}\rho_{\mathrm{eff}} \tag{4-1}$$

$$\begin{aligned}\Delta T(r,\varphi,t) &= T(r,\varphi,t) - T_0 \\ &= \frac{q}{4\pi\lambda_{\mathrm{eff}}}\exp\left(\frac{Ur}{2\alpha}cos\varphi\right)\int_0^{\frac{4\alpha t}{r^2}}\frac{1}{\beta}\exp\left(-\frac{1}{\beta}-\frac{U^2r^2\beta}{16\alpha^2}\right)d\beta\end{aligned} \tag{4-2}$$

The average temperature of the circulating fluid (ΔT_{f}) over time is calculated with the borehole thermal resistance and the temperature response (ΔT) when r is assigned to the borehole radius (r_{bh}) in Eq. 4-3. Meanwhile, ΔT_{f} without considering the groundwater flow can be approximately expressed as the linear equation with the logarithmic time when $\frac{\alpha t}{r^2} > 5$ is satisfied in Eq. 4-4. The apparent effective thermal conductivity is then estimated in Eq. 4-5.

$$\Delta T_{\mathrm{f}}(t) = T_{\mathrm{f}}(t) - T_0 = \frac{1}{2\pi}\int_0^{2\pi} T(r_{\mathrm{bh}},\varphi,t)d\varphi + R_{\mathrm{bh}}q \tag{4-3}$$

$$\begin{aligned}\Delta T_{\mathrm{f}}(t) &= \frac{\mathrm{q}}{4\pi\lambda_{\mathrm{eff}}}Ei\left(\frac{r^2}{4\alpha t}\right) + R_{\mathrm{bh}}q \\ &\approx \frac{q}{4\pi\lambda_{\mathrm{eff}}}\ln(t) + \frac{q}{4\pi\lambda_{\mathrm{eff}}}\left\{\ln\left(\frac{4\alpha}{r_{\mathrm{bh}}^2}\right) - \gamma\right\} + R_{\mathrm{bh}}q\end{aligned} \tag{4-4}$$

$$\lambda_{\mathrm{eff}} = \frac{q}{4\pi k} \tag{4-5}$$

Where Ei is the exponential integral function. k is temperature slope

The principle of the temporal superposition can provide the temperature response of the assumed borehole wall by considering the time-dependent heat flux [31–34]. When this method is utilized with the MLS model, the average temperature changes of the circulating fluid are

reproduced like the TRT temperature results, which are varied in response to the heat injection. The MLS model applied to the temporal superposition can express the average fluid temperature in accordance with the time-varying heat flux in Eq 4-6.

$$\Delta T_{\mathrm{f}}(t) = T_{\mathrm{f}}(t) - T_0 = \sum_{i=1}^{N} \frac{q_i - q_{i-1}}{4\pi\lambda_{\mathrm{s}}} \int_0^{\pi} \int_0^{\frac{4\alpha(t_N - t_{i-1})}{r^2}} \frac{1}{\pi} \exp\left(\frac{Ur}{2\alpha} cos\varphi\right) \frac{1}{\beta} \exp\left(-\frac{1}{\beta} - \frac{U^2 r^2 \beta}{16\alpha^2}\right) d\beta + R_{\mathrm{bh}} q_N \quad (4\text{-}6)$$

Here, the borehole thermal resistance (R_{bh}) was calculated by using a finite volume model (FVM) with the commercial software, ANSYS FLUENT, based on the previous work [20,43] in the permeable backfilled conditions.

4.3.2. Estimation of the groundwater velocity and effective thermal conductivity in the multi-layer

This research introduces the 'relaxation time of temperature (RTT)' to classify the ground into layers grouped with similar thermal properties of the soils. The RTT (t_r) is defined as the moment when the circulating fluid temperature recovers a certain level. In this study, the certain level is set that ΔT_{f} at a time when the heat supply is stopped (t') is reduced by the ratio of the temperature decrement (ω): $\Delta T_{\mathrm{f}}(t_r) = \omega \Delta T_{\mathrm{f}}(t')$. Here, ω is in the range between 0 and 1 ($0 < \omega < 1$). RTT (t_r) depends on end time of the TRT (t'), the effective thermal conductivity (λ_{eff}) and the groundwater velocity (v), which affects the intensity of the heat transfer around the borehole. Fig. 4-3 illustrates the dimensional temperature variation ($\Delta T_{\mathrm{f}}^*(t)$) and the dimensional RTT (t_r/t') according to the groundwater velocity when ω is 0.5. $\Delta T_{\mathrm{f}}^*(t)$ is shown in Eq. (4-8), based on Eq. 4-6. When the groundwater flow speed was large, the RTT was getting smaller.

$$t_r = f(\lambda_{\mathrm{eff}}, v, t') \quad (4\text{-}7)$$

$$\Delta T_{\mathrm{f}}^*(t) = \Delta T_{\mathrm{f}}(t) / \Delta T_{\mathrm{f}}(t') \quad (4\text{-}8)$$

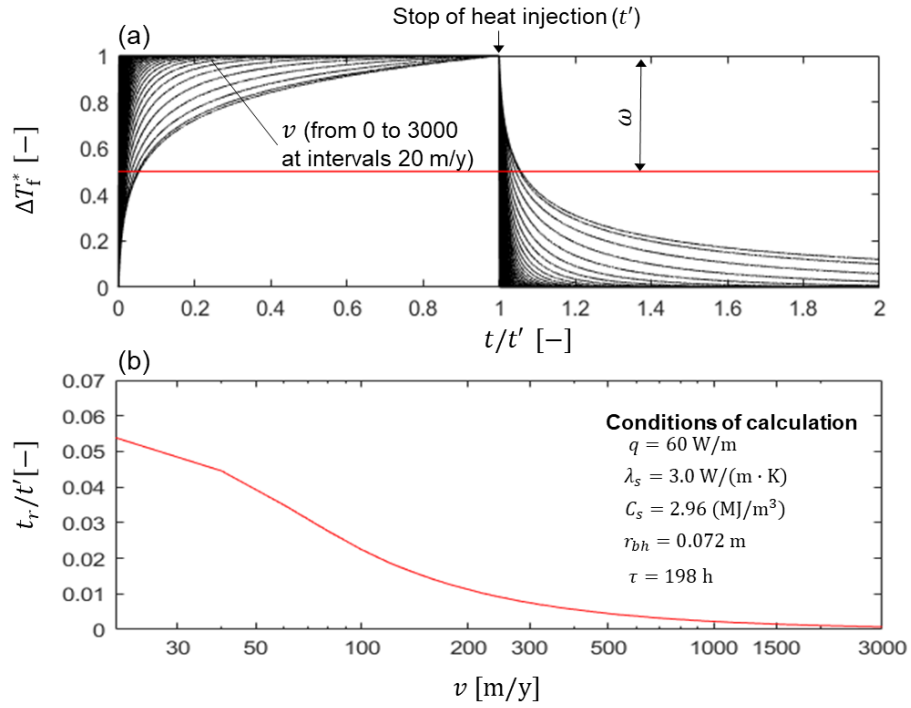

Fig. 4. 3 Relationship between dimensional temperature and the dimensional RTT

For the determination of the grouped layer (Zone) length, the vertical distribution of the RTT (t_{r,L_i}) is calculated from the recovery temperature of each depth measured by the DTS. The length of the Zone is sequentially determined by using standard RTTs ($t_r^*(N)$). The standard $t_r^*(N)$ is decided, depends on the number of the Zone to be divided based on the TRT data. Here, N is the number of the Zone. The depth of one layer was adopted to 0.5 m on which the optical fiber DTS can measure the data.

The heat exchange rate of each zone is calculated by the temperature changes of the circulating fluid in each layer. These temperature changes in each layer are observed from the optical fiber DTS during the heat injection period. The heat exchange rate of each zone is calculated by the average heat exchange rate of the grouped layers, shown in Eq. 4-9.

$$q_{L_i} = \frac{C\dot{m}}{L_i}\sum_{L_{i,start}}^{L_{i,end}}\left(\Delta T_{\mathrm{fin},i} + \Delta T_{fout,i}\right) \tag{4-9}$$

Finally, the groundwater velocity and the effective thermal conductivity is determined by the comparison of the temperature increment between TRT data and calculated results at the end time of the TRT. The temperature ($T_{\mathrm{f}}(t)$) calculated by Eq. 4-3 is iterated to find the best fitting with the TRT data. Fig. 4.4 indicates the flow chart of the calculation.

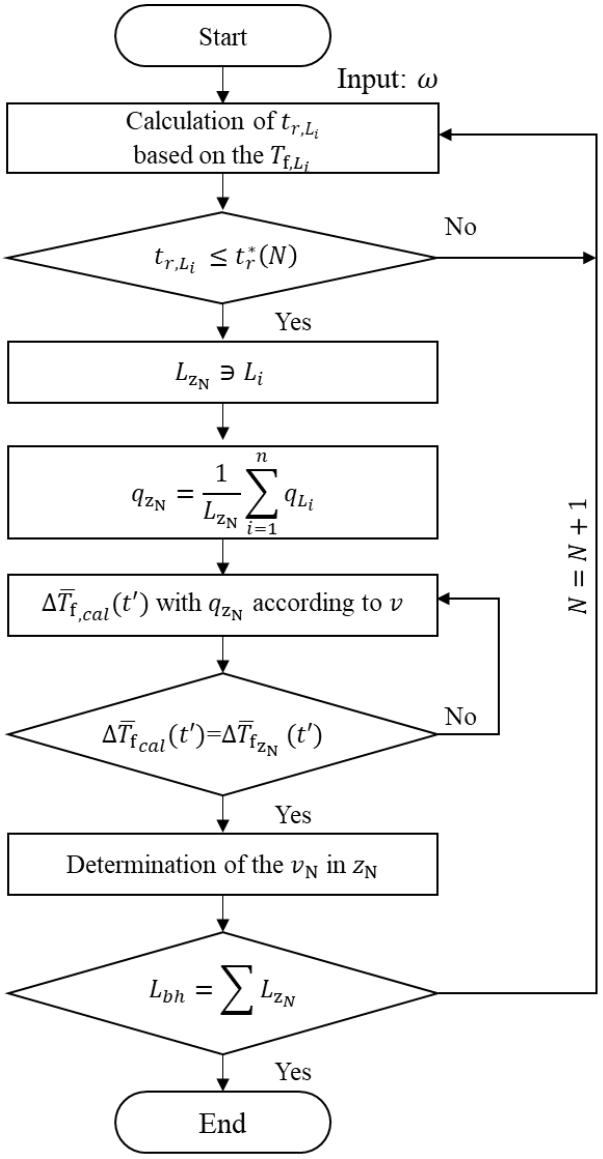

Fig. 4. 4 Flow chart of calculation

4.4. Multi-layer TRT analysis method

4.4.1. Standard TRT results

Figure. 5 shows the measurement data of the TRT. The temperature difference between the inlet and the outlet pipes was almost constant to be 4.6 ℃ in Fig. 4.5 (a). The flow rate and heat injection approximately were 20 L/min and 60.6 kW during the heat injection period in Fig. 4.5 (b). As a result of the conventional TRT analysis, the temperature gradient was 0.51 ℃/ln(t), and the apparent effective thermal conductivity was 9.5 $\mathrm{W/(m \cdot K)}$ for 12-60 h [35].

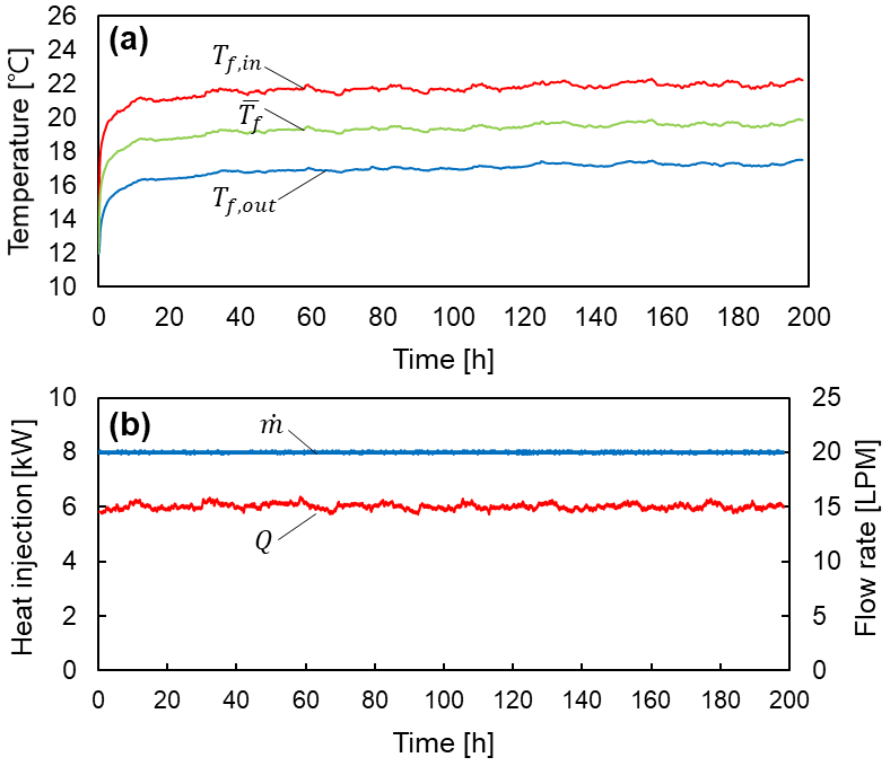

Fig. 4. 5 Measurement data of the TRT; (a) temperature data of inlet, outlet and average of Pt-100 sensors, (b) heat injection and flow rate

4.4.2. Determination of the depths of the zone

Fig. 4.6 indicates the dimensional average temperature variation of the circulating fluid. The average temperature variation at the inlet and outlet pipes during the heat injection was measured by the Pt100 sensor and the optical fiber DTS. The recovery temperature after stopping the heat injection was the average temperature of the optical fiber DTS in all layers. The black one shown in the Fig. 4.6 is the calculated result by Eq 4-8 when λ_{eff} was 3 $\text{W/(m}\cdot\text{k)}$ in the condition without the groundwater flow. The calculated result has the maximum thermal diffusivity in the condition of the test site when the groundwater velocity is 0 m/y. The dimensionless standard RTTs ($t_r^{*\prime}$) are determined by these data of the optical fiber DTS and the calculated result.

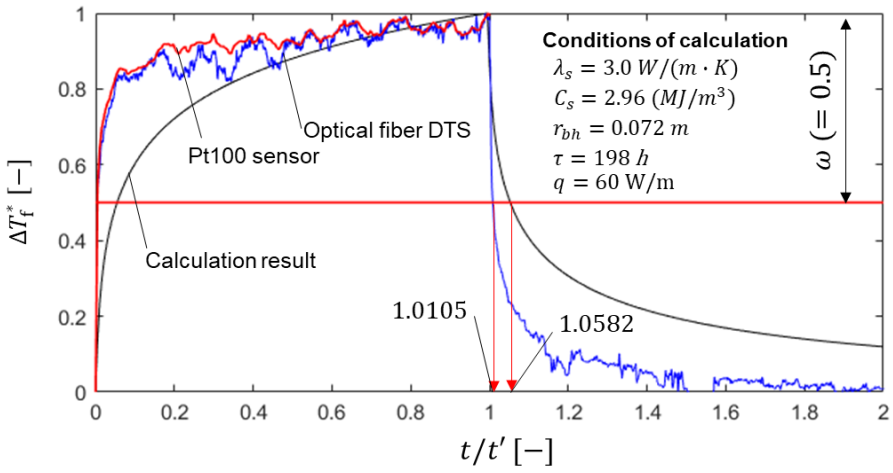

Fig. 4. 6 Dimensional temperature variation and RTT of the measurement data and calculated results

In the study, the ground was vertically divided into three zones based on the standard RTTs ($t_r^* = t_r^{*\prime} \times t'$): the strong influence of the groundwater flow (Zone 1), the intermediate influence of the groundwater flow (Zone 2), the weak influence of the groundwater flow (Zone 3). Fig. 4.7 shows the RTT according to the groundwater velocity when ω was 0.5. Here, the calculating conditions in Fig. 4.7 are set when λ_{eff} is in range of 1 to 3 $\text{W/(m}\cdot\text{K)}$ at an interval of 0.5 which is the expected range at a test site. The operating time of the TRT (t') is 198 h. Each zone divided by standard RTTs indicates the similar tendency on the RTT variation. The RTT change in Zone 1 was low and converged. In the Zone 2, The RTT change of each condition is high, and its changes were equalized over 70 m/y of the groundwater velocity. The RTT change in the Zone 3 are different in the conditions.

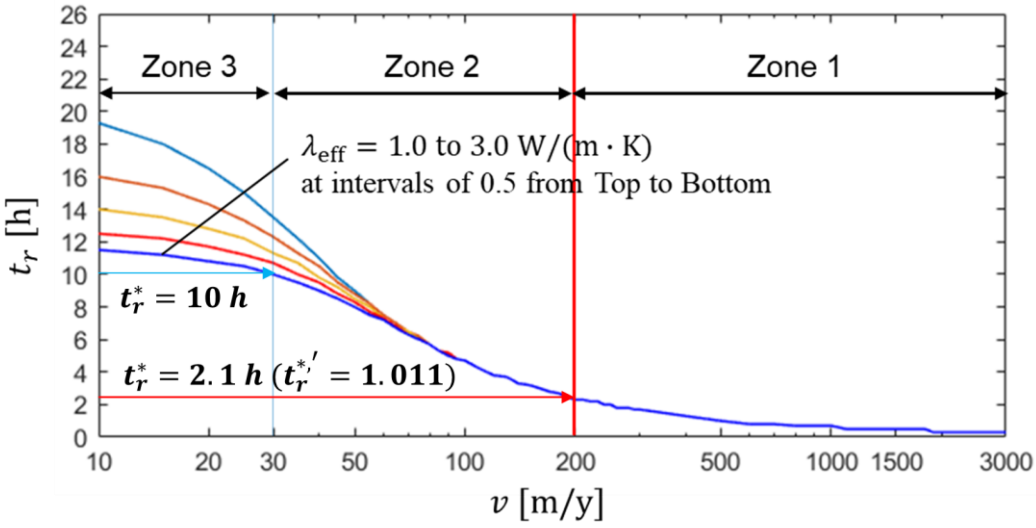

Fig. 4. 7 RTT according to the groundwater velocity

Figure. 8 shows the vertical distribution of the RTT when $\Delta T_f(t_r) = 0.5 \times \Delta T_f(t')$. The standard RTTs are derived from Fig. 4.6 ($t_r^* = t_r^{*\prime} \times t'$) and its time values are 2.1 h and 10 h, respectively. First, the Zone 1 with the rapid groundwater flow was decided when the RTT in each layer is lower than 2.1 h. Second, the Zone 3 without the groundwater flow was determined when the RTT is higher than 10 h of the standard RTT. The undecided layers were then allocated to the intermediate Zone (Zone 2). As a result, the length of the Zone 1, Zone 2 and Zone3 were 40, 28 and 32 m, respectively. Table 1 indicates the conditions of Zone.

Table 4. 1 Conditions of Zones

Layer	t_r **[h]**	v **[m/y]**	L **[m]**
Zone 1	$t_{r,L_i} < t_r^*(1) = 2.1$ h	$200 < v(L_i)$	0-40
Zone 2	$t_r^*(1) < t_{r,L_i} \leq t_r^*(2)$	$30 < v(L_i) \leq 200$	40-68
Zone 3	$t_r^*(2) = 10$ h $\leq t_{r,L_i}$	$v(L_i) \leq 30$	68-100

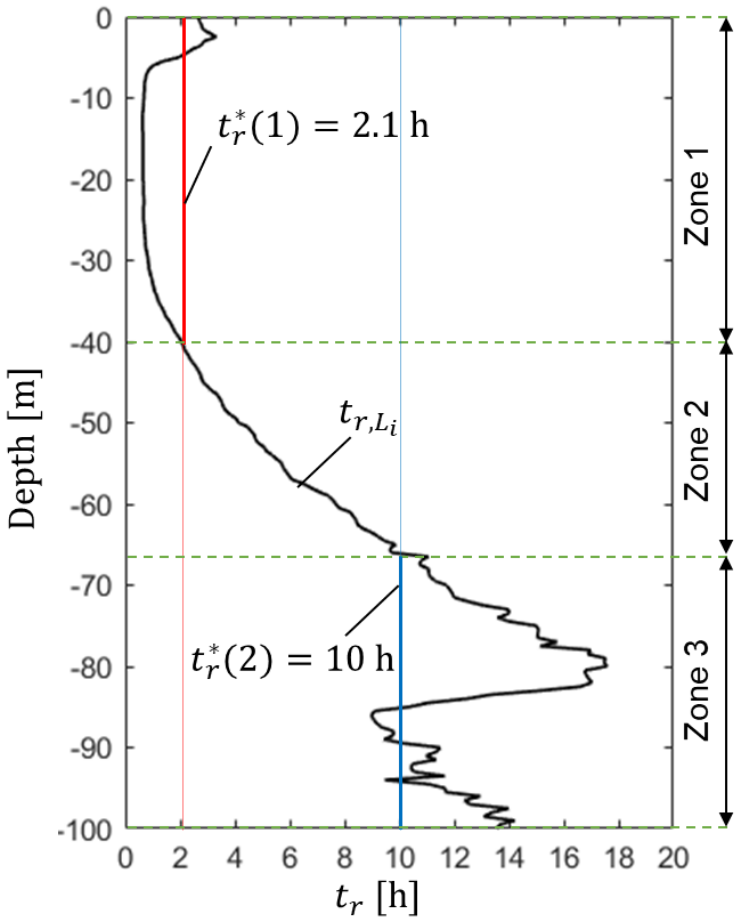

Fig. 4. 8 Vertical distribution of the RTT

Fig. 4.9 indicates the vertical temperature distribution during the heat injection period and the heat transfer rate of each zone. The heat exchange rate was calculated from Eq. 4-9 and was changed over time in each Zone. In particular, the heat exchange rate in Zone 1 gradually is increased. This reason was that the temperature difference between the circulating fluid and the ground increases. Whereas the temperature of the circulating fluid is increased by the heat injection, the ground temperature in Zone 1 is converged by the effect of the advection. To apply the heat exchange rate to calculation, average heat exchange rates in each Zone were calculated for 12 to 60 h, based on the standard procedure of the TRT in Japan [35]. As a result, the average heat exchange rates of each zone were calculated to 92.8, 31.9 and 27.6, respectively.

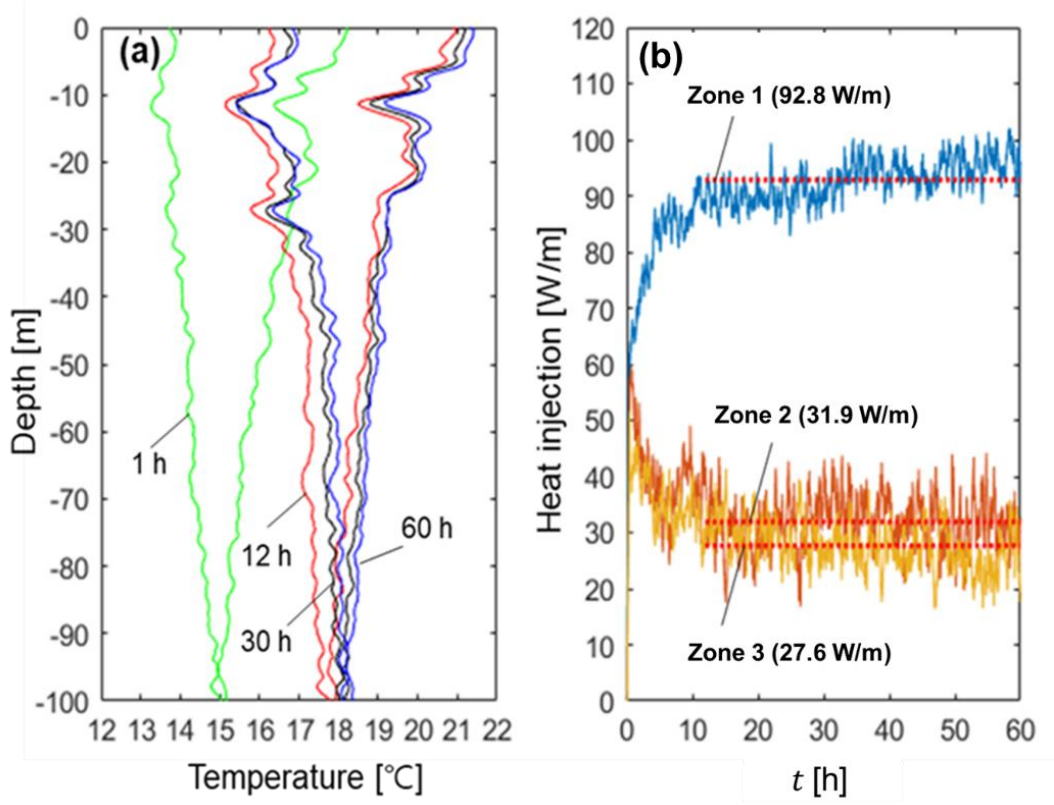

Fig. 4. 9 Vertical temperature distribution during the heat injection period (a) and the heat transfer rate of each zone (b)

4.4.3. Estimation of the groundwater velocity in the zones

The MLS model is a two-dimensional heat transfer analysis solution and is calculated by the temperature response on the borehole wall and the borehole thermal resistance. The temperature response of the circulating fluid differs when the thermal properties of each layer differ. On the other hand, in practice, the average temperature of the circulating fluid in each layer is almost similar because the fluid continuously circulates in the U-tube, even though the thermal properties of each layer differ. Therefore, the temperatures between the TRT data and calculated results were compared using the temperature increment at the TRT end time to estimate the parameters based on the heat exchanger rate. The method is derived from the temperature identity that the temperature response is the same at any time if the estimated parameters are correct. Fig. 4.10 demonstrates the temperature increment according to the groundwater velocity and the effective thermal conductivity in each zone. The method is the iterative parameter estimation, and the blue line was calculated by Eq. 4-6. The temperature results $\Delta T_f(t')$ are applied to the heat exchanger

rates in each zone and the groundwater velocity at the TRT end time. The effective thermal conductivity in Zone 1 and 2was applied to the thickness-weighted average value of the ground. In these Zones, ΔT_f has no significant influence by the thermal conductivity but mainly depends on the effect of the groundwater flow. In Zone 3, ΔT_f was calculated by changing the effective thermal conductivity in the range of 1-3 $W/(m \cdot k)$). The groundwater velocity or the effective thermal conductivity was determined at a point where the red line (TRT data) intersected with the blue lines (calculated results). As a result, the groundwater velocity was 2750, 58 and 0 m/y, and the thermal conductivity was 2.4, 2.4 and 2.1 $W/(m \cdot k)$ in each zone.

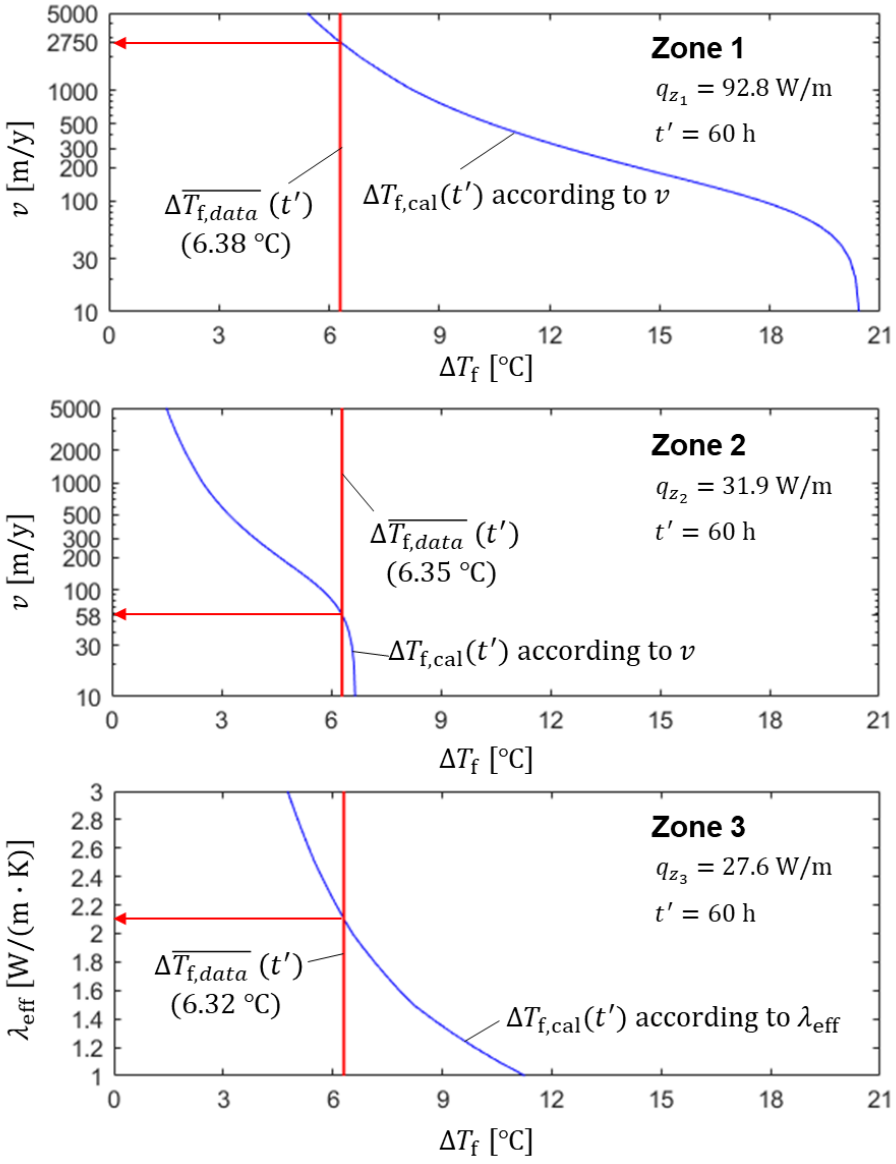

Fig. 4. 10 Temperature increment according to the heat exchanger rate and the groundwater velocity at the end of the TRT

4.5. Validation of the methodology

4.5.1. Comparison with calculated results and TRT data

The design parameters in Chapter 4.4 were estimated based on the TRT data for 60 h. These design parameters were applied to the MLS model to compare the TRT data, using Eqs. 4-10 to 4-12. The calculated period was also expanded to 198 h for comparison with the TRT data. Fig. 4.11 shows the temperature variation of the calculated results and TRT data. The RMSEs and temperature error of each data were under 0.16 K and 3 % for 198 h. These results show the well-matched estimation of the parameters.

$$\overline{T}_{\mathrm{f}}(t) = \frac{1}{L_{\mathrm{bh}}}\sum_{z=1}^{3}\left(\frac{Q_z}{4\pi\lambda_{\mathrm{eff}}}\int_0^{\pi}\int_0^{\frac{4\alpha t}{r^2}}\frac{1}{\pi}\exp\left(\frac{Ur}{2\alpha}cos\varphi\right)\frac{1}{\beta}\exp\left(-\frac{1}{\beta}-\frac{U^2r^2\beta}{16\alpha^2}\right)d\beta\, d\varphi + R_{\mathrm{bh}}Q_z\right) \tag{4-10}$$

$$T_{\mathrm{f,in}}(t) = \overline{T}_{\mathrm{f}}(t) + \frac{\sum_{z=1}^{3} Q_z}{2\rho_{\mathrm{f}}c_{\mathrm{f}}\dot{m}_{\mathrm{f}}} \tag{4-11}$$

$$T_{\mathrm{f,out}}(t) = \overline{T}_{\mathrm{f}}(t) - \frac{\sum_{z=1}^{3} Q_z}{2\rho_{\mathrm{f}}c_{\mathrm{f}}\dot{m}_{\mathrm{f}}} \tag{4-12}$$

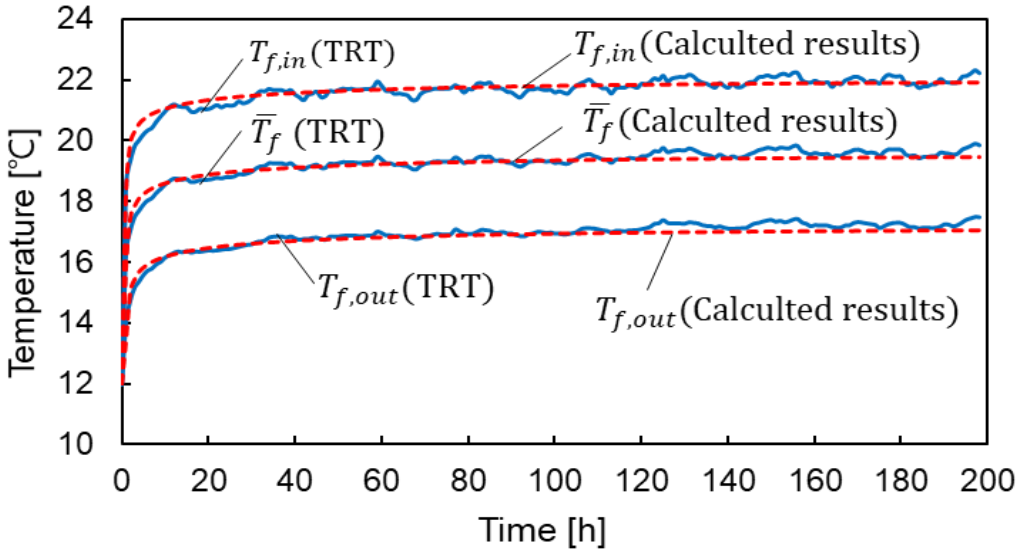

Fig. 4. 11 Comparison between the calculated results and the TRT data

4.5.2. Analysis results of the thermal parameters according to the end time of the TRT

Fig. 4.12 demonstrates the temperature change based on the design parameters according to the end time of TRT. The TRT end time was referred from previous studies: 60 h [35], 48 h [18] and 96 h [36]. Table 2 indicates the results of each case. The design parameters of each Case were slightly different, but not significantly different. The reason for slightly different parameters is that the heat exchanger rates differed a little by the TRT end time. The TRT data to the calculation of the heat exchange rate might contain measurement errors or be affected by the surrounding environment. Nevertheless, the heat exchange rate could become converged gradually as the TRT time passed. Based on the estimated thermal parameter at each end time, the temperature results of Case 1 and Case 3 were similar but slightly different from that of Case 2, compared with the measurement data of the DTS. Although the longer TRT time can give the more accurate the design parameters, it makes the construction time and effort increase. Since the optimal TRT time depends on the location of the test, a future study will be carried out to determine the optimal TRT time based on the TRT results in the other site.

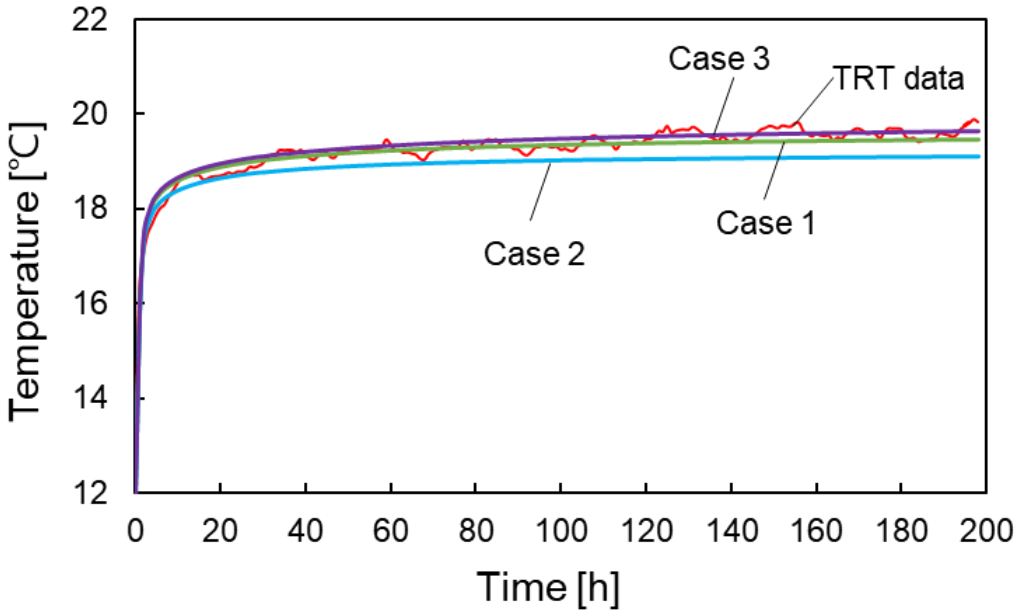

Fig. 4. 12 Temperature variation according to the end time of the TRT

Table 4. 2 Results of the thermal parameter according to the end time

Case		Case 1 [end time =60 h]	Case 2 [end time =60 h]	Case 3 [end time =60 h]
Zone 1	q [W/m]	92.8	91.8	94
	λ_{eff} [W/(m · K)]	2.4	2.4	2.13
	v [m/y]	2750	3250	2730
Zone 2	q [W/m]	31.9	32.1	31.1
	λ_{eff} [W/(m · K)]	2.4	2.4	2.36
	v [m/y]	58	89	28
Zone 3	q [W/m]	27.6	28.4	26.1
	λ_{eff} [W/(m · K)]	2.1	2.36	1.97
	v [m/y]	0	0	0

4.6. Comparison between single and multi-layer parameters for the design of the GSHP

The conventional TRT analysis method has yielded the parameters of the single layer to design the GSHP system. The estimated parameters are the thickness-weighted average values in response to the total length of the BHE. Although suggesting the number of the BHEs for the heating and cooling of the building, these parameters cannot figure out the depth of the BHEs to decrease the installation cost of the system. On the other hand, the TRT analysis method presented in this study divided the ground into the zones according to the recovery temperature of the circulating fluid after stopping the heat supply. It also estimated the design parameters in each zone. This method has an advantage significantly to consider the depth of the BHEs as well as the number of the BHEs for the design of the GSHP system. In particular, it is expected that the larger the required number of the BHEs for heating and cooling of the building should bring economic benefits about the initial installation cost, by applying to the estimated parameters in multi-layer to design the GSHP system. The evidence as mentioned above is demonstrated in the following Sections, compared with the conventional TRT analysis method. Table 4.3 shows the condition of cases according to the results of the TRT analysis.

Table 4. 3 Condition of cases according to the results of the TRT analysis

Case		L_b ($L_{z_1}/L_{z_2}/L_{z_3}$) [m]	λ_{eff} ($\lambda_{\mathrm{eff},z_1}/\lambda_{\mathrm{eff},z_2}/\lambda_{\mathrm{eff},z_3}$) [W/(m · K)]	v ($v_{z_1}/v_{z_2}/v_{z_3}$) [m/y]
Case 1 (proposed method)	Case 1-1 (3 zones)	100 (40/28/32)	2.4/ 2.4/ 2.1	2750/ 58/ 0
	Case 1-2 (2 zones)	68 (40/28)	2.4/ 2.4	2750/ 58
	Case 1-3 (mono-zone)	40	2.4	2750
Case 2 (conventional TRT analysis method)	Case 2-1	100	9.5	0
	Case 2-2	68	9.5	0
	Case 2-3	40	9.5	0
Case 3 (Chapter 3)	Case 3-1	100	4.7	120
	Case 3-2	68	4.7	120
	Case 3-3	40	4.7	120

4.6.1. Comparison between the proposed method and the conventional TRT analysis method

Fig 4.13 shows the average temperature variations of the circulating fluid. These temperatures were calculated for two years, based on the parameters estimated from the proposed method and the conventional TRT analysis method. The heating and cooling load were also the same condition of the target building in Section 5.3. Case 1-1 was considered both λ_{eff} and v of three zones, while Case 2-1 was considered only λ_{eff}. The temperature variation of Case 2-1 had a large fluctuation of -2.7 to 1.9 ℃ based on Case 1-1. That is, the GSHP system designed by the parameters without the consideration of v might be over-designed.

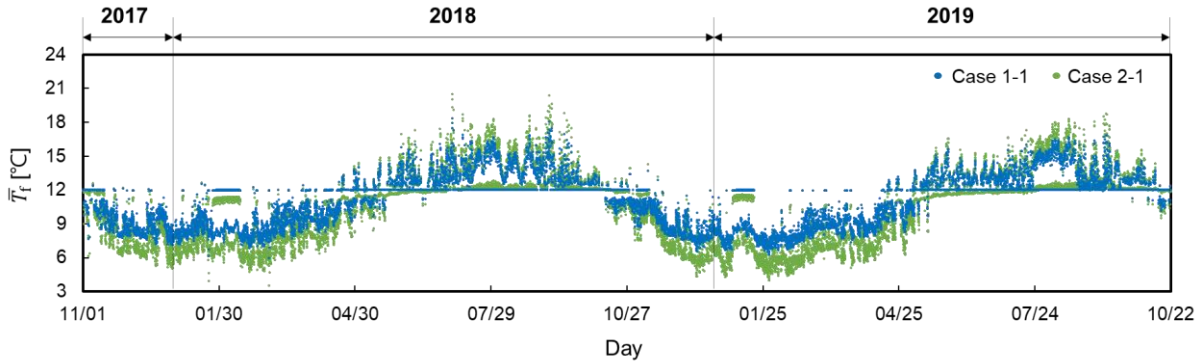

Fig. 4. 13 Average temperature variation of the circulating fluid; Comparison between the proposed method and the conventional TRT analysis method

4.6.2. Comparison between multi-layer and single layer for design parameters

Fig 4.14 shows the average temperature variations of the circulating fluid. The temperature of Case 3-1 was considered both λ_{eff} and v in a single layer in response to 100 m borehole depth [20]. In the comparison result between Case 1-1 and Case 3-1, the temperature error was 0.3 %. It was regarded that both methods were suitable for the design of the GSHP system in response to the 100 m borehole depth. On the other hand, Fig 4.15 shows the average temperature variations of the circulating fluid when the depth of the borehole was 40 m. The temperature variation of Case 3-3 had a large fluctuation of -3.0 to 1.8 ℃ based on Case 1-3, and its temperature error was 9.2 %. In other words, although the single layer method [20] could be suitable for 100 m borehole depth, it cannot figure out the optimal design of the borehole depth.

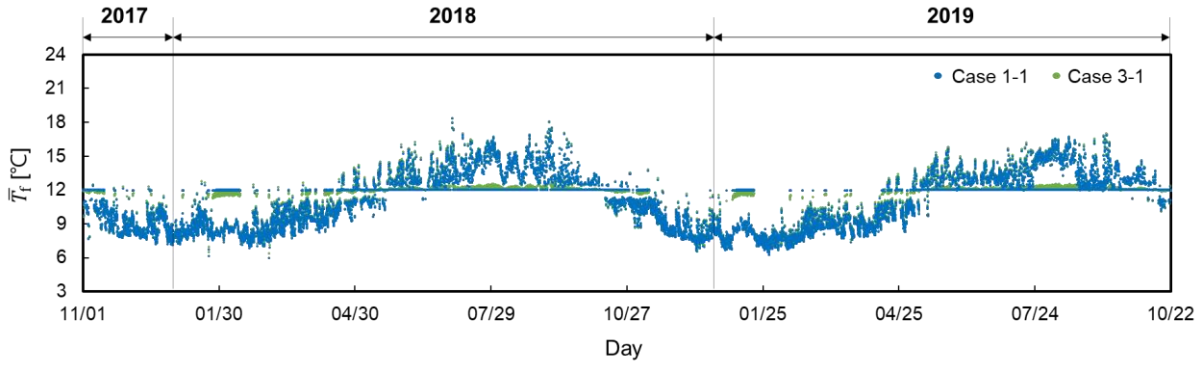

Fig. 4. 14 Average temperature variation of the circulating fluid; Comparison between multi-layer and single layer for design parameters

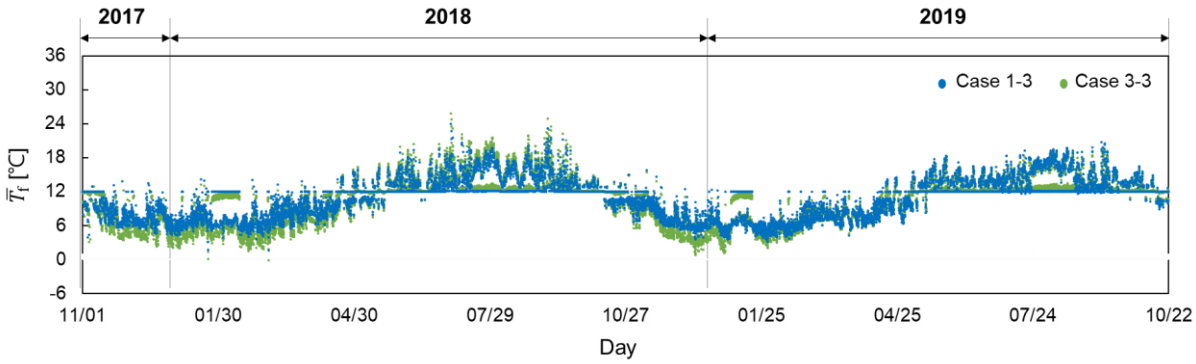

Fig. 4. 15 Average temperature variation of the circulating fluid; Comparison between multi-layer and single layer for design parameters when depth of the borehole was 40 m

4.6.3. Comprehensive review of each method

Fig 4.16 indicates the average temperature of the circulating fluid during the heating and cooling season. In Case 1, the average temperature of the circulating fluid did not change significantly even though the depth of the BHE was shortened since the groundwater velocity was fast in Zone 1. Based on Case 1-1, the average temperature of the circulating fluid of Case 1-3 decreased -1.47 °C in the heating season, and increased 1.23 °C in the cooling season, respectively. On the other hand, in Case 3, the average temperature of the circulating fluid changed significantly. Based on Case 3-1, the average temperature of the circulating fluid of Case 3-3 decreased -4.94 °C in the heating season, and increased 3.07 °C in the cooling season, respectively.

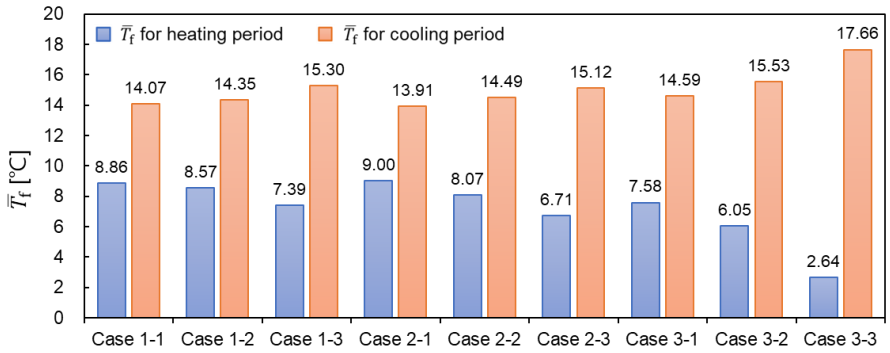

Fig. 4. 16 Average temperature of the circulating fluid during the heating and cooling season

4.7. Summary

In this Chapter, the ground was divided into three zones according to the effect of the groundwater flow, and the groundwater velocity in each zone was estimated. The reaching time was also proposed to determine the depth of the zones by considering the temperature recovery of the circulating fluid after stopping the heat supply. The temperature increments based on the heat exchange rate in each zone were then calculated according to the groundwater velocities. These results are compared with the average temperature increments measured from each zone, and its best-fitting value yields the groundwater velocities. As a result, the groundwater velocity was 2750, 58 and 0 m/y, and the thermal conductivity was 2.4, 2.4 and 2.1 $W/(m \cdot k)$ in each zone.

These estimated velocities with the other parameters were applied to the simulation tool to calculate the temperatures of the circulating fluid. These calculated temperature results were validated by comparing with the measurement data of the circulating fluid in the target building, and it was well-matched. In addition, the temperatures of the circulating fluid were calculated according to the depth of the BHE, based on the parameters estimated from the proposed method and the conventional TRT analysis method. The design parameters obtained from the proposed method could reflect the heat transfer of the ground more reasonably. It was possible to design the proper depth of the BHEs for the GSHP system.

4.8. Reference

[1] O. Ozgener, A. Hepbasli, L. Ozgener, A parametric study on the exergoeconomic assessment of a vertical ground-coupled (geothermal) heat pump system, Build. Environ. 42 (2007) 1503–1509. doi:10.1016/j.buildenv.2005.12.019.

[2] O. Ozgener, A. Hepbasli, Performance analysis of a solar-assisted ground-source heat pump system for greenhouse heating: An experimental study, Build. Environ. 40 (2005) 1040–1050. doi:10.1016/j.buildenv.2004.08.030.

[3] Y. Nam, R. Ooka, S. Hwang, Development of a numerical model to predict heat exchange rates for a ground-source heat pump system, Energy Build. 40 (2008) 2133–2140. doi:10.1016/j.enbuild.2008.06.004.

[4] J.C. Choi, S.R. Lee, D.S. Lee, Numerical simulation of vertical ground heat exchangers: Intermittent operation in unsaturated soil conditions, Comput. Geotech. 38 (2011) 949–958. doi:10.1016/j.compgeo.2011.07.004.

[5] P. Mogensen, Fluid to duct wall heat transfer in duct system heat storages.pdf, (1983) 652–657.

[6] H.S. Carslaw, J.C. Jeager, Conduction of Heat in solids, Oxford University Press, Oxford, 1959.

[7] S. Signorelli, S. Bassetti, D. Pahud, Thomas Kohl, Numerical evaluation of thermal response tests, Geothermics. 36 (2007) 141–166.

[8] A. Angelotti, L. Alberti, I. La Licata, M. Antelmi, Energy performance and thermal impact of a Borehole Heat Exchanger in a sandy aquifer: Influence of the groundwater velocity, Energy Convers. Manag. 77 (2014) 700–708.

[9] J.C. Choi, J. Park, S.R. Lee, Numerical evaluation of the effects of groundwater flow on borehole heat exchanger arrays, Renew. Energy. 52 (2013) 230–240. doi:10.1016/j.renene.2012.10.028.

[10] J. Hecht-Méndez, M. De Paly, M. Beck, P. Bayer, Optimization of energy extraction for vertical closed-loop geothermal systems considering groundwater flow, Energy Convers. Manag. 66 (2013) 1–10. doi:10.1016/j.enconman.2012.09.019.

[11] C.K. Lee, H.N. Lam, A modified multi-ground-layer model for borehole ground heat exchangers with an inhomogeneous groundwater flow, Energy. 47 (2012) 378–387. doi:10.1016/j.energy.2012.09.056.

[12] H. Wang, C. Qi, H. Du, J. Gu, Thermal performance of borehole heat exchanger under groundwater flow: A case study from Baoding, Energy Build. 41 (2009) 1368–1373.

doi:10.1016/j.enbuild.2009.08.001.

[13] V. Wagner, P. Blum, M. Kübert, P. Bayer, Analytical approach to groundwater-influenced thermal response tests of grouted borehole heat exchangers, Geothermics. 46 (2013) 22–31. doi:10.1016/j.geothermics.2012.10.005.

[14] S.J. Austin WAI, Yavuzturk C, Development of an insitu system and analysis procedure for measuring ground thermal properties, ASHRAE Trans. (2000) 1–19.

[15] P.R. Smith MD, In situ testing and thermal conductivity testing, Proc. Geoexchange Tech. Conf. Expo. Stillwater, Oklahoma State Univ. (1999).

[16] S.P. Kavanaugh, L. Xie, C. Martin, Investigation of Methods for Determining Soil and Rock Formation Thermal Properties From Short-Term Field Tests, Atlanta. (2000).

[17] S.E.A. Gehlin, G. Hellström, Comparison of four models for thermal response test evaluation, ASHRAE Trans. 109 (2003) 131–142.

[18] ASHRAE, ASHRAE handbook - HVAC applications, chapter 34 Geothermal energy, 2011.

[19] V. Wagner, P. Bayer, G. Bisch, M. Kubert, P. Blum, M. Kübert, P. Bayer, Hydraulic characterization of aquifers by thermal response testing: Validation by large-scale tank and field experiments, WATER Resour. Res. 46 (2014) 71–85. doi:10.1016/j.geothermics.2012.10.005.

[20] H. Chae, K. Nagano, Y. Sakata, T. Katsura, T. Kondo, Estimation of fast groundwater flow velocity from thermal response test results, Energy Build. 206 (2020) 109571. doi:10.1016/j.enbuild.2019.109571.

[21] Y. Sakata, T. Katsura, K. Nagano, Multilayer-concept thermal response test: Measurement and analysis methodologies with a case study, Geothermics. 71 (2018) 178–186. doi:10.1016/j.geothermics.2017.09.004.

[22] Y. Sakata, T. Katsura, K. Nagano, M. Ishizuka, Field analysis of stepwise effective thermal conductivity along a borehole heat exchanger under artificial conditions of groundwater flow, Hydrology. 4 (2017) 1–12. doi:10.3390/hydrology4020021.

[23] J. Kallio, N. Leppäharju, I. Martinkauppi, M. Nousiainen, Geoenergy research and its utilization in Finland, Spec. Pap. Geol. Surv. Finl. 2011 (2011) 179–185.

[24] H. Fujii, H. Okubo, K. Nishi, R. Itoi, K. Ohyama, K. Shibata, An improved thermal response test for U-tube ground heat exchanger based on optical fiber thermometers, Geothermics. 38 (2009) 399–406. doi:10.1016/j.geothermics.2009.06.002.

[25] U. Günzel, H. Wilhelm, Estimation of the in-situ thermal resistance of a borehole using the Distributed Temperature Sensing (DTS) technique and the Temperature Recovery

Method (TRM), Geothermics. 29 (2000) 689–700. doi:10.1016/S0375-6505(00)00028-6.

[26] B.M. Freifeld, S. Finsterle, T.C. Onstott, P. Toole, L.M. Pratt, Ground surface temperature reconstructions: Using in situ estimates for thermal conductivity acquired with a fiber-optic distributed thermal perturbation sensor, Geophys. Res. Lett. 35 (2008) 3–7. doi:10.1029/2008GL034762.

[27] T. Saito, S. Hamamoto, E.E. Mon, T. Takemura, H. Saito, T. Komatsu, P. Moldrup, Thermal properties of boring core samples from the Kanto area, Japan: development of predictive models for thermal conductivity and diffusivity, Soils Found. 54 (2014) 116–125.

[28] G. Dalla Santa, F. Peron, A. Galgaro, M. Cultrera, D. Bertermann, J. Mueller, A. Bernardi, 19. Laboratory Measurements of Gravel Thermal Conductivity: An Update Methodological Approach, Energy Procedia. 125 (2017) 671–677. doi:10.1016/j.egypro.2017.08.287.

[29] I.N. Hamdhan, B.G. Clarke, 20. Determination of Thermal Conductivity of Coarse and Fine Sand Soils, Proc. World Geotherm. Congr. 2010. (2010) 1–7. doi:10.1137/120866701.

[30] N. Diao, Q. Li, Z. Fang, Heat transfer in ground heat exchangers with groundwater advection, Int. J. Therm. Sci. 43 (2004) 1203–1211. doi:10.1016/j.ijthermalsci.2004.04.009.

[31] C. Eklöf, S. Gehlin, A Mobile Equipment for Thermal Response Test, (Master's Thesis). Lulea Univ. Technol. Sweden. (1996). https://pure.ltu.se.

[32] J. Raymond, R. Therrien, L. Gosselin, R. Lefebvre, A Review of Thermal Response Test Analysis Using Pumping Test Concepts, Ground Water. 49 (2011) 932–945. doi:10.1111/j.1745-6584.2010.00791.x.

[33] C. Yavuzturk, J.D. Spitler, Short time step response factor model for vertical ground loop heat exchangers, ASHRAE Trans. 105 (1999) 475–485.

[34] W. Choi, R. Ooka, Interpretation of disturbed data in thermal response tests using the infinite line source model and numerical parameter estimation method, Appl. Energy. 148 (2015) 476–488. doi:10.1016/j.apenergy.2015.03.097.

[35] K. Nagano, Standard Procedure of Standard TRT, version 2.0; Heat Pump and Thermal Storage Technology Center of Japan, 2011.

[36] L. Lamarche, J. Raymond, C.H.K. Pambou, Evaluation of the internal and borehole resistances during thermal response tests and impact on ground heat exchanger design, Energies. 11 (2018). doi:10.3390/en11010038.

Chapter 5.

Validation of proposed TRT analysis and determination of borehole size:

Life cycle cost analysis and cost reduction

5.1. Introduction

As social issues of energy demand and carbon emissions have been increased gradually, many countries have enacted energy reduction policies and have funded projects to develop high-performance and environmental-friendly systems [1]. In particular, they have striven to reduce energy consumption in the building sector, which consumes more than 40% of the total energy [2]. The systems utilizing renewable resources such as solar and wind energy have been developed and applied to the buildings to solve environmental problems [3,4]. The efficiency of these systems depends on geographical characteristics, although they can supply high-efficiency and environmental-friendly energy. Since they also require large installation spaces to cover the total loads of the buildings, it is unsuitable for the metropolis where many commercial and residential buildings in expensive neighborhoods are concentrated. On the other hand, a ground source heat pump (GSHP) system utilizing the heat source of the ground that maintains a relatively constant annual temperature has been recognized as a highly efficient system. The GSHP systems with vertical closed-loops are suitable for the cities because it is high-efficient as well as requires small installation spaces. Despite the advantages, the design of the borehole heat exchanger (BHE) without pre-investigation of geological thermal properties has brought about an expensive installation cost by the over/under-designing the system. The over-designed system results in a high initial cost, or the under-designed system needs additional heat sources. The incorrect design also has given a wrong impression of the system and is a hindrance to the growth of the market for the GSHP system.

The essential step to design the BHEs, which are the main component of the GSHP system, is to determine the thermal properties of the ground. The conventional method for determining the thermal properties of the soil is the thermal response test (TRT) proposed by Mogensen [5]. The TRT is an onsite test to continuously inject the heat to circulating fluid in U-tubes and measure their temperature changes at an inlet and outlet of the U-tube. The measured data is then analyzed by using an infinite line source model with least-squares approximation [6]. The analyzed results provide the effective thermal conductivity of the soil and the borehole thermal resistance, which are critical parameters for the design of the GSHP system. The results represent the thickness-weighted average values corresponding to the borehole length in a site. Many studies have proposed various methods to determine more accurate parameters, such as the period of the TRT analysis [7–11], the effect of disturbance from the external environments [12,13], the utilization of additional measuring equipment [14–16]. The numerical methods also made it possible to

perform the TRT under various conditions; the variation of heat injection rates, the borehole sizing, and the thermal properties of materials [12,17–20]. However, the conventional TRT analysis method does not reflect the groundwater flow because it considers only the conduction heat transfer in the ground as homogeneous medium.

The ground in practice is a porous media consisted of complex structures such as water content, particle size and porosity. The ground structures and regional topography decide the intensity of the groundwater flow affecting the performance of the GSHP systems. Many studies have reported on the advection effect and the performance of the GSHP systems [21–25]. Although their reports are available to understand the influence of the groundwater flow on the performance of the GSHP systems, it is challenging to estimate the groundwater velocities in the field sites and to apply their values to the design of the GSHP systems.

As an alternative to the conventional TRT analysis, a moving line source (MLS) model introduced by Carslaw and Jaeger [6] was modified to consider the heat conduction and advection in the ground environment by Diao [26]. The MLS model was utilized in the TRT analysis to simultaneously estimate the thermal conductivity of the soil and the groundwater velocity [27–30]. Their methods were essentially an iterative parameter estimation to find the minimum root mean square error (RMSE) between the TRT data and the calculated results. They determined the design parameters from the conditions of the minimum RMSE, and their RMSE results were under 0.1 K between the calculated results and TRT data. These methods made it possible to predict the performance of the GSHP system during the long-term operation in areas where the groundwater flows rapidly.

The optimal design minimizes the initial installation and the operating cost while maintaining the target performance. Many studies predicted the performance of the GSHP system for long-term operation based on the thickness-weighted average values corresponding to the borehole length. Although their designs are appreciated to predict the performance of the system, they could not provide the appropriate BHE size to reduce the initial cost by figuring out the layers with the high thermal dispersion. In terms of the initial cost of the GSHP system, the cost of the BHE accounts for half of the total cost [31]. Therefore, it is necessary to reduce the total borehole length while maintaining the target performance of the system. To suggest the appropriate size of the BHEs, our research team [32] proposed the TRT method that estimates the thermal properties of the soils in multi-layer, analyzing the temperature recovery in each layer after stopping the TRT. The method utilizing the optical fiber distributed temperature sensors (DTS) effectively figured out the layers with the high thermal dispersion to provide the

appropriate BHE sizing.

For reduction of the initial cost of the GSHP system, this study verifies the effectiveness of the multi-layer TRT analysis method. First, the numerical simulation is carried out to validate the design parameters in the multi-layer, comparing with the TRT data. Second, the required borehole number is determined based on the system performance in the 30^{th} year after operating the GSHP system and the parameters estimated by the TRT analysis methods. Finally, the initial and operating costs are calculated to analyze the life cycle cost (LCC) of the GSHP system. The return of investment (ROI) period is analyzed comparing with an air source heat pump system. In addition, the new TRT method utilizing actively heated fiber optics distributed temperature sensing (A-TRT) is introduced. This method is straightforward than the conventional TRT method on the test set-up and analysis process of the thermal properties in the multi-layer. The groundwater velocities of each layer are estimated, based on the relationship between the effective thermal conductivity and the apparent thermal conductivity suggested in previous studies, which carried out the A-TRT. The LCC of the GSHP system according to the borehole size in the test sites is also calculated for 30 years.

5.2. Heating and cooling load for target building

Fig. 5.1 shows the floor plan and the three dimension modeling of the target building. The building is a six-story office building, and the total floor area is 4672.2 m^2. The spaces in this building are divided into the air conditioning zone and the non-air conditioning zone. The air conditioning zone is 85% of the total area (3971.4 m^2) where the people work in the office space. The hourly building load is calculated by using software tools 'EnergyPlus' and 'OpenStudio'. The weather data are used by TMY3 dataset which is typical meteorological data derived from hourly weather data through 2018 in the ISD (US NOAA's Integrated Surface Database). The building operation schedule is 08:00 to 18:00 on weekdays, and the operating setpoint for heating and cooling is 22℃ and 26℃, respectively. Table. 5. 1 indicates the detailed building information.

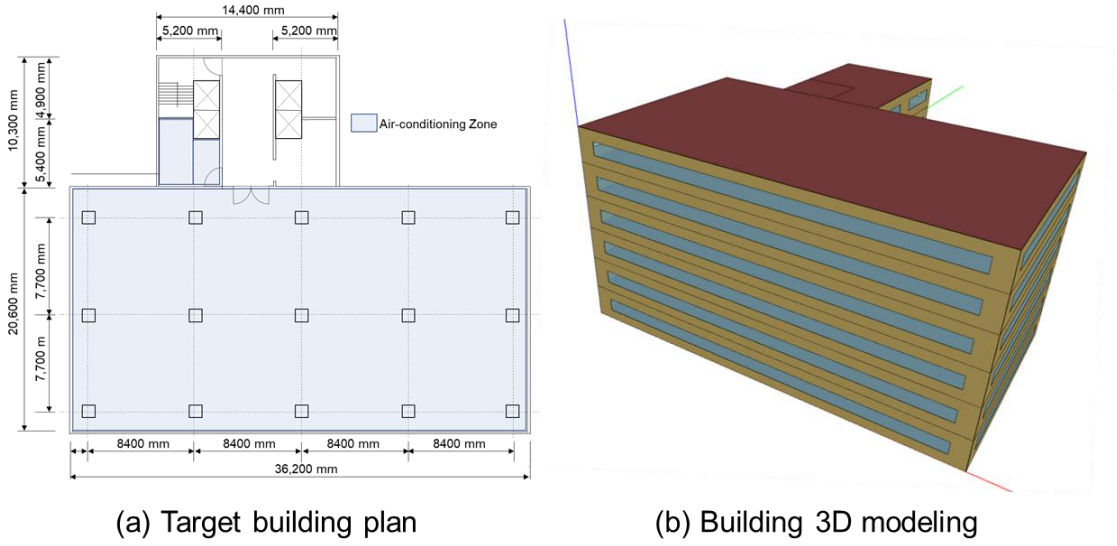

Fig. 5. 1 Target building

Table 5. 1 Building information and parameters

Building information	Value
Building area	Floor area: 778.68 m^2 (height: 3 m) Air-condition zone area: 658.44 m^2 Number of stories: 6 Window-wall ratio: 42.5%
U-value [$W/(m^2\ K)$]	Wall: 0.33, Roof: 0.28, Floor: 0.46, Windows: 3.26
Internal heat gain [W/m^2]	People: 0.15 ($person/m^2$), Lighting: 25, Equipment: 7
Air change rate	25 $m^3/(person\ h)$
Setting temperature [℃]	Heating: 22, Cooling: 26
Operating schedule	08:00-18:00 (from Mon to Fri)

5.3. Numerical model

A numerical model was developed in the ANSYS FLUENT software, which is based on the finite volume method to build the BHEs environment under the ground. The model is fully discretized with a three-dimensional unsteady-state model. The model considers both conduction and advection heat transfer of the ground. The geometry of the ground is composed of three layers with different thermal properties of the material in each layer. The following is a detailed description of the numerical model.

5.3.1. Governing Equation

To study the conjunction of fluid and porous domains, the conservation equations of mass, momentum, and energy in three-dimensional and unsteady state forms are solved simultaneously in three-dimensional geometry. The following assumptions are applied to solve the model in this study:

1) The ground domains are classified under three layers with different thermal properties.
2) The fluid inside the U-tube is incompressible.
3) The boundary on the soil wall and the groundwater temperature are constant regardless of the depth.
4) The heat loss/gain on the ground surface are neglected.

The numerical solution of the mass, the momentum, and the energy conservation in three-dimensional and unsteady state forms were solved as following equations [33].

Mass conservation equation

The equation for conservation of mass, or continuity equation, can be written as follows;

$$\frac{\partial \rho_{\mathrm{f}}}{\partial t} + \nabla \cdot (\rho_{\mathrm{f}} \vec{v}) = 0 \qquad (5\text{-}1)$$

$\vec{v}$ is velocity vector [m/s]

Momentum conservation equation

The porous media models for multiphase flows use a superficial velocity porous formulation based on the volumetric flow rate in a porous region. The momentum equation for the porous media is added to the momentum source term S_i from the standard fluid flow equation.

$$\frac{\partial \rho}{\partial t}(\rho_{\mathrm{f}}\vec{v}) + \nabla \cdot (\rho_{\mathrm{f}}\vec{v}\vec{v}) = -\nabla p + \nabla \cdot (\bar{\bar{\tau}}) + \rho_{\mathrm{f}}\vec{v} + \vec{F} + S_i \tag{5-2}$$

p is the static pressure [N/m^2], $\bar{\bar{\tau}}$ is the stress tensor (N/m^2), $\rho_{\mathrm{f}}\vec{v}$ and $\vec{F}$ are the gravitation body force and external body forces, respectively. S_{mon} is a momentum source term in the simple homogeneous porous media calculated by Eq. 5-3

$$S_i = \mu \frac{150}{D_{\mathrm{p}}^2}\frac{(1-\varepsilon)^2}{\varepsilon^3}\vec{v} + \frac{3.5}{2D_{\mathrm{p}}}\frac{(1-\varepsilon)}{\varepsilon^3}\rho|v|\vec{v} \tag{5-3}$$

μ is the dynamic viscosity [Ps · s], D_{p} is the mean particle diameter [m], and ε is the porosity[-].

In laminar flows through porous media, the pressure drop is typically proportional to velocity. Ignoring convective acceleration and diffusion, the porous media model then reduces to Darcy's Law:

$$\nabla p = -\frac{\mu}{\alpha}\vec{v} \tag{5-4}$$

Energy equitation in porous media

For simulations in which the porous media and fluid flow are assumed to be in thermal equilibrium, the conduction flux in the porous media uses an effective conductivity and the transient term includes the thermal inertia of the solid region on the media:

$$\begin{aligned}\frac{\partial}{\partial t}(\varepsilon\rho_{\mathrm{f}}E_{\mathrm{f}} - (1-\varepsilon)\rho_{\mathrm{s}}E_{\mathrm{s}}) + \nabla \cdot \left(\vec{v}(\rho_{\mathrm{f}}E_{\mathrm{f}} + p)\right) \\ = S_{\mathrm{f}}^h + \nabla \cdot [\lambda_{\mathrm{eff}}\nabla T - (\bar{\bar{\tau}} \cdot \vec{v})]\end{aligned} \tag{5-5}$$

Where, E_{f} is total fluid energy, E_{s} is total solid media energy, ρ_{f} is fluid density, $\rho_{\mathrm{s}}$is solid media density, λ_{eff} is effective thermal conductivity of the media, S_{f}^h is fluid enthalpy source term.

The effective thermal conductivity in the porous media, λ_{eff} is calculated by the volume average of the fluid conductivity and the solid conductivity:

$$\lambda_{\text{eff}} = \varepsilon\lambda_{\text{f}} + (1-\varepsilon)\lambda_{\text{s}} \tag{5-6}$$

Turbulence model

The standard $\kappa-\varepsilon$ model is a model based on model transport equations for the turbulence kinetic energy (κ) and its dissipation rate (ε) on the wall of the U-tube, the standard $\kappa-\varepsilon$ model is used. It provides superior performance for the flows on the boundary layers and offers accurate and fast convergence for high Reynolds number applications. Two-equation turbulence models allow the determination of both a turbulent length and time scale by solving two separate transport equations as follows;

$$\frac{\partial}{\partial t}(\rho\kappa) + \frac{\partial}{\partial x_i}(\rho\kappa v_i) = \frac{\partial}{\partial x_j}\left[(\mu + \frac{\mu_t}{\sigma_\kappa})\frac{\partial\kappa}{\partial x_j}\right] + G_\kappa + G_b - \rho\varepsilon - Y_M + S_\kappa \tag{5-7}$$

$$\frac{\partial}{\partial t}(\rho\varepsilon) + \frac{\partial}{\partial x_i}(\rho\varepsilon v_i) = \frac{\partial}{\partial x_j}\left[(\mu + \frac{\mu_t}{\sigma_\varepsilon})\frac{\partial\varepsilon}{\partial x_j}\right] + C_{1\varepsilon}\frac{\varepsilon}{\kappa}(G_\kappa + C_{3\varepsilon}G_b) - C_{2\varepsilon}\rho\frac{\varepsilon^2}{\kappa} + S_\varepsilon \tag{5-8}$$

Where κ is the turbulent kinetic energy per unit mass (J/kg), ε is the rate of dissipation of turbulent kinetic energy per unit mass (m^2/s^3). G_κ and G_b are the source terms of turbulence kinetic energy due to the mean velocity gradients and buoyancy. Y_M represents the source terms which is contribution of the fluctuating dilatation in compressible turbulence to the overall dissipation rate. The turbulent viscosity, μ_t is computed by combining κ and ε as follows:

$$\mu_t = \rho C_\mu \frac{\kappa^2}{\varepsilon} \tag{5-9}$$

The model constants $C_{1\varepsilon}$, $C_{2\varepsilon}$, C_μ, σ_κ and σ_ε have the flowing values, respectively.

$C_{1\varepsilon} = 1.44,\ C_{2\varepsilon} = 1.92,\ C_\mu = 0.09,\ \sigma_\kappa = 1.0,\ \sigma_\varepsilon = 1.3$

5.3.2. Discretized domain

The discretized model is illustrated in Fig. 5.2 and the geometry has dimensions of 10×10× 105 m (length×width×depth). The geometry consists of three main domains; the fluid domain, borehole domain, surround soils. The fluid domain located in a U-tube was filled with water and the borehole consisted of the backfilled material. The surrounding soil is the porous media with the saturated water-soils and is divided into three layers with different materials.

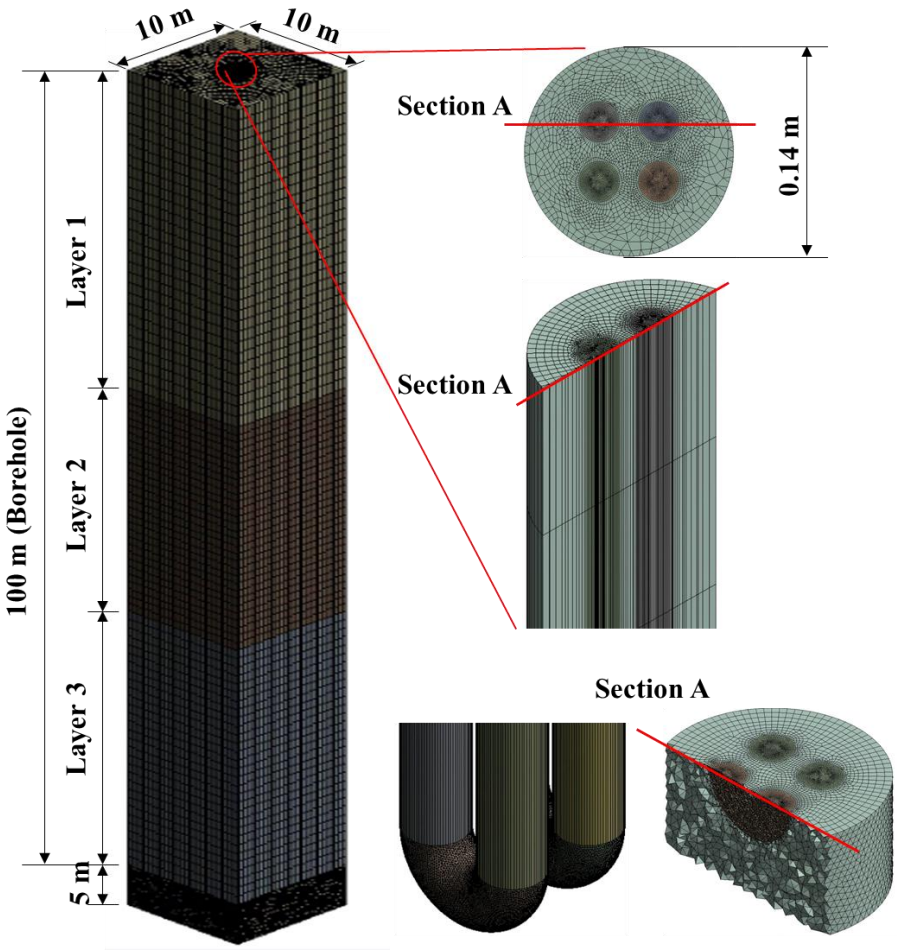

Fig. 5. 2 Discretized numerical model

For effective and appropriate mesh generation, the geometry is divided into sub-domains to optimize mesh element numbers and decrease computation time. In particular, the smaller mesh size was applied to the U-tube and the borehole (generally approximately 1 and 5 mm) to figure

out the energy dissipation and pressure gradient. The sweep meshing method is also used in sweep divisions number of 200 slices with the vertical direction. The U-tube bending part, the bottom part of the borehole and the bottom portion of the soil are meshed by tetrahedron elements. The total mesh element number is 1.46×10^6 elements with average skewness mesh quality of 95%. Table. 5.2 indicates the conditions of the borehole heat exchanger, the U-tube, the circulating fluid and the TRT set-up.

Table 5. 2 Conditions of the thermal response test

Parameter [unit]		Value
Borehole Heat exchanger	Borehole depth [m]	100
	Borehole diameter [m]	0.14
U-tube	Outer/inner diameter of pipe [m]	0.32/0.26
	Shank spacing between pipe centers [m]	0.06
	Thermal conductivity [W/(m K)]	0.45
Circulating fluid; Water	Flow rate [L/min]	20
	Thermal conductivity [W/(m K)]	0.6
Heat injection rate during TRT [kW]		6.0
Initial temperature of ground [℃]		12.2

5.3.3. Boundary conditions

Selecting the boundary conditions is an important process to have an accurate solution. A user-defined function developed by previous studies [34,35] was applied to the variable temperature conditions at the inlet boundaries of the U-tubes in Eq. 5-10. The temperature conditions are considered by the outlet temperature of the U-tube of the previous time step, the flowrate of the circulating fluid and the heat injection. The upper and bottom sides of soil are considered as constant temperature. The boundary conditions applied in the computational fluid dynamic (CFD) model are indicated in Table. 5.3.

$$T_{\mathrm{f,in}}(t) = T_{\mathrm{f,out}}(t-1) + \frac{Q}{\rho_{\mathrm{f}} c_{\mathrm{f}} \dot{m}} \tag{5-10}$$

Table 5. 3 Boundary conditions applied in CFD model

Boundary	Conditions	Value
The upper side of soils	Dirichlet	15 ℃
Front, back, bottom side of soils	Dirichlet	12 ℃
Right and left side of soils	Dirichlet, velocity inlet/pressure outlet	12 ℃, v m/y (depends on cases)
Inlet of U-tube	Dirichlet (time-varying), velocity inlet	Eq. (9), -20 L/min
Outlet of U-tube	Well-type, Pressure outlet	20 L/min

5.4. Life cycle analysis of GSHP system according to TRT analysis methods

5.4.1. Design parameters in multi-layer

In the previous study [32], the practical method for the TRT was proposed to estimate the groundwater velocity and effective thermal conductivity in the multi-layer, using the relaxation time of temperature (RTT), which is the moment when the temperature recovers to a certain level after stopping the heat injection. The vertical temperature profile was measured by the optical-fiber distributed temperature sensors (DTS) located in the supply and return sides of the U-tube. The ground in the test site was divided into three layers, based on the groundwater velocity. The estimated parameters of the soils in each layer are shown in Table. 5.4. The borehole backfill material as permeable materials was assumed to be the same parameter values of the surrounding soil in each layer.

Table 5. 4 Conditions of parameters in each layer

Layer	Depth [m]	λ_{eff} [W/(m K)]	v [m/y]
Layer 1	0-40	2.4	2750
Layer 2	40-68	2.4	58
Layer 3	68-100	2.1	0

5.4.2. Determination of the depths of the zone

The numerical simulation is carried out to emulate a thermal response test (TRT) during the heating and recovery period to validate the multi-layer TRT analysis method. The three-dimensional transient model consists of three layers with the thermal properties, based on the Table. 5.4. The RMSE and temperature average error are used to compare the calculated results with the measured data of the TRT in Eqs. 5-11 and 5-12. Fig. 5.3 shows the temperature change of the TRT data and calculated results at the inlet and outlet pipe for 198 hours. It is noticeable that the results are a good agreement between the developed model results and the TRT data, and the RMSE and an average error value were 0.16℃ and 0.8%, respectively.

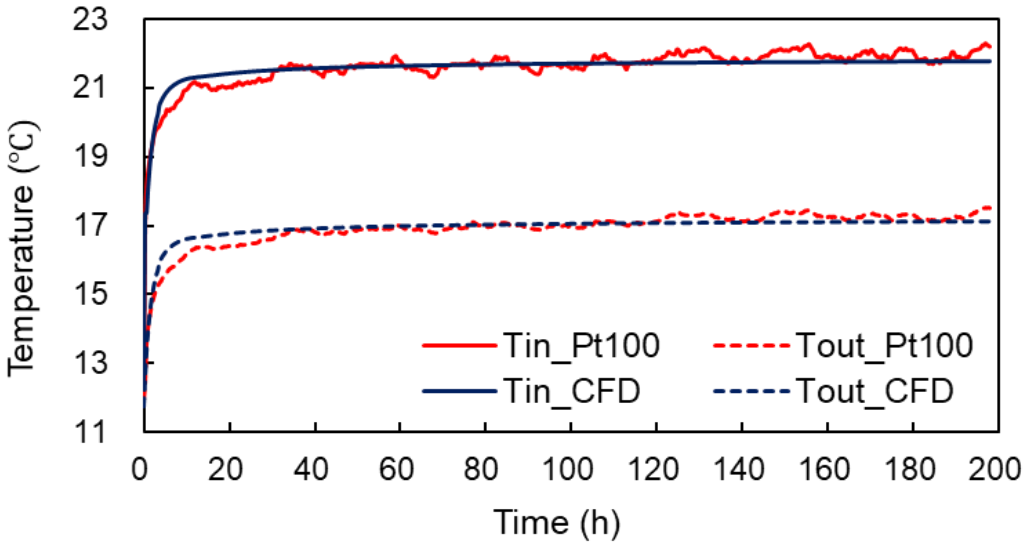

Fig. 5. 3 Comparison of temperature variation between TRT data and CFD results at inlet and outlet pipes

The second step is to validate the parameters in each layer with the different thermal properties of the soil and the groundwater velocities. The numerical simulation is conducted both for heating and after stopping heating periods. The boundary conditions of the CFD model are changed to calculate the temperature recovery after stopping heat injection. The boundary of inlet and outlet domains is also changed from the time-varying temperature to the heat flux of 0 W. The circulating flow rate in the U-tubes is changed from 20 to 0 L/min. Fig. 5.4 indicates the average temperature change of the circulating fluid in each layer between the CFD results and TRT data measured by the DTS. The DTS were inserted in the supply and retune sides of the U-tube and measured the circulating fluid temperature at intervals of 0.5 m during both periods [32]. The experimental and numerical temperature responses in three layers were similar to each other, and the RMSE and average error values were indicated in Table. 55. Fig. 5.5 (a) describes the temperature distribution of the circulating fluid over depth at 10, 60 and 190 h. The temperature distribution in Layer 1 measured from the DTS was unstable. The reason for the temperature fluctuation in Layer 1 was assumed that the DTS was contacted with the inner pipe surface and affected by surrounding soil. The CFD results and the measured data were well-matched except for layer 1. Fig. 5.5 (b) demonstrates the temperature distribution inside the borehole at depths of -20, -55 and -85 m. It illustrated that the groundwater flow affects the temperature distribution in the borehole. In particular, the borehole temperature at a depth of -20 m was higher than that of a depth of -85 m because of being affected by the fast groundwater velocity.

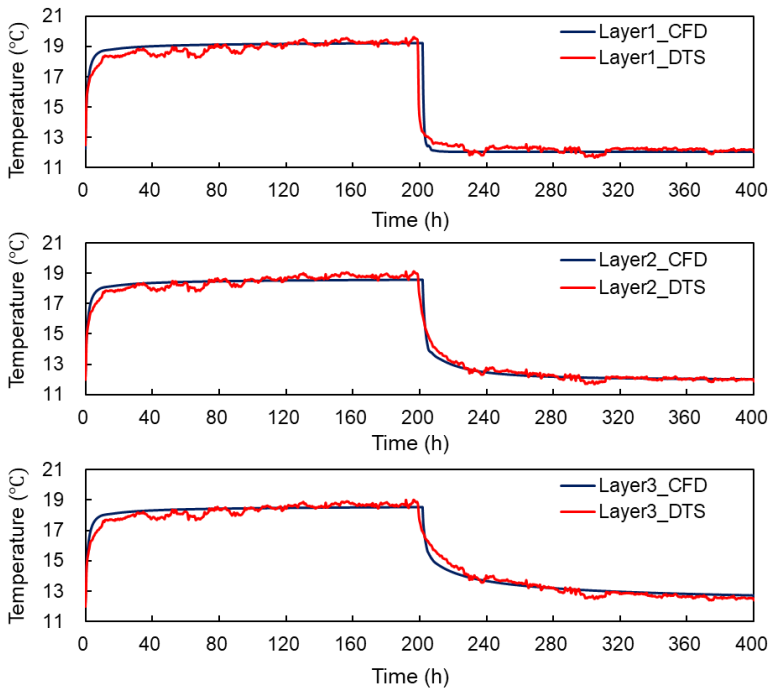

Fig. 5. 4 Temperature change of circulating fluid in each layer

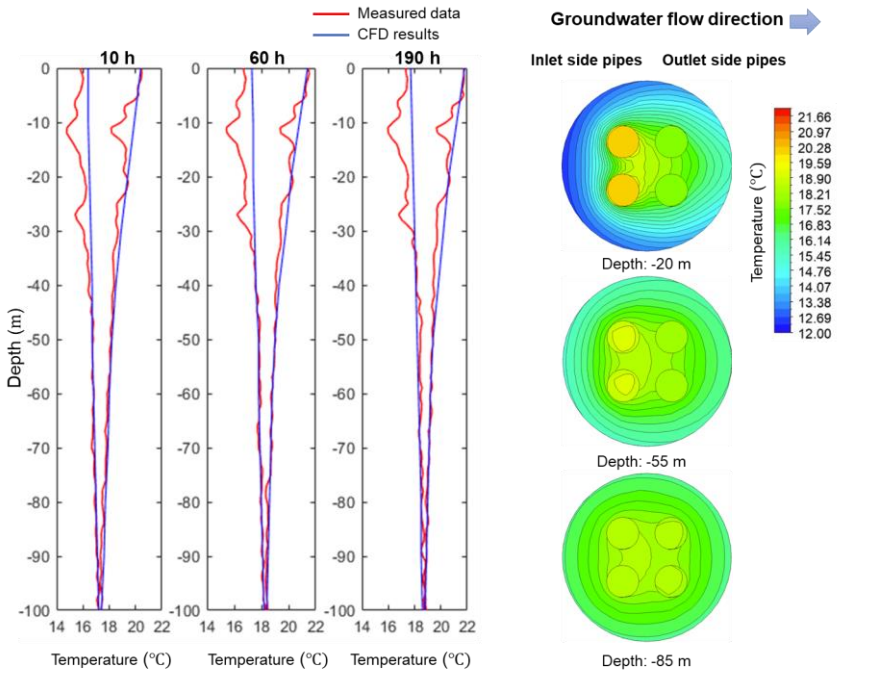

Fig. 5. 5 Temperature distribution over depth; (a) temperature comparison between the CFD results and the DTS data over depth, (b) temperature distribution in the borehole at 60 h after heat injection

Table 5. 5 RMSE and temperature error in each layer

Error	Period (h)	Layer1	Layer2	Layer3
RMSE (℃)	Heating (0-198)	0.27	0.25	0.25
RMSE (℃)	After stopping heating (198-400)	1.44	1.39	1.40
Error (%)	Heating (0-198)	0.31	0.16	0.22
Error (%)	After stopping heating (198-400)	2.32	1.22	1.62

5.4.3. Estimation of the groundwater velocity in the zones

In general, geothermal energy is regarded as the inexhaustible potential source as the heat source/sink. However, the operation of the GSHP system where the many BHEs are installed in the restricted areas can deplete the geothermal potential by the unbalanced building load. It leads to degradation of the system performance due to the temperature increase/decrease of the ground. In particular, the long-term operation of the GSHP system causes the sequential degradation of the system performance over time when the ground is regarded as the solid domain considering thermal diffusion. In practice, the ground is the porous media consisted of the solid and fluid matrix where the heat is dispersed by conduction and advection. The effect of advection by the groundwater flow can prevent depletion of the geothermal potential, effectively. Therefore, it is necessary that the GSHP system that can be used semi-permanently is designed by predicting the ground temperature and the system performance during the long-term operation, considering both the groundwater flow rate and thermal conductivity. This study evaluates the system performance and the LCC during long-term operation. The GSHP system is designed by using the parameters estimated by the TRT analysis results, based on the previous study [29,32]. The conditions of each case are described as follows, and the design parameters of the cases are summarized in Table 7.

1) Case 1: Results of the TRT analysis considering both heat conduction and advection in multi-layer.
2) Case 2: Results of the TRT analysis considering both heat conduction and advection in single layer.
3) Case 3: Results of the conventional TRT analysis considering only heat conduction.
4) Case 4: Determination of the appropriate borehole length; the estimated parameters are obtained from the layer with high thermal dispersion based on Case 1.

The heating and cooling load of the office building was calculated to design the GSHP

system corresponding to the weather data in the test site, based on the building conditions in Chapter 5.2. Fig. 5.6 shows the heating and cooling load of the building in Kazuno City (40°19′ N and 140°78′ E), Japan where the TRT was carried out [32]. Kazuno City is located in the north area of Japan. The maximum, minimum, and average outdoor temperatures were 35.6, -18.4, and 9.6℃, respectively. Table. 5.6 indicates the monthly amount of heating and cooling loads. The heating load is 2.6 times higher than the cooling load.

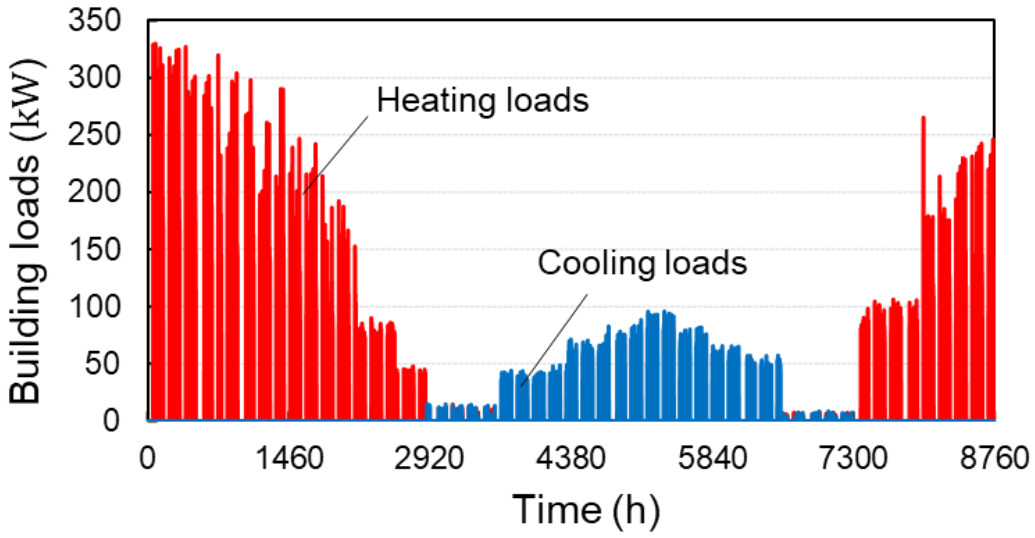

Fig. 5. 6 Heating and cooling loads of building

Table 5. 6 Monthly heating and cooling loads

Load	Jan	Feb	Mar	Apr	May	Jun	Jul	Aug	Sep	Oct	Nov	Dec	Total
Heating Load [GJ]	123.4	105.6	81.3	31.9	1.6	0.0	0.0	0.0	0.0	1.3	46.1	92.9	484.0
Cooling Load [GJ]	0.0	0.0	0.0	0.8	2.2	32.0	52.0	57.2	39.1	1.2	0.0	0.0	184.5

The GSHP simulation tool “Ground Club” is used to calculate the ground temperature, the entering water temperature (EWT) and the coefficient of performance (COP) of the GSHP system during a long-term period. The simulation tool calculates the temperature variation on the borehole walls applied to the moving infinite cylinder source model considering the groundwater flow and time-varying heat flux conditions in the multiple BHEs and the multi-layer

environments. The theoretical details of the simulation tool were explained in previous studies [36–38], and the accuracy of the results was verified by the comparison between the calculated results and the long-term operating data of the GSHP system in the previous study [32]. The COP for heating and cooling is calculated by a simplified linear formula for the performance curve, which is driven by the relationship between the COP of the heat pump and EWT as indicated in Eqs. 5-13 and 5-14.

$$COP_{\mathrm{h}} = 0.1T + 3.686 \tag{5-13}$$

$$COP_{\mathrm{c}} = -0.158T + 9.487 \tag{5-14}$$

Fig. 5.7 shows the required borehole number to achieve target performance in the 30th year after operating the GSHP system. The required number of the BHEs in each case was determined to maintain the COP of 3.5 for heating in response to the building load. The boreholes are installed at intervals of 5 m in the assumed site area (40×40 m^2), increasing the borehole number from 10 to 64 sequentially. Fig. 5.7 demonstrates the required borehole numbers in each case, based on the COP in the 30th year. The required borehole number in Cases 1 and 2, which considered the groundwater velocity and thermal conductivity, were similar, whereas Case 3, which considered only thermal conductivity, needed more borehole numbers. Fig. 5.8 shows the temperature change of the ground for 30 years. Here, the ground temperature is the average temperature on all borehole surfaces in conditions of the required borehole numbers of the cases. The ground temperature in Case 3, which considers thermal diffusion by the conduction heat transfer, decreased over time, whereas the ground temperature in Case 1, 2 and 4 became stable owing to the effect of advection. The performance of the GSHP system mainly depends on the ground temperature. To prevent the over-design of the GSHP system, it is necessary to design the BHEs by predicting the system performance considering both the groundwater velocity and the effective thermal conductivity. In particular, the rate of change of COP in Case 4 considering the layer with the high thermal dispersion was higher than that of other cases because the ground temperature maintained a relatively high temperature. The total length of the BHEs in Case 4 could reduce 16.8% compared with Case 3. Table. 5.7 shows the calculation condition and the total length of the BHEs. Determining the borehole size considering the layers with high thermal dispersion in multi-layer made it possible to reduce the initial investment cost of the GSHP system.

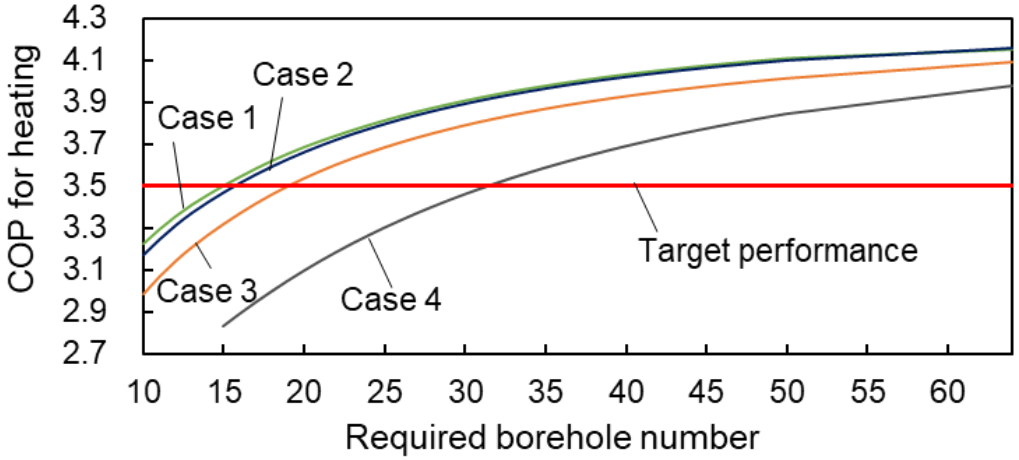

Fig. 5. 7 Required borehole numbers based on COP of the 30th year

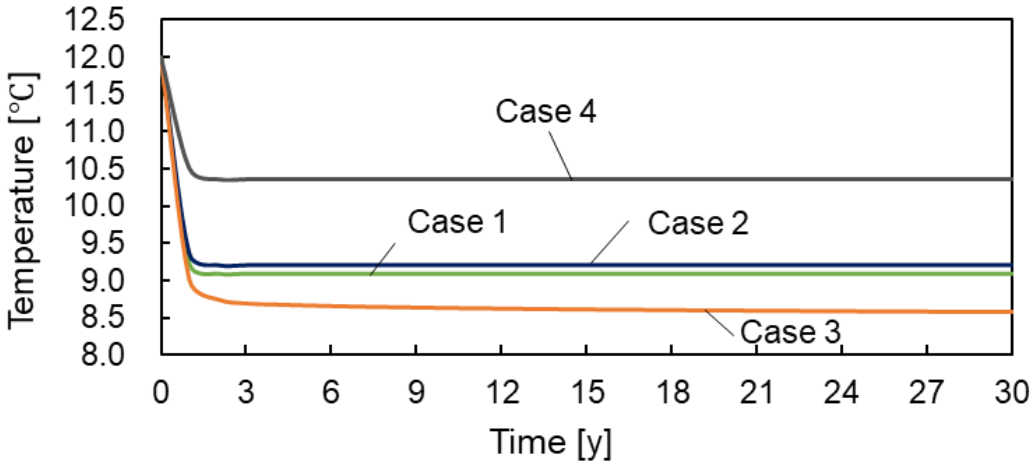

Fig. 5. 8 Temperature change of the ground for 30 years

Table 5. 7 Calculation conditions and total length of BHEs

Case	λ_{eff} [W/(m K)]	v [m/y]	L_{bh} [m]	Borehole number	Total L_{bh} [m]
Case 1	2.4/2.4/2.1	2750/58/0	40/28/32	15	1500
Case 2	4.7	120	100	16	1600
Case 3	9.5	0	100	20	2000
Case 4	2.4	2750	40	31	1240

5.4.4. Life cycle cost analysis

For analysis of the LCC, the present value method in Eq. 5-15 was used for non-continuous costs, such as initial costs. The present value is defined as the present value of the future net cash flows from an investment. Annual recurring costs, such as electric charges and maintenance costs, were applied to the present worth of annuity factor (PWAF) method in Eq. 5-16, and lifetime cost was analyzed with the sum of the two equations in Eq. 5-17.

$$PV(y) = (1 - C_{sub}) \times \frac{IC}{(1 + r_t)^y} \tag{5-15}$$

$$PWAF(y) = \big(OC(y) + MC(y)\big) \times \frac{(1 + r_t)^y - 1}{r_t(1 + r_t)^y} \tag{5-16}$$

$$P(y) = PV(y) + PWAF(y) \tag{5-17}$$

Here, IC is initial cost, C_{sub} is government subside, y is number of compounding periods, OC is annual cost of the operating system, and MC is maintenance cost. r_t is interest rate and assumed to be a target of the Japan government (r_t= 3%).

Fig. 5.9 shows the cost rate of each section of the GSHP system in the previous studies [31,39,40]. According to the report of Department of Energy and Climate Change [41], the initial cost of the BHE is over 50% in the GSHP system, and the drilling cost is over 60% on the part of the BHE. Regardless of country or location, the rate of the system cost is similar, and the BHE is around half of the total system cost. On the other hand, the equipment or drilling costs are sensitive and depend on its cost in each country or company. In this study, the initial cost of the GSHP system is calculated by approximate cost functions in the previous study [41]. This study carried out the inquiry survey about initial costs of the GSHP system in Japan, and derived approximated functions of capital costs for borehole heat exchangers and heat pumps. To calculate the payback period of the GSHP system, the life cycle cost of an air-source heat pump (ASHP) system was calculated. The initial cost of the ASHP system was assumed to be 9,000 U.S dollars/10 kW, considering the product pricing lists of Japanese companies.

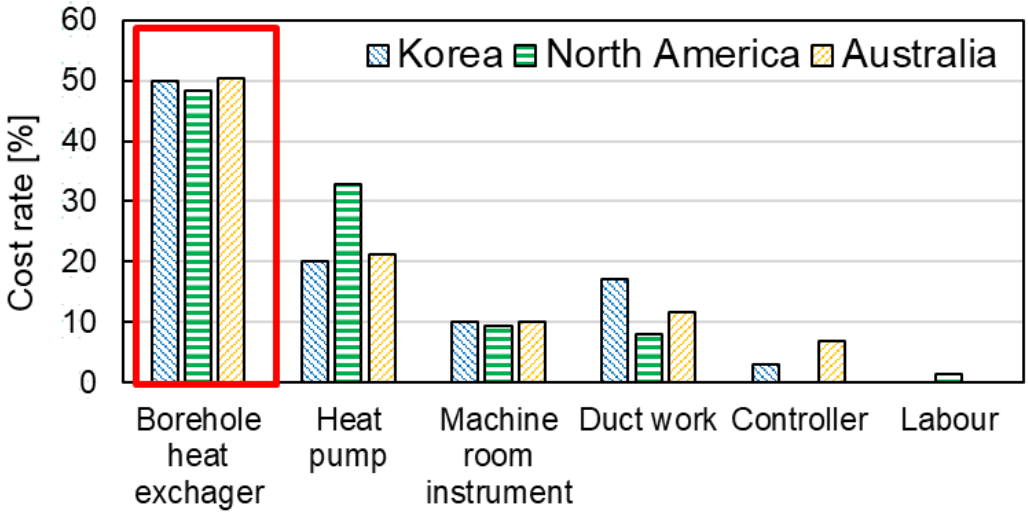

Fig. 5. 9 Cost rate of each section of the GSHP system in the previous studies [31,39,40]

The operating costs of the GSHP system were calculated in Eq. 5-18, based on the electric power consumption for 30 years. The COP is calculated from the performance curve of the heat pump. The COP of the ASHP system is calculated by the relationship between the COP and ambient temperature [42]. The maintenance and replacement price does not cost every year, unlike operating costs, and its cost depends on the equipment. Additional costs were considered in response to the periods with reference to the previous study [39].

$$OC = \sum_{h=1}^{8760} \frac{Q(t)}{COP(t)} E_{cost} \tag{5-18}$$

Here, E_{cost} used as the public rates at 2020 fiscal year of the electric company (0.21 U.S dollars /kWh).

Fig. 5.10 shows the life cycle cost for 30 years according to the government subsidy. Table. 5.8 shows the initial cost of each case in the condition without the government subsidy. Based on Case 3, the initial cost could save 12.8% (Case 1), 10.2% (Case 2), 16.8% (Case 4). As a result of the approximate initial cost, the GSHP systems were about 2-2.5 times more expensive than the ASHP system. On the other hand, the operating costs of the GSHP system and the ASHP system

for the first year were calculated to be 18.8 and 51.3 U.S. dollars, respectively. The Japanese government has subsidized to encourage the installation of the renewable system. The government subsidy has been paid as the extra charge on the initial investment cost, but the extra charges have been applied differently for each local government. In this study, the government subsidy is decided so that the investment cost can be recovered within 10 years, considering the extra charge of 15 and 30%. The ROI could be recovered within 10 years in cases considering the groundwater flow when 30% of the government subsidy is subsidized. Fig. 5.11 shows the return of investment period according to the government subsidy. The GSHP system has high efficiency but an expensive system. Notwithstanding, the introduction of the GSHP system in the test site is considered reasonable and economical when the government subsidy is subsidized.

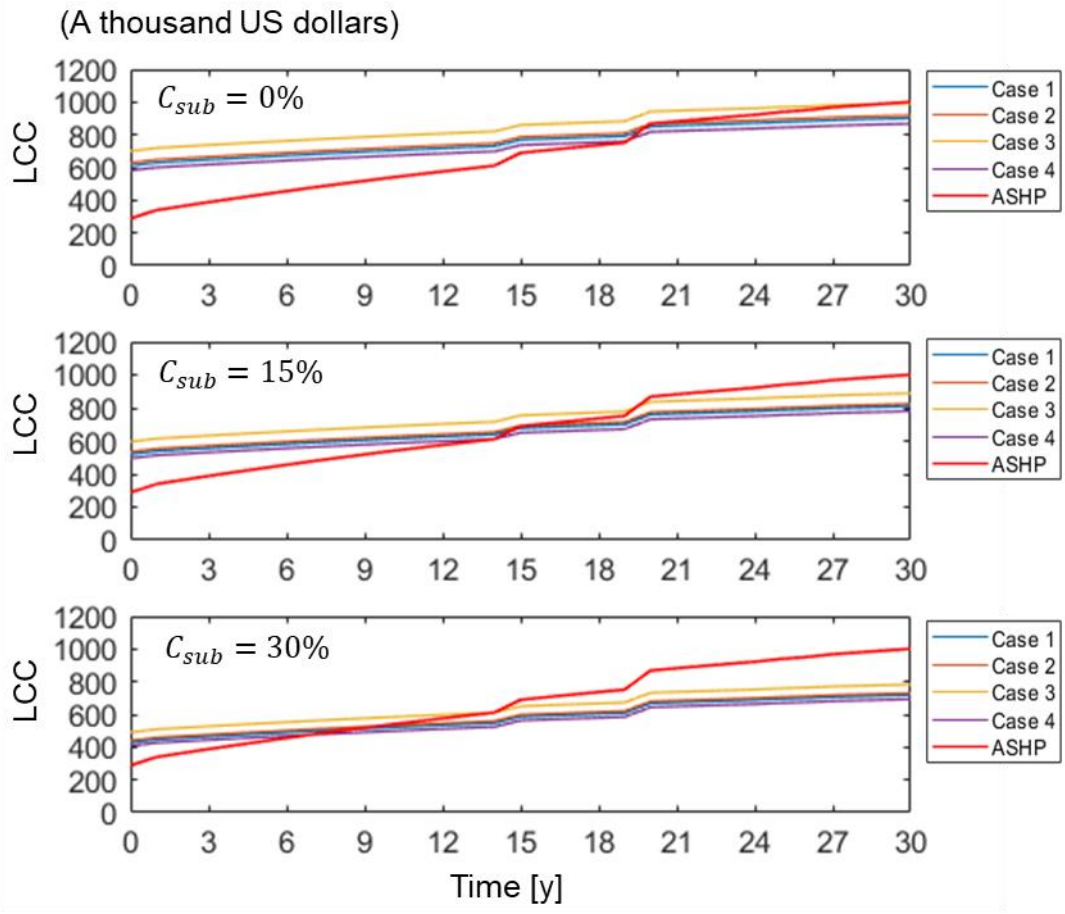

Fig. 5. 10 Life cycle cost according to the government subsidy

Table 5. 8 Initial cost in each case

Case	Part of BHE		Part of Heat pump	
	Cost (A thousand U.S dollars)	**Cost rate (%)**	**Cost (A thousand U.S dollars)**	**Cost rate (%)**
Case 1	307.5	50.4	303.1	49.6
Case 2	325.7	51.8	303.1	48.2
Case 3	397.2	56.7	303.1	43.3
Case 4	279.3	48.0	303.1	52.0

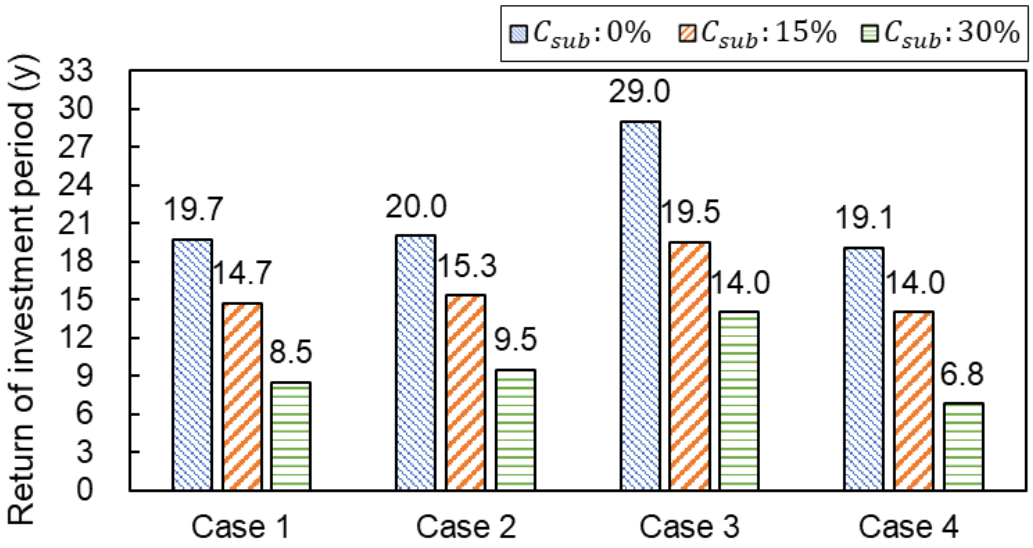

Fig. 5. 11 Return of investment period according to the government subsidy

5.5. Calculation of appropriate borehole length by using the multi-layer TRT analysis

5.5.1. Thermal response test utilizing the actively heated fiber optics distributed temperature sensing

The conventional TRT method monitors the temperature of the circulating fluid in the U-tubes. The temperature change is dominated by the heat injection and the circulating flow rate throughout the whole borehole. This method could not quantify the groundwater flow and thermal conductivity in the distributed layers along the boreholes. The previous study [32] focused on temperature recovery after stopping heat injection. Although the method is effective to observe the natural thermal dispersion and determine the design parameters in the multi-layers, it needs tests during both heating and recovering periods. It is also a difficult process to identify the heat exchanger rate calculated by the temperature gradients of the fluid in each layer. As an alternative to the conventional TRT method, a new method has been proposed for the thermal response test utilizing the actively heated fiber optics distributed temperature sensing (A-DTS). The A-DTS integrated between the heating cable and sensing cable could inject the constant heat flux and measure the fluid temperature in the U-tube throughout the whole borehole without circulating fluid. This chapter examines the previous studies [43,44] conducted on the TRT utilizing the A-DTS and estimates the groundwater velocities. The appropriate borehole size is proposed in the areas where the TRT was performed.

5.5.2. Analysis results of the thermal parameters according to the end time of the TRT

The previous studies [43,44] investigated the effective thermal conductivity (λ_{eff}) of the soils through the laboratory measurements of core samples and estimated the apparent effective thermal conductivity (λ_{a}) including the effect of both conduction and advection in each layer. Fig. 5.12 (a) and Fig. 5.13 (a) were the results of the multi-layer TRT analysis in Guelph (Canada), and Changzhou (China). Based on their results, the groundwater velocities were estimated by using a moving line source (MLS) model. First, the boundary was set up by the average rate of λ_{a} to λ_{eff} of all layers shown in Fig. 5.12 (b) and 5.13 (b). The groups of the layers were formed by the values of the rate of λ_{a} to λ_{eff}, based on the boundary to simply calculate the performance of the GSHP system in the multi-layer condition. The λ_{a} and λ_{eff} of the grouped layers were

represented by their average values. The groundwater velocities were determined by the relationship among the λ_a, λ_{eff} and v in Fig. 5.14. The relationship was calculated by using MLS model in Eqs. 5-19 to 5-21. The λ_a was calculated by temperature slop for 12 to 60 h in Eq. 5-22. Fig. 5.12 (c) and Fig. 5.13 (c) were the calculated groundwater velocities in layers. Since the thermal properties of layer 1 in Area 1 and Area 2 were not provided, these layers were applied to the average thermal conductivity in the condition without groundwater flow. Table. 5.9 and 5.10 show the λ_a, λ_{eff} and v of each layer in Area 1 and Area 2.

$$T(\lambda_{eff}, v, r, \varphi, t) - T_0 = \frac{q}{4\pi\lambda_{eff}} \exp\left(\frac{Ur}{2\alpha} cos\varphi\right) \int_0^{\frac{4\alpha t}{r^2}} \frac{1}{\beta} \exp\left(-\frac{1}{\beta} - \frac{U^2 r^2 \beta}{16\alpha^2}\right) d\beta \tag{5-19}$$

$$T_f(t) = \frac{1}{2\pi} \int_0^{2\pi} T(\lambda_{eff}, v, r_{bh}, \varphi, t) d\varphi + R_{bh} q + T_0 \tag{5-20}$$

$$U = v c_w \rho_w / c_{eff} \rho_{eff} \tag{5-21}$$

$$\lambda_a = \frac{q}{4\pi k}, \tag{5-22}$$

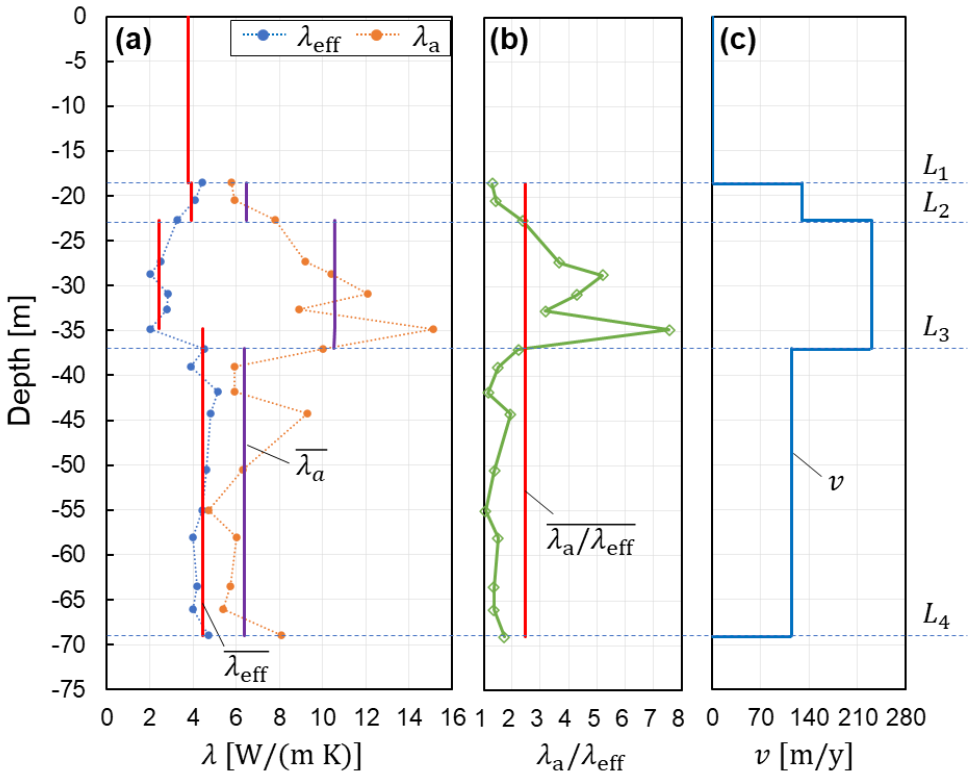

Fig. 5. 12 Geological conditions and groundwater velocity in Area 1 (Canada) [44]

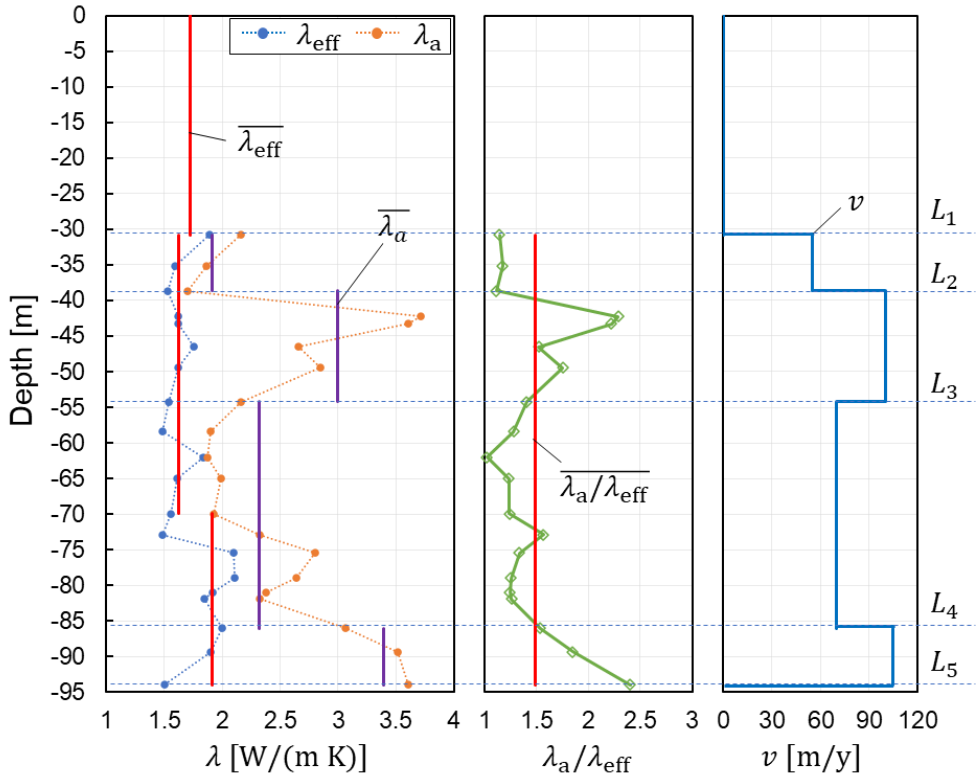

Fig. 5. 13 Geological conditions and groundwater velocity in Area 2 (China) [43]

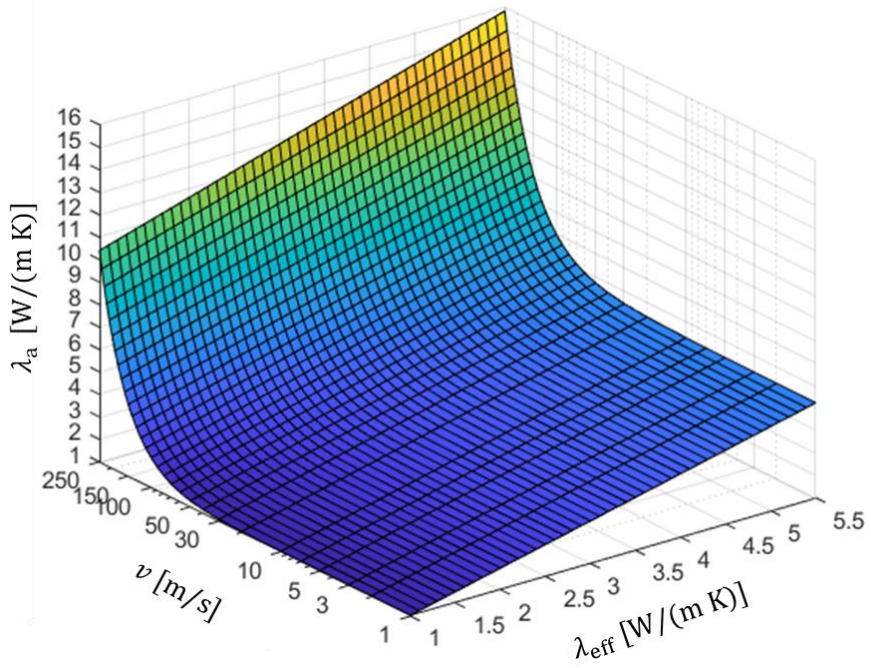

Fig. 5. 14 Relationship among the λ_a, λ_{eff} and v

Table 5. 9 Thermal properties of each layer in Area 1

Area 1	Start depth of layer [m]	End depth of layer [m]	Length [m]	λ_{eff} [W/(m K)]	λ_a [W/(m K)]	v [m/y]
Layer 1	0	18.5	18.5	3.78	-	0
Layer 2	18.5	23	4.5	3.92	6.48	130
Layer 3	23	37	14	2.42	10.51	230
Layer 4	37	69	32	4.43	6.37	115

Table 5. 10 Thermal properties of each layer in Area 2

Area 1	Start depth of layer [m]	End depth of layer [m]	Length [m]	λ_{eff} [W/(m K)]	λ_a [W/(m K)]	v [m/y]
Layer 1	0	31	31	1.72	-	0
Layer 2	31	38.5	7.5	1.62	1.81	55
Layer 3	38.5	54	15.5	1.62	3.00	100
Layer 4	54	86	32	1.74	2.30	70
Layer 5	86	94	8	1.91	3.39	105

5.5.3. Appropriate borehole sizing and LCC analysis

Fig. 5.15 shows the heating and cooling loads of the buildings in the areas where the TRTs were carried out in previous studies [43,44]. Area 1 is located in Guelph, Canada [44]. This area has cold winters and warm, humid summers. The climate in Area 2 located in Changzhou, China is a humid subtropical region with cool winters and hot and humid summers [43]. The hourly building loads were calculated in the same building conditions as mentioned in Chapter 5.2, applying to weather data of Area1 and Area 2.

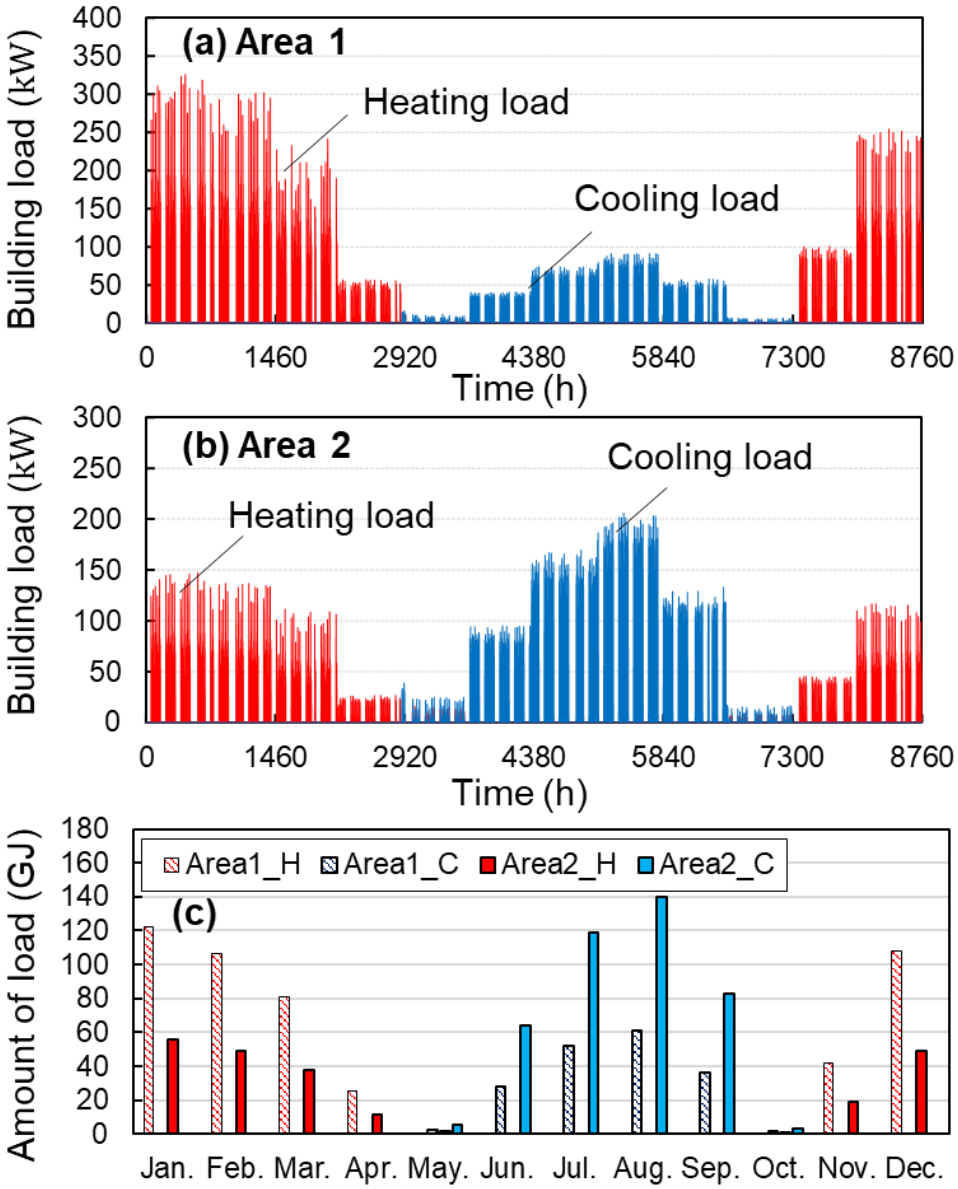

Fig. 5. 15 Heating and cooling loads of the buildings; (a) Area 1 (Guelph, Canada), (b) Area 2 (Changzhou, China) and (c) monthly amount of heating and cooling loads

For the design of the appropriate borehole size, the required borehole number in Area 1, the cold area, was determined to maintain the COP of 3.5 for heating in response to the building load. On the other hand, the required borehole number in Area 2, the humid subtropical region, was calculated to maintain the COP of 4.0 for cooling. For each case under the conditions in Area 1 and Area 2, the baseline of the cases consists of the total layers where the TRT is carried out (four layers in Area 1, five layers in Area 2). The borehole length in the following cases is determined

by subtracting the bottom layer, progressively. Table. 5.11 indicates the conditions of each case in Area 1 and Area 2. The case conditions consisted of a design parameter considering only the apparent effective thermal conductivity and both the effective thermal conductivity and the groundwater velocity to calculate the performance of the GSHP system.

Table 5. 11 Conditions of each case in Area 1 and Area 2

Area	Case	Design parameter	L_{bh} (m)	Layer
Area 1	A1-1-1	λ_a	69	Layer 1 to 4
	A1-1-2		37	Layer 1 to 3
	A1-2-1	λ_{eff} and v	69	Layer 1 to 4
	A1-2-2		37	Layer 1 to 3
Area 2	A2-1-1	λ_a	94	Layer 1 to 5
	A2-1-2		86	Layer 1 to 4
	A2-1-3		54	Layer 1 to 3
	A2-2-1	λ_{eff} and v	94	Layer 1 to 5
	A2-2-2		86	Layer 1 to 4
	A2-2-3		54	Layer 1 to 3

Fig. 5.16 and 5.17 shows the required borehole number to achieve target performance and the temperature change of the ground over time in Area 1 and 2. The required borehole number was determined to achieve a target performance by changing the borehole number from 10 to 64 in the same conditions mentioned in Chapter 5.3. The required borehole numbers in Area 1 were 24, 62, 16 and 37, and the required borehole numbers in Area 2 were 30, 34, 20, 24 and 49 except for A2-1-3, respectively. In both Areas, the design of the BHEs considering the groundwater flow was able to reduce 30-40% of the total BHE length by effect of advection. Meanwhile, the total BHE length in Area 2 was longer than that of Area 1. The main reason is that the effective thermal conductivity and the groundwater velocity in Area 1 were about 2 times higher than that of Area 2 despite different conditions such as the building loads, the outdoor temperature and the initial

temperature of the ground. The performance of A2-1-3 in the 30th year could not be obtained 4.0 of COP for cooling, even though the maximum numbers of boreholes (64 boreholes) were installed in the test site. As a result, the total borehole length in both Areas was the shortest in the whole borehole size where the TRT was carried out. The reason is that the thermal dispersion in both Areas was high in the bottom layer.

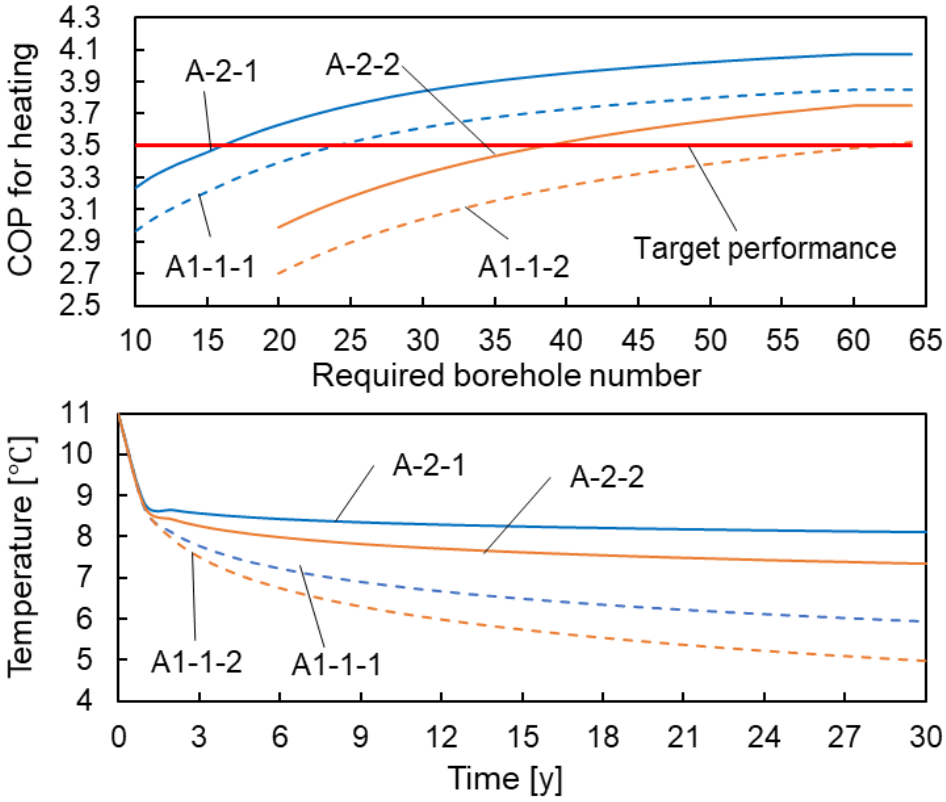

Fig. 5. 16 Required borehole numbers and the temperature change of the ground over time (Area 1 [Guelph, Canada])

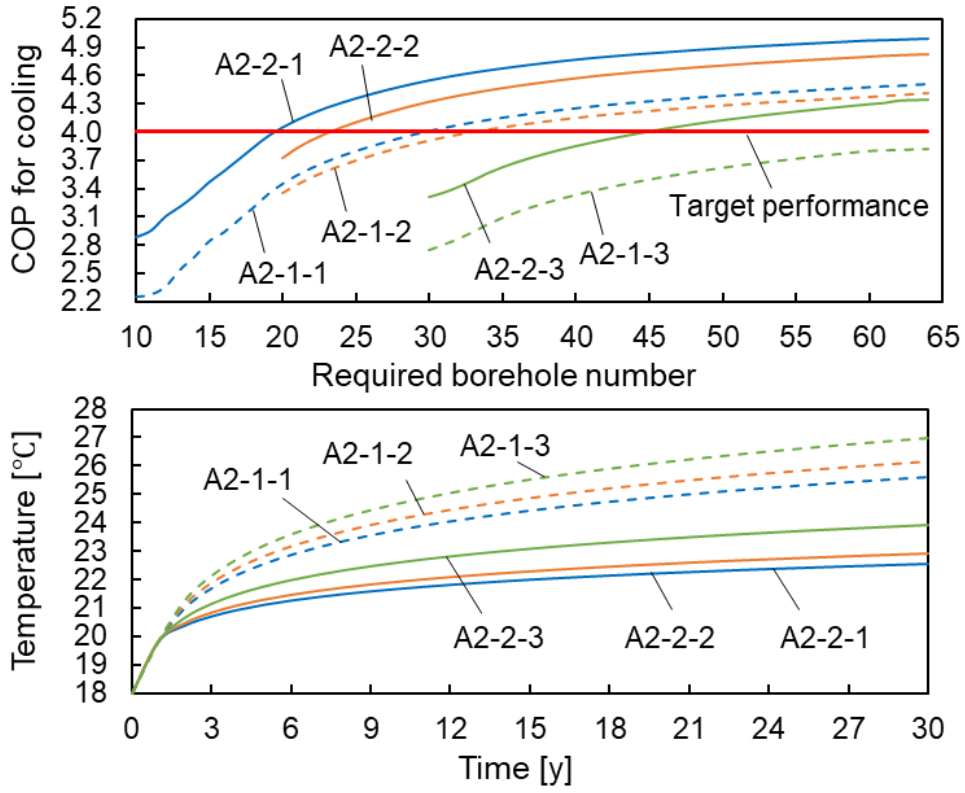

Fig. 5. 17 Required borehole numbers and the temperature change of the ground over time (Area 2 [Changzhou, China])

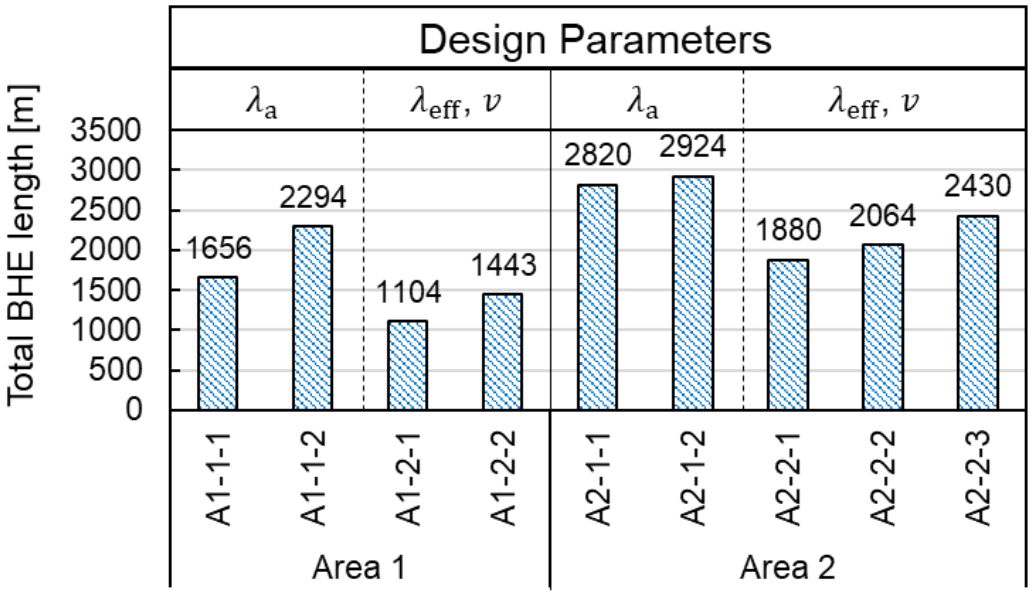

Fig. 5. 18 Total borehole length in each case

Fig. 5.19 and 5.20 show the life cycle cost for 30 years according to the government subsidy in Area 1 and 2. The initial and operating cost was calculated the same way in Chapter 5.4. In Area 1, A1-2-1 with the shortest total BHE length was able to recover the initial investment cost within 10 years, regardless of government subsidies. On the other hand, the initial investment cost in Area 2 could not be recovered within 30 years without government subsidies. In Area 2, when the government subsidy of 60% was supported to reduce the initial cost of the GSHP system, only A2-2-1 was able to recover the initial investment cost within 10 years. The main reason for the difference in the payback period between Area 1 and 2 recovery years was not only the thermal properties of the ground but also the performance of the ASHP system, which is affected by the outside temperature. In Area 1 as the cold region, the operating cost of the GSHP system was cheaper than that of the ASHP system. However, in Area 2 as the subtropical region, the operating cost difference between the GSHP and the ASHP systems was relatively small.

This study proposed the method minimizing the total BHEs length while maintaining the target performance of the system. It confirmed the usefulness of the multilayer TRT analysis methods, which is a prerequisite for the minimum BHEs length. It was possible to reduce the initial investment cost by 10-35%, compared with the conventional design method. On the other hand, the ROI period depended on the thermal properties of the ground and the climatic environment in the test site, compared with the ASHP system. The GSHP systems have a high-efficiency system compared to other heat sources, but the expensive investment cost is a big obstacle to encourage the application of the system. To reduce the initial investment cost, it is necessary to improve the high efficiency of the borehole heat exchanger and the hole drilling method.

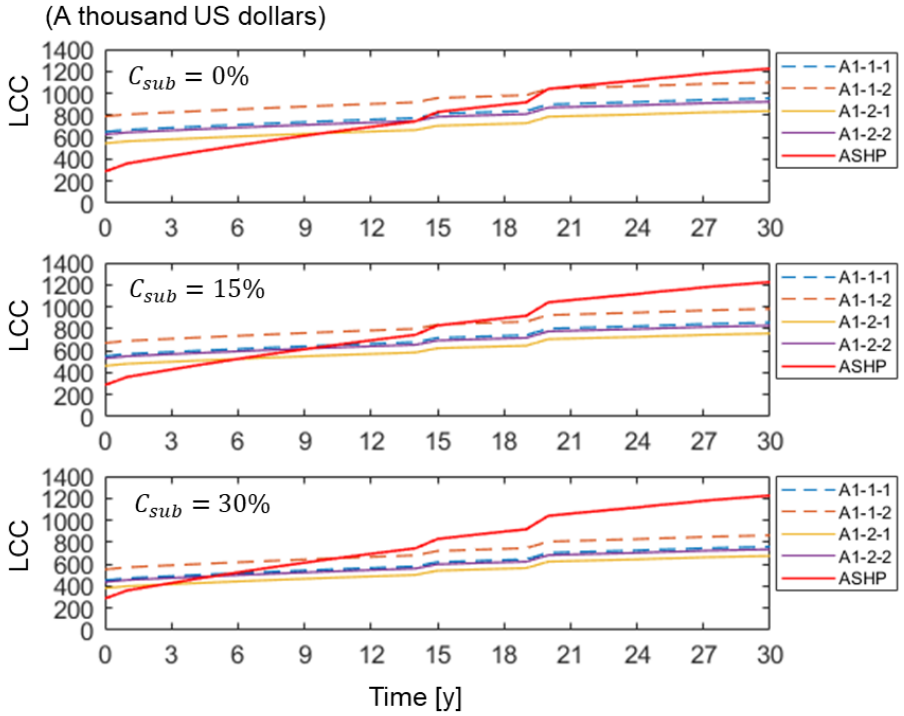

Fig. 5. 19 Life cycle cost according to the government subsidy (Area 1 [Guelph, Canada])

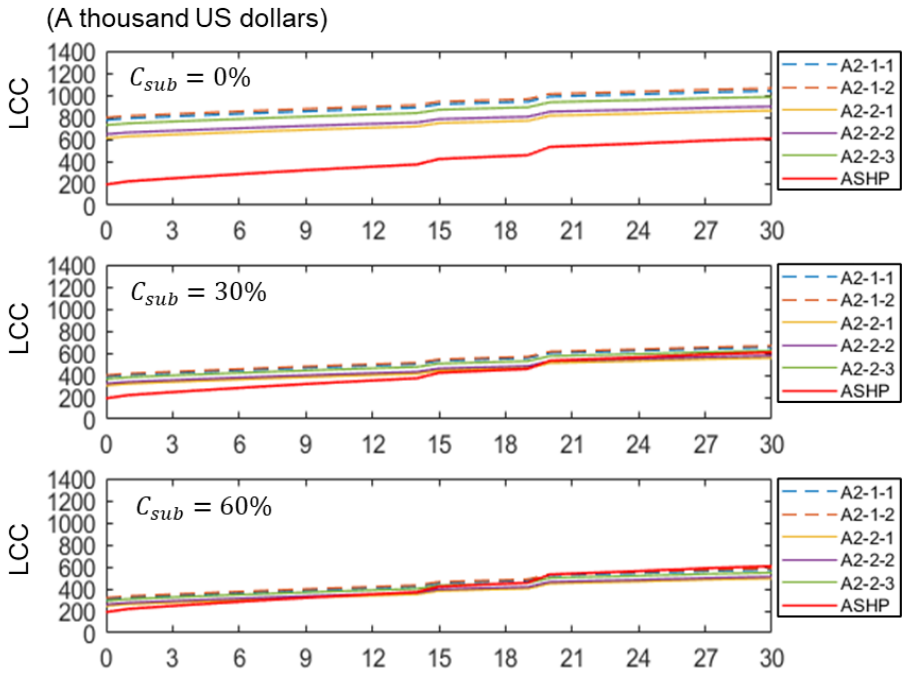

Fig. 5. 20 Life cycle cost according to the government subsidy (Area 2 [Changzhou, China])

5.6. Summary

This Chapter validated the effectiveness of the multi-layer TRT analysis method, reflecting both groundwater flow and effective thermal conductivity. The method could provide an appropriate borehole length by determining the layers with high thermal dispersion to reduce the construction investment of the BHEs. The numerical simulation was carried out to emulate the TRT during the heating and recovery period. The RMSE and the temperature error were under 0.27 K and 0.31% in all layers. The effect of the TRT analysis methods on the long-term operation of the GSHP system was evaluated. Based on the thermal properties of the soils estimated by the TRT analysis methods, the ground temperature change and the performance of the GSHP system were predicted for 30 years according to the building loads. As a result, the GSHP system designed by considering the layer with high thermal dispersion could save 16.8% of the initial investment, compared with the system designed by the conventional TRT method. The ROI period is 19.1, 14.0 and 6.8 years according to 0, 15, 30% of government subsidies, compared with the ASHP system.

In addition, as an alternative to the conventional TRT method, the new method utilizing actively heated fiber optics distributed temperature sensing was introduced. The groundwater velocities in the multi-layer were estimated by the relationship among the λ_{a}, λ_{eff} and v, utilizing the moving line source model. Based on the thermal parameters of the multi-layer, an appropriate borehole length in Area 1 and 2 was determined. As a result, in both Areas, the design of the BHEs considering the groundwater flow was able to reduce 30-40% of the total BHE length by the effect of advection. The borehole length where the TRT was carried out was appropriate in both Areas because the bottom layer has a high thermal dispersion. Meanwhile, A1-2-1 in Area 1 was able to recover the initial investment cost within 10 years, regardless of government subsidies. On the other hand, A2-2-1 in Area 2 could recover the initial investment cost within 10 years when the government subsidy of 60% was supported. The proposed method could provide a reasonable design of the borehole to reduce the risk of performance degradation and the initial investment cost of the GSHP system.

5.7. Reference

[1] S. Royston, J. Selby, E. Shove, Invisible energy policies: A new agenda for energy demand reduction, Energy Policy. 123 (2018) 127–135. doi:10.1016/j.enpol.2018.08.052.

[2] C. Robinson, B. Dilkina, J. Hubbs, W. Zhang, S. Guhathakurta, M.A. Brown, R.M. Pendyala, Machine learning approaches for estimating commercial building energy consumption, Appl. Energy. 208 (2017) 889–904. doi:10.1016/j.apenergy.2017.09.060.

[3] V. Kumar, A.S. Pandey, S.K. Sinha, Grid integration and power quality issues of wind and solar energy system: A review, Int. Conf. Emerg. Trends Electr. Electron. Sustain. Energy Syst. ICETEESES 2016. 2011 (2016) 71–80. doi:10.1109/ICETEESES.2016.7581355.

[4] P. Nema, R.K. Nema, S. Rangnekar, A current and future state of art development of hybrid energy system using wind and PV-solar: A review, Renew. Sustain. Energy Rev. 13 (2009) 2096–2103. doi:10.1016/j.rser.2008.10.006.

[5] P. Mogensen, Fluid to duct wall heat transfer in duct system heat storages.pdf, (1983) 652–657.

[6] H.S. Carslaw, J.C. Jeager, Conduction of Heat in solids, Oxford University Press, Oxford, 1959.

[7] P.R. Smith MD, In situ testing and thermal conductivity testing, Proc. Geoexchange Tech. Conf. Expo. Stillwater, Oklahoma State Univ. (1999).

[8] C. Yavuzturk, J.D. Spitler, Short time step response factor model for vertical ground loop heat exchangers, ASHRAE Trans. 105 (1999) 475–485.

[9] S.P. Kavanaugh, L. Xie, C. Martin, Investigation of Methods for Determining Soil and Rock Formation Thermal Properties From Short-Term Field Tests, Atlanta. (2000).

[10] ASHRAE, ASHRAE handbook - HVAC applications, chapter 34 Geothermal energy, 2011.

[11] S.E.A. Gehlin, G. Hellström, Comparison of four models for thermal response test evaluation, ASHRAE Trans. 109 (2003) 131–142.

[12] W. Choi, R. Ooka, Effect of disturbance on thermal response test, part 2: Numerical study of applicability and limitation of infinite line source model for interpretation under disturbance from outdoor environment, Renew. Energy. 85 (2016) 1090–1105. doi:10.1016/j.renene.2015.07.049.

[13] W. Choi, R. Ooka, Effect of disturbance on thermal response test, part 1: Development

of disturbance analytical model, parametric study, and sensitivity analysis, Renew. Energy. 85 (2016) 306–318. doi:10.1016/j.renene.2015.06.042.

[14] H. Fujii, H. Okubo, K. Nishi, R. Itoi, K. Ohyama, K. Shibata, An improved thermal response test for U-tube ground heat exchanger based on optical fiber thermometers, Geothermics. 38 (2009) 399–406. doi:10.1016/j.geothermics.2009.06.002.

[15] Y. Sakata, T. Katsura, K. Nagano, Multilayer-concept thermal response test: Measurement and analysis methodologies with a case study, Geothermics. 71 (2018) 178–186. doi:10.1016/j.geothermics.2017.09.004.

[16] Y. Sakata, T. Katsura, K. Nagano, M. Ishizuka, Field analysis of stepwise effective thermal conductivity along a borehole heat exchanger under artificial conditions of groundwater flow, Hydrology. 4 (2017) 1–12. doi:10.3390/hydrology4020021.

[17] S. Signorelli, S. Bassetti, D. Pahud, T. Kohl, Numerical evaluation of thermal response tests, Geothermics. 36 (2007) 141–166. doi:10.1016/j.geothermics.2006.10.006.

[18] X. Yu, Y. Zhang, N. Deng, J. Wang, D. Zhang, J. Wang, Thermal response test and numerical analysis based on two models for ground-source heat pump system, Energy Build. 66 (2013) 657–666. doi:10.1016/j.enbuild.2013.07.074.

[19] V. Wagner, P. Bayer, M. Kübert, P. Blum, Numerical sensitivity study of thermal response tests, Renew. Energy. 41 (2012) 245–253. doi:10.1016/j.renene.2011.11.001.

[20] J. Raymond, L. Lamarche, M. Malo, Extending thermal response test assessments with inverse numerical modeling of temperature profiles measured in ground heat exchangers, Renew. Energy. 99 (2016) 614–621. doi:10.1016/j.renene.2016.07.005.

[21] A. Angelotti, L. Alberti, I. La Licata, M. Antelmi, Energy performance and thermal impact of a Borehole Heat Exchanger in a sandy aquifer: Influence of the groundwater velocity, Energy Convers. Manag. 77 (2014) 700–708. doi:10.1016/j.enconman.2013.10.018.

[22] J.C. Choi, J. Park, S.R. Lee, Numerical evaluation of the effects of groundwater flow on borehole heat exchanger arrays, Renew. Energy. 52 (2013) 230–240. doi:10.1016/j.renene.2012.10.028.

[23] C.K. Lee, H.N. Lam, A modified multi-ground-layer model for borehole ground heat exchangers with an inhomogeneous groundwater flow, Energy. 47 (2012) 378–387. doi:10.1016/j.energy.2012.09.056.

[24] J. Hecht-Méndez, M. De Paly, M. Beck, P. Bayer, Optimization of energy extraction for vertical closed-loop geothermal systems considering groundwater flow, Energy Convers. Manag. 66 (2013) 1–10. doi:10.1016/j.enconman.2012.09.019.

[25] H. Wang, C. Qi, H. Du, J. Gu, Thermal performance of borehole heat exchanger under groundwater flow: A case study from Baoding, Energy Build. 41 (2009) 1368–1373. doi:10.1016/j.enbuild.2009.08.001.

[26] N. Diao, Q. Li, Z. Fang, Heat transfer in ground heat exchangers with groundwater advection, Int. J. Therm. Sci. 43 (2004) 1203–1211. doi:10.1016/j.ijthermalsci.2004.04.009.

[27] V. Wagner, P. Bayer, G. Bisch, M. Kübert, P. Blum, Hydraulic characterization of aquifers by thermal response testing: Validation by large-scale tank and field experiments, Water Resour. Res. 50 (2014) 71–85. doi:10.1002/2013wr013939.

[28] V. Wagner, P. Blum, M. Kübert, P. Bayer, Analytical approach to groundwater-influenced thermal response tests of grouted borehole heat exchangers, Geothermics. 46 (2013) 22–31. doi:10.1016/j.geothermics.2012.10.005.

[29] H. Chae, K. Nagano, Y. Sakata, T. Katsura, T. Kondo, Estimation of fast groundwater flow velocity from thermal response test results, Energy Build. 206 (2020) 109571. doi:10.1016/j.enbuild.2019.109571.

[30] M. Verdoya, G. Imitazione, P. Chiozzi, M. Orsi, E. Armadillo, C. Pasqua, Interpretation of Thermal Response Tests in Borehole Heat Exchangers Affected by Advection, World Geotherm. Congr. 2015. (2015) 19–25.

[31] Q. Lu, G.A. Narsilio, G.R. Aditya, I.W. Johnston, Economic analysis of vertical ground source heat pump systems in Melbourne, Energy. 125 (2017) 107–117. doi:10.1016/j.energy.2017.02.082.

[32] H. Chae, K. Nagano, Y. Sakata, T. Katsura, A.A. Serageldin, T. Kondo, Analysis of Relaxation Time of Temperature in Thermal Response Test for Design of Borehole Size, Energies. 13 (2020). doi:10.3390/en13133297.

[33] Inc. ANSYS, ANSYS FLUENT Theory Guide, 2013. doi:10.1016/0140-3664(87)90311-2.

[34] A.A. Serageldin, Y. Sakata, T. Katsura, K. Nagano, Performance enhancement of borehole ground source heat pump using single U-tube heat exchanger with a novel oval cross-section (SUO) and a novel spacer, Sustain. Energy Technol. Assessments. 42 (2020) 100805. doi:10.1016/j.seta.2020.100805.

[35] A.A. Serageldin, Y. Sakata, T. Katsura, K. Nagano, Thermo-hydraulic performance of the U-tube borehole heat exchanger with a novel oval cross-section: Numerical approach, Energy Convers. Manag. 177 (2018) 406–415. doi:10.1016/j.enconman.2018.09.081.

[36] T. Katsura, Y. Shoji, Y. Sakata, K. Nagano, Method for calculation of ground temperature in scenario involving multiple ground heat exchangers considering groundwater advection, Energy Build. 220 (2020). doi:10.1016/j.enbuild.2020.110000.

[37] T. Katsura, K. Nagano, Y. Sakata, H. Wakayama, A design and simulation tool for ground source heat pump system using energy piles with large diameter, Int. J. Energy Res. (2019) 1505–1520. doi:10.1002/er.4372.

[38] T. Katsura, K. Nagano, S. Takeda, Method of calculation of the ground temperature for multiple ground heat exchangers, Appl. Therm. Eng. 28 (2008) 1995–2004. doi:10.1016/j.applthermaleng.2007.12.013.

[39] K.C. Lee, J.H. Hong, H.J. Kong, A Study of Comparative Economic Evaluation for the System of Ground Source Heat Pump and District Heating and Cooling:Focusing on the Analysis of Operation Case, Korean J. Air-Conditioning Refrig. Eng. 28 (2016) 103–109. doi:10.6110/kjacr.2016.28.3.103.

[40] D. Tanguay, Fundamental Economic Analysis of Ground Source Heat Pump Markets in North America, 12th IEA Heat Pump Conf. (2017) 1–11.

[41] Department of Energy and Climate, Potential Cost Reductions for Ground Source Heat Pumps, 2016.

[42] C. Huan, S. Li, F. Wang, L. Liu, Y. Zhao, Z. Wang, P. Tao, Performance analysis of a combined solar-assisted heat pump heating system in Xi'an, China, Energies. 12 (2019) 1–20. doi:10.3390/en12132515.

[43] B. Zhang, K. Gu, B. Shi, C. Liu, P. Bayer, G. Wei, X. Gong, L. Yang, Actively heated fiber optics based thermal response test: A field demonstration, Renew. Sustain. Energy Rev. 134 (2020). doi:10.1016/j.rser.2020.110336.

[44] C.H. Maldaner, J.D. Munn, T.I. Coleman, J.W. Molson, B.L. Parker, Groundwater Flow Quantification in Fractured Rock Boreholes Using Active Distributed Temperature Sensing Under Natural Gradient Conditions, Water Resour. Res. 55 (2019) 3285–3306. doi:10.1029/2018WR024319.

Chapter 6.

Application of ground source heat pump system for nearly-zero energy building

6.1. Introduction

As the population grows and industrialization progresses, energy consumption has been increasing. According to the U.S. Energy Information Administration's latest International Energy Outlook 2020 (IEO2020), energy consumption increased by 25% from 1990 to 2015 and is expected to increase by 28% between 2015 and 2040 (Fig. 6.1) [1]. It has been industrialized and enriched for the human race materially, but the use of fossil fuels has caused environmental problems such as air pollution, the city heat island effect, and global warming. To solve this problem, "Transforming Our World: the 2030 Agenda for Sustainable Development" was adopted at the UN Summit for Sustainable Development on 25 September 2015 [2]. The agenda includes a set of 17 Sustainable Development Goals (SDGs) to end poverty, fight inequality and injustice and tackle climate change by 2030. In our field to achieve the 7th goal "Ensure access to affordable, reliable, sustainable and modern energy for all", it is necessary to propose methods of providing clean and sustainable energy by increasing the use of renewable energy and improving energy efficiency.

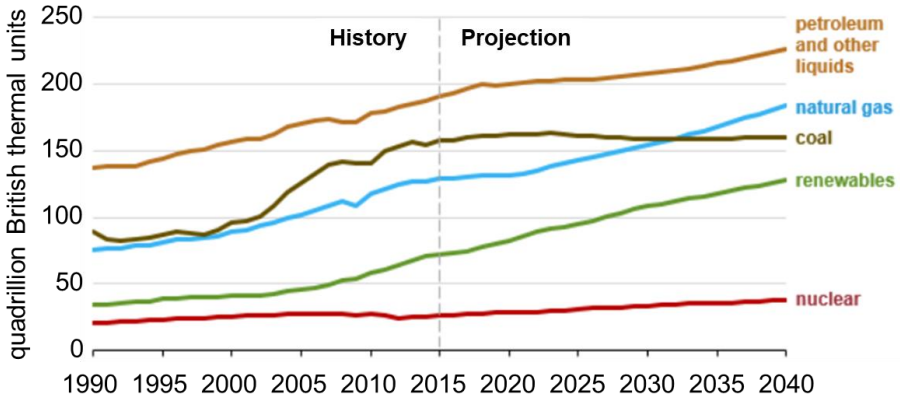

Fig. 6. 1 World energy consumption by energy source (1990-2040, source: International Energy Outlook 2020)

Fig. 6. 2 Sustainable Development goals (source: United Nations)

As social issues of energy demand and carbon emissions have been increased gradually, many countries have enacted energy reduction policies and have funded projects to develop high-performance and environmental-friendly systems [3]. In particular, they have striven to reduce energy consumption in the building sector, which consumes more than 40% of the total energy [4]. The research on Zero Energy/Emission Buildings (ZEBs) has attracted to reduce a large share of the world's primary energy in the building sector. The ZEB adopts high-performance insulation and high airtight windows to minimize energy loss with an 'Active system', which applies high-efficiency equipment and renewable energy. It contributes to users living without additional energy supply from the outside by enhancing the energy performance of the building.

6.1.1. Concept of zero energy building

The ZEB is made of an advanced architectural design that actively utilizes natural energy and adopting passive technology. In addition, it also has a goal of realizing significant energy saving and achieving zero annual primary energy consumption while maintaining the air quality in the indoor environment with a high-efficiency system. In Japan, a policy goal "Energy Basic Plan" is set to achieve the ZEB by 2030 for new public buildings. The ZEB consists of the following steps in Table. 6.1 and Fig. 6. 3.

Table 6. 1 Classification of zero energy building

Classification	Definition	Qualification
ZEB	Buildings with net zero or negative annual primary energy consumption	- More than 50% reduction in primary energy consumption by applying a passive system. - Reduce energy consumption by more than 100% by using renewable energy.
Nearly ZEB	Buildings satisfying ZEB Ready requirements and near-zero annual primary energy consumption.	- More than 50 % reduction in primary energy consumption by applying a passive system. - Reduce energy consumption by 75-100 % by using renewable energy.
ZEB Ready	Buildings with high thermal insulation and high-efficiency energy-saving equipment.	- More than 50 % reduction in primary energy consumption by applying a passive system.

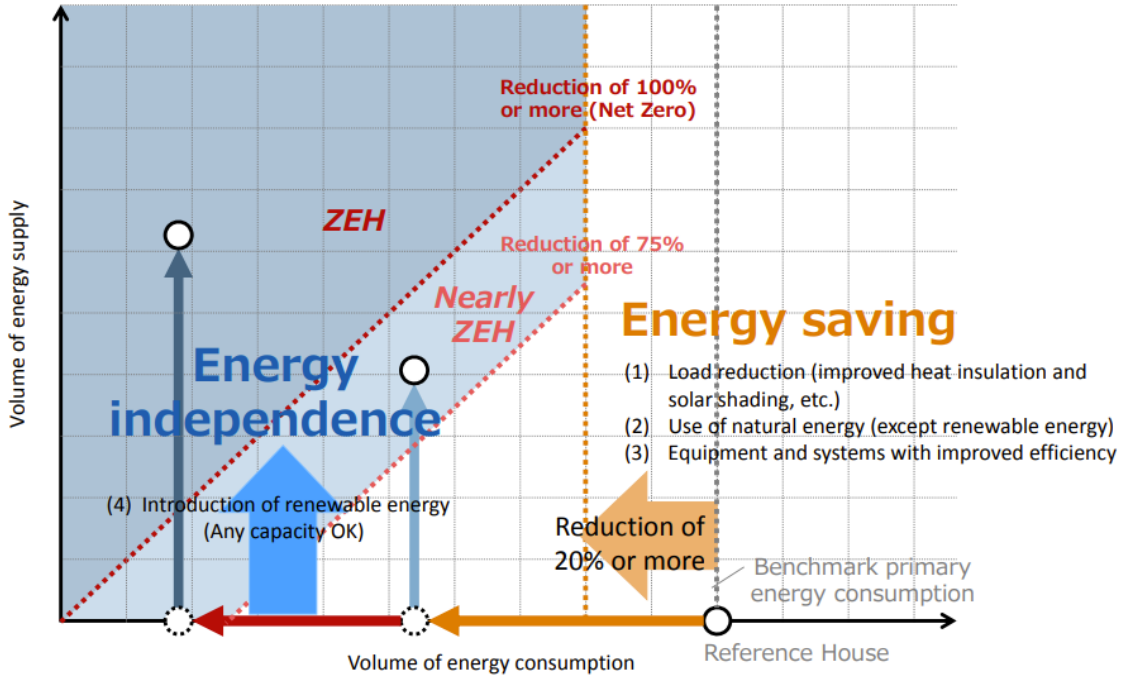

Fig. 6. 3 Image of ZEB definition

6.1.2. Investigation instance of facility technology in ZEB

While global attention has recently been focused on environmental problems, issues related to global warming and the depletion of energy resources have emerged in Japan. Fossil energy (coal, oil, natural gas, LP gas) accounts for about 80% of Japan's energy consumption, but the self-sufficiency rate is only 4%. Most of the fossil energy is dependent on imports. Japan's government has implemented various policies to promote the distribution of the GSHP system on which energy can alleviate environmental problems. In Japan, the installed number of the GSHP systems has steadily increased since Geothermal Utilization Promotion Association was established in 2001 (Fig. 6.4). The GSHP systems could be combined with other heat source systems to realize zero energy buildings. In the chapter, the cases of the ZEB in the world are demonstrated.

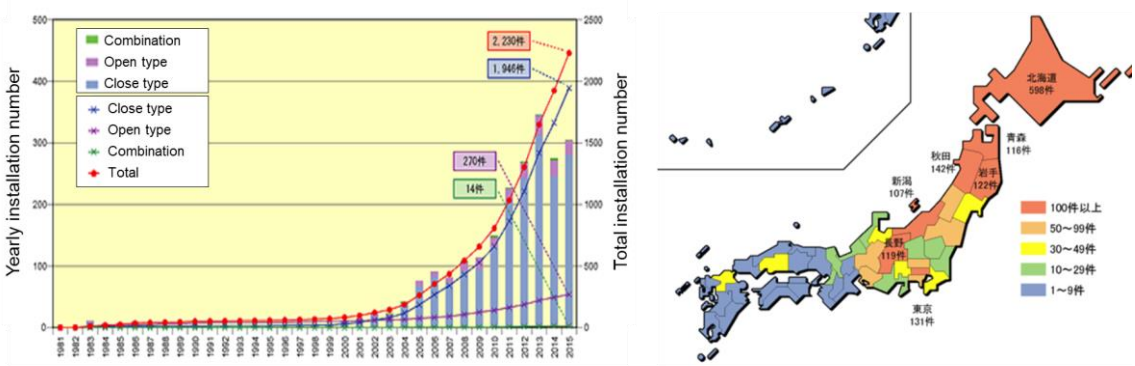

(a) Yearly installation number of GSHP system (Japan Ministry of Environment, 2017)

(b) Installation number of GSHP system in Japan (Japan Ministry of Environment, 2017)

Fig. 6. 4 Installed number of the GSHP systems in Japan

■ Japan

1) Kitakyushu Dormitory

- Construction location: Kitakyushu City
- Building Use: Dormitory
- Year of construction: February 2012
- Structural type: RC-steel frame
- Number of floors: 7 stories
- Building area: 2,066 m^2
- Total floor area: 9,374 m^2

Fig. 6. 5 Figure of Kitakyushu Dormitory

Kitakyushu Dormitory is a relatively large dormitory with 230 rooms and has applied new and renewable energy technology with the aim of realizing a “next-generation single dormitory”. The 'smart heat pump system' that effectively utilizes renewable energy systems was applied to the building, based on the core technology of the GSHP system. In addition, the electrical consumption was reduced by 20% compared to conventional facilities in which fossil fuels are used, by recycling waste heat. Fig 6.6 shows the schematic diagram of the system in Kitakyushu Dormitory.

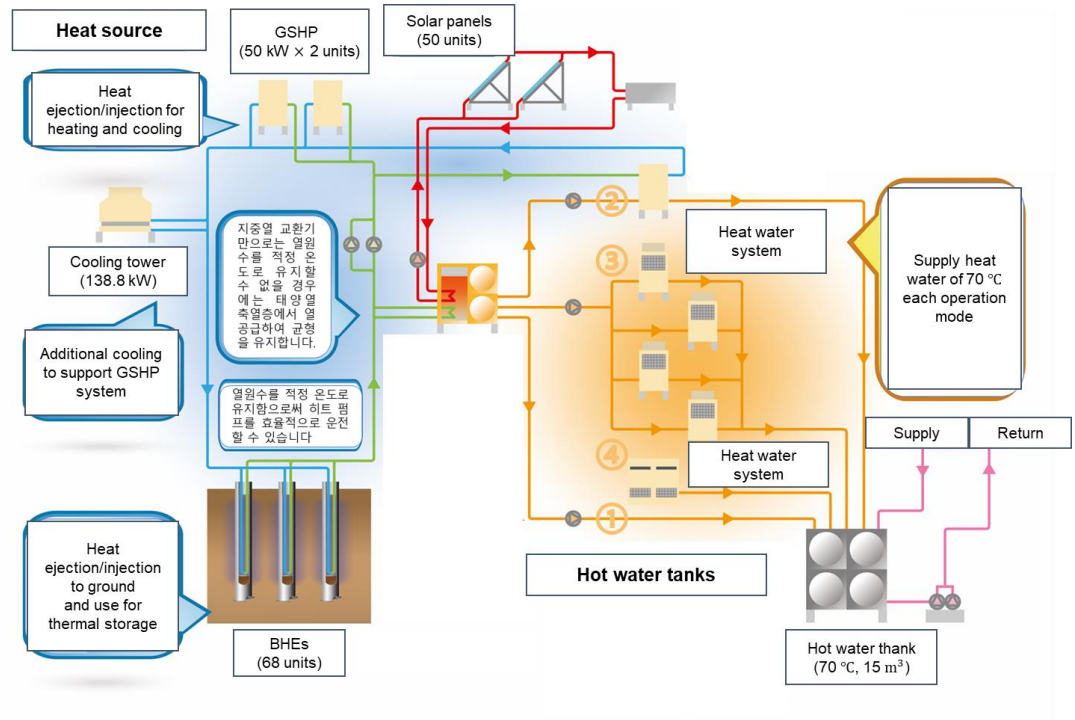

Fig. 6. 6 Schematic diagram of the system Kitakyushu Dormitory

2) Forrester Hirosaki Park

- Construction location: Aomori City
- Building Use: Apartment
- Structural type: Reinforced concrete
- Number of floors: 15 stories
- Building area: 2083.9 m^2

Fig. 6. 7 Figure of Forrester Hirosaki Park

In cold regions, snow melting in parking lots and public areas causes economic losses. In order to reduce such economic loss, 'Forrester Hirosaki Park' used the GSHP system to remove snow from the parking lot and the access part of the apartment. During the snow melting period (November–February), the fuel cost of snow melting using boilers was about 570,000 yen (90 yen/L) per household, whereas the cost reduction of snow melting using the GSHP system was about 35,000 yen per household. In 'Forrester Hirosaki Park', Sixteen GSHPs with a heating capacity of 10 kW were installed, and the amount of power consumption was suppressed by installing heat pumps with a small heating capacity. The GSHP systems were automatically controlled with and 3.7 of the COP during snow melting. Fig. 6.8 shows the figures of the snow melting system in Forrester Hirosaki Park. Fig 6.9 shows buildings targeting ZEB in various regions in Japan.

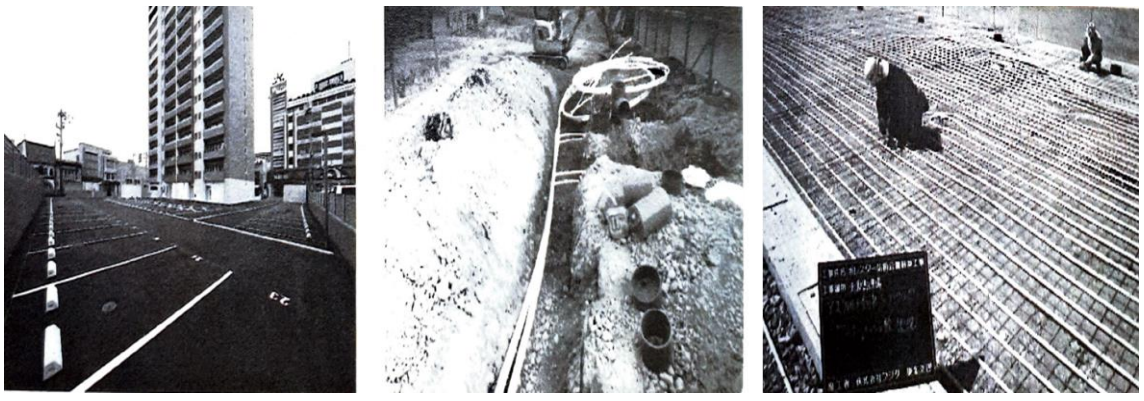

Fig. 6. 8 figures of the snow melting system in Forrester Hirosaki Park

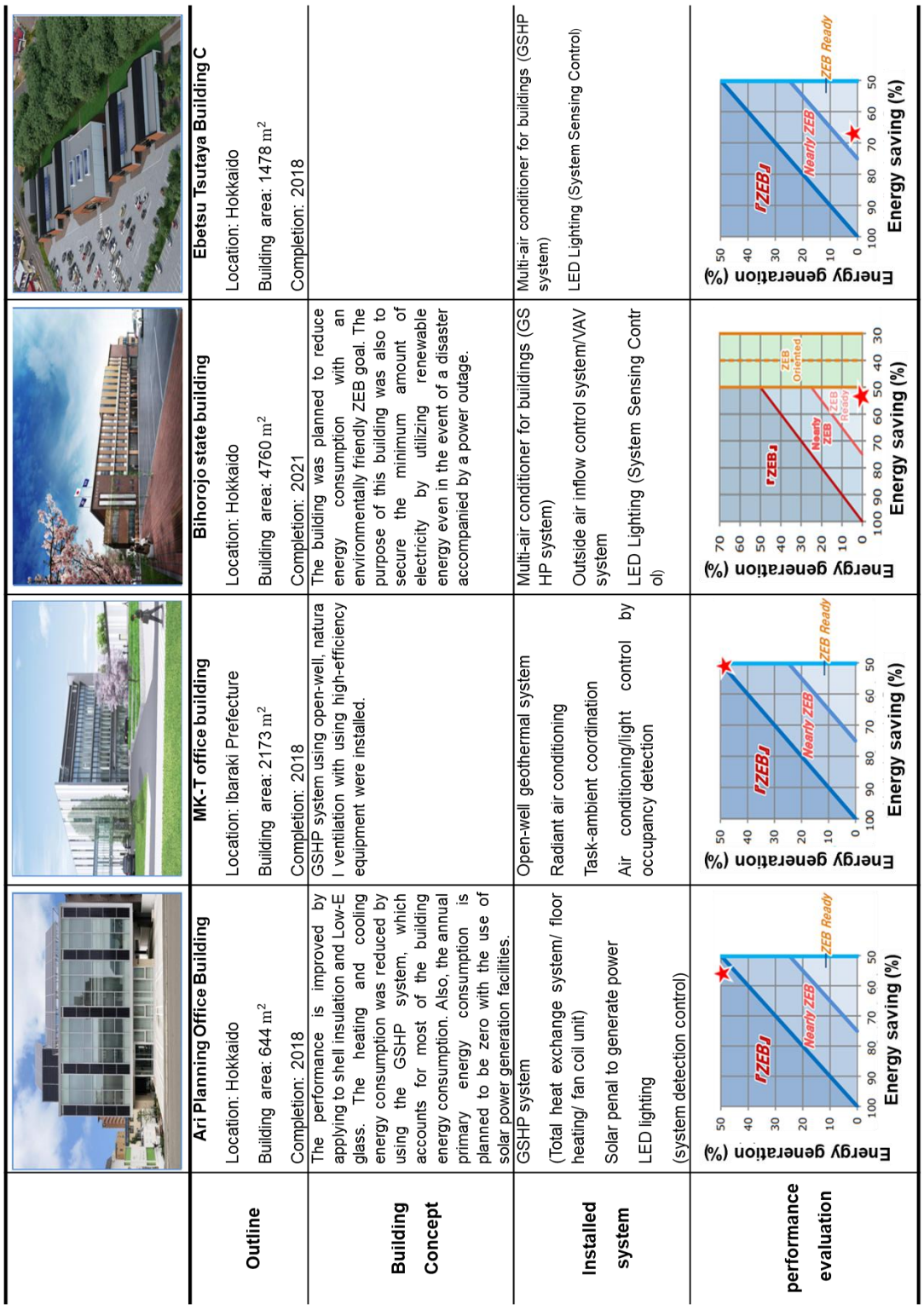

Fig. 6. 9 shows buildings targeting ZEB in various regions in Japan

■ South Korea

1) Green Tomorrow

- Construction location: Gyeonggi-do
- Building Use: House
- Year of construction: 2009
- Certification: LEED Platinum
- Building area: 676.1 m^2
- Construction company: Samsung

Fig. 6. 10 Figure of Green Tomorrow

In Green Tomorrow, 68 technologies were applied in building such as heating and cooling and ventilation systems, renewable energy and information technology. In addition, the Green Tomorrow was designed by rooftop greening to reduce the heating and cooling loads through the insulation effect and was used of water (purified water). As a passive technology, triple-glazed windows, super-insulation materials, high-insulation and high-tight fire doors were used to strengthen the insulation and airtightness, and the efficiency of the shell was increased through the double-shell system in Fig. 5.11.

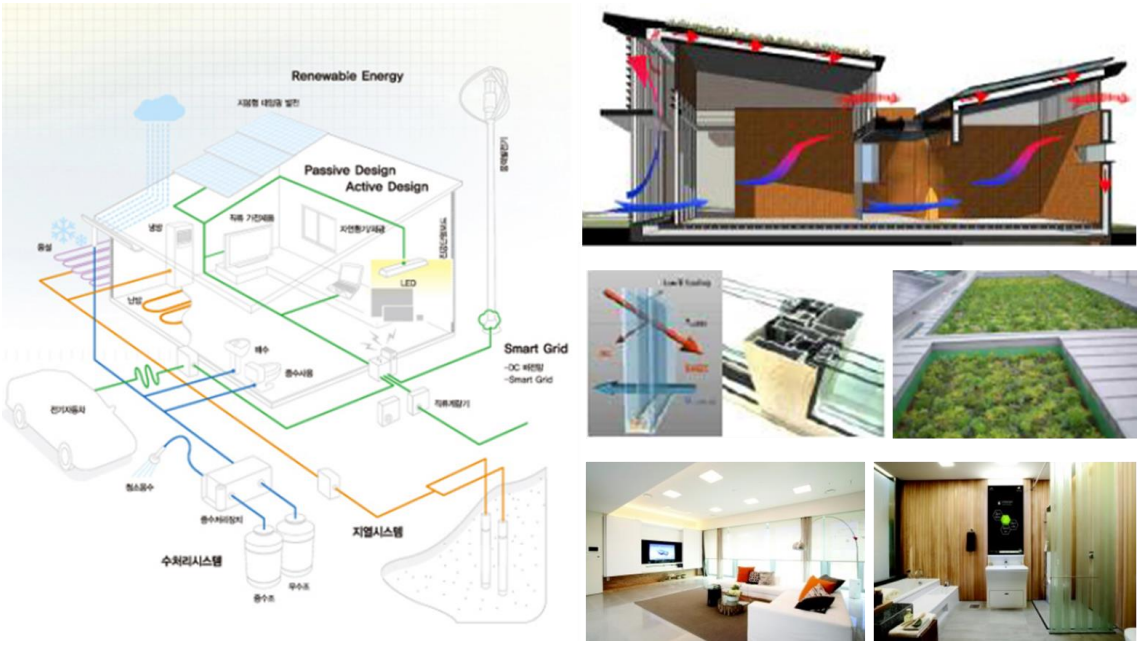

Fig. 6. 11 Concept of applied system in Green Tomorrow and figures

2) Eco-3L house

- Construction location: Deajeon
- Building Use: Apartment House
- Year of construction: 2006
- Building area: 3,200 m^2
- Construction company: Daelim

Fig. 6. 12 Figure of Eco-3L house

Fig 6.13 indicates the schematic diagram of the applied system in the Eco-3L house. Detail description of the applied systems is as follows:

① Solar power generation system (renewable energy): Power generation by using solar power as a semiconductor.

② Wind power generation system (renewable energy): Converts wind power into rotational power to generate induced electric power.

③ Geothermal system (renewable energy): Energy technology that utilizes heat from underground.

④ Underground duct system (renewable energy): Utilizes geothermal heat below freezing depth by heat exchange with air.

⑤ Rooftop greening (load reduction / securing green space): Insulation effect of buildings using vegetation, improvement of rainwater storage function.

⑥ Rainwater Utilization Facility (Water Resource Utilization): Store rainwater and use it as sanitary water, landscaping water.

⑦ Natural lighting system (load reduction / light environment): Energy saving by supplying natural sunlight to dark rooms such as basements.

⑧ Super external insulation (load reduction): Minimizes condensation and thermal bridges and greatly improves insulation performance.

⑨ High-performance windows (load reduction): Performance improvement with high-performance glass such as triple glazing and system windows with airtightness.

⑩ Ventilation system (air environment / load reduction): Automatic operation of indoor air and fresh outdoor air by CO_2 sensor.

⑪ LED lighting (load reduction / light environment): Energy efficiency is improved up to 20 times compared to existing luminaires.

⑫ Floor impact sound reduction material (load reduction / sound environment): Minimize noise between floors and block heat transfer from floor to floor.

Fig. 6. 13 Schematic diagram of the applied system in the Eco-3L house

■ **The other countries**

1) Case 1

- Construction location: Hämeenlinna, Finland
- Building Use: Commercial/Industrial
- Year of construction: 2015
- Construction company: Ruukki Construction

Fig. 6. 14 Figure of ZEB (Case 1)

Finland's first nearly zero-energy "big-box" type single-story building for commercial, logistic or industrial use was designed and constructed to meet an objective to be a building with an economic lifecycle that saves energy and uses existing renewable energy sources.

Building envelope

The outer walls of the building are fitted with a sandwich panel system with ultra-right panels. The sandwich panels are composed of a glass-wool insulating layer between two thin steel sheets. The insulation thickness in both the wall and the corner panels is 230 mm, with a U-value of 0.16 W/m^2K. The building's roof incorporates a new type of prefabricated PIR roof elements with a U-value of 0.12 W/m^2K.

Heating, cooling and ventilation systems

The radiation profiles generate either cool or heat the interior, depending on the season and the desired indoor temperature of the building. Radiant profiles work with a low-temperature difference to the ambient air, allowing the heat pump installed in the building to perform well. The mechanical ventilation machine is equipped with an 80%heat recovery system.

Renewable heating energy system

Geothermal energy is utilized for the building's heating and cooling requirements. In total, 60 energy piles with a diameter of 115 mm and 11m in length under the floor and columns are incorporated in the foundation to use renewable energy to heat the building. A total of 24 m^2 of solar collectors are installed on the roof of the building's technical area. Solar collectors accumulate thermal energy from the sun and transfer it to the soil through the energy piles.

Building Integrated Solar Energy Solution

Solar power is also used in the outer walls of the building. On-wall solar panels, which generate electricity from the sun's light for the building's network, are installed on its southern façade. A total of 61 m^2 PV (Photovoltaic) panels with total peak power of 10 kW are incorporated in the wall.

Monitoring of the Building

The building is equipped with a large number of energy meters and other measuring devices to ensure extensive monitoring and ascertain the real energy performance of the building. In particular, the energy pile and solar heat systems are monitored carefully to study the soil behavior in the long run. Some building elements are also equipped with thermal moisture sensors to monitor their condition throughout their life-cycle. Furthermore, the snow on the roof is also monitored with a application based on strain gauge measuring of the metal roof structure. Fig. 6.15 shows the installed system in the building of Case 1.

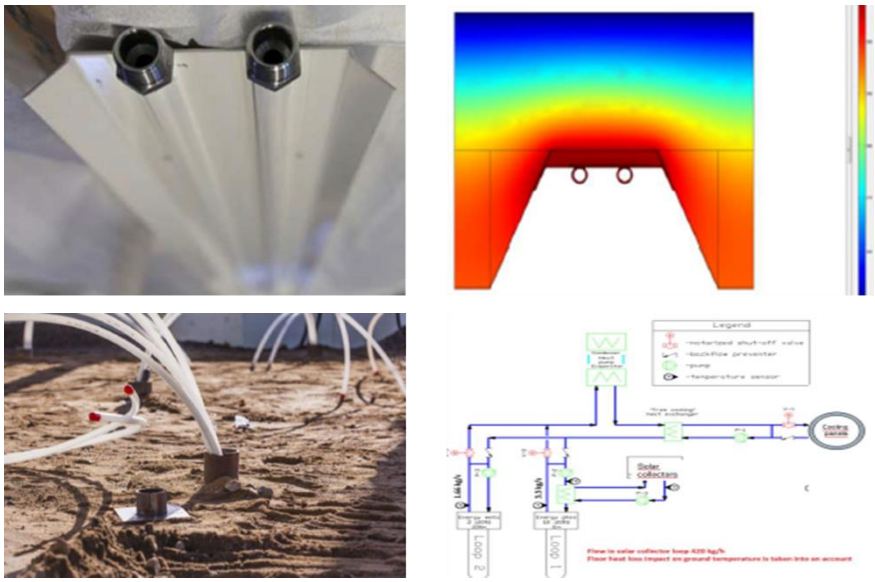

Fig. 6. 15 Installed system in the building in Case 1

1) Case 2

- Construction location: K-Rauta, Finland
- Building Use: Commercial/Industrial
- Year of construction: 2008
- Construction company: Ruukki Construction

Fig. 6. 16 Figure of ZEB (Case 2)

Most recent energy efficiency research has concentrated mainly on residential buildings and office buildings. New concepts utilizing simple techniques in a very innovative way decrease considerably heating and cooling energy as well as lighting energy thus creating promising possibilities. The developed solutions are applied to the building of Case 2 with cost and production efficiency. Fig. 6.17 shows the installed system in the building of Case 2.

(a) Energy pipe GSHP system (b) Building integrated photovoltaics

Fig. 6. 17 Installed system in the building of Case 2.

Some of the identified technical solutions includes:

① Using foundation piles that support the buildings as ground heat harvesters.

② Integrating solar photovoltaic panels directly into the exterior wall structures.

③ Using highly isolative translucent panels to maximize natural light without compromising commercial aspects.

④ Supporting natural ventilation with exterior wall components to form a hybrid with efficient heat recovery systems.

6.1.3. Strategy for ZEB

In recently, zero energy buildings [5,6] and energy flexible buildings [7–9] have been attending to reduce the energy consumption in the building sector. The GSHP systems are highly desirable for the ZEBs and energy flexible buildings. The generated electricity from photovoltaic panels can readily be consumed with the GSHP system for a very high-efficiency heating/cooling on-site. With the development of the GSHP system and photovoltaic thermal (PVT) system, the GSHP combining PVT (GSHP-PVT) systems have proposed to solve features of thermal imbalance for geothermal energy and intermittency for photovoltaic system in the building energy field. There is a lot of research focused on the design and optimization of GSHP-PVT systems in recent years. Abu-Rumman et al. [10] mentioned that the GSHP-PVT hybrid system can improve 9.5 % of the electricity production efficiency and 30% of the average coefficient of performance (COP) of the heat pump. Sakellariou et al. [11] carried out the numerical simulation to clarify the energy performance of GSHP-PVT. The optimal operation strategies are also proposed under different operation modes for the GSHP-PVT system [12–14]. Although studies combining various renewable systems have been reported, an integrated simulation tool for realizing ZEB has not yet been provided. Therefore, it is necessary for a simulation tool to realize ZEB, including various system components under the conditions of each regional characteristic.

6.2. Building characteristics

6.2.1. Building information

This chapter aims to develop a ZEB simulation tool. The target building is a childcare support center built in a cold region located in Rusutsu (42°74'N and 140°87'E), Hokkaido island, and it is used as an evacuation spot in case of disaster. The childcare support center is a one-story wooden house. Fig. 6.18 shows the building floor plan and the figures of each area. A building area is 6299.8 m^2, and a total floor area of 1499.8 m^2. The insulation specifications of the building material in each part are shown in Table. 6.2-6.4. The childcare support is used a high insulation performance aiming to realize ZEB ready. Windows is the triple glass of argon-filled glass windows, and the U value is 1.22 $W/(m^2 K)$. Based on the thermal insulation specifications, the heat loss coefficient (Q value) of this building is 0.93 $W/(m^2 K)$. The low Q value leads the building to achieve zero energy building.

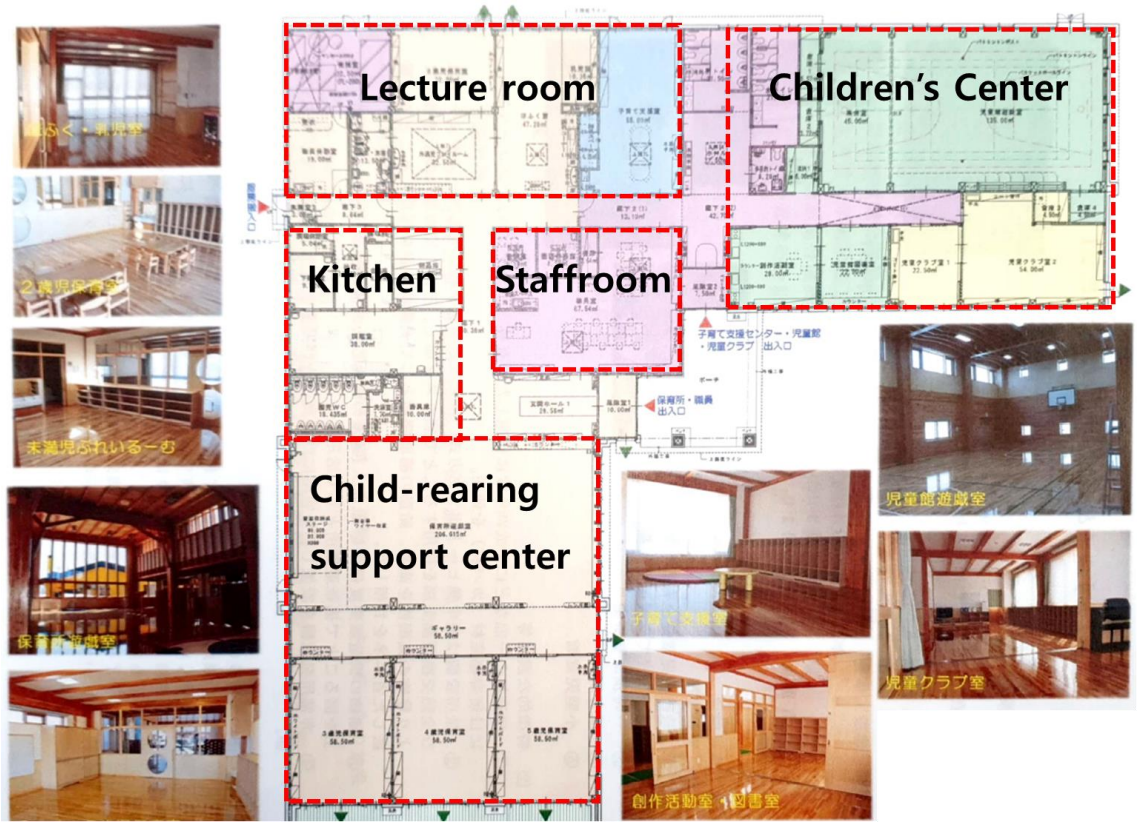

Fig. 6. 18 Building floor plan and figures of each area

Table 6. 2 Thermal conductivity and thickness on the wall

Material	Thermal conductivity [W/(m K)]	Thickness [mm]
Steel	45	0.4
Hardboard	0.22	18
Glass wool (32K)	0.04	100
Plywood	0.19	9
Glass wool (24K)	0.042	100
Drywall	0.17	12.5
Total thermal resistance	5.24 $[(m^2 K)/W]$	
Overall heat transfer coefficient	0.19 $[W/(m^2 K)]$	

Table 6. 3 Thermal conductivity and thickness on the ceiling

Material	Thermal conductivity [W/(m K)]	Thickness [mm]
Steel	45	0.4
Rigid Urethane Foam	0.028	30
Plywood	0.19	12
Rigid Urethane Foam	0.028	200
Plywood	0.19	24
Drywall	0.17	12.5
Total thermal resistance	5.75 $[(m^2 K)/W]$	
Overall heat transfer coefficient	0.17 $[W/(m^2 K)]$	

Table 6. 4 Thermal conductivity and thickness on the floor

Material	Thermal conductivity [W/(m K)]	Thickness [mm]
Plywood	0.19	27
Concrete	1.4	220
Polyethylene foam board	0.044	100
Gravel	0.62	50
Total thermal resistance	2.65 $[(m^2 K)/W]$	
Overall heat transfer coefficient	0.37 $[W/(m^2 K)]$	

6.2.2. Building equipment system for HVAC

Fig. 6.19 shows a schematic diagram of the equipment system. The GSHP system as the renewable energy use is applied to the building for heating and cooling. It is also involved with the solar collector, the energy recovery ventilator with the earth tube system.

The three GSHPs (maximum output of 28 kW per unit) are installed, shown in Fig. 6.20. The refrigerant of R410 circulating into the compressor, the condenser, the expansion valve and the evaporator is used for the heat pump. These HPs are connected with the fifteen borehole heat exchangers (BHE). The boreholes are filled with the single U-tube and the backfilled material. The diameter and length of the borehole are 0.14 and 85 m, respectively. The 40 % ethylene glycol circulates in the U-tubes. The ground consists of clay and volcanic ash, and the water table depth is 9 m. The TRT is carried out to determine the apparent effective thermal conductivity and borehole thermal resistance. As a result, the apparent effective thermal conductivity and borehole thermal resistance are 1.41 $W/(m\,K)$ and 0.060 $(m\,K)/W$. The initial ground temperature was measured to be 9.8 ℃.

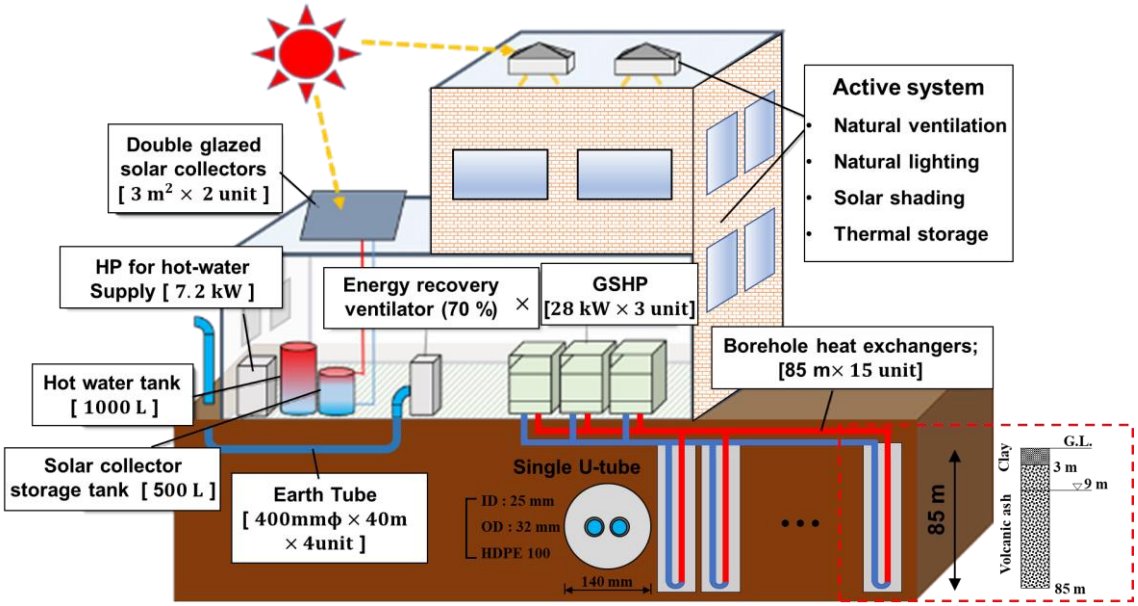

Fig. 6. 19 Conceptual diagram of equipment system

Fig. 6. 20 Figure of the ground source heat pump

The two solar collectors made of the double glazed vacuum pipes collector are installed to supply the hot water, and its area of each collector is 3.23 m2. The heat collecting efficiency of the solar collector is 0.95, and the volume of the solar collector storage tank is 500 L. The maximum heating capacity of the heat pump for the hot water is 7.2 kWh, and the volume of the heat water tank is 1000 L.

The energy recovery ventilator with an efficiency of 70 % is introduced to the building. The system goes through the energy recovery process in residential and commercial HVAC systems that exchanges the energy contained in normally exhausted air of a building or conditioned space, using it to treat the incoming outdoor ventilation air. During the warmer seasons, the system pre-cools and dehumidifies. During cooler seasons, the system humidifies and pre-heats. The system can maintain a 40-50 % indoor relative humidity and reduce total HVAC equipment capacity and energy consumption. The childcare support center is installed with the earth tube system to reduce the ventilation load. The ventilation rate is 1,600-5,300 m^3/h. The earth tubes made of PVC pipe with a diameter of 400 mm are buried in G.L. -2.8 m, and four pipes of 40 m are laid along the foundation of the building. Fig. 6.21 shows the Figures of the earth tube system on the construction site.

Fig. 6.22 illustrates the schematic diagram of the installed system of the building. The distributed system is the floor heating system with 13A pipes. These pipes are installed in 90 mm from the building floor at intervals with 150 mm. The supply water temperature and the flow rate are controlled.

Fig. 6. 21 Figures of earth tube system on construction site

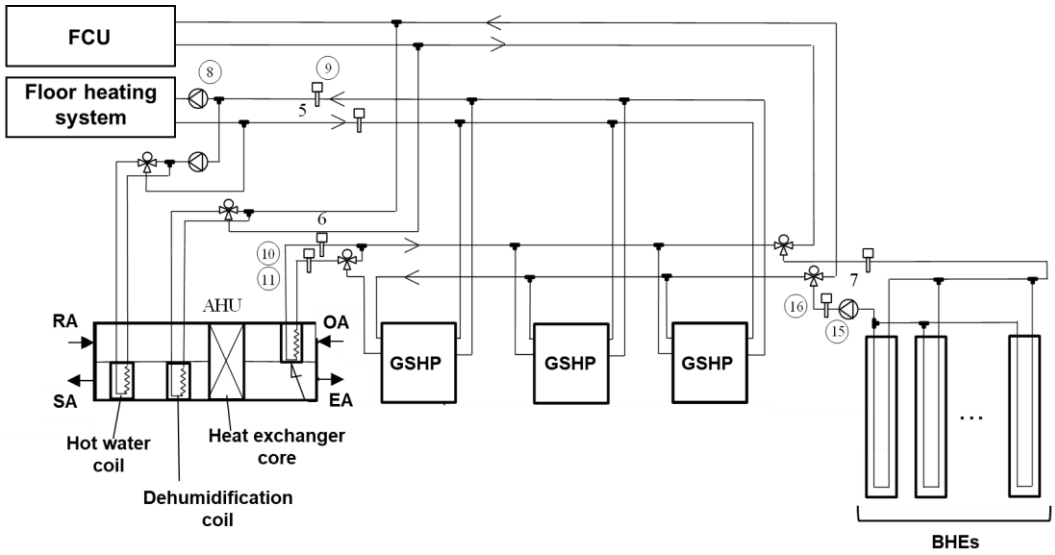

Fig. 6. 22 Schematic diagram of the systems

6.3. Features of ZEB simulation tool

The ZEB simulation tool is developed to predict the energy consumption of the building, based on the GSHP system being able to calculate multi-borehole configuration under the conditions with the multi-layer with groundwater flows. This tool also calculates the indoor temperature and power consumption for each hour when the floor heating or fan coil systems are operated for heating and cooling. The indoor temperature is determined by the heat balance, considering the heat transfer on the walls, the floor, the ceiling, the glass, the ventilation rate and internal heat generation. The systems operate to maintain the set-point temperatures of the rooms. The mathematical method of each component is described as the following chapters.

6.3.1. Calculation of Room temperature

The heat loss coefficient (Q value) is a basic parameter used in the calculation of heat transfer problems. The Q value represents the insulation performance of the building. The low Q value of the building leads to high insulation performance. In Japan, the "Energy Conservation Act" in 1979 and 'Energy Conservation Standards for Buildings" in 1980 were enacted, and the standard of Q value for each region has suggested corresponding to regional characteristics for energy saving [15]. The value is an important parameter in the operating strategy of the heating and cooling system.

Table 6. 5 Q value for each region [15]

Region	Q value $[W/(m^2 K)]$
Hokkaido	1.6
Aomori, Iwate, Akita	1.9
Miyagi, Yamagata, Fukushima, Ibaraki, Tochigi, Gunma, Niigata, Toyama, Ishikawa, Fukui, Yamanashi, Nagano, Gifu, Shiga	2.4
Saitama, Chiba, Tokyo, Kanagawa, Shizuoka, Aichi, Mie, Kyoto, Osaka, Nara, Wakayama, Tottori, Shimane, Okayama, Hiroshima, Yamaguchi, Tokushima, Kagawa, Ehime, Kochi, Fukuoka, Saga, Nagasaki, Kumamoto, Oita	2.7
Miyazaki, Kagoshima	2.7
Okinawa	3.7

The Q value of the building as the amount of heat loss coefficient is determined by the rate of heat flow through the buildings' envelope when a temperature difference exists between the indoor air and the outdoor air under steady-state conditions. The total heat flow is the sum of the heat flow by conduction through the various parts and the heat flow by air infiltration through the building. The Q value is derived from Eq. 6-1. Here, the heat flow on the floor is modified by a correction factor of 0.5 because the floor does not connect with the outdoor. The Q value of the target building is calculated to be 0.84. The target building can reduce more than 50 % of primary energy consumption comparing with the conventional building.

$$Q \text{ value} = \frac{K_{wall}A_{wall} + K_{glass}A_{glass} + K_{roof}K_{roof} + K_{wall}A_{wall} + \frac{K_{floor}A_{floor}}{2} + q_{vent}}{A_{floor}} \quad (6\text{-}1)$$

Fig 6.23 shows the conceptual diagram of the heat balance for the calculation of the indoor temperature and the heating and cooling loads. The indoor volume of the building keeps the setpoint temperature for all weather conditions, using heating and cooling energy. In general, the setpoint temperature is 22 during the heating period and 26 during the cooling period. The extend of all heat flows dependent on external or internal influence factors. These heat flows can be arranged into three categories; factors by the external heat loss, factors by the internal heat loss and the heat loss by the infiltration and the ventilation. The factors by the external heat loss depend on the structure of the building, climate of the location and orientation. The solar radiation from the sun also affects the external heat loss, significantly. The factors by the internal heat loss are the people, the lighting and the applications which make the heat.

The heat loss in the wall and ceiling is obtained by the temperature difference between the wall surface and room. The wall surface in the outdoor is applied to solar-air temperature (SAT) considered the solar absorption rate on the wall. The heat gain by the floor heating system is calculated by the floor surface temperature (T_{floor}), the room temperature and the convective heat transfer coefficient (α) in the room. The calculation method of the floor surface temperature is explained in more detail in the next Chapter. The heat loss in the window is calculated by the temperature difference and the heat gain by solar radiation. The ventilation loads are calculated by considering the ventilation efficiency (E_{vent}) of the energy recovery ventilator. Internal heat generation is applied to be 6 $\mathrm{W/m^2}$ during the day when the people stay in the building. Each heat loss calculation describes Eqs. 6-2 to 6-10. The indoor temperature is calculated by Eq. 6-11 at interval of 60 s.

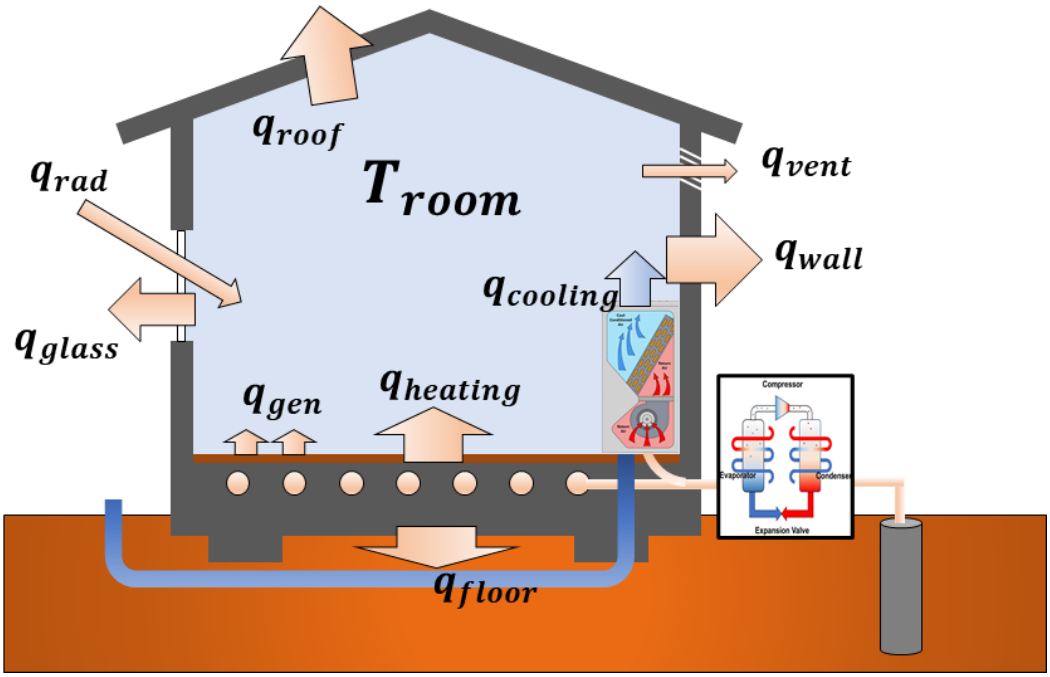

Fig. 6. 23 Conceptual diagram of the heat balance

Heat loss through Walls

$$q_{\text{wall}} = K_{\text{wall}} A_{\text{wall}} (SAT - T_{\text{room}}) \tag{6-2}$$

$$q_{\text{ceiling}} = K_{\text{ceiling}} A_{\text{ceiling}} (SAT - T_{\text{room}}) \tag{6-3}$$

$$q_{\text{floor}} = h_c A_{\text{floor}} (T_{\text{floor}} - T_{\text{room}}) \tag{6-4}$$

$$SAT = T_{\text{out}} + \frac{a_{\text{w}} I_{\text{sun}}}{h_{\text{out}}} \tag{6-5}$$

$$K = \frac{1}{R} = \frac{1}{\sum l/\lambda \ + 1/h_{\text{in}} + 1/h_{\text{out}}} \tag{6-6}$$

Heat loss through glasses

$$q_{\text{glass}} = K_{\text{glass}} A_{\text{glass}} (T_{\text{out}} - T_{\text{room}}) \tag{6-7}$$

$$q_{\text{rad}} = I_{\text{sun}} K_{\text{s}} A_{\text{glass}} \tag{6-8}$$

Heat loss by ventilations and internal heat gain

$$q_{\text{vent}} = nCV(1 - E_{\text{vent}})(T_{\text{out}} - T_{\text{room}}) \tag{6-9}$$

$$q_{\text{gen}} = \dot{q_{\text{gen}}} A_{\text{floor}} \tag{6-10}$$

Indoor temperature

$$C\rho_{air} V_{room} \frac{dT_{\text{room}}}{dt} = q_{\text{wall}} + q_{\text{celling}} + q_{\text{floor}} + q_{\text{glass}} + q_{\text{rad}} + q_{\text{vent}} + q_{\text{gen}} \tag{6-11}$$

6.3.2. Floor heating system

The floor temperature is solved with a two-dimensional polygonal finite difference method (FEM). Figure. 6.24 shows the conceptual diagram of the floor heating system. Half of the pipe is divided into 5 areas in the X-direction and 8 areas in the Z-direction. The parts of the pipe are enhanced by fine meshes. In addition, the mesh of the pipe has a regular octagon shape, and a mesh of the parts of the pipe is 1/8 of the circumference of the pipe. The pipes in Y-direction assume the infinite length of the pipes. The condition of the boundary surface is the adiabatic condition. The initial temperature of each mesh is 20 ℃. Eq. 12 indicates the objective function of the temperature in the floor.

$$C(x,z)\rho(x,z)\frac{\partial T(x,z)}{dt} = \frac{\partial}{\partial x}\left(\lambda(x,z)\frac{\partial T(x,z)}{\partial x}\right) + \frac{\partial}{\partial z}\left(\lambda(x,z)\frac{\partial T(x,z)}{\partial z}\right) \tag{6-12}$$

Each mesh has the information of the material in each layer (Table. 6.4) including the specific volume capacity, thermal conductivity. The heat flow is calculated by using the net thermal resistance between adjacent meshes, shown in Fig. 6.25.

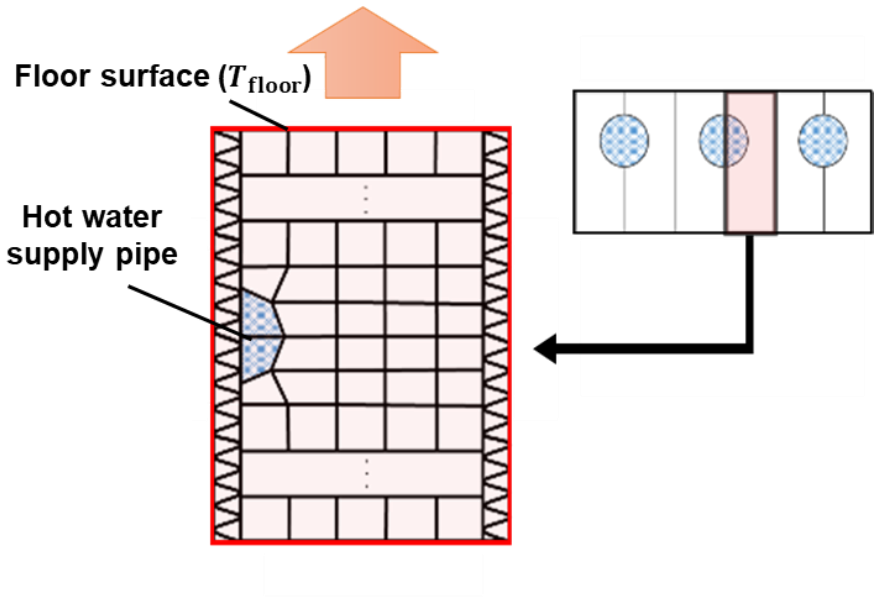

Fig. 6. 24 Conceptual diagram of the floor heating system

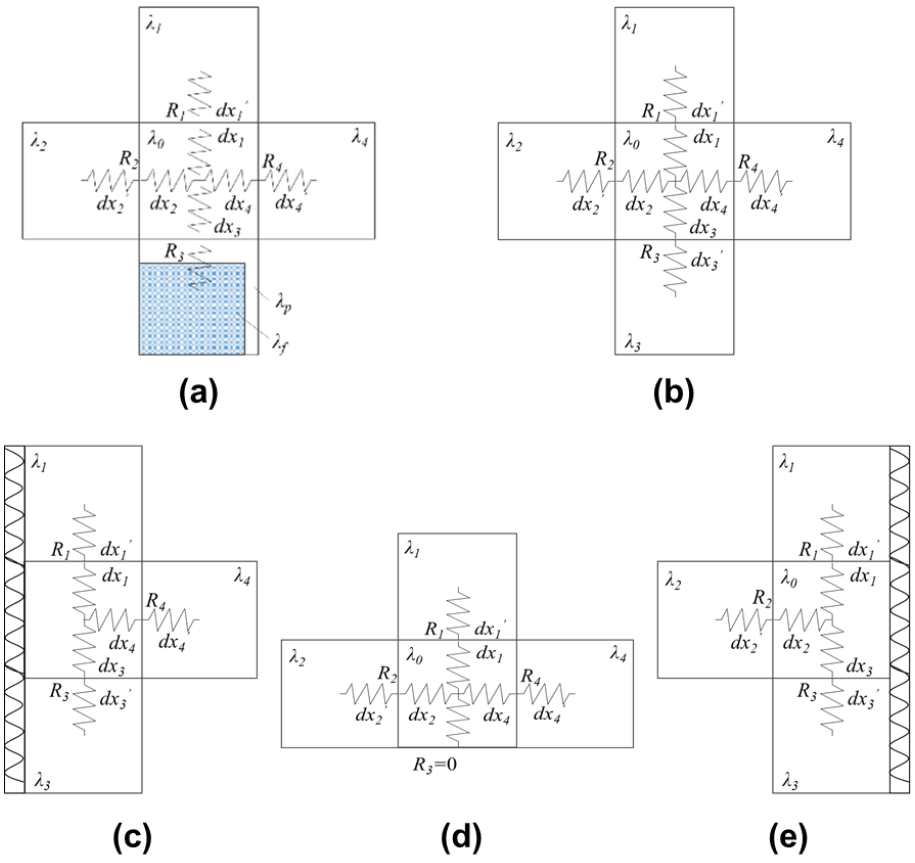

Fig. 6. 25 Net thermal resistance between adjacent meshes

The thermal resistance of the fluid in pipe in Fig. 6.25 (a) are determined by the flow rate of circulating fluid and are calculated in Eqs 6-13 and 6.14.

Flow rate = 0 m/y

$$R_3 = \frac{dx_3}{\lambda_0} + \frac{r_{\mathrm{p,out}}\, ln\left(\frac{r_{\mathrm{p,out}}}{r_{\mathrm{p,in}}}\right)}{\lambda_{\mathrm{p}}} + \frac{dx_3{}'}{\lambda_{\mathrm{f}}} \tag{6-13}$$

Flow rate > 0 m/y

$$R_3 = \frac{dx_3}{\lambda_0} + \frac{r_{\mathrm{p,out}}\, ln\left(\frac{r_{\mathrm{p,out}}}{r_{\mathrm{p,in}}}\right)}{\lambda_{\mathrm{p}}} + \frac{1}{h_{\mathrm{c}}} \tag{6-14}$$

$$h_{\mathrm{c}} = \frac{\lambda_{\mathrm{f}}}{r_{\mathrm{p,in}}} Nu \tag{6-15}$$

$$Nu = 1.62\left(\frac{Re\, Pr\ r_{\mathrm{p,in}}}{L}\right)^{\frac{1}{3}} \quad (\ Re < 2100\ ) \tag{6-16}$$

$$Nu = 0.023\, Re^{0.8}\, Pr^{0.4} \quad (\ Re > 2100\ ) \tag{6-17}$$

The temperature in each mesh over time is calculated in Eq. 6-18 with the overall heat transfer coefficient ($cc_{1\sim4}$).

$$T^{n+1} = cc_0 T^n + cc_1 T_1^n + cc_2 T_2^n + cc_3 T_3^n + cc_4 T_4^n \tag{6-18}$$

$$cc_{1\sim4} = \frac{\frac{dl}{c\rho S}}{\sum \frac{dx}{\lambda}} \tag{6-19}$$

$$cc_0 = 1 - \sum_{k=1}^{4} cc_k dt \tag{6-20}$$

Eq. 6-21 indicates the equation of the supply water temperature over time, taking into account the heat balance of the building loads to maintain the room temperature to the setpoint temperature. Fig. 6.26 shows the conceptual diagram of the supply water pipe.

$$T_{\mathrm{f}}^{n+1} = T_{\mathrm{f}}^{n} - \frac{Q_2}{c\rho V_{\mathrm{f}}} + \frac{m_2 \Delta t}{V_{\mathrm{f}}}\left(T_{2,\mathrm{out}} - T_{2,\mathrm{in}}\right) \tag{6-21}$$

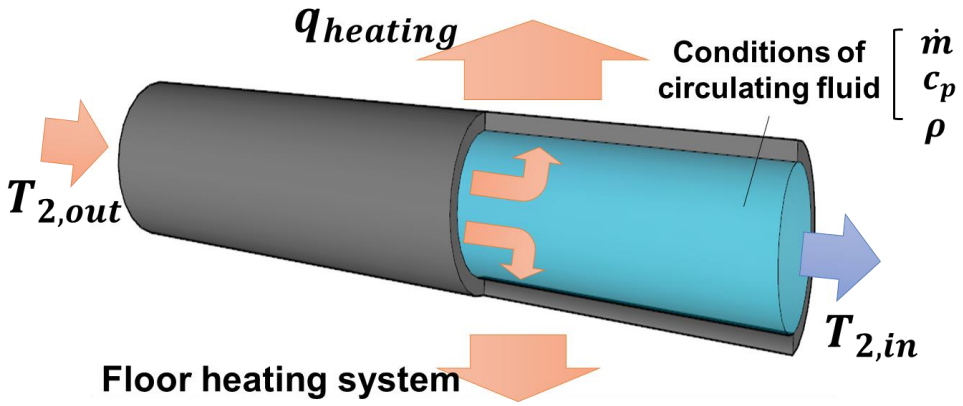

Fig. 6. 26 Conceptual diagram of the supply water pipe

Finally, the temperature of the floor surface is calculated by Eq. 6-22.

$$T_{floor} = \frac{q_{rad} + cc_1 c\rho S T_{floor} + (h_c + h_r) T_{room}}{cc_1 c\rho S + (h_c + h_r)} \tag{6-22}$$

$$h_c = 2.18\,|T_{\text{room}} - T_{\text{floor}}|^{1.31} \tag{6-23}$$

$$h_r = 5.67 \times 10^{-8} \left\{ \left(T_{floor} + 273.15\right)^4 - \left(T_{room} + 273.15\right)^4 \right\} \tag{6-24}$$

Here, h_c is convective heat transfer coefficient, and h_r is radiative heat transfer coefficient.

6.3.3. Ground source heat pump system

The calculation module of the circulating fluid and the ground temperature is applied based on the "Ground Club", which is the GSHP simulation tool developed in Hokkaido university. The module calculates the entering water temperature (EWT) and the coefficient of performance (COP) of the GSHP system during a long-term period, applying the moving infinite cylinder source model considering the groundwater flow and time-varying heat flux conditions in the multiple BHEs and the multi-layer environments [16–18]. The average temperature of the borehole wall is obtained in Eqs. 6-25 to 6-28. Here, the dimensionless parameters are derived by the approximate expressions in the previous research [16–18].

$$\frac{1}{\mathrm{L}}\int_0^L T_s(r_{\mathrm{bh}},z,t)dz = \underbrace{\frac{1}{\mathrm{L}}\int_0^L \Delta T_{s1}(r_{\mathrm{bh}},z,t)dz}_{\text{Temperature variation affected by heat injection/extraction}} + \underbrace{T_{s0}}_{\text{Initial temperature}} \tag{6-25}$$

$$\frac{1}{\mathrm{L}}\int_0^L \Delta T_{s1}(r_{\mathrm{bh}},z,t)dz = \Delta T_{\mathrm{s,i,j}}(r_{\mathrm{bh}},t) + \sum_{j=1}^{m}\Delta T_{\mathrm{s,i,j}}\left(r_{\mathrm{d,i,j}},t\right) \tag{6-26}$$

Temperature variation on the borehole wall

$$\Delta T_{\mathrm{s,i,j}}(r_{\mathrm{bh}},t) \cong \frac{1}{2\pi\lambda_{\mathrm{eff}}}\sum_{j=1}^{n} q_{\mathrm{i,j}}\Delta T_C^*\left(r_{\mathrm{bh}}^*, t_{\mathrm{bh}}^* - t_{\mathrm{bh,i}}^*\right) \tag{6-27}$$

Average surface temperature variation due to the heat injection/extraction via the neighboring boreholes

$$\Delta T_{\mathrm{s,i,j}}\left(r_{\mathrm{d,i,j}},t\right) \cong \frac{1}{2\pi\lambda_{\mathrm{eff}}}\sum_{j=1}^{n} q_{\mathrm{i,j}}\Delta T_L^*\left(r_{\mathrm{d,i,j}}^*, t_{\mathrm{d}}^* - t_{\mathrm{d,i}}^*\right) \tag{6-28}$$

The performance of the GSHP system was determined by the entering water temperature ($T_{1,\mathrm{in}}$) as a result of the BHEs calculation and the supply water temperature ($T_{2,\mathrm{out}}$) to the building in Eq. 6-29. The power consumption of the heat pump can be obtained from the following Eq. 6-30.

$$COP = f(T_{1,\text{in}}, T_{2,\text{out}}) \tag{6-29}$$

$$E = Q_2/COP \tag{6-30}$$

The heat exchange rate (Q_1) in the primary side can be calculated by the following Eq. 6-31, using Q_2 and E. The leaving water temperature ($T_{1\text{out}}$) in the primary side can be calculated using the following Eq. 6-32.

$$Q_1 = Q_2 - E \tag{6-31}$$

$$T_{1,\text{out}} = T_{1,\text{in}} - \frac{Q_1}{c_{1,\text{f}}\rho_{1,\text{f}}\dot{m}_{1,\text{f}}} \tag{6-32}$$

6.4. Results of the simulation tool for ZEB

6.4.1. Building load

The heating and cooling load of the building was calculated, based on the building conditions in Chapter 6.2. Fig. 6. 27 indicates the outdoor temperature variation and the global radiation at the test site. The data was measured at interval of 1 hour. The average, maximum and minimum annual temperatures are 8.7 ℃, 30.5 ℃ and -14.5 ℃.

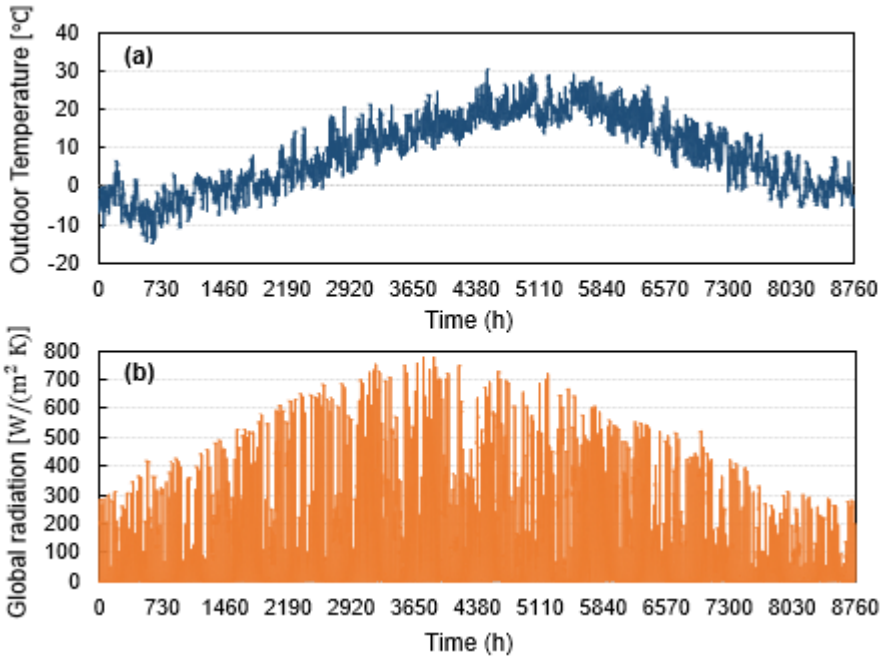

Fig. 6. 27 Weather data; (a) outdoor temperature and (b) global radiation

Fig. 6.28 and 6.29 show the heating and cooling load of the building. The building loads were calculated based on the heat balance of the building to maintain the indoor temperature to the setpoint temperatures. The setpoint temperatures for heating and cooling were 22 ℃ and 26 ℃, respectively. The peak load was 26.4 kW in winter season. The amount of the loads for heating and cooling was 76.5 GJ and 34.2 GJ, respectively. The total heating loads is 2.24 times higher than total cooling loads. The annual load per area was 10.2 W/m^2 for heating and 6.3 W/m^2 for cooling. These values are very small compared with conventional buildings of the loads. It can realize the ZEB to reduce primary energy consumption by applying a passive system.

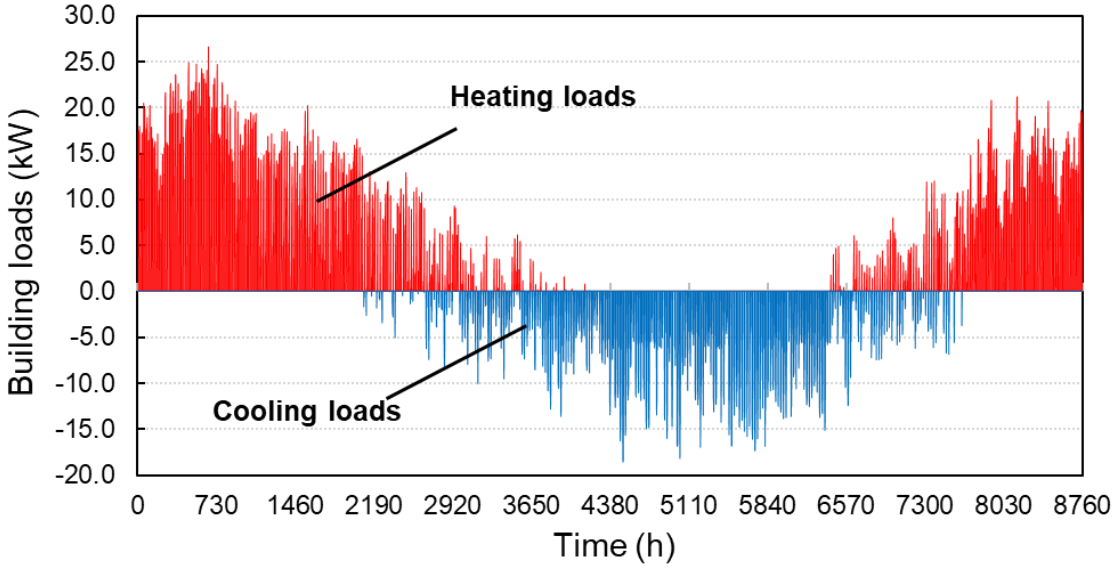

Fig. 6. 28 Heating and cooling loads of building

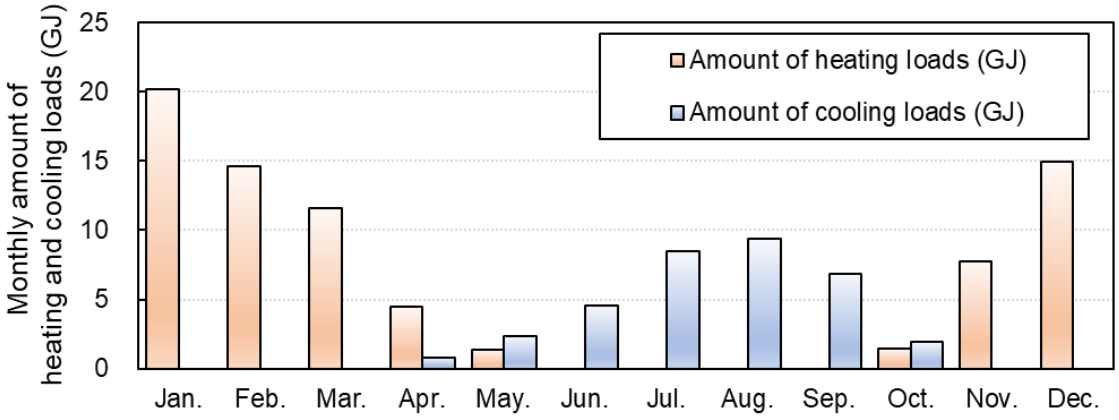

Fig. 6. 29 Monthly amount of heating and cooling loads

Table 6. 6 Monthly amount of heating and cooling loads

Load	Jan	Feb	Mar	Apr	May	Jun	Jul	Aug	Sep	Oct	Nov	Dec	Total
Heating Load [GJ]	20.2	14.7	11.6	4.4	1.3	0.0	0.0	0.0	0.0	1.5	7.8	15.0	76.5
Cooling Load [GJ]	0.0	0.0	0.0	0.7	2.3	4.5	8.5	9.4	6.8	1.9	0.0	0.0	34.2

6.4.2. Control of supply water temperature for floor heating and cooling system

A floor heating and cooling system was used to maintain the indoor temperature in response to heat loss of the building; the temperature change over time becomes zero based on the Eq. 6-11. To maintain the constant value of the indoor temperature, the circulating water in the pipe is suppled and controlled according to the building loads. Fig. 6.30 and Fig. 6.31 were the results of the floor surface temperature and the supplied water temperature. As a result, the average supplied water temperature for the heating and cooling period was 29.7 ℃ and 22.5 ℃, respectively.

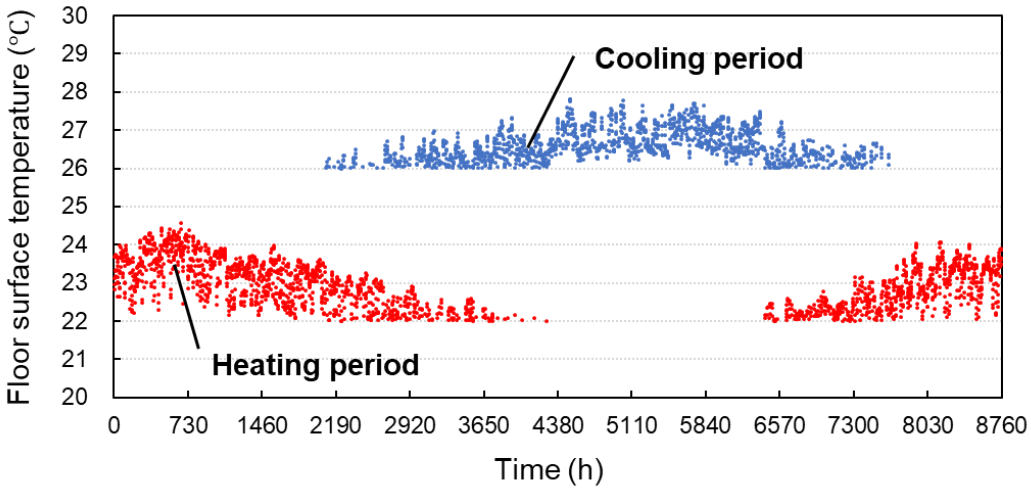

Fig. 6. 30 Floor surface temperature over time.

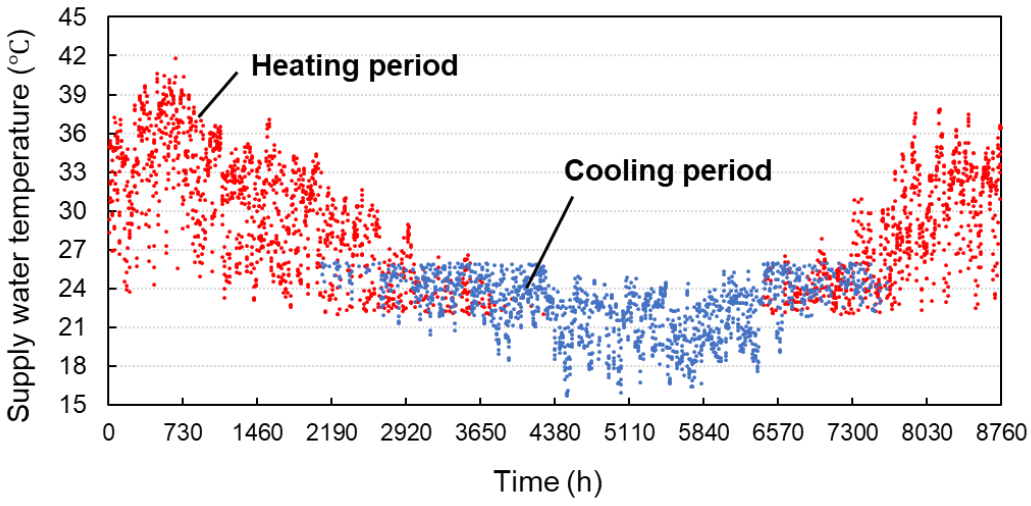

Fig. 6. 31 Supplied water temperature for heating and cooling

6.4.3. Prediction of the performance on the GSHP system

The GSHP system in the target building is connected with fifteen BHEs. The diameter and length of the borehole are 0.14 and 85 m, respectively. As a result of the TRT, the apparent effective thermal conductivity and borehole thermal resistance are 1.41 $\mathrm{W/(m\,K)}$ and 0.060 $\mathrm{(m\,K)/W}$. The initial ground temperature was 9.8 ℃. The spacing between boreholes was 5 m. Based on these conditions, the EWT ($T_{1,\mathrm{in}}$) and the system coefficient of performance (SCOP) are predicted. Fig. 6.32 shows the variation of the EWT ($T_{1,\mathrm{in}}$) for a year. The EWT was in the range of 2.3-18.3 ℃. The average temperature of the EWT for a year was 9.5 ℃. Fig. 6.32 (b) and (c) show the variation of the EWT in the typical days for heating and cooling. The temperatures were increased and decreased according to the building load. The temperature recovered to the initial temperature of the ground. The number of BHEs was enough to obtain the high performance of the GSHP system, based on the results of the temperature recovery. Fig. 6.33 indicates the variation of the SCOP for a year. The SCOPs of the heating and cooling for a year have relatively stable values of 4.02 for heating and 6.6 for cooling.

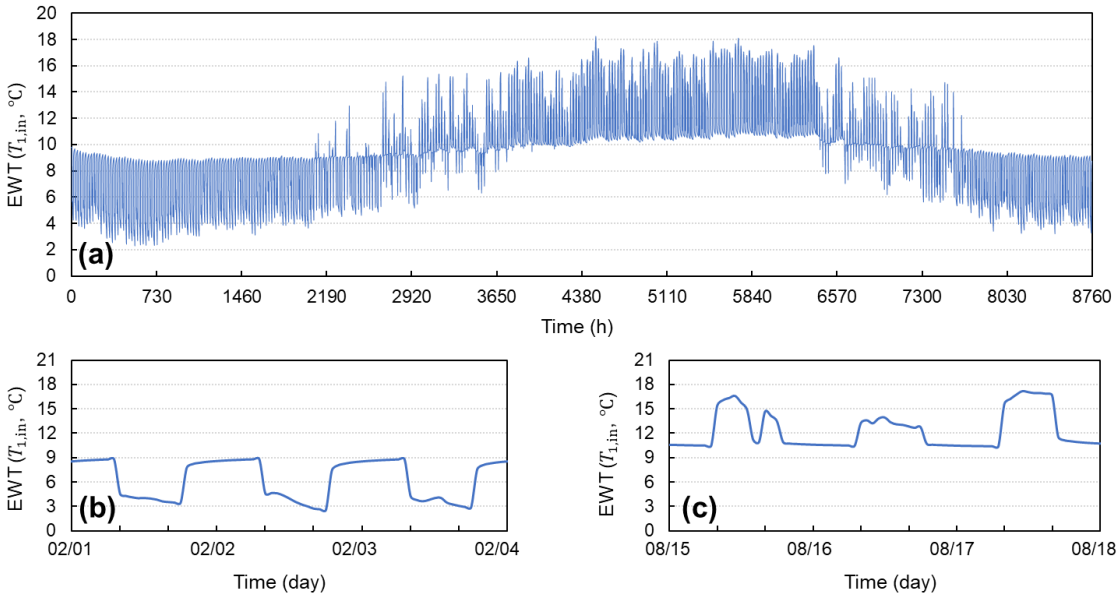

Fig. 6. 32 Variation of the EWT ($T_{1,\mathrm{in}}$)

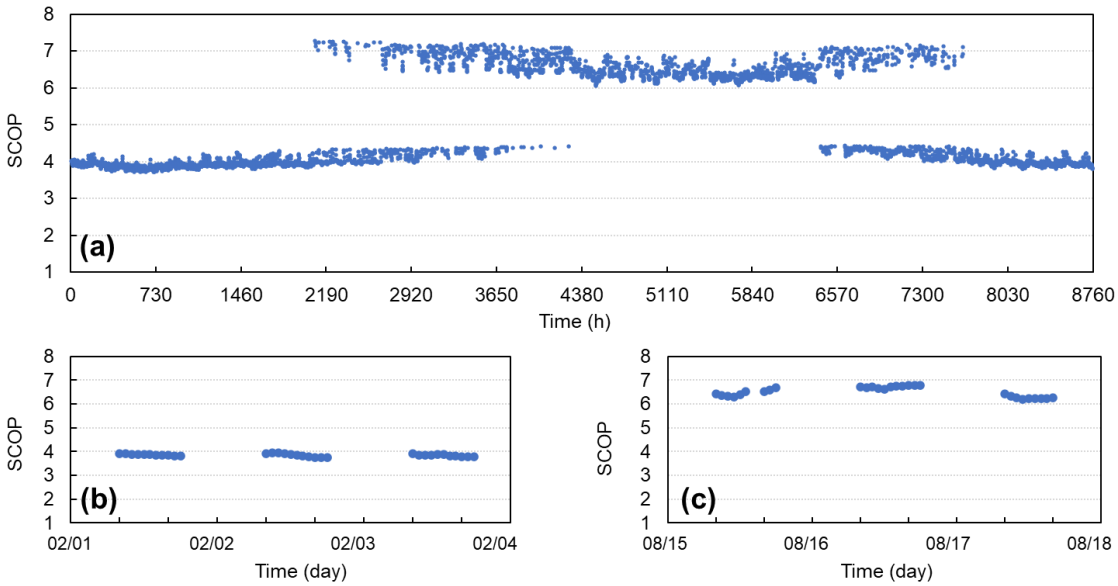

Fig. 6. 33 Variation of SCOP over time

6.4.4. Long-term simulation for GSHP system according to groundwater velocity and borehole number

Fig. 6. 34 indicates the calculated results for 30 years according to borehole number. The borehole was considered to change the BHEs from 5 to 25 at intervals of 2 units in a single layer under conditions without groundwater flow. In the results of the comparison between the first year and 30 years after operating the GSHP system in 5 BHEs conditions, the annual average ground temperature and SCOP were decreased 1.4°C and 0.07, respectively, and the electric consumption increased from 26.7 GJ to 27.2 GJ. On the other hand, in 25 BHEs, the annual average ground temperature and SCOP were decreased by 0.5°C and 0.03, respectively, and the electric consumption increased by 0.13 GJ. An appropriate number of the borehole was regarded to about 10 BHEs because the temperature difference when the BHEs was over 10 BHEs did not differ significantly.

Fig. 6. 35 and 36 shows the calculated results for 30 years according to groundwater velocity. The ground was divided to two layers, and the layer length of each case differ. The depth of layer 1 in Case 1 (Fig. 6. 35) was 20 m, and the depth of layer 1 in Case 2 (Fig. 6. 36) was 40 m. In the results of the comparison of the layer depth where the groundwater flows, the Case 2 was about 2.5 % higher performance than Case 1. In particular, the annual electric consumption decreased by about 0.1 GJ.

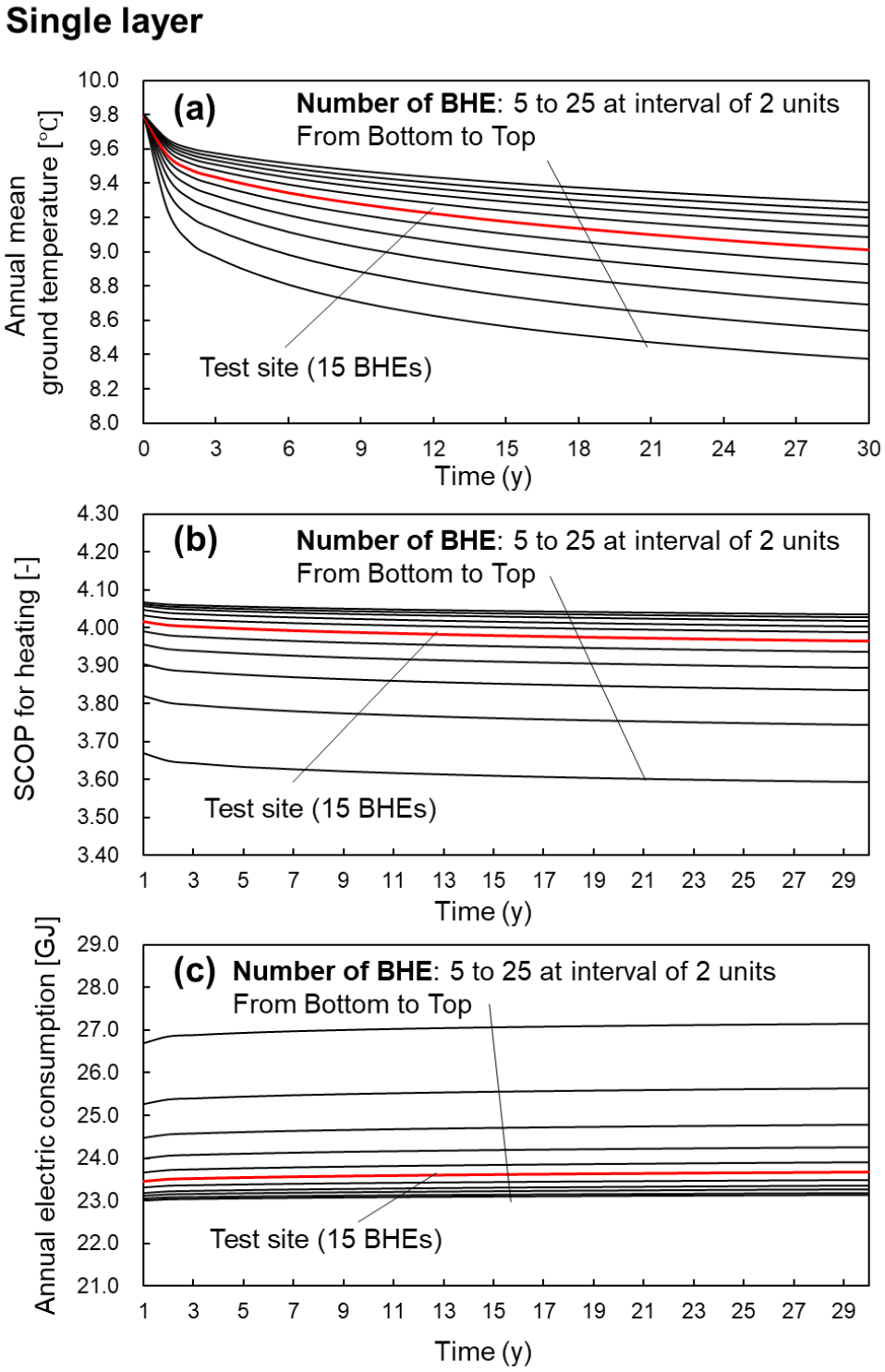

Fig. 6. 34 Calculated results for 30 years according to borehole number: (a) annual mean ground temperature, (b) SCOP for heating and (c) annual electric consumption

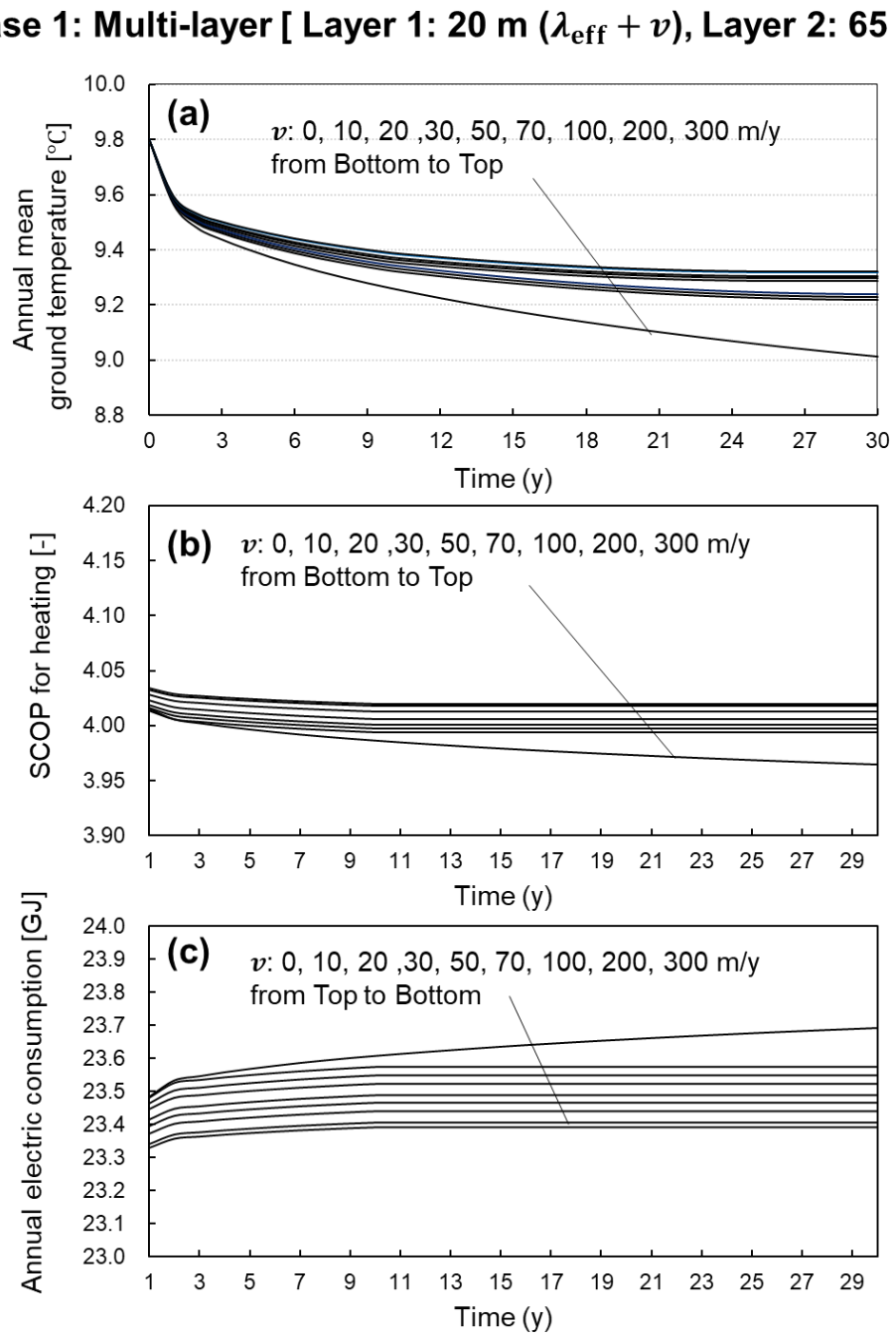

Fig. 6. 35 Calculated results (Case 1) for 30 years according to groundwater velocity [Layer 1: 20 m ($\lambda_{eff} + v$), Layer 2: 65 m (λ_{eff})]: (a) annual mean ground temperature, (b) SCOP for heating and (c) annual electric consumption

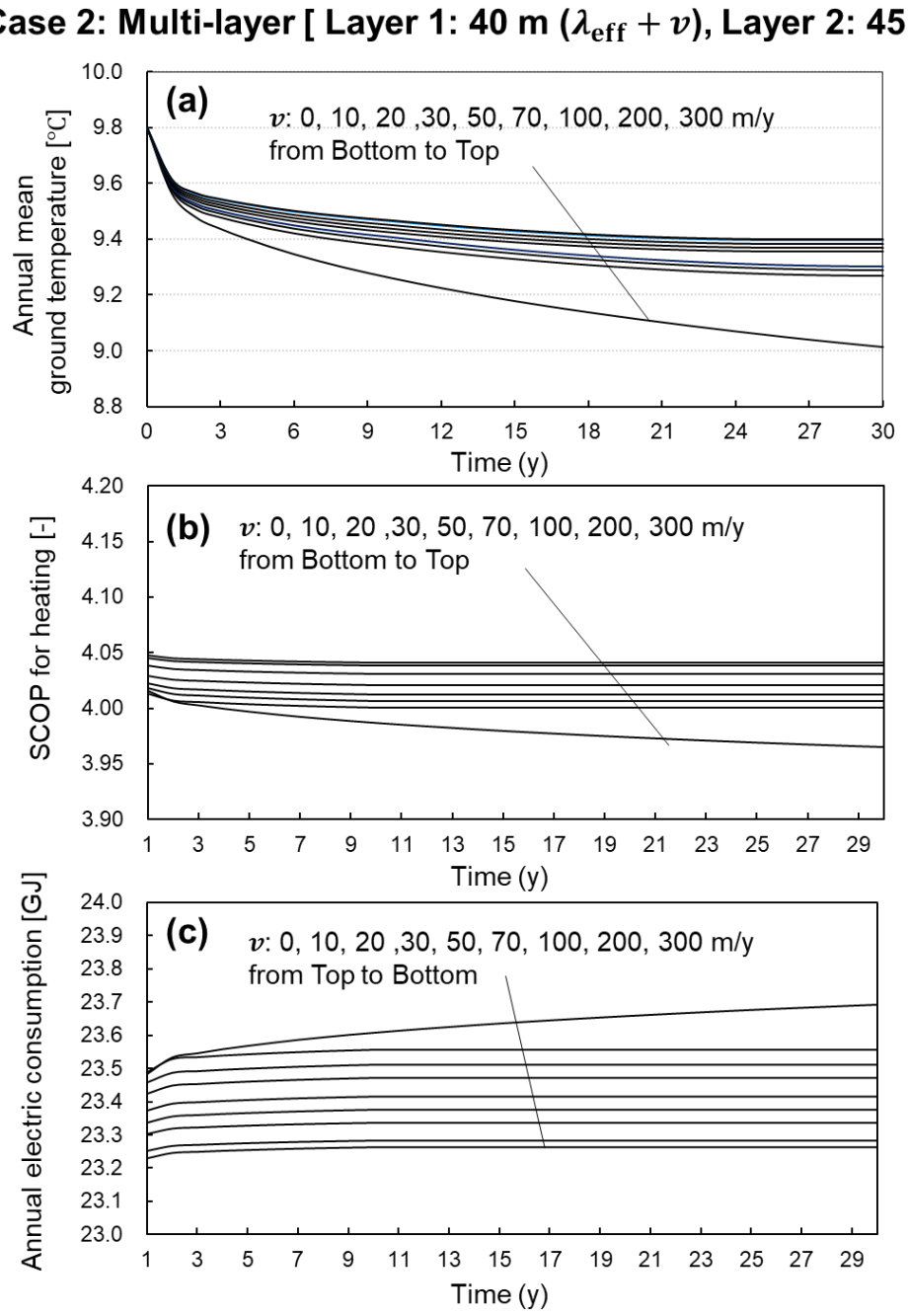

Fig. 6. 36 Calculated results (Case 2) for 30 years according to groundwater velocity [Layer 1: 40 m ($\lambda_{eff} + v$), Layer 2: 45 m (λ_{eff})]: (a) annual mean ground temperature, (b) SCOP for heating and (c) annual electric consumption

6.5. Summary

The Chapter introduced an application of a ground source heat pump system for nearly zero energy building. The application tool was developed to predict the energy consumption of the building, based on the GSHP system being able to calculate multi-borehole configuration under the conditions with the multi-layer with groundwater flows. Also, it could calculate the building loads installed in the floor heating and cooling system. Based on the application, a GSHP system was operated and predicted the system performance and the ground temperature in a nearly zero energy building located in the cold region.

The amount of the building loads for heating and cooling was 76.5 GJ and 34.2 GJ, respectively. The total heating loads were 2.24 times higher than total cooling loads. The annual load per area was 10.2 W/m^2 for heating and 6.3 W/m^2 for cooling. The supply water temperatures depended on the outdoor temperature and the SAT to maintain the indoor temperature of 22 ℃ for heating and 26 ℃ for cooling.

The ground temperature, system performance and the electric consumption were calculated in the various conditions: borehole number, groundwater velocity, layer depth. Based on the conditions of the target building, it was considered that the BHEs were needed over 10 to maintain high performance while reducing the initial investment cost. In addition, the depth of the layer where the groundwater flows affected the system performance, and the increased 20 m lengths of layer 1 improved the system performance by 2.5 % and reduced the electric consumption by 0.07 %.

6.6. Reference

[1] L. Capuano, International Energy Outlook 2020 (IEO2020), US Energy Inf. Adm. 2020 (2020) 1–7. https://www.eia.gov/outlooks/ieo/pdf/ieo2020.pdf.

[2] N. Ferri, United nations general assembly, Int. J. Mar. Coast. Law. 25 (2010) 271–287. doi:10.1163/157180910X12665776638740.

[3] S. Royston, J. Selby, E. Shove, Invisible energy policies: A new agenda for energy demand reduction, Energy Policy. 123 (2018) 127–135. doi:10.1016/j.enpol.2018.08.052.

[4] C. Robinson, B. Dilkina, J. Hubbs, W. Zhang, S. Guhathakurta, M.A. Brown, R.M. Pendyala, Machine learning approaches for estimating commercial building energy consumption, Appl. Energy. 208 (2017) 889–904. doi:10.1016/j.apenergy.2017.09.060.

[5] R. Dufo-López, J.L. Bernal-Agustín, New methodology for the generation of hourly wind speed data applied to the optimization of stand-alone systems, Energy Procedia. 14 (2012) 1973–1978. doi:10.1016/j.egypro.2011.12.1097.

[6] L. Danza, L. Belussi, G. Guazzi, I. Meroni, F. Salamone, Durability of technologies in the keeping of ZEB's performances, Energy Procedia. 148 (2018) 138–145. doi:10.1016/j.egypro.2018.08.041.

[7] S.Ø. Jensen, A. Marszal-Pomianowska, R. Lollini, W. Pasut, A. Knotzer, P. Engelmann, A. Stafford, G. Reynders, IEA EBC Annex 67 Energy Flexible Buildings, Energy Build. 155 (2017) 25–34. doi:10.1016/j.enbuild.2017.08.044.

[8] R. Li, G. Dane, C. Finck, W. Zeiler, Are building users prepared for energy flexible buildings?—A large-scale survey in the Netherlands, Appl. Energy. 203 (2017) 623–634. doi:10.1016/j.apenergy.2017.06.067.

[9] G. Reynders, R. Amaral Lopes, A. Marszal-Pomianowska, D. Aelenei, J. Martins, D. Saelens, Energy flexible buildings: An evaluation of definitions and quantification methodologies applied to thermal storage, Energy Build. 166 (2018) 372–390. doi:10.1016/j.enbuild.2018.02.040.

[10] M. Abu-Rumman, M. Hamdan, O. Ayadi, Performance enhancement of a photovoltaic thermal (PVT) and ground-source heat pump system, Geothermics. 85 (2020) 101809. doi:10.1016/j.geothermics.2020.101809.

[11] E.I. Sakellariou, A.J. Wright, P. Axaopoulos, M.A. Oyinlola, PVT based solar assisted ground source heat pump system: Modelling approach and sensitivity analyses, Sol. Energy. 193 (2019) 37–50. doi:10.1016/j.solener.2019.09.044.

[12] L. Xia, Z. Ma, G. Kokogiannakis, S. Wang, X. Gong, A model-based optimal control strategy for ground source heat pump systems with integrated solar photovoltaic thermal collectors, Appl. Energy. 228 (2018) 1399–1412. doi:10.1016/j.apenergy.2018.07.026.

[13] L. Xia, Z. Ma, G. Kokogiannakis, Z. Wang, S. Wang, A model-based design optimization strategy for ground source heat pump systems with integrated photovoltaic thermal collectors, Appl. Energy. 214 (2018) 178–190. doi:10.1016/j.apenergy.2018.01.067.

[14] S. Andrew Putrayudha, E.C. Kang, E. Evgueniy, Y. Libing, E.J. Lee, A study of photovoltaic/thermal (PVT)-ground source heat pump hybrid system by using fuzzy logic control, Appl. Therm. Eng. 89 (2015) 578–586.

doi:10.1016/j.applthermaleng.2015.06.019.

[15] 知久多喜真,ゴム工場における省エネルギー
最近のエネルギー事情と省エネルギー対策, 日本ゴム協会誌. 53 (1980) 521–524.

[16] T. Katsura, Y. Shoji, Y. Sakata, K. Nagano, Method for calculation of ground temperature in scenario involving multiple ground heat exchangers considering groundwater advection, Energy Build. 220 (2020). doi:10.1016/j.enbuild.2020.110000.

[17] T. Katsura, K. Nagano, Y. Sakata, H. Wakayama, A design and simulation tool for ground source heat pump system using energy piles with large diameter, Int. J. Energy Res. (2019) 1505–1520. doi:10.1002/er.4372.

[18] T. Katsura, K. Nagano, S. Takeda, Method of calculation of the ground temperature for multiple ground heat exchangers, Appl. Therm. Eng. 28 (2008) 1995–2004. doi:10.1016/j.applthermaleng.2007.12.013.

Chapter 7.

General conclusion and development toward zero carbon society

7.1. General conclusion

With growing concern about energy exhaustion and increasing environmental problems, the GSHP system has been regarded as a promising solution to the problem. In addition, interest in Zero-energy building has recently increased, and it has become a good opportunity for the GSHP system applicable to ZEB to be more widely distributed. Furthermore, the research proposed an appropriate borehole depth by estimating the effective thermal conductivity and groundwater velocity in the multi-layer to reduce the initial cost of the GSHP system, which is high compared to other types of systems. As part of the effort, this study presented several research topics in each chapter and could make conclusions.

In Chapter 1, "Introduction" described the outline of the GSHP system and the significance of its introduction in perspective of carbon dioxide emission reduction effects.

In Chapter 2, "Previous study orientation of this study" focused on the methodology on heat transfer process between the BHEs and the ground and the historical review of TRT to determine the design parameters of the GSHP system. In addition, The purpose and originality of this study were described to contribute to the development of the research field.

In Chapter 3, "Estimation of fast groundwater flow" proposed a practical approach for the determination of the groundwater flow velocity and the effective thermal conductivity of soil using the MLS theory, simultaneously. The TRT was carried out in Kazuno City, Japan, and the conventional TRT analysis results presented that apparent effective thermal conductivity was 9.14 W/(m K). The borehole thermal resistance was calculated by numerical simulation, considering the groundwater velocity under the conditions that inside borehole was filled by the porous material having a high permeability. The radius of an equivalent single pipe instead of the borehole radius was applied to the MLS model to calculate the circulating fluid temperature, including the temperature increase by the grout thermal resistance. The approximate expression of the equivalent radius calculated by linear regression analysis was suggested. The groundwater velocity and the effective thermal conductivity of the soil are determined by using root mean square error between the calculated results and the TRT data. As a result, the groundwater velocity based on the effective thermal conductivity of the ground column section was calculated in 120 m/y and 4.7 W/(m K). The practical approach method could use standard TRT data for

analysis without additional auxiliary equipment and complex simulation algorithms, designing the BHE in response to the annual building heat loads.

In Chapter 4, "Analysis of relaxation time of temperature for thermal response test" suggested that the ground was divided into three zones according to the effect of the groundwater flow, and the groundwater velocity in each zone was estimated. The reaching time was also proposed to determine the depth of the zones by considering the temperature recovery of the circulating fluid after stopping the heat supply. The temperature increments based on the heat exchange rate in each zone were then calculated according to the groundwater velocities. These results are compared with the average temperature increments measured from each zone, and its best-fitting value yields the groundwater velocities. As a result, the groundwater velocity was 2750, 58 and 0 m/y, and the thermal conductivity was 2.4, 2.4 and 2.1 $W/(m \cdot k)$ in each zone.

These estimated velocities with the other parameters were applied to the simulation tool to calculate the temperatures of the circulating fluid. These calculated temperature results were validated by comparing with the measurement data of the circulating fluid in the target building, and it was well-matched. In addition, the temperatures of the circulating fluid were calculated according to the depth of the BHE, based on the parameters estimated from the proposed method and the conventional TRT analysis method. The design parameters obtained from the proposed method could reflect the heat transfer of the ground more reasonably. It was possible to design the proper depth of the BHEs for the GSHP system.

In Chapter 5, "Validation of proposed TRT analysis and determination of borehole size" validated the effectiveness of the multi-layer TRT analysis method, reflecting both groundwater flow and effective thermal conductivity. The method could provide an appropriate borehole length by determining the layers with high thermal dispersion to reduce the construction investment of the BHEs. The numerical simulation was carried out to emulate the TRT during the heating and recovery period. The RMSE and the temperature error were under 0.27 K and 0.31% in all layers. The effect of the TRT analysis methods on the long-term operation of the GSHP system was evaluated. Based on the thermal properties of the soils estimated by the TRT analysis methods, the ground temperature change and the performance of the GSHP system were predicted for 30 years according to the building loads. As a result, the GSHP system designed by considering the layer with high thermal dispersion could save 16.8% of the initial investment, compared with the system designed by the conventional TRT method. The ROI period is 19.1, 14.0 and 6.8 years according to 0, 15, 30% of government subsidies, compared with the ASHP system.

In addition, as an alternative to the conventional TRT method, the new method utilizing actively heated fiber optics distributed temperature sensing was introduced. The groundwater velocities in the multi-layer were estimated by the relationship among the λ_a, λ_{eff} and v, utilizing the moving line source model. Based on the thermal parameters of the multi-layer, an appropriate borehole length in Area 1 and 2 was determined. As a result, in both Areas, the design of the BHEs considering the groundwater flow was able to reduce 30-40% of the total BHE length by the effect of advection. The borehole length where the TRT was carried out was appropriate in both Areas because the bottom layer has a high thermal dispersion. Meanwhile, A1-2-1 in Area 1 was able to recover the initial investment cost within 10 years, regardless of government subsidies. On the other hand, A2-2-1 in Area 2 could recover the initial investment cost within 10 years when the government subsidy of 60% was supported. The proposed method could provide a reasonable design of the borehole to reduce the risk of performance degradation and the initial investment cost of the GSHP system.

In Chapter 6, "Application of ground source heat pump system for nearly-zero energy building" introduced an application of a ground source heat pump system for nearly zero energy building. The application tool was developed to predict the energy consumption of the building, based on the GSHP system being able to calculate multi-borehole configuration under the conditions with the multi-layer with groundwater flows. Also, it could calculate the building loads installed in the floor heating and cooling system. Based on the application, a GSHP system was operated and predicted the system performance and the ground temperature in a nearly zero energy building located in the cold region.

The amount of the building loads for heating and cooling was 76.5 GJ and 34.2 GJ, respectively. The total heating loads were 2.24 times higher than total cooling loads. The annual load per area was 10.2 W/m^2 for heating and 6.3 W/m^2 for cooling. The supply water temperatures depended on the outdoor temperature and the SAT to maintain the indoor temperature of 22 ℃ for heating and 26 ℃ for cooling.

The ground temperature, system performance and the electric consumption were calculated in the various conditions: borehole number, groundwater velocity, layer depth. Based on the conditions of the target building, it was considered that the BHEs were needed over 10 to maintain high performance while reducing the initial investment cost. In addition, the depth of the layer where the groundwater flows affected the system performance, and the increased 20 m lengths of layer 1 improved the system performance by 2.5 % and reduced the electric consumption by 0.07 %.

To sum up, the GSHP systems are greatly attractive in terms of saving operating costs and reducing the emission of greenhouse gas. Although there still hurdles for the GSHP system to overcome, it is strongly believed that research in terms of its various aspects throughout the world will finally bring us the more developed technology. Furthermore, interest in ZEB applied to the GSHP system brings about the positive factors for the GSHP market to spread out and more high efficiency with collaborating the other system.

The world has been facing environmental issues during recent decades. As a part of an effort to solve the problem, low-carbon air conditioning through the GSHP systems is highly suggested.

7.2. Development toward zero carbon society

7.2.1. Plan to activate distribution of the GSHP system

In Japan, the installed number of GSHP systems has steadily increased since Geothermal Utilization Promotion Association was established in 2001. However, it is difficult to accept that government policies affect the supply of the GSHP systems in the private sector. Although the key factor for market expansion of the GSHP system in the private sector is the supply in large-scale building groups such as apartments, there are not many GSHP applications in apartment houses. Nevertheless, the applications of the GSHP systems in large-scale building groups are increasing recently, and the market size is likely to grow. As the GSHP systems can be competitive in new construction projects, it is expected that the distribution of the GSHP system in multi-unit dwellings will be activated if the technology can provide convenience and reliability to the users.

The special advantage of applying the GSHP system to large-scale buildings is that the system can efficiently supply the heating and cooling and hot water supply using a stable underground heat source (10~20℃), and it is possible to reduce energy by more than 30% compared to the existing air heat source. In addition, various design options for the energy supply can be provided through optimal capacity design according to the installation area. Because it is easy to converge with other energy systems, energy fusion between buildings or convergence with other building groups can be realized. Compared to other renewable systems, the GSHP system has the advantage that it does not affect the building façade or floor plan and does not require a cooling tower or outdoor unit space.

Geothermal cooling and heating technology has gone through many trials and errors over the past 20 years. Its technology has reached the level of advanced countries and is gaining stability and reliability. The geothermal application is expanding from the public sector to the household, and successful cases have been reported, so it is expected to be applied continuously in the future.

In recent years, apartments or office buildings have become high-rise buildings, and the centralized GSHP systems are expected to increase transport power, heat loss in pipes. There are also several difficulties in applying the GSHP system to large-scale buildings, such as unbalancing heating and cooling loads.

There are ways to solve this problem.

First, it is essential to secure an installation space for the BHEs and reduce the construction

period and cost. The various technologies can be introduced, such as vertical sealing type, horizontal type, low-depth modular type.

Second, the imbalance of heating and cooling loads will be solved to utilize units that respond to loads of individual rooms. It could satisfy the economic efficiency through number division and capacity optimization design.

The third is to install a small heat pump to enable individual heating and cooling and optimally design the entire pipe zoning. Therefore, it is necessary to develop a heat pump and secondary side unit that can respond to individual methods.

Finally, GSHP system could be integrated with the other system. The optimal operation strategies have proposed under different operation modes for the GSHP-PVT system [1–3]. In this case, the GSHP systems are more utilized in ZEBs [4,5] and energy flexible buildings [6–8].

7.2.2. State-of-the-art facility element technology for zero carbon society

Vacuum insulation panel

A vacuum insulated panel (VIP) is a form of thermal insulation consisting of a gas-tight enclosure surrounding a rigid core, from which the air has been evacuated. It is used in building construction, refrigeration units, and insulated shipping containers to provide better insulation performance than conventional insulation materials.

Heat transfer occurs by three modes: convection, conduction and radiation. Creating a vacuum practically eliminates convection, since this relies on the presence of gas molecules able to transfer heat energy by bulk movement. A small decrease in pressure has no effect on the thermal conductivity of a gas, because the reduction in energy-carrying molecules is offset by a reduction in collisions between molecules. However, at sufficiently low pressure, the distance between collisions exceeds the size of the vessel, and then the conductivity does reduce with pressure.

Since the core material of a VIP is similar in thermal characteristics to materials used in conventional insulation, VIPs therefore achieve a much lower thermal conductivity (k-value) than conventional insulation, or in other words a higher thermal resistance per unit of thickness. Typically, commercially available VIPs achieve a thermal conductivity of 0.004 $W/(m\,K)$ across the center of the panel, or an overall value of 0.006-0.008 $W/(m\,K)$ after allowing for

thermal bridging (heat conduction across the panel edges) and the inevitable gradual loss of vacuum over time.

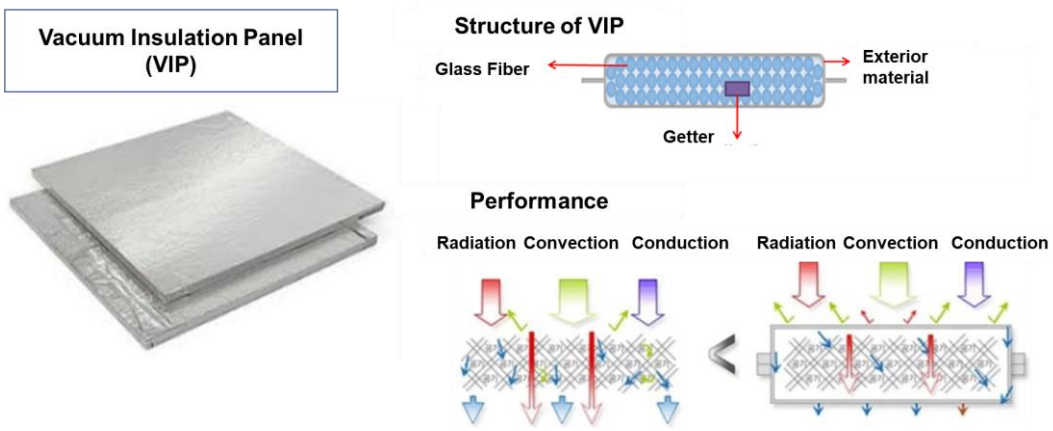

Fig. 7. 1 Conceptual image of vacuum insulation panel

Energy-storage system

An energy-storage system, also called home or solar battery, captures electricity during the day, and then it can use at another time. For example, you can store the electricity your solar panels generate during the day and use it at night. Big tech brands including Samsung and Tesla sell home-energy storage systems. This relatively new technology could utilize with the GSHP system.

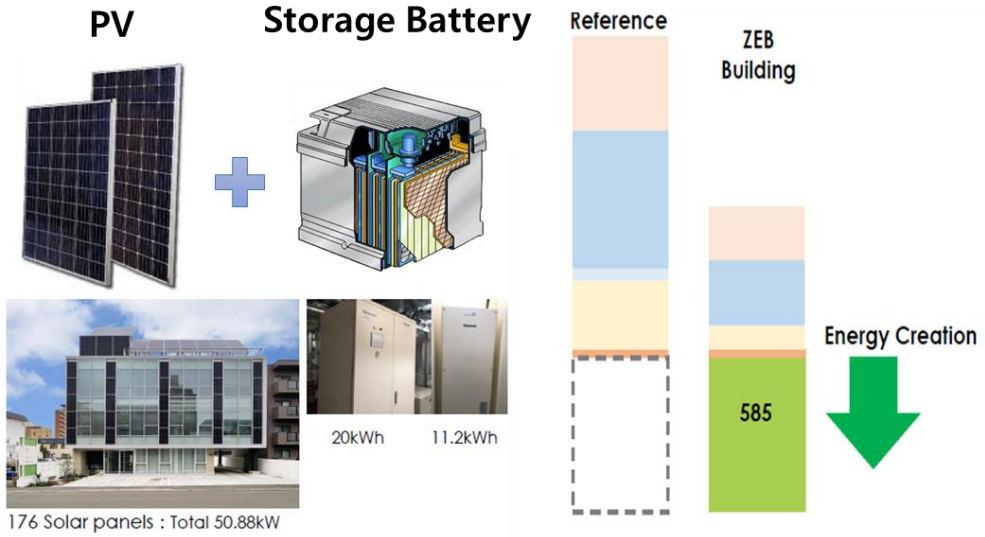

Fig. 7. 2 Conceptual image of energy-storage system

Building Energy Management System

The IEA uses the following description of a Building Energy Management Systems (BEMS): "an electrical control and monitoring system that has the ability to control monitoring points and an operator terminal. The system can have attributes from all facets of building control and management functions such as heating, ventilation and air conditioning (HVAC) to lighting, fire alarm system, security, maintenance and energy management. Another common description is that Building Energy Management Systems are control systems for individual buildings or groups of buildings that use computers and distributed microprocessors for monitoring, data storage and communication. Other terms frequently used for this technology are Building Management System (BMS) and Energy Management System (EMS).

As such, the Building Energy Management Systems technology is a broad concept of building control and can have a variety of characteristics. However, the term BEMS is limited to use for sophisticated and advanced control systems. Therefore, while all buildings require and have some form of the control system, Building Energy Management Systems technology is substantially different from previous control systems. The main point in which a Building Energy Management System (BEMS) differs from other control systems is the characteristic of communication: information of the processes and functions of the building can be received and controlled at a central, single operating unit. Therefore, decisions can be made based upon the received information. This is a critical aspect of a BEMS as it allows for optimization of the system. For instance, the central and single operating units can receive information on temperature and building occupancy and can make the decision to lower the temperature in parts of the building that are not occupied. These decisions therefore can increase energy efficiency. Figure 1 illustrates a possible BEMS configuration in which multiple buildings are connected to each other and are connected via the internet to a central operating unit to allow smooth cooperation among the buildings and increase efficiency. Increased cooperation among different buildings through the BEMS allows for additional increased energy efficiency, as functions of the different buildings can be coupled.

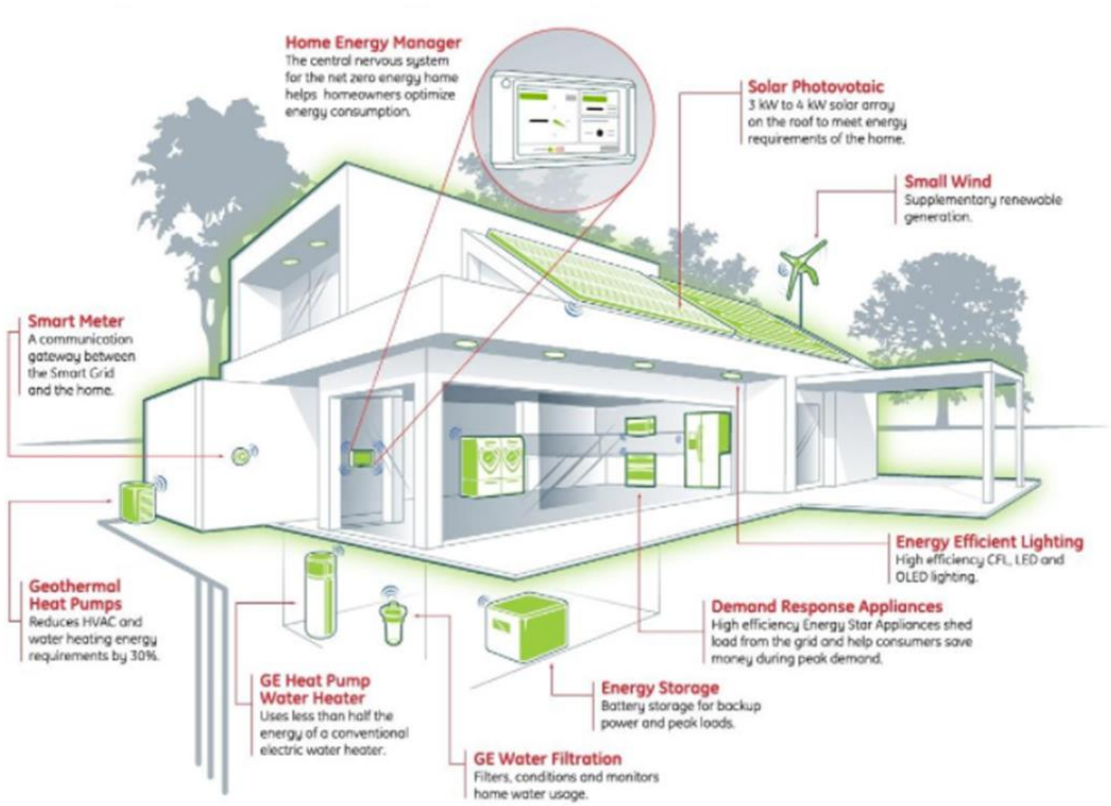

Fig. 7. 3 Conceptual image of Building Energy Management System

7.3. Reference

[1] L. Xia, Z. Ma, G. Kokogiannakis, S. Wang, X. Gong, A model-based optimal control strategy for ground source heat pump systems with integrated solar photovoltaic thermal collectors, Appl. Energy. 228 (2018) 1399–1412. doi:10.1016/j.apenergy.2018.07.026.

[2] L. Xia, Z. Ma, G. Kokogiannakis, Z. Wang, S. Wang, A model-based design optimization strategy for ground source heat pump systems with integrated photovoltaic thermal collectors, Appl. Energy. 214 (2018) 178–190. doi:10.1016/j.apenergy.2018.01.067.

[3] S. Andrew Putrayudha, E.C. Kang, E. Evgueniy, Y. Libing, E.J. Lee, A study of photovoltaic/thermal (PVT)-ground source heat pump hybrid system by using fuzzy logic control, Appl. Therm. Eng. 89 (2015) 578–586. doi:10.1016/j.applthermaleng.2015.06.019.

[4] R. Dufo-López, J.L. Bernal-Agustín, New methodology for the generation of hourly wind speed data applied to the optimization of stand-alone systems, Energy Procedia. 14 (2012) 1973–1978. doi:10.1016/j.egypro.2011.12.1097.

[5] L. Danza, L. Belussi, G. Guazzi, I. Meroni, F. Salamone, Durability of technologies in the keeping of ZEB's performances, Energy Procedia. 148 (2018) 138–145. doi:10.1016/j.egypro.2018.08.041.

[6] S.Ø. Jensen, A. Marszal-Pomianowska, R. Lollini, W. Pasut, A. Knotzer, P. Engelmann, A. Stafford, G. Reynders, IEA EBC Annex 67 Energy Flexible Buildings, Energy Build. 155 (2017) 25–34. doi:10.1016/j.enbuild.2017.08.044.

[7] R. Li, G. Dane, C. Finck, W. Zeiler, Are building users prepared for energy flexible buildings?—A large-scale survey in the Netherlands, Appl. Energy. 203 (2017) 623–634. doi:10.1016/j.apenergy.2017.06.067.

[8] G. Reynders, R. Amaral Lopes, A. Marszal-Pomianowska, D. Aelenei, J. Martins, D. Saelens, Energy flexible buildings: An evaluation of definitions and quantification methodologies applied to thermal storage, Energy Build. 166 (2018) 372–390. doi:10.1016/j.enbuild.2018.02.040.

Acknowledgements

Acknowledgements

Firstly, I would like to express my deepest appreciation to my supervisor, Professor Nagano. His guidance and motivation helped me grow up as a researcher. The five years I spent in his laboratory were a valuable time to experience various research fields in my life. Also, I am grateful for his encouragement during the toughest period of my life. Without his support and persistent help, this dissertation would not have been possible. I will become a better researcher based on all the guidance of Professor Nagano. Thank you again for giving me the opportunity to have a valuable experience and support.

I would like to thank Professor Katsura. His dedicated support and guidance have made an inspiring experience for me in the research field. I was able to learn a lot of research approaches from kindly your guidance.

I would like to say special thanks to Professor Sakata, for supporting me with a sincere heart whenever I face problems. His advice and encouragement have been a valuable time for me to develop my research knowledge. Also, I would like to say thanks to Dr. Award and Dr. Ali for giving me a lot of academic advice.

I would like to thank Professor Hamada and Professor Tabe for their service and precious comments on my doctoral committee for developing my research.

I would like to say thanks to all Korean members, Professor Lee and Dr. Seol. I used to be encouraged by Korean group especially when I feel depressed. I also would like to thank many students in our laboratory.

Especially, I am grateful for Professor Nam. He is always been my spiritual mainstay, and his encouragement allowed me to focus on my research. Thank you again for your continued encouragement and support.

During the doctoral course, I sometimes used to feel alone. I would like to thank my friends Min Kwan-hong and Lee kyung-sik for cheering me up.

Finally, I would like to dedicate this thesis to my parents, Father and Mother. I always have felt as if he is standing behind me to support me. Always respect and love you. To

my sister, thank you for helping, and I will not forget your support. Lastly, I will try to be a better person and researcher to repay your devotional sacrifice.

2021. 08. 23

With All My Heart

Hobyung Chae